Electrochemically Modulated Generation/Delivery of Nitric Oxide (NO) from Nitrite for Biomedical Applications

by

Hang Ren

A dissertation submitted in partial fulfillment
of the requirements for the degree of
Doctor of Philosophy
(Chemistry)
in the University of Michigan
2016

Doctoral Committee:

Professor Mark E. Meyerhoff, Chair
Associate Professor Bart Bartlett
Associate Professor Stephen Maldonado
Associate Professor Chuanwu Xi

© Hang Ren 2016

DEDICATION

To my family.

ACKNOWLEDGEMENTS

First and foremost, I would express my gratitude to my advisor Dr. Mark E. Meyerhoff. His passion for science always inspires me. None of this work would have been possible without his support and encouragement. I really appreciate the freedom he has given me to pursue the research described in this dissertation.

I would also like to thank my committee members, Dr. Bart Bartlett, Dr. Stephen Maldonado and Dr. Chuanwu Xi for their time and effort. I appreciate their suggestions and recommendations on various aspects of the projects reported herein.

Special thanks to my collaborators from Dr. Xi's Lab, Dr. Robert Bartlett's Lab and Dr. Lehnert's Lab. I would like to especially thank Dr. Chuanwu Xi and Dr. Jianfeng Wu for providing invaluable facilities and expertise in the field of microbiology. I am grateful for their suggestions ranging from experimental design to manuscript writing. I would also like to thank Dr. Robert Bartlett and all the ECMO team for all of their help with the animal experiments reported in this thesis. I am especially thankful to Dr. Terry Major, Dr. Alvaro Rojas-Pena and Dr. Megan Coughlin, not only for their fantastic surgical skills and tremendous commitment to the experiments, but also for their insights and suggestions for the projects. I would also like to express my gratitude to Dr. Nicolai Lehnert for taking me on as a rotation student when I first came to Michigan, and for the suggestions on the project regarding the use of Cu(II)-ligand complexes as mediators to

generate NO. Dr. Lauren Goodrich-Berto and Dr. Tim Berto, thank you for your help and guidance during the rotation, and Andrew Hunt, thank you for all the discussions and experiments on the projects that utilized the Cu(II)-ligand complexes.

During the past five years, I feel very lucky to have had the opportunity to work with all the amazing people in Meyerhoff Lab: Dr. Dipankar Koley, Dr. Gary Jenson, Dr. Kun Liu, Dr. Natlie Crist, Dr. Bo Peng, Dr. Si Yang, Dr. Wenyi Cai, Dr. Elizabeth Brisbois, Dr. Andrea Bell, Dr. Alex Wolf, Dr. Yu Qin, Dr. Xuewei Wang, Dr. Gergely Lautner, Dr. Woong Hee Lee, Dr. Joanna Zajda, Alex Ketchum, Zheng Zheng, Yaqi Wo, Kyoung Ha Cha, Stephen Ferguson, Josh Doverspike, Alessandro Colletta, Anant Balijepalli, Ian Vonwald, and Anna Mokrushina. Thank you all for your support and friendship.

My sincere appreciation goes to my many friends here in Michigan. Sheng Zheng, Chuan Leng, Tao Jiang, our basketball is full of fun. I am also very grateful to all my friends from college, especially Jie Zhu, Zhongming Li, Yuwen Xu, Xiwen Guan, Weiqi Hou and Guohong Huang. Thank you all for your belief in me and support over the years, and for always being there for me.

I would like to thank my family, especially my parents, Hong Li and Nailin Ren for their unconditional love, patience and belief in me. I'm also grateful to my grandparents Zhanlan Gao and Fucai Li, my mother-in-law Yuehong Jin and fatheter-in-law Zhitao Yang.

Finally, to my wife, Jinjing Yang. I can never thank you enough for your love, belief, support and encouragement. Thank you for being with me now and in all the journeys the lie ahead of us.

TABLE OF CONTENTS

DEDICATION ..... **ii**

ACKNOWLEDGEMENTS ..... **iii**

LIST OF FIGURES ..... **viii**

LIST OF TABLES ..... **xx**

LIST OF ABBREVIATIONS ..... **xxi**

ABSTRACT ..... **xxiv**

CHAPTER 1. Introduction **1**

1.1 Challenges for Implantable Medical Devices 1

1.2 Current Strategies/Efforts 5

1.3 Nitric Oxide to the Rescue 8

1.4 Statement of Research 18

1.5 References 22

CHAPTER 2. Optimization of Cu^0 Wire-Based Electrochemically Modulated NO Release from Inorganic Nitrite **29**

2.1 Introduction 29

2.2 Experimental Details 32

2.3 Results and Discussion 36

2.4 Conclusions 46

2.5 References 48

CHAPTER 3. Electrochemically Modulated NO Releasing Biomedical Devices via Copper(II)-Tri(2-pyridylmethyl)amine Mediated Reduction of Nitrite 52

3.1 Introduction 52

3.2 Experimental Details 54

3.3 Results and Discussion 59

3.4 Conclusions 74

3.5 References 76

CHAPTER 4. Improved In Vivo Performance of Amperometric Oxygen (PO_2) Sensing Catheters via Electrochemical NO Generation/Release 79

4.1 Introduction 79

4.2 Experimental Details 81

4.3 Results and Discussion 86

4.4 Conclusions 97

4.5 References 99

CHAPTER 5. Dosage Effect of Nitric Oxide (NO) and Its Synergy with Antibiotic Against Pseudomonas Aeruginosa Biofilm Using Controlled Release of NO from an Electrochemical System 101

5.1 Introduction 101

5.2 Experimental Details 103

5.3 Results 107

5.4 Discussion 114

5.5 Conclusions 119

5.6 References 121

CHAPTER 6. Experimental and Simulation Studies of Transport of NO Through Biomedical Grade Polymers and Its Effect on Local NO Flux Distribution on Medical Devices 124

6.1 Introduction 124
6.2 Theory 126
6.3 Experimental and Simulation Methods 132
6.4 Results and Discussion 138
6.5 Conclusions 154
6.6 References 156
CHAPTER 7. Electrochemical Generation of NO for Potential Application in Inhaled NO Therapy 159
7.1 Introduction 159
7.2 Experimental Details 161
7.3 Results and Discussion 164
7.4 Conclusions 173
7.5 References 175
CHAPTER 8. Conclusions and Future Directions 178
8.1 Conclusions 178
8.2 Future Directions 181
8.3 References 188
Appendix A. Summary of Behavior of Various Cu(II)-Ligand Complexes as Catalysts for NO Generation via Electrochemical Reduction of Nitrite 189
A.1 Summary of the Electrochemical Properties Cu-Ligand Complexes 189
A.2 Study of Cu(II)Me_3TACN as Catalyst for NO Generation from Nitrite .. 191
A.3 Side Reaction of CuMe_3TACN—Disproportionation of Cu(I) 193
A.4 References 197

LIST OF FIGURES

Figure 1.1. Development of bacterial biofilms on surfaces. 3

Figure 1.2. Sequence of events that lead to the formation of thrombus induced by a foreign surface. 4

Figure 1.3. NO production from a two-step oxidation L-arginine via nitric oxide synthase (NOS). 9

Figure 1.4. Schematics of NO release from a diazeniumdiolate blended polymer. 11

Figure 1.5. Frost diagram of nitrogen species in acidic (blue) and basic (black) solutions. 15

Figure 1.6. Mechanism of electrochemical generation of NO from nitrite and an iron porphyrin catalyst in aqueous solution. (Reprinted from Chi et. al. *Inorg. Chem.* **2004**, *43*, 8437.) [94] 16

Figure 1.7. Schematic of the electrochemical NO generating catheter configuration. A copper wire serves as the working electrode and silver/silver chloride wire serves as the reference electrode. PTFE coating prevents the two wires from short-circuit. The inner filling solution contains $NaNO_2$, NaCl, EDTA, Na_2HPO_4, NaH_2PO_4, pH 6.8. [95] 16

Figure 1.8. Electromodulated NO generation in silicone rubber catheter tube (see Fig. 1.7). (A) NO flux from surface of silicone rubber tubing over a 24 h period, with the applied -0.7 V (3 min)/+0.2 V (3 min) (vs. NHE); pulse sequence initiated for 1 h every 2 h. (B) Expanded view of 2 h segment when voltage cycle is "off" and then

turned "on" (oscillating between -0.7 V and +0.2 V vs. NHE). (Reprint from Hofler et. al. *RSC Adv.* **2012**, *2*, 6765.)[95] 18

Figure 2.1. Schematic of a single-lumen electrochemically modulated NO releasing catheter. 36

Figure 2.2. Effect of pulse cycle on NO release profile from surface of the silicone catheter from a copper wire electrode: (a) Schematic of applied voltage pulse sequence; (b) NO release profile from 6 min cycles using old pulse sequence (as in ref 23); with an anodic pulse of 3 min at 0 V and a cathodic pulse of 3 min at -0.92 V (vs. Ag/AgCl wire); (c) NO release profile of 6 min cycles and 30 s cycles, with an anodic pulse of +0.2 V and a cathodic pulse of -1.3 V (vs. Ag/AgCl wire). 38

Figure 2.3. Effect of cathodic pulse voltage on NO release from a single-lumen catheter at 25 ℃. Each pulse cycle includes a 15 s cathodic voltage pulse and a 15 s anodic voltage pulse. The potentials are vs. Ag/AgCl wire. 39

Figure 2.4. NO release from a single-lumen silicone catheter using repeated pulse cycles of 15 s at -1.3 V and 15 s at +0.2 V at 37 ℃. The dotted line indicates a surface NO flux of 1.0×10^{-10} mol min^{-1} cm^{-2}. Note that the catheter is intentionally turned "off" periodically to demonstrate the NO release can be modulated. The potentials are vs. a Ag/AgCl wire. 39

Figure 2.5. Effect of solution phase O_2 concentration on NO release from a single-lumen silicone catheter (37 ℃). Repeated pulse cycles of 15 s at -1.3 V and 15 s at +0.2 V are applied. Note that NO release is turned "off" when changing the purging gas. 40

Figure 2.6. Antithrombotic effect of NO releasing catheters (NRC) in 7 h rabbit experiment: a) representative photos of high flux (NRC (High) ~1.1×10^{-10} mol min^{-1} cm^{-2}), low flux (NRC (Low) ~0.7×10^{-10} mol min^{-1} cm^{-2}) and control (Control, < 0.1×10^{-10} mol min^{-1} cm^{-2}) catheters after explantation; b) thrombus surface coverage quantified by counting the red pixels on the catheters from the photos (Low flux

catheters: n = 3 rabbits, * $p < 0.05$; High flux catheters: n = 3 rabbits, **$p < 0.01$). 41

Figure 2.7. *S. aureus* biofilms developed on single-lumen catheters in a drip flow biofilm reactor for 48 h with the electrochemical NO release turned "on" continuously (only for NO release catheters) throughout the entire period of the biofilm growth. Plate counts of viable bacteria attached to the catheter surface after this period (n = 3, **$p < 0.01$). 43

Figure 2.8. *E. coli* biofilm developed on single-lumen catheters in a drip flow biofilm reactor for a) 48 h and b) 96 h and NO release was then turned "on" only at the end of these periods for 3 h. Plate counts of viable bacteria attached to the catheter surface (n = 4 for both experiments, **$p < 0.01$). 44

Figure 2.9. Representative fluorescent micrographs of surfaces of a) control and b) NO releasing catheters with live/dead staining. *E. coli* biofilms was grown for 48 h and NO is turned "on" for the NO releasing catheter for 3 h at the end of the growth before the imaging. 45

Figure 3.1. Experiment setup for bulk electrolysis of Cu(II)TPMA and nitrite solution. 55

Figure 3.2. Cyclic voltammograms of 1 mM Cu(II)TPMA in 0.1 M MOPS buffer (pH 7.2) on a 0.0314 cm^2 gold disc electrode with different levels of nitrite in solution saturated with N_2. Scan rate is 50 mV/s. Inset: structure of Cu(II)TPMA. 59

Figure 3.3. Cyclic voltammograms of 1 mM CuTPMA in 0.1 M MOPS buffer (pH 7.2) in a bulk solution experiment using a) 0.0707 cm^2 glassy carbon (GC) disk electrode; and b) 0.0314 cm^2 platinum disc electrode with different levels of nitrite in N_2 environment. Scan rate: 50 mV/s. 60

Figure 3.4. Modulation of NO generation in bulk solution by applying -0.2 V, -0.3 V and -0.4 V (vs. 3 M Cl^- Ag/AgCl) on a 0.071 cm^2 GC electrode. The solution contains 2 mM Cu(II)TPMA, 100 mM nitrite and 0.1 M MOPS buffer (pH 7.2). 61

Figure 3.5. a) Gas phase IR spectra of headspace N_2O solution standards. Inset: calibration curve from integration of N_2O feature peaks at 2235 and 2212 cm^{-1}; b) gas-phase N_2O produced from bulk electrolysis of CuTPMA with different levels of nitrite present in the solution phase. 62

Figure 3.6. Cross sectional geometries of a) dual lumen and b) single lumen silicone catheters employed in these studies. 63

Figure 3.7. Schematics of a) single and b) dual lumen electrochemically modulated NO releasing catheter configurations examined in this work. 64

Figure 3.8. The concentration profile of 7, 5 and 3 cm catheters with 1 cm long active Pt surface; concentration profile 100 μm away from catheter surfaces of b) 7 cm c) 5 cm d) 3 cm in length along the direction of the white line at different time points; e) integration of concentration of a 7 cm catheter, with 1, 2 and 3 cm along a line 100 μm away from catheter surface near the exposed Pt electrode. 65

Figure 3.9. Modulation of NO flux from a single lumen catheter with 0.0798 cm^2 Pt wire. The solution contains 4 mM Cu(II)TPMA, 0.4 M $NaNO_2$, 0.2 M NaCl and 0.5 M MOPS (pH 7.2). Flux calculated based on the 3 cm silicone surface area near the Pt wire. Potentials are vs. 0.2 M Cl^- Ag/AgCl. 66

Figure 3.10. Nitric oxide release from a 7.5 cm long single lumen catheter with 0.080 cm^2 Pt wire. Inner solution contains 2 mM Cu(II)TPMA, 0.4 M $NaNO_2$, 0.2 M NaCl and 0.5 M MOPS (pH 7.2). NO turned "on" (- 0.4 V vs. 0.2 M Cl^- Ag/AgCl reference) for 8 d; periods of applied potential being turned "off" are also indicated. 67

Figure 3.11. Antithrombotic effect of e-chem NO releasing catheters in veins of six rabbits for 7 h. Representative pictures of a) single and b) dual lumen catheters after removal from the vein; c) thrombosis coverage percentage on the catheters (single lumen: SL 1–3, dual lumen: DL 1–3). 69

Figure 3.12. Distribution of NO concentration around the cross-section of a dual lumen silicone catheter (via COMOSOL Multiphysics): a) color map of NO concentration after 30 min of NO generation from the electrode surface; b) concentration vs. time at 100 μm from left- and right-side of the catheter surface (indicated by pink star in the color map; c) concentration profile on the cut line crossing the electrode (yellow dashed line in the color map). 71

Figure 3.13. *E. coli* biofilm developed on dual lumen catheters in a drip flow reactor for 3 d with NO turned on for 3 h each day. a) and b): Plate count of the number of viable bacteria attached to the catheter surface and channel surface; c) picture shows the dramatic reduction of biofilm (indicated by arrow) formed on the channel with NO releasing catheter. 73

Figure 4.1. Schematic of dual-lumen catheter-type electrochemical NO generating/releasing PO_2 sensor with cross section geometry of catheter. 84

Figure 4.2. Distribution of NO levels around a dual lumen catheter after 900 s in the presence of air from simulation via Comsol Multiphysics®: a) Concentration color map near catheter surface; b) concentration of NO outside the catheter along the lines dissecting the catheter at 0 °, 45 °, 90 ° and 135 °, as indicated in a). 87

Figure 4.3. Calibration curve of PO_2 sensing catheters on the benchtop with NO generation/release switched "on" and "off" as indicated. 88

Figure 4.4. Stability of the PO_2 sensing catheters over 3 d: a) calibration curve of three sensors on different days with continuous NO generation/release; b) summary of the change in sensitivity over 3 d period for each of the three sensors. 89

Figure 4.5. Typical reversible response of the electrochemical NO generation PO_2 sensing catheter under investigation. 90

Figure 4.6. NO release profile from an electrochemical NO generation/release PO_2 sensing catheter. NO release was switched "off" at ~ the 8^{th} h to demonstrate the control of the release. 91

Figure 4.7. Performance of electrochemical NO generating/releasing PO_2 sensors implanted in rabbit veins for 7 h: a) representative response for a NO releasing sensor (black) and a control sensor (red) compared with blood draw *in vitro* test values (blue square); the FiO_2 levels were changed purposely between 100% to 21% (dash dot) to vary venous PO_2; b) representative photo illustrating the degree of clot formation on the surface of the control and the NO releasing sensors after being explanted; c) average thrombus coverage on NO releasing sensors vs. control sensors ($n = 5$ rabbits, $p < 0.05$); d) average deviation of the NO releasing sensors (black) and control sensors (red) from the reference method (blue). Error bars indicate standard deviations. 94

Figure 4.8. Performance of electrochemical NO generating/releasing PO_2 sensors implanted in pig arteries for 21 h: a) representative current response for a NO releasing sensor (black) and a control sensor (red) compared with blood draw *in vitro* test values (reference method, blue square). Arrows indicate where FiO_2 changes from 21% to 100%; b) average deviation of the NO release sensors (black) and control sensors (red) from the reference method (blue). Error bars indicate standard deviations..... 95

Figure 4.9. Comparison of measured PO_2 from catheter-type sensors *in vivo* vs. reference method from blood samples. Data contain all the measurements > 4 h time point in rabbit experiments and > 6 h time point in pig experiments. Black squares represent results from the NO generating/releasing sensors. The red triangles represent the measurements from the control sensors. Dash lines and solid line indicate ±20% error and 0% error, respectively. 97

Figure 5.1. Schematic of the electrochemical NO releasing catheter employed in this study, with cutaway view showing the inside configuration of the catheter. 104

Figure 5.2. Modulation of surface NO fluxes from an electrochemical NO releasing catheter by different applied voltages applied to the metal wire electrodes. 108

Figure 5.3. Imaging 7 d *P. aeruginosa* biofilms with 3 h of NO release at surface flux of 1.5×10^{-10} mol min^{-1} cm^{-2}: A) Illustration of the experiment procedure and areas on the catheter that are under imaging; B) representative images of NO release catheter and its biofilm at 0 and 3 h; C) representative images of control catheter and its biofilm at 0 and 3 h. 109

Figure 5.4. Dosage response of 3 h NO release on 7 d *P. aeruginosa* biofilms. Viable bacteria counts A) on the surface of catheters and B) within the media after NO release for 3 h in the PBS. Asterisk denotes statistical significance at each flux compared with 0 flux (n.s.: $p > 0.05$, * $p < 0.05$, ** $p < 0.01$). 110

Figure 5.5. Effect of 3 h and 24 h NO release (1.5 flux unit) treatment towards *P. aeruginosa* biofilms (7 d) on the catheters and its planktonic counterparts in the PBS. Asterisk denotes statistical significance (n.s.: $p > 0.05$, * $p < 0.05$, ** $p < 0.01$, *** $p < 0.001$). 111

Figure 5.6. Combination of NO release with different concentrations of gentamicin against 7 d *P. aeruginosa* biofilms. A) Surface attached bacterial biofilm after 3 h treatment of gentamicin (gentamicin), and gentamicin with simultaneous NO release at 1.5 flux (gentamicin/NO); B) biofilm-detached/released bacteria vs. planktonic suspension control in the media with different treatments: 3 h exposure to different concentration of gentamicin (gentamicin); 3 h NO release at 1.5 flux in the presence of varied concentration of gentamicin (gentamicin/NO). 113

Figure 5.7. Effect of O_2 environment and diffusivity of NO on the NO concentration profile near the catheter surface via simulation. A) Illustration of the 1-D axial symmetry model. Point O represents axial symmetric line for the catheter; Point A is catheter surface where constant NO at 1.5 flux is released; Point B represents semi-infinite boundary condition where concentration of NO is 0. *R* is the radius of the catheter. B) NO concentration profile after NO release is "on" for 5 min: normal diffusivity (diffusivity in water) with ambient air (solid line); 60% diffusivity (slower diffusion in biofilms) with ambient air (short-dotted line) and 60% diffusivity in anoxic environment (deep inside biofilms, dashed line). 117

Figure 6.1. Schematic for NO permeation through polymer film/wall with thickness of *L*. 127

Figure 6.2. Schematic for the diffusion experiment performed in this study. The polymeric membrane is clamped between two parts of the diffusion cells. The left cell is filled with KI and H_2SO_4 to generate NO when nitrite is added. The right cell is connected directly to nitric oxide analyzer (NOA). 134

Figure 6.3. Geometry and meshing for (A) single lumen, (B) commercial dual lumen, and (C) proposed symmetric triple lumen catheter used in the finite element analysis. 136

Figure 6.4. Typical NO flux profile (J_{NO}, black) and amount of permeated NO (Q_{NO}, red) vs. time for 368 μm E5-325 polyurethane at 25 ℃ in a diffusion experiment. Red dotted line denotes the asymptote used for deriving the time lag. 138

Figure 6.5. Specific density (ρ) of polymers vs. log of diffusion coefficient for NO (D_{NO}). Correlation coefficient r = -0.75 for ρ vs. the log D_{NO}. 140

Figure 6.6. Cells of typical morphology (lamellae, spheres and cylinders) for block copolymers with phase separation. 141

Figure 6.7. Diffusion coefficient of NO (D_{NO}) vs. volume fraction of PDMS (X_A) in polymer based on different morphology for (A) Silicone-PU, and (B) Polycarbonate-Silicone-PU. 143

Figure 6.8. NO release profile for electrochemical NO releasing catheters made from silicone and PU SG80A determined by a nitric oxide analyzer. The catheters are 2.6 mm in o.d. and ~0.3 mm in wall thickness. 146

Figure 6.9. Effect of diffusion and partition on NO release profile from electrochemical NO releasing catheters as determined by simulation. 146

Figure 6.10. Local surface flux of NO on a Cook 7 Fr dual lumen PDMS catheter at room temperature in N_2 and in air. A) illustration of the polar angel for the dual lumen

catheter; B) polar graph showing the local surface flux at different time in 0% and C) in 21% O_2; D) Maximum surface flux ratio vs. time under 0 and 21% O_2. .. 149

Figure 6.11. Experiment probing the distribution of NO by around a dual lumen catheter. A) experimental setup of catheter immobilization using agar; B) cumulative NO in the left and right domain of the catheter as measured by the agar immobilization experiment (dot) and simulation (line). 150

Figure 6.12. Effect of diffusion coefficient (D) on distribution of NO on a catheter (same configuration of the Cook 7 Fr dual lumen catheter as shown in Figure 6.10) at 20 min. Partition coefficient K = 2.5. A) Polar graph of distribution of NO flux at catheter surface at 0% O_2; B) maximum flux ratio vs. time at 0% O_2; C) Polar graph of distribution of NO flux at catheter surface at 21% O_2; D) maximum flux ratio vs. time at 21% O_2. 151

Figure 6.13. Effect of partition coefficient (K) on distribution of NO for Cook 7 Fr dual lumen catheter at 20 min in 0% O_2 and 21% O_2. Diffusion coefficient $D = 2 \times 10^{-6}$ cm^2 s^{-1}. A) Polar graph of distribution of NO flux at catheter surface without O_2; B) maximum flux ratio vs time without O_2; C) Polar graph of distribution of NO flux at catheter surface with 21 %; D) maximum flux ratio vs time with 21% O_2. 153

Figure 6.14. Effect of diffusion coefficient (D) and partition coefficient (K) of NO in the polymer on the maximum ratio of local flux on an electrochemical NO releasing catheters with a more symmetric design as shown in Figure 6.3C. A) varied D with K = 2; B) varied K with $D = 2 \times 10^{-6}$ cm^2 s^{-1}. 154

Figure 7.1. Experimental setup for chemiluminescence detection of NO_2. The sample is passed through a UV photochemical reactor and NO_2 is converted to NO, which is subsequently detected by nitric oxide analyzer (NOA). 164

Figure 7.2. Schematic of bulk electrolysis cell for INO generation. WE: working electrode (Pt mesh); CE: counter electrode (Au mesh). The solution contains 7 mM $CuMe_3TACN$, 1.0 M $NaNO_2$ and 0.5 M HEPES buffer (pH 7.3). 164

Figure 7.3. Modulation of NO concentration in gas phase by applying different constant currents. The bubbling gas is N_2 at 1 L/min. The solution contains 7 mM $CuMe_3TACN$, 1.0 M $NaNO_2$ and 0.5 M HEPES buffer (pH 7.3). 165

Figure 7.4. Current vs. NO concentration in the gas phase at different flow rates and the corresponding faradaic efficiency. The solution contains 7 mM $CuMe_3TACN$, 1.0 M $NaNO_2$ and 0.5 M HEPES buffer (pH 7.3). 166

Figure 7.5. Effect of flow rate on NO concentration in the gas phase and current efficiencies at A) 1 mA and B) 6 mA. 167

Figure 7.6. Electrochemical NO generation for INO at 3L/min from the same 80 mL solution at 36 mA. 169

Figure 7.7. NO generation from the same solution at 0.5 mA for 4 h each day. The solution is stored at ambient conditions for up to 60 days. 169

Figure 7.8. NO generation in gas phase using air as bubbling gas. Flow rate of air is 0.2 L/min. 171

Figure 7.9. NO_2 produced from reaction of NO at different concentration with air in the gas phase vs. duration of the reaction based on rate equation $d[NO_2]/dt=2\ k\ [NO]^2[O_2]$, where $k = 6.0 \times 10^3\ M^{-2}\ s^{-1}$. 171

Figure 7.10. Silicone rubber bundle design for gas exchange in electrolysis solution for INO generation. 172

Figure 7.11. NO generation from using silicone rubber bundle in the electrolysis solution for gas exchange. The bundles contain 8 silicone tubing (i.d. 0.51 mm, o.d. 0.94 mm, length 16 cm). Flow rate of N_2 passing the bundles is 2 L/min. 173

Figure 8.1. Structures of new TACN derivatives and Cu(II) complexes that can be investigated in future work. A) $Cu(II)R_3TACN(X)_2$, R = -Et, -*i*Pr, $-CH_2CH_2OH$, or -*i*PrOH; B) asymmetric TACN derivatives: R' = H (alcohol group) or carbonyl (carboxylate group); C) BMPA-carboxylate derivatives; n = 1–3; D)

Cu(II)TAPMA(X)]. X = NO_2^-, H_2O/HO^-, CH_3COO^-, or Cl^-, depending on experimental conditions. 182

Figure 8.2. Various approaches to immobilize Cu(II)-ligand catalysts onto different electrode surfaces. A) Click chemistry to bind catalyst onto a graphitic surface; B) electro-grafting by coupling of an aryl radical to the graphitic surface via electrochemical oxidation of an aryl carboxylic acid; and C) attachment of catalyst to gold surface by a cystamine mediated self-assembly monolayer. 183

Figure 8.3. Attachment of Cu(II)-tridentate-ligand complexes to A) poly(vinylpyridine) and B) poly(vinylimidazole). 184

Figure 8.4. Concept of circulating/changing the inner filling nitrite solution for electrochemical NO release. 185

Figure A.1. Structures of ligands that form strong Cu(II) complexes that have been studied in this work for electrochemical reduction of nitrite. 190

Figure A.2. Cyclic voltamogram of 1 mM Cu(II)Me_3TACN in 0.1 M HEPES buffer (pH 7.3) in the presence of different concentrations of $NaNO_2$. 192

Figure A.3. NO release to gas phase from a 5 mL solution of 1 mM Cu(II)Me_3TACN, 50 mM $NaNO_2$, 0.1 M HEPES (pH 7.3), 0.1 M NaCl by different applied potential to a 2 mm diameter Pt working electrode. Solution was continuously purged with nitrogen at flow rate of 50 mL/min. 192

Figure A.4. NO release from a single lumen catheter (i.d. 1.47 mm; o.d. 1.96 mm, 6 cm) using 0.5 mM Cu(II)Me_3TACN, 0.5 M $NaNO_2$, 0.4 M HEPES and 0.16 M NaCl as inner solution. Pt wire (o.d. 0.127 mm) was exposed for 2 cm and Ag/AgCl wire was exposed for 4 cm and coiled. Applied potential was -0.3 V vs Ag/AgCl wire. 193

Figure A.5. Cyclic voltammogram of 2 mM CuMe_3TACN in 0.1 M HEPES buffer on a 25 μm Pt microelectrode at different scan rates. The peak on the anodic scan near -0.05 V correspond to the stripping of Cu^0 on the electrode surface. 194

Figure A.6. Simulated CV of 2 mM $CuMe_3TACN$ on a 25 μm Pt microelectrode at different scan rate. The reaction of disproportionation of Cu(I) was included.. 195

Figure A.7. Comparison of deposited Cu from experiment and simulation. The stripping peak at ~-0.05 V was used to calculate amount of deposited Cu^o. 195

LIST OF TABLES

Table 3.1. Boundary conditions used for simulating the NO diffusion from electrode surface through silicone rubber. 58

Table 3.2. Effect of nitrite concentration on the current efficiency and gaseous product ratio between NO and N_2O using CuTPMA mediated nitrite electrochemical reduction. 62

Table 3.3. Potential applied, NO flux, and NO current efficiency in the single lumen catheter. 66

Table 3.4. Result of 7 day Cu leaching experiment determined by ICP-OES. 74

Table 5.1. Effect of NO flux on dispersing and killing of mature 7 d *P. aeruginosa* biofilms. 111

Table 6.1. Chemical properties of silicone and polyurethanes used in this study. 133

Table 6.2. Parameters used in finite element analysis 137

Table 6.3. Summary of diffusion coefficients and partition coefficients of NO in various polymers obtained in this study. 139

Table A.1. Summary of electrochemical properties of catalyst in aqueous solution.[†] .. 191

LIST OF ABBREVIATIONS

BDO	1,4-butanediol
BMPA-Pr	3-[bis(2-pyridylmethyl)amino]propionate
BMPA-*S*Et	2-ethylthio-*N*,*N*-bis(pyridin-2-yl) methylethanamine
CABSI	Catheter-associated bloodstream infection
CAUTI	Catheter-associated urinary tract infection
CDC	Centers for Disease Control and Prevention
CoNS	Coagulase-negative staphylococci
CuTPMA	Copper(II) tris-2-pyryidalmethylamine
CV	Cyclic voltammogram
DL	Dual lumen
E.coli	*Escherichia coli*
E-chem	Electrochemical
eNOS	Endothelial nitric oxide synthase
FEA	Finite element analysis
FiO_2	Fraction of inspired oxygen
GC	Glassy carbon
HAI	Healthcare-associated infection
HEPES	4-(2-hydroxyethyl)-1-piperazineethanesulfonic
HIT	Heparin induced thrombocytopenia
HMDI	4,4′-methylene-bis(cyclohexyl isocyanate)

ICP-OES	Inductively coupled plasma optical emission spectroscopy
ICU	Intensive care unit
INO	Inhalation of nitric oxide
iNOS	Inducible nitric oxide synthase
IV	Intravascular
MDI	4,4′-methylene-bis(phenyl isocyanate)
Me_3TACN	1,4,7-trimethyl-1,4,7-triazacyclononane
Me_6TREN	Tris[2-(dimethylamino)ethyl]amine
MOPS	Morpholinopropane-1-sulfonic
nNOS	Neuronal nitric oxide synthase
NOA	Nitric oxide analyzer
nor	Nitric oxide reductase
NOS	Nitric oxide synthase
OxyHb	Oxyhemoglobin
P. aeruginosa	*Pseudomonas aeruginosa*
PBS	Phosphate buffer saline
***P*O_2**	Oxygen partial pressure
PDMS	Poly(dimethylsiloxane)
PHEC	Poly(1,6-hexyl 1,2-ethyl carbonate)
PHMG	Poly(hexamethylene oxide)
PTFE	Poly(tetrafluoroethylene)
PTMG	Poly(tetramethylene oxide)
PU	Polyurethane
PVC	Poly(vinyl chloride)
PVI	Poly(vinylimidazole)

PVPy	Poly(vinylpyridine)
RSNO	*S*-nitrosothiol
S. aureus	*Staphylococcus aureus*
SL	Single lumen
TACN	1,4,7-triazacyclononane
TPMA	Tri(2-pyridylmethyl)amine
TREN	Tris(2-aminoethyl)amine
VAP	Ventilator-associated pneumonia
vWbp	von Willebrand factor binding protein
vWF	von Willebrand factor

ABSTRACT

ELECTROCHEMICALLY MODULATED GENERATION/DELIVERY OF NITRIC OXIDE (NO) FROM NITRITE FOR BIOMEDICAL APPLICATIONS

by

Hang Ren

Chair: Mark E. Meyerhoff

In this dissertation research, the development of a new electrochemically modulated NO generation/delivery approach was examined. Further, the potential application of this approach in devising advanced thromboresistant/bactericidal intravascular catheters and a new NO inhalation therapy system was explored.

Nitric oxide can be generated from nitrite via two electrochemical approaches: 1) using a Cu^0 wire and an applied anodic/cathodic potential pulse sequence to electrochemically reduce nitrite to NO (Chapter 2); and 2) using Pt/Au or other working electrodes and a soluble Cu(II)-ligand complex as mediator to reduce nitrite to NO (Chapter 3). The temporal pattern of NO generation can be precisely modulated in the latter system by the applied potential or current. This electrochemical NO release system was first incorporated within intravascular catheters, which exhibited much reduced clotting (~85 %)

in vivo and significantly less (>99.9%) microbial biofilm *in vitro* compared to non-NO release control devices. Further, this NO release concept was combined with an amperometric oxygen sensor (PO_2 sensor) within a dual-lumen catheter configuration (Chapter 4) for intravascular continuous monitoring of PO_2 levels. Electrochemical NO release was fully compatible with PO_2 sensing and yielded more accurate PO_2 measurements (vs. controls) when implanted in arteries of pigs for 20 h. In Chapter 5, the electrochemical NO release catheters were used for controlled delivery of NO to elucidate the dosage effect of NO on mature *P. aeruginosa* biofilm. Fluxes of NO $>0.5 \times 10^{-10}$ mol min^{-1} cm^{-2} showed 99% killing of the biofilm in 3 h, and such an effect was in synergy with added gentamicin. In Chapter 6, the new electrochemical NO delivery method was employed for developing a gas phase NO inhalation (INO) system. Relatively pure gas phase NO in the range of 1–150 ppmv can be created by this system. Finally, the partitioning and diffusion properties of NO within several biomedical polymers was examined (Chapter 7), with silicone rubber exhibiting the optimal transport of NO.

Overall, electrochemical delivery of NO provides both a tool for fundamental biological studies, as well as a means to improve the biocompatibility of medical devices.

CHAPTER 1.

INTRODUCTION

1.1 Challenges for Implantable Medical Devices

1.1.1 Risk of Infection

Implanted medical devices are frequently used in hospitals for therapeutic and diagnostic purposes. There is a wide variety of such devices ranging from central venous catheters for infusion and blood draw, to implanted artificial heart valves for valvular heart disease, and to urinary catheters to facilitate urine drainage. These devices are designed to facilitate diagnosis and treatment and to improve the quality of health care. However, the use of many of these medical devices, especially the invasive ones, are often associated with increased risk of infection. Indeed, three device-associated infections – catheter-associated bloodstream infection (CABSI), catheter-associated urinary tract infection (CAUTI) and ventilator-associated pneumonia (VAP), have been listed among the four major healthcare-associated infections (HAI) by Centers for Disease Control and Prevention (CDC). [1] An estimated 250,000 CABSIs occur each year in the US alone, leading to prolonged hospital stays, substantially increased medical costs ($2.3 billion per year), and as many as 28,000 deaths.[1,2] On the other hand, CAUTIs contribute to 0.5-0.7 million nosocomial infections,[3] with a cumulative incidence of 3-6% per day of

catheterizations (50% at 10 days, >90% at 28 days, 100% long term)[4] leading to complications, and approximately ten thousand deaths annually.[5]

These infections are caused by invasion of pathogenic microbes. For example, coagulase-negative *staphylococci* (CoNS), *Staphylococcus aureus*, *enterococci*, and *Candida* species account for ~70% of CABSIs,[6,7] while *Escherichia coli*, *Candida* species, *Enterococcus* species and *Pseudomonas aeruginosa* account for >60% of CAUTIs.[8] One challenge for treating such infections is the formation of biofilms by these pathogenic microbes. Biofilms are groups of sessile cells embedded in a self-produced extracellular polymeric substance (EPS) matrix that are attached to a surface (e.g., catheter surface, etc.). Formation of biofilms starts with the attachment of planktonic cells to surfaces, followed by development via cell growth/colonization, maturation by formation of EPS, and finally dispersal to start of a new cycle (Figure 1.1). Once formed, biofilms are usually associated with significantly increased antibiotic-resistance and are therefore notoriously hard to cure. Unfortunately, 80% of all nosocomial bacterial infections are associated with the formation of biofilms.[9] In the case of a catheter, the biofilms formed are so resistant that they are virtually impossible to eradicate unless the whole device is physically removed.[10]

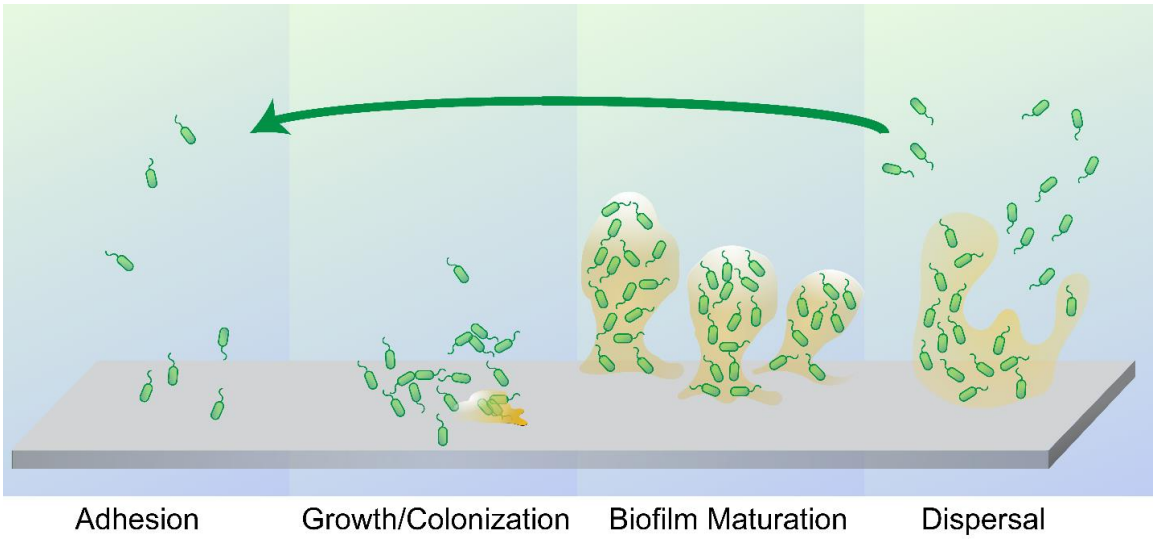

Figure 1.1. Development of bacterial biofilms on surfaces.

1.1.2 Risk of Clotting

Another challenge with medical devices that are in contact with flowing blood is thrombosis, or clotting. Once a device is in contact with blood, a foreign surface induced coagulation cascade can be triggered. The cascade starts with adsorption of proteins in the blood in seconds, including von Willebrand factor (vWF), fibrinogen, fibronectin, and vitronectin. This is followed by platelet adhesion and activation, and amplification reactions with the formation of thrombin and fibrin, and finally the formation of a mature clot within hours (see Figure 1.2).[11]

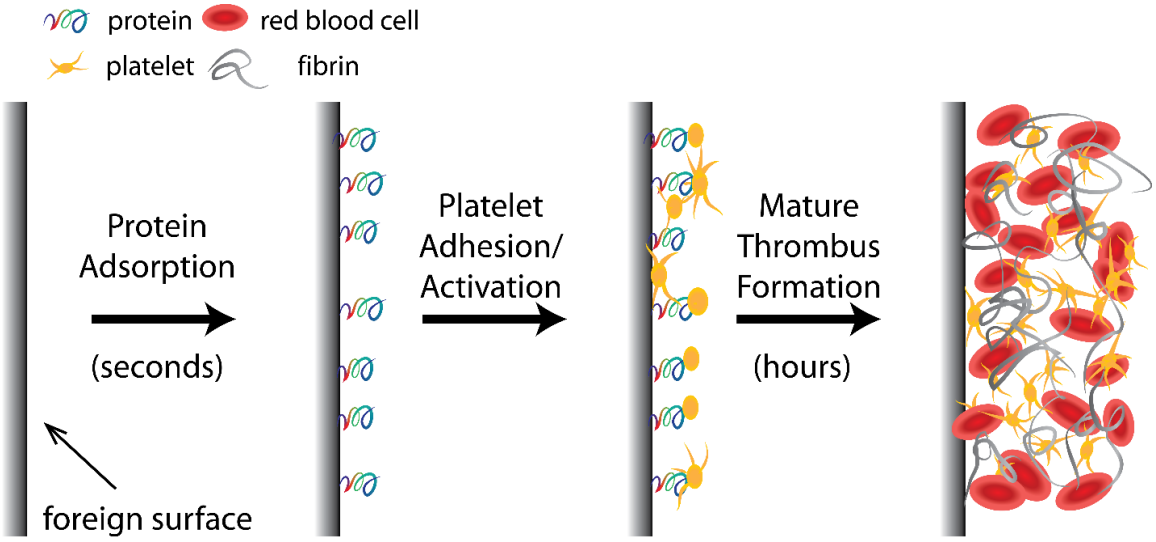

Figure 1.2. Sequence of events that lead to the formation of thrombus induced by a foreign surface.

Such foreign surface induced clotting has a severe impact on the functions of many medical devices, including bloodstream catheters, dialysis catheters, oxygenators, artificial heart valves, and implantable sensors. For example, the formation of a clot on the tip of a bloodstream catheter often impedes/prevents blood draw or infusion of drugs/nutrients. Consequently, the dysfunctional catheter has to be surgically removed and replaced. Another such example involves intravascular chemical sensors that could potentially measure blood gases, pH, electrolytes, glucose, lactate and other chemicals continuously in the blood. The clots formed on the surface of the sensors can isolate the sensors from the analytes in the blood, yielding inaccurate/unreliable results. More importantly, foreign surface induced clotting/thrombosis can often pose severe medical complications to the patients, leading to clots that can potentially dislodge, which significantly increases the risk of stroke, heart attack, and other life-threatening complications.[12]

It should be noted that although usually treated separately as different challenges (from a therapeutic/drug standpoint), thrombosis and infection are actually closely linked.

Bacteria can induce clot formation both directly and indirectly. Pathogenic bacteria such as *S. aureus* can secrete crucial factors including coagulase and von Willebrand factor binding protein (vWbp), which promote clotting.[13] Recently, it has also been shown that bacteria, including *Bacillus cereus* and *Bacillus anthracis*, can cluster and directly initiate blood clot formation.[14] This suggests that when addressing the overall issue of thrombosis, infection induced clotting should also be taken into account. It is, therefore, desirable to develop new strategies that can contend with both the risks of infection and thrombosis simultaneously.

1.2 Current Strategies/Efforts

1.1.1 Anti-Infection Strategies

Currently, the prevention of device-associated infections focuses on different aspects from standardization of clinical practices (e.g., handling of the devices, sterilization, etc.) to improvement/intervention in the devices themselves. Clinical practice guidelines for preventing HAIs have been drafted by the CDC, instructing clinical practitioners to comply with hygiene recommendations and emphasizing the disinfection of the devices.[15] However, device-associated infections still occur frequently. Treatment of such infections relies heavily on prolonged exposure to high-dose antibiotics.[16] However, the dose of such antibiotics are sometimes inappropriate and can induce antibiotic resistance.[17] Moreover, traditional antibiotics are designed to eradicate planktonic bacteria, but, as stated earlier, many infections are associated with bacterial biofilms, which are not effectively targeted by traditional antibiotics.

To fight infections more effectively, many different strategies involving modification of medical devices themselves have been proposed. Most of these can be classified into two categories: passive surface modification and active chemical release. Passive surface modification refers to changing the physiochemical properties of the surfaces to prevent the attachment of bacteria to the surface, or to kill the bacteria near the surface. To this end, surfaces have been modified by attaching polyethylene glycol (PEG),[18] poly(ethylene oxide) brushes,[19] hydrophilic polyurethane,[20] side chains with negative charges,[21] poly-cations (especially quaternary ammonium salts),[22] and antimicrobial peptides.[23] Surfaces have also been patterned with arrays of submicron-/nano-structure,[24-26] and infused with a fluorinated oil liquid to lower the surface energy for initial attachment.[27] However, the effectiveness of these modifications varies widely between different bacterial species. Furthermore, a conditioning film (e.g., protein) often forms on the surface under physiological conditions and can change or mask the surface properties provided by these different surface modification strategies.

The second class of strategies – the active release strategies – are based on the release of antimicrobial agents from the surface of the devices to inhibit/kill the bacteria from initial adhesion, or to disturb the formation of biofilms.[28] Antimicrobial impregnated catheters have been developed and clinically used, but dosage is hard to control as susceptibility varies with different bacterial species.[29] Inappropriate dosage could promote antibiotic resistance, or even the formation of biofilms.[30] In clinical studies, reduction of CAUTIs via the use of antimicrobial-impregnated catheters was not regarded as clinically useful.[31] Silver-alloy particles have also been applied as coatings for urinary catheters.[32] However, these coatings have proved clinically ineffective in reducing the incidence of

CAUTIs.[31] Release of antibodies[33] and quorum sensing inhibitors[34,35] have also been proposed, either to prevent biofilm formation or to disperse existing biofilms.

Despite all these efforts, the problem of device-induced infections has yet to be solved. Neither has the toxicity of some strategies against human cells/tissues been addressed. The development of new, more powerful techniques to prevent/reduce biofilms while being benign to healthy human cells or tissues is therefore of utmost importance.

1.1.2 Anti-Clotting Strategies

To address the problem of clotting/thrombosis, heparin, a highly sulfated glycosaminoglycan polymer with a very high negative charge density, has been routinely used. For example, dilute heparin solution has been intermittently or continuously injected into vascular catheters as a lock solution. However, the usage of heparin poses the risk of systemic anticoagulation (especially with inadvertent overdose). Moreover, heparin induced thrombocytopenia (HIT)[36] and heparin sensitivity/resistance is also a concern.[37] More importantly, heparin, acts as an anticoagulant by inactivating thrombin and factor Xa through an antithrombin-dependent mechanism[38] and therefore it does not address the primary event in the foreign surface induced thrombosis process; that is platelet activation/adhesion and aggregation.

Strategies to modify device surfaces have also been attempted, including using ultra smooth silicone rubber[39] or polyurethane,[40] immobilizing poly(ethylene oxide),[41] pre-exposure to albumin[42] or other coating proteins,[43] and binding of heparin in an ionic [44] or covalent fashion.[45] Surface patterning/texturing,[46] as well as infusion with non-stick liquid has also been pursued.[47] Unfortunately, these approaches have not solved the clotting

problem completely. On the other hand, as stated in Section 1.1.2, clotting can also be induced by bacterial infection and the problem of infection and clotting should really be considered jointly.

1.3 Nitric Oxide to the Rescue

1.1.3 Background/Properties of Nitric Oxide

To combat infection and clotting for medical devices, the use of nitric oxide (NO), a natural molecule in the human body, has been proposed.[48-50] Nitric oxide is a diatomic gas radical molecule that is involved in many different physiological processes, including vasodilation,[51] anti-clotting,[52] antimicrobial,[53] neuron transmission,[54] and wound healing,[55] just to name a few. In the body, NO is produced by a two-step oxidation of L-arginine to citrulline and NO via the enzyme nitric oxide synthase (NOS) (Figure 1.3). Three types of NOS isozymes have been discovered, including iNOS (inducible NOS), eNOS (endothelial NOS) and nNOS (neuronal NOS), and their activities are associated immune response, vascular functions and neuron transmission, respectively.[56] The healthy endothelium cells secrete NO through eNOS at fluxes from (0.5–4.0) $\times 10^{-10}$ mol cm^{-2} min^{-1} (0.5–4.0 flux unit) and the NO emitted acts as a powerful anti-clotting and anti-thrombotic agent at the interface of the endothelial cells and flowing blood.[57] The mechanisms by which NO is able to temporarily inhibit or anesthetize platelets are both direct and indirect.[58] In the blood, NO has a short lifetime (< 1 s),[59] and the excess NO is scavenged immediately by oxyhemoglobin (OxyHb) in red blood cells to form non-toxic nitrate.[60] Consequently, those platelets in circulating blood exposed to the endothelium are inhibited temporarily,

while those distant from the surface remain functional. It is precisely this close proximity effect and short lifetime of NO (no systemic effects) that makes the use of NO release very attractive for biomedical applications, since the therapeutic process will mimic what occurs physiologically at the endothelium surface.

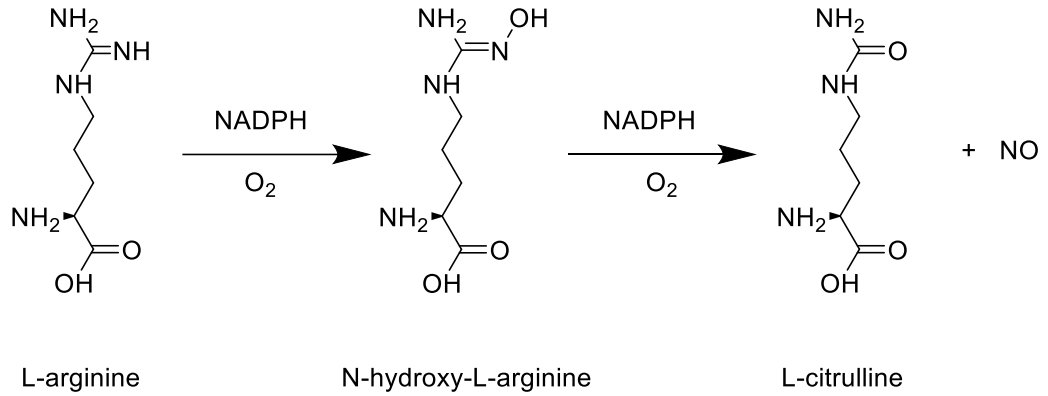

Figure 1.3. NO production from a two-step oxidation L-arginine via nitric oxide synthase (NOS).

Nitric oxide is also recognized as a potent endogenous antimicrobial and antifungal agent.[61] In fact, nasal epithelial cells are known to produce NO at high levels to prevent airway infection.[62] Nitric oxide and peroxynitrite ($ONOO^-$), formed by phagocytes undergoing simultaneous oxidative burst, have been shown to be bactericidal against numerous pathogens.[63] Furthermore, NO has also been shown to act as a signaling molecule for the dispersal of biofilms.[64] The combination of the killing and dispersal effects of NO towards bacteria and their biofilms suggests that NO can be an excellent candidate species to combat medical device induced infections.

1.1.4 Previous Research on NO Release from Polymeric Materials

Since NO is a gas molecule and has a relatively short lifetime in blood, appropriate delivery methods/mechanisms are necessary for its application, especially in medical devices. Specifically, NO needs to be delivered to the place where it is needed, e.g. at the surface of a given medical device, before it is consumed/scavenged by red cell hemoglobin. To this end, many different classes of NO donors have been developed, including organic nitrates, organic nitrites, metal-NO complexes, diazeniumdiolates, *S*-nitrosothiols, etc.[65,66] Among these, diazeniumdiolates and *S*-nitrosothiols have been extensively investigated in the development of NO releasing polymers, particularly because of their appropriate release mechanism.

Diazeniumdiolates are formed by the reaction of secondary amines with NO under high pressure. In the presence of protons, diazeniumdiolates can decompose and release NO according to Reaction 1.1. This is the major NO release mechanism for diazeniumdiolates, although thermal decomposition also occurs slowly at room temperature.[67] Different diazeniumdiolates have been synthesized and their half-lives range from seconds to days in phosphate buffered saline (PBS).[68,69] To better enhance their lifetime as well as to apply them into medical devices, diazeniumdiolates have been blended into,[49] as well as covalently attached to different biopolymers including polyurethanes[70] and silicone rubber.[71] When these diazeniumdiolates containing polymers are in contact with blood/water, the protons in the blood/water can trigger the NO release (Figure 1.4). Lipophilic diazeniumdiolates have also been prepared to slow the leaching of these donors from the polymers.[72]

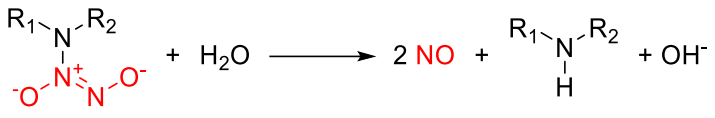

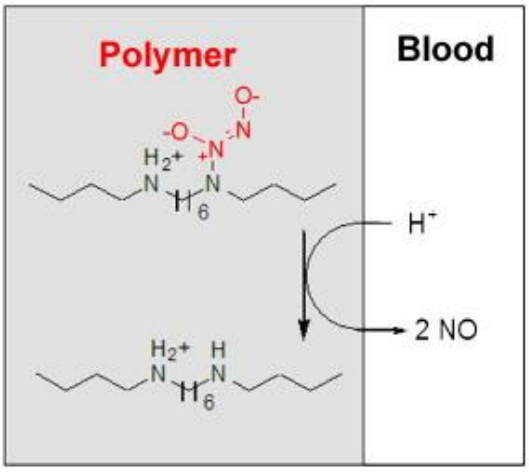

Figure 1.4. Schematics of NO release from a diazeniumdiolate blended polymer.

The second class of NO donors that have been investigated to prepare NO releasing biomedical polymers is *S*-nitrosothiols (RSNOs). *S*-nitrosothiols are naturally present in the human body and *S*-nitroso-human serum albumin and *S*-nitrosoglutathione are the two major forms in blood.[73] These endogenous RSNOs are thought to serve as reservoirs/carriers for NO, as NO itself has a limited diffusion range in blood.[74] The RSNOs can decompose and release NO via several different mechanisms, as shown in Reaction 1.2, including heat, light or catalytic species (e.g., copper(I/II), organo-selenium).[75] To develop NO releasing polymers, *S*-nitrosothiols have also been blended[76,77] or impregnated[78] into polymers, as well as covalently attached to the polymer backbones[79] and polymer fillers such as silica particle.[80] The release of NO can be triggered by the expedited decomposition of RSNOs at body temperature (37 ℃).

Temporal and spatial control of NO release by an external light source has also been demonstrated.[80]

$$2\ RSNO \xrightarrow{light/\ heat/\ Cu^{2+}} RS\text{-}SR + 2\ NO \quad \text{(Reaction 1.2)}$$

Although these NO donor incorporated polymers have been shown to exhibit much improved anti-clotting/antimicrobial properties, none have yet been used in clinical settings. Several issues have limited their commercialization. First, most diazeniumdiolates and RSNOs containing polymers are unstable at body temperature or in buffer—that is how NO release is usually triggered. Such instability actually resides in the basic chemistry of these NO donors—the diazeniumdiolate are moisture and heat sensitive, whereas the RSNOs are light and heat sensitive, which increases the costs for storage and shipping of such NO releasing polymers. Secondly, leaching of the donors and their degradation products hinder their potential clinical application, until it can be clearly shown that these products are non-toxic. The leaching process not only significantly reduces the duration of NO release, but also poses potential health risks to the hosts, especially for diazeniumdiolates, which can back-react with NO oxidation products to form carcinogenic nitrosamines.[48]

A strategy based on NO generation from endogenous RSNOs has also been attempted. Instead of incorporating NO donors, the polymers are simply coated with RSNO decomposition catalysts, such as lipophilic copper(II) complexes and organoselenium species.[81-84] Once in contact with blood, the endogenous RSNOs in the blood can decompose catalytically and release NO at the polymer surfaces. However, the endogenous RSNOs exist in limited amounts in the body, and the level of these can vary

greatly from one individual to another, which creates challenges for the application of this type of NO generation strategy.[85]

1.1.5 Electrochemically Modulated NO Release Method

Most of the above mentioned NO release strategies, except for the photo-initiated NO release from RSNOs, are passive and uncontrolled. Once triggered (sometimes even simply by storing in buffer), the NO release cannot be paused, and this might waste a significant amount of the NO donor capability before the device is ever implanted into a patient. In contrast, modulated release can save the NO donors by releasing NO only when needed, or boost the therapeutic effect by easily switching to higher flux of NO release. In addition, fast temporal control of precise NO fluxes enabled by such a modulated release strategy can greatly facilitate fundamental studies where the effect of a precise and steady release of NO needs to be defined.

To better control the release of NO, new strategies using electrochemical methods have been proposed, and electrochemical NO generation from diazeniumdiolates and RSNOs has been attempted.[86-88] For the diazeniumdiolate systems, protons generated locally at the surface of an electrode by electrochemical water oxidation can occur, which triggers the NO release from diazeniumdiolate in the solution.[89] Efforts have also been attempted to generate NO from direct electrochemical reduction of RSNOs.[86] However, both diazeniumdiolates and RSNOs are generally unstable in solution. Another drawback of these systems is that the product composition is usually complex, especially for reduction of RSNOs.[86]

In contrast to diazeniumdiolates and RSNOs, inorganic nitrates and nitrites are relatively stable in solution and cost-effective. To investigate the possibility of NO generation from inorganic nitrates and nitrites, thermodynamic data of nitrogen species are summarized in an oxidation state diagram (Frost diagram) in Figure 1.5.[90] The *y*-axis of the Frost diagram (n*E*) is the standard redox potential of the reaction from nitrogen species to N_2, times the number of electrons transferred, which is proportional to the Gibbs free energy. It can be seen that reduction of both nitrate and nitrite to NO is thermodynamically downhill, although N_2 and ammonia are the most stable forms under standard conditions. However, this diagram is based on thermodynamics and therefore shows no kinetic information. Indeed, the reduction of nitrate and nitrite are generally kinetically controlled and usually requires an overpotential to occur on most inert electrodes (e.g., platinum[91]). Yet another challenge for NO generation from nitrite or nitrate is the selectivity. Indeed, it may be difficult to control the electrochemical reduction of nitrite or nitrate to yield only NO, as the product composition is usually complex with different reduced nitrogen species being formed (including N_2O).[91] Catalysts are therefore generally required to improve the turnover numbers as well as the selectivity for these reduction reactions. Although development of a selective and robust catalyst for NO generation can be challenging, in nature, bacteria can selectively and efficiently perform the nitrate reduction and nitrite reduction enzymatically in the denitrification pathway using nitrate reductase and nitrite reductase, respectively.[92]

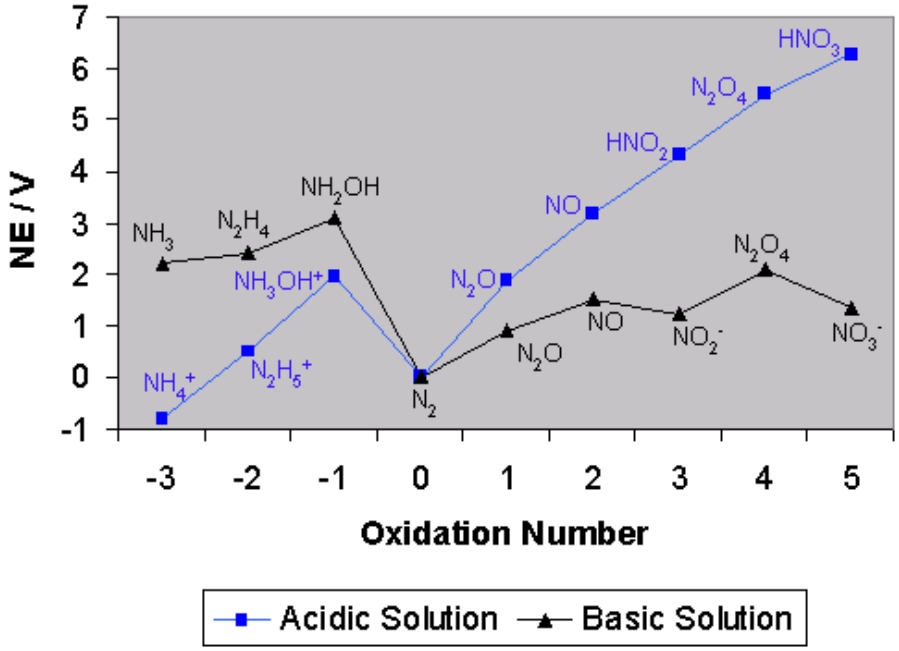

Figure 1.5. Frost diagram of nitrogen species in acidic (blue) and basic (black) solutions.

To generate NO from nitrate and nitrite in aqueous solution by electrochemical methods, a few systems have been suggested. One involves NO generation from the reaction between nitric acid with Cu^0 formed by electrochemical reduction of Cu(II).[93] Another example utilizes iron *meso*-tetrakis (4-*N*-methylpyridiniumyl) porphyrin ($[Fe^{III}(TMPyP)]^{5+}$) to generate NO from nitrite in a flow cell.[94] The first step involves the electrochemical reduction of $[Fe^{III}(TMPyP)]^{5+}$and nitrite to $[Fe^{II}(NO_2^-)_2(TMPyP)]^{2+}$ and $[Fe^{II}(NO)(TMPyP)]^{4+}$ sequentially. In the second step, the newly formed $[Fe^{II}(NO)(TMPyP)]^{4+}$ is further electrochemically oxidized back to $([Fe^{III}(TMPyP)]^{5+}$to complete the catalytic cycle (see the diagram of the mechanism in Figure 1.6).

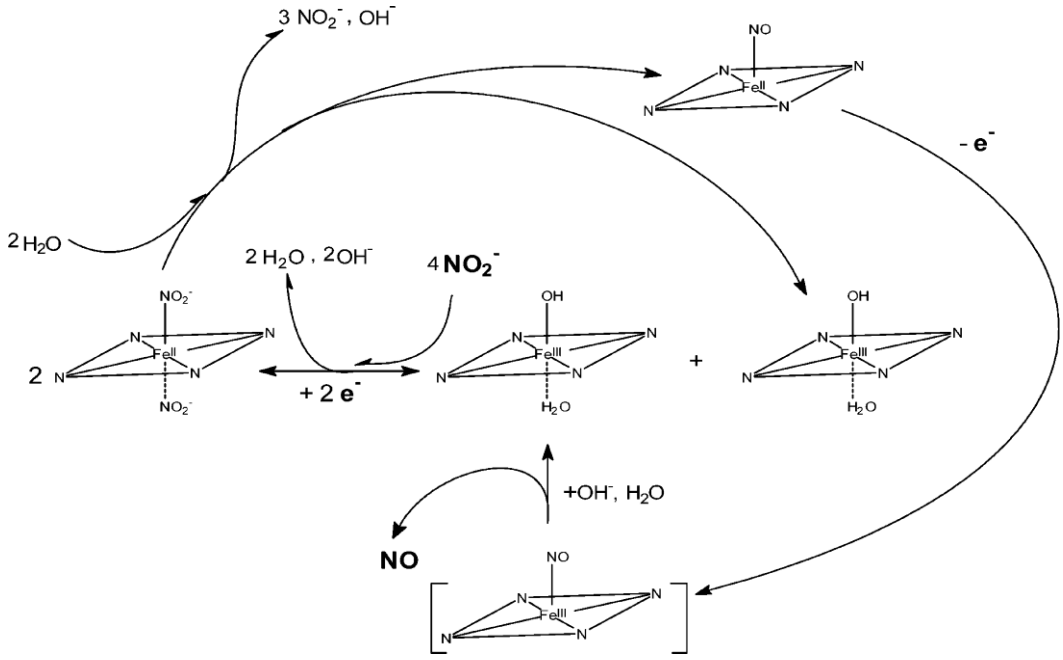

Figure 1.6. Mechanism of electrochemical generation of NO from nitrite and an iron porphyrin catalyst in aqueous solution. (Reprinted from Chi et. al. *Inorg. Chem.* **2004**, *43*, 8437.) [94]

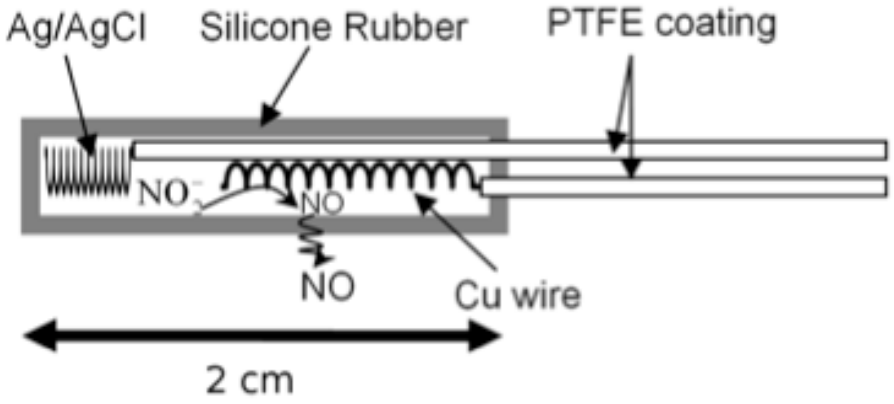

Figure 1.7. Schematic of the electrochemical NO generating catheter configuration. A copper wire serves as the working electrode and silver/silver chloride wire serves as the reference electrode. PTFE coating prevents the two wires from short-circuit. The inner filling solution contains $NaNO_2$, NaCl, EDTA, Na_2HPO_4, NaH_2PO_4, pH 6.8. [95]

In our lab, Hofler *et al.*[95] pioneered an electrochemical NO releasing method from inorganic nitrite and a Cu^0 electrode. A copper wire (working electrode), and silver/silver chloride wire (reference and counter electrode), were sealed inside a silicone tubing filled with concentrated nitrite solution (see Figure 1.7 for the schematic). Electrochemical potential pulses, with potentials periodically oscillating between anodic and cathodic, were used to generate NO. The anodic pulses generate Cu(I) species which reduce nitrite to NO. Cathodic pulses reduce/clean the passivating mixed copper oxide and hydroxide layer formed during the anodic pulses. By continually repeating the electrochemical pulse cycles, NO can be continuously generated, which then diffuses through the silicone rubber wall of the catheter. The NO flux can be turned "on" and "off" on demand (Figure 1.8). A catheter incorporating such electrochemical NO release reduced biofilm formation on the catheter surface, which demonstrated the potential of the electrochemical NO release method in antibiofilm application. However, the highest flux of NO released from these catheters is ~0.6 flux units, which is at the lower end of the physiological range; therefore, their antithrombogenic application *in vivo* has not yet been demonstrated. In addition, the pulse cycles in this system requires relatively more complex circuits.

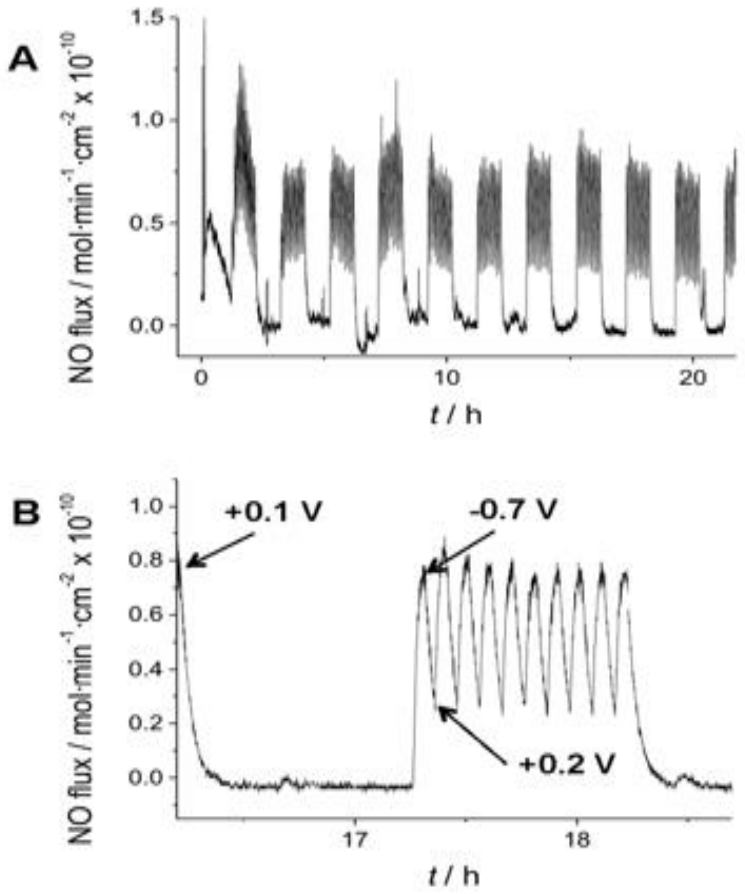

Figure 1.8. Electromodulated NO generation in silicone rubber catheter tube (see Fig. 1.7). (A) NO flux from surface of silicone rubber tubing over a 24 h period, with the applied -0.7 V (3 min)/+0.2 V (3 min) (vs. NHE); pulse sequence initiated for 1 h every 2 h. (B) Expanded view of 2 h segment when voltage cycle is "off" and then turned "on" (oscillating between -0.7 V and +0.2 V vs. NHE). (Reprint from Hofler et. al. *RSC Adv.* **2012**, *2*, 6765.)[95]

1.4 Statement of Research

The incomparable advantage of the electrochemical NO release method is the facile control of the NO release profile, which can not only extend the lifetime for NO release from medical devices when continuous NO release is not necessary (e.g., urinary catheters), but also provide a powerful tool for fundamental research on the dosage effect of NO. The

frequent presence of wire electrodes in medical devices such as pacemakers, and temperature sensing catheters suggests that incorporation of the electrochemical NO release system into medical devices is practical and feasible.

The purpose of this dissertation is to further improve and test the current copper wire-based electrochemical NO release system, and to develop a completely new electrochemical NO release systems using water-soluble Cu(II)-ligand catalysts that mimic the bacterial nitrite reductase. This dissertation also aims to apply these electrochemical NO release systems to various medical devices to reduce clotting and infection. It should be noted that this dissertation is prepared using a multiple manuscript/publication format, and hence the introduction sections in the chapters may be somewhat repetitive.

Chapter 2 will discuss the improvement of the Cu^0 wire electrode-based electrochemical NO release system first developed by Hofler *et. al.*,[95] and demonstrate its *in vivo* anticlotting ability/activity in a catheter model. This work was published in *Bioelectrochemistry* (H. Ren, A. Colletta, D. Koley, J. F. Wu, C. W. Xi, T. C. Major, R. H. Bartlett, M. E. Meyerhoff, *Bioelectrochemistry* **2015**, *104*, 10-16).

Chapter 3 focuses on utilizing a copper(II) tri-2-pyryidalmethylamine (CuTPMA) complex as a catalyst for electrochemical NO generation from inorganic nitrite. The study of the catalytic effect using cyclic voltammetry, the control of NO release profile by different applied voltages, and the application of this new catheter system in anti-biofilm and anti-clotting (*in vivo*) experiments will be presented. This work was published in *ACS Applied Materials and Interfaces* (H. Ren, J. Wu, C. Xi, N. Lehnert, T. Major, R. H. Bartlett, M. E. Meyerhoff, *ACS Applied Materials & Interfaces* **2014**, *6*, 3779-3783).

Chapter 4 will demonstrate the incorporation of the newly developed electrochemical NO release system (Chapter 3) into a catheter-type PO_2 sensors. Both

bench top validation and *in vivo* experiments in veins and arteries of rabbit and pig models are described. This work was published in *Analytical Chemistry* (H. Ren, M. A. Coughlin, T. C. Major, S. Aiello, A. Rojas Pena, R. H. Bartlett, M. E. Meyerhoff, *Analytical Chemistry* **2015**, *87*, 8067-8072.).

Chapter 5 will further utilize the advantage of facile control of the NO release profile enabled by the new electrochemical NO release system to study the dosage effect of NO on mature *Pseudomonas aeruginosa* biofilms. The synergy between NO release and antibiotic treatment in creating a powerful antibiofilm strategy will also be examined experimentally and the results discussed in detail. The work presented in this chapter has been submitted to *Journal of Antimicrobial Chemotherapy (2016).*

Chapter 6 will detail the experimental and simulation studies of NO transport properties through different biomedical grade polymers and discusses the compatibility of these polymers with the new electrochemical NO release system. Finite element analysis (FEA) is used to simulate the distribution of NO around catheters of different design. Such FEA can help better understand and design NO release catheters and other devices.

Chapter 7 will focus on the development of an NO inhalation (INO) device using the electrochemical NO release method. A constant voltage method and a constant current method will be compared and the gas phase product composition will be examined. This INO device can serve as a potential substitute for the expensive NO gas tanks for inhalation therapies in hospitals as well as portable INO device at home.

Chapter 8 will summarize the major conclusions from this dissertation and provide suggestions for future directions.

Finally, Appendix A will outline the preliminary studies of other Cu(II)-ligand complexes for electrochemical NO generations from nitrite. Catalyst efficiency, turnover number, as well as long-term stability will be discussed.

1.5 References

(1) Magill, S. S.; Edwards, J. R.; Bamberg, W.; Beldavs, Z. G.; Dumyati, G.; Kainer, M. A.; Lynfield, R.; Maloney, M.; McAllister-Hollod, L.; Nadle, J.; Ray, S. M.; Thompson, D. L.; Wilson, L. E.; Fridkin, S. K. *N. Engl. J. Med.* **2014**, *370*, 1198.

(2) Klevens, R. M.; Edwards, J. R.; Richards, C. L.; Horan, T. C.; Gaynes, R. P.; Pollock, D. A.; Cardo, D. M. *Public Health Rep.* **2007**, *122*, 160.

(3) Stringham, J.; Young, N. *Perspectives in Health Information Management / AHIMA, American Health Information Management Association* **2005**, *2*, 12.

(4) Smith, P. W.; Nicolle, L. E. *Infect. Control Hosp. Epidemiol.* **2001**, *22*, 316.

(5) Klevens, R. M.; Edwards, J. R.; Richards, C. L.; Horan, T. C.; Gaynes, R. P.; Pollock, D. A.; Cardo, D. M. *Public Health Rep.* **2007**, *122*, 160.

(6) Edmond, M. B.; Wallace, S. E.; McClish, D. K.; Pfaller, M. A.; Jones, R. N.; Wenzel, R. P. *Clin. Infect. Dis.* **1999**, *29*, 239.

(7) Wisplinghoff, H.; Bischoff, T.; Tallent, S. M.; Seifert, H.; Wenzel, R. P.; Edmond, M. B. *Clin. Infect. Dis.* **2004**, *39*, 309.

(8) Sievert, D. M.; Ricks, P.; Edwards, J. R.; Schneider, A.; Patel, J.; Srinivasan, A.; Kallen, A.; Limbago, B.; Fridkin, S.; National Healthcare Safety Network, T.; Participating, N. F. *Infect. Control Hosp. Epidemiol.* **2013**, *34*, 1.

(9) Römling, U.; Balsalobre, C. *J. Intern. Med.* **2012**, *272*, 541.

(10) Bjarnsholt, T. *APMIS* **2013**, *121*, 1.

(11) Hanson, S. R.; Tucker, E. I. In *Biomaterials Science (Third Edition)*; Lemons, B. D. R. S. H. J. S. E., Ed.; Academic Press: 2013, p 551.

(12) Burns, K. E. A.; McLaren, A. *Can. Respir. J.* **2009**, *16*, 163.

(13) McAdow, M.; Missiakas, D. M.; Schneewind, O. *J. Innate Immun.* **2012**, *4*, 141.

(14) Kastrup, C. J.; Boedicker, J. Q.; Pomerantsev, A. P.; Moayeri, M.; Bian, Y.; Pompano, R. R.; Kline, T. R.; Sylvestre, P.; Shen, F.; Leppla, S. H.; Tang, W.-J.; Ismagilov, R. F. *Nat. Chem. Biol.* **2008**, *4*, 742.

(15) Umscheid, C. A.; Agarwal, R. K.; Brennan, P. J. *Am. J. Infect. Control*, *38*, 264.

(16) Aslam, S. *Am. J. Infect. Control* **2008**, *36*, S175.e9.

(17) Roberts, J. A.; Kruger, P.; Paterson, D. L.; Lipman, J. *Crit. Care Med.* **2008**, *36*, 2433.

(18) Kingshott, P.; Wei, J.; Bagge-Ravn, D.; Gadegaard, N.; Gram, L. *Langmuir* **2003**, *19*, 6912.

(19) Kaper, H. J.; Busscher, H. J.; Norde, W. *J. Biomater. Sci. Polym. Ed.* **2003**, *14*, 313.

(20) Nagel, J. A.; Dickinson, R. B.; Cooper, S. L. *J. Biomater. Sci. Polym. Ed.* **1996**, *7*, 769.

(21) Jansen, B.; Kohnen, W. *J. Ind. Microbiol.* **1995**, *15*, 391.

(22) Tiller, J. C.; Liao, C.-J.; Lewis, K.; Klibanov, A. M. *Proceedings of the National Academy of Sciences* **2001**, *98*, 5981.

(23) Nguyen, L. T.; Haney, E. F.; Vogel, H. J. *Trends Biotechnol.*, *29*, 464.

(24) Truong, V. K.; Lapovok, R.; Estrin, Y. S.; Rundell, S.; Wang, J. Y.; Fluke, C. J.; Crawford, R. J.; Ivanova, E. P. *Biomaterials* **2010**, *31*, 3674.

(25) Pogodin, S.; Hasan, J.; Baulin, Vladimir A.; Webb, Hayden K.; Truong, Vi K.; Phong Nguyen, The H.; Boshkovikj, V.; Fluke, Christopher J.; Watson, Gregory S.; Watson, Jolanta A.; Crawford, Russell J.; Ivanova, Elena P. *Biophys. J.*, *104*, 835.

(26) Xu, L. C.; Siedlecki, C. A. *Acta Biomater.* **2012**, *8*, 72.

(27) Epstein, A. K.; Wong, T. S.; Belisle, R. A.; Boggs, E. M.; Aizenberg, J. *Proc. Natl. Acad. Sci. U. S. A.* **2012**, *109*, 13182.

(28) Hetrick, E. M.; Schoenfisch, M. H. *Chem. Soc. Rev.* **2006**, *35*, 780.

(29) Wassil, S. K.; Crill, C. M.; Phelps, S. J. *The Journal of Pediatric Pharmacology and Therapeutics : JPPT* **2007**, *12*, 77.

(30) Hoffman, L. R.; D'Argenio, D. A.; MacCoss, M. J.; Zhang, Z.; Jones, R. A.; Miller, S. I. *Nature* **2005**, *436*, 1171.

(31) Pickard, R.; Lam, T.; MacLennan, G.; Starr, K.; Kilonzo, M.; McPherson, G.; Gillies, K.; McDonald, A.; Walton, K.; Buckley, B.; Glazener, C.; Boachie, C.; Burr, J.; Norrie, J.; Vale, L.; Grant, A.; N'Dow, J. *The Lancet* **2012**, *380*, 1927.

(32) Furno, F.; Morley, K. S.; Wong, B.; Sharp, B. L.; Arnold, P. L.; Howdle, S. M.; Bayston, R.; Brown, P. D.; Winship, P. D.; Reid, H. J. *J. Antimicrob. Chemother.* **2004**, *54*, 1019.

(33) Rojas, I. A.; Slunt, J. B.; Grainger, D. W. *J. Control. Release* **2000**, *63*, 175.

(34) Weng, L.; Zhang, Y.; Yang, Y.; Wang, L. *Int. J. Mol. Sci.* **2014**, *15*, 6328.

(35) Feldman, M.; Shenderovich, J.; Al-Quntar, A. A.; Friedman, M.; Steinberg, D. *Antimicrob. Agents Chemother.* **2015**, *59*, 2265.

(36) Arepally, G. M.; Ortel, T. L. *N. Engl. J. Med.* **2006**, *355*, 809.

(37) Finley, A.; Greenberg, C. *Anesth. Analg.* **2013**, *116*, 1210.

(38) Hirsh, J.; Anand, S. S.; Halperin, J. L.; Fuster, V. *Arterioscler. Thromb. Vasc. Biol.* **2001**, *21*, 1094.

(39) Kolobow, T.; Stool, E. W.; Weathersby, P. K.; Pierce, J.; Hayano, F.; Suaudeau, J. *Trans. Am. Soc. Artif. Intern. Organs* **1974**, *20A*, 269.

(40) Szycher, M. *J. Biomater. Appl.* **1988**, *3*, 297.

(41) Tan, J.; McClung, W. G.; Brash, J. L. *J. Biomed. Mater. Res. A* **2008**, *85*, 873.

(42) Edmunds, L. H., Jr. *ASAIO J.* **1995**, *41*, 824.

(43) Didisheim, P. *ASAIO J.* **1994**, *40*, 230.

(44) Kim, S. W.; Jacobs, H. *Blood Purif.* **1996**, *14*, 357.

(45) Larm, O.; Larsson, R.; Olsson, P. *Biomater. Med. Devices Artif. Organs* **1983**, *11*, 161.

(46) Fujisawa, N.; Poole-Warren, L. A.; Woodard, J. C.; Bertram, C. D.; Schindhelm, K. *Biomaterials* **1999**, *20*, 955.

(47) Leslie, D. C.; Waterhouse, A.; Berthet, J. B.; Valentin, T. M.; Watters, A. L.; Jain, A.; Kim, P.; Hatton, B. D.; Nedder, A.; Donovan, K.; Super, E. H.; Howell, C.; Johnson, C. P.; Vu, T. L.; Bolgen, D. E.; Rifai, S.; Hansen, A. R.; Aizenberg, M.; Super, M.; Aizenberg, J.; Ingber, D. E. *Nat. Biotech.* **2014**, *32*, 1134.

(48) Mowery, K. A.; Schoenfisch, M. H.; Saavedra, J. E.; Keefer, L. K.; Meyerhoff, M. E. *Biomaterials* **2000**, *21*, 9.

(49) Smith, D. J.; Chakravarthy, D.; Pulfer, S.; Simmons, M. L.; Hrabie, J. A.; Citro, M. L.; Saavedra, J. E.; Davies, K. M.; Hutsell, T. C.; Mooradian, D. L.; Hanson, S. R.; Keefer, L. K. *J. Med. Chem.* **1996**, *39*, 1148.

(50) Nablo, B. J.; Chen, T.-Y.; Schoenfisch, M. H. *J. Am. Chem. Soc.* **2001**, *123*, 9712.

(51) Palmer, R. M.; Ferrige, A.; Moncada, S. *Nature* **1987**, 327, 524..

(52) Radomski, M.; Palmer, R.; Moncada, S. *The Lancet* **1987**, *330*, 1057.

(53) Fang, F. C. *J. Clin. Invest.* **1997**, *99*, 2818.

(54) Bult, H.; Boeckxstaens, G.; Pelckmans, P.; Jordaens, F.; Van Maercke, Y.; Herman, A. *Nature* **1990**, *345*, 346.

(55) Broughton 2nd, G.; Janis, J. E.; Attinger, C. E. *Plast. Reconstr. Surg.* **2006**, *117*, 12S.

(56) Nathan, C.; Xie, Q.-w. *Cell* **1994**, *78*, 915.

(57) Vaughn, M. W.; Kuo, L.; Liao, J. C. *Am. J. Physiol. Heart Circ. Physiol.* **1998**, *274*, H2163.

(58) Radomski, M. W.; Palmer, R. M.; Moncada, S. *Biochem. Biophys. Res. Commun.* **1987**, *148*, 1482.

(59) Lancaster, J. R., Jr. *Proc. Natl. Acad. Sci. U. S. A.* **1994**, *91*, 8137.

(60) Gardner, P. R.; Gardner, A. M.; Martin, L. A.; Salzman, A. L. *Proc Natl Acad Sci U S A* **1998**, *95*, 10378.

(61) Jones, M.; Ganopolsky, J.; Labbé, A.; Wahl, C.; Prakash, S. *Appl. Microbiol. Biotechnol.* **2010**, *88*, 401.

(62) Rouby, J. *Am. J. Respir. Crit. Care Med.* **2003**, *168*, 265.

(63) Xia, Y.; Zweier, J. L. *Proc. Natl. Acad. Sci. U. S. A.* **1997**, *94*, 6954.

(64) Barraud, N.; Hassett, D. J.; Hwang, S. H.; Rice, S. A.; Kjelleberg, S.; Webb, J. S. *J. Bacteriol.* **2006**, *188*, 7344.

(65) Wang, P. G.; Xian, M.; Tang, X.; Wu, X.; Wen, Z.; Cai, T.; Janczuk, A. J. *Chem. Rev.* **2002**, *102*, 1091.

(66) Bill Cai, T.; Wang, P. G.; Holder, A. A. In *Nitric Oxide Donors*; Wiley-VCH Verlag GmbH & Co. KGaA: 2005, p 1.

(67) Shaikh, N.; Valiev, M.; Lymar, S. V. *J. Inorg. Biochem.* **2014**, *141*, 28.

(68) Hrabie, J. A.; Keefer, L. K. *Chem. Rev.* **2002**, *102*, 1135.

(69) Keefer, L. K. *ACS Chem. Biol.* **2011**, *6*, 1147.

(70) Saavedra, J. E.; Southan, G. J.; Davies, K. M.; Lundell, A.; Markou, C.; Hanson, S. R.; Adrie, C.; Hurford, W. E.; Zapol, W. M.; Keefer, L. K. *J. Med. Chem.* **1996**, *39*, 4361.

(71) Zhang, H.; Annich, G. M.; Miskulin, J.; Osterholzer, K.; Merz, S. I.; Bartlett, R. H.; Meyerhoff, M. E. *Biomaterials* **2002**, *23*, 1485.

(72) Batchelor, M. M.; Reoma, S. L.; Fleser, P. S.; Nuthakki, V. K.; Callahan, R. E.; Shanley, C. J.; Politis, J. K.; Elmore, J.; Merz, S. I.; Meyerhoff, M. E. *J. Med. Chem.* **2003**, *46*, 5153.

(73) Tyurin, V. A.; Tyurina, Y. Y.; Liu, S. X.; Bayir, H.; Hubel, C. A.; Kagan, V. E. *Methods Enzymol.* **2002**, *352*, 347.

(74) Jourd'heuil, D.; Hallen, K.; Feelisch, M.; Grisham, M. B. *Free Radic. Biol. Med.* **2000**, *28*, 409.

(75) Al-Sa'doni, H. H.; Ferro, A. *Curr. Med. Chem.* **2004**, *11*, 2679.

(76) Shishido, S. M.; Seabra, A. B.; Loh, W.; De Oliveira, M. G. *Biomaterials* **2003**, *24*, 3543.

(77) Brisbois, E. J.; Handa, H.; Major, T. C.; Bartlett, R. H.; Meyerhoff, M. E. *Biomaterials* **2013**, *34*, 6957.

(78) Colletta, A.; Wu, J.; Wo, Y.; Kappler, M.; Chen, H.; Xi, C.; Meyerhoff, M. E. *ACS Biomater. Sci. Eng.* **2015**, *1*, 416.

(79) Bohl, K. S.; West, J. L. *Biomaterials* **2000**, *21*, 2273.

(80) Frost, M. C.; Meyerhoff, M. E. *J. Am. Chem. Soc.* **2004**, *126*, 1348.

(81) Oh, B. K.; Meyerhoff, M. E. *J. Am. Chem. Soc.* **2003**, *125*, 9552.

(82) Hwang, S.; Cha, W.; Meyerhoff, M. E. *Angew. Chem. Int. Ed. Engl.* **2006**, *45*, 2745.

(83) Cha, W.; Meyerhoff, M. E. *Biomaterials* **2007**, *28*, 19.

(84) Yang, J.; Welby, J. L.; Meyerhoff, M. E. *Langmuir* **2008**, *24*, 10265.

(85) Wu, Y.; Meyerhoff, M. E. *Talanta* **2008**, *75*, 642.

(86) Peng, B.; Meyerhoff, M. E. *Electroanalysis* **2013**, *25*, 914.

(87) Peng, B. *Studies of Miniature Tear Glucose Sensors and Electromodulated Nitric Oxide Delivery Devices*, 2013.

(88) Suchyta, D., University of Michigan-Ann Arbor, 2012.

(89) Davies, K. M.; Wink, D. A.; Saavedra, J. E.; Keefer, L. K. *J. Am. Chem. Soc.* **2001**, *123*, 5473.

(90) Bard, A. J.; Parsons, R.; Jordan, J.; International Union of, P.; Applied, C. *Standard potentials in aqueous solution*; M. Dekker: New York, 1985.

(91) Rosca, V.; Duca, M.; de Groot, M. T.; Koper, M. T. M. *Chem. Rev.* **2009**, *109*, 2209.

(92) Carlson, C. A.; Ingraham, J. L. *Appl. Environ. Microbiol.* **1983**, *45*, 1247.

(93) Shirazi, S. Z.; Zhelyaskov, V. Method and Apparatus for the Generation of Nitric Oxide. U.S. Patent 5827420, Oct 27, 1998.

(94) Chi, Y.; Chen, J.; Aoki, K. *Inorg. Chem.* **2004**, *43*, 8437.

(95) Hofler, L.; Koley, D.; Wu, J.; Xi, C.; Meyerhoff, M. E. *RSC Adv.* **2012**, *2*, 6765.

CHAPTER 2.

OPTIMIZATION OF CU^0 WIRE-BASED ELECTROCHEMICALLY MODULATED NO RELEASE FROM INORGANIC NITRITE

2.1 Introduction

As described in Chapter 1, catheters play an indispensable role in facilitating infusion, drug administration and drainage for hospitalized patients every day. However, these biomedical devices also provide a potential source of entry for microbes into the human body that can lead to severe infection, the most common being catheter-associated bloodstream infections (CABSIs) and catheter-associated urinary tract infections (CAUTIs).[1] It has been estimated that 250,000 cases of CABSIs[2] and 500,000 incidences of CAUTIs[3] occur in hospitals annually in the U.S., thus contributing considerably to increasing healthcare costs.[4] Some 80% of CABSIs and CAUTIs are associated with biofilm formation, thus representing a significant challenge to many clinical treatments, especially conventional antibiotic therapies.[5] Indeed, since the extracellular polymeric matrices of biofilms protect bacterial cells, most antibiotic treatments are ineffective.[6] Several strategies, such as modified surfaces,[7] silver particle doped materials[8,9] and anti-quorum sensing drugs[10,11] have been suggested over the last decades to either prevent or exterminate biofilms. Yet, the problem of biofilm formation and concomitant catheter

induced infections persists, suggesting that other novel and more effective strategies are needed.

In the case of intravascular catheters, another significant health risk factor is the activation of the clotting cascade and formation of surface thrombus, which can occlude a lumen of the catheter, potentially leading to complete dysfunction of the device and establishing risk for life-threatening complications via thrombus dislodgment.[12,13] This problem is currently managed by injecting intermittent heparin "lock" solutions into the catheters. Unfortunately, this approach increases the risk of systemic anticoagulation (mostly due to inadvertent overdoses) and heparin allergic response (e.g., heparin induced thrombocytopenia).

Nitric oxide (NO) releasing catheters provide a promising solution to both the biofilm-induced infection and thrombosis issues that plague current biomedical catheters. Endothelial cells produce NO to attenuate platelet activation, adhesion, and aggregation. Hence, the use of NO release agents can be useful in developing therapeutic strategies that aim to avert arterial thrombotic disorders.[14] This free radical gas molecule is also a principle component of the innate immune system and functions as a potent antimicrobial agent. Indeed, macrophages release high levels of NO as cytotoxic agent to efficiently neutralize bacteria, viruses and helminths.[15] Recent studies have also demonstrated that NO, in small doses, can act as a signaling molecule to disperse biofilms.[16] Thus, with the goal of preventing implant-associated infections, several approaches have been developed to deliver NO by either doping or modifying polymeric materials with *S*-nitrosothiols (RSNO) or diazeniumdiolate-based NO donors. These NO releasing materials have been shown to exhibit effective antibacterial properties.[17-19] Nevertheless, the innate drawback

of these NO donor-based approaches is their instability, with RSNOs being sensitive to light and heat[20] and diazeniumdiolates being very susceptible to decomposition by moisture and potentially yielding toxic nitrosamines.[21,22] These issues have impeded their commercialization within medical devices.

Instead of *S*-nitrosothiols and diazeniumdiolates, inorganic nitrite is a much more attractive NO source because of its low cost and high stability. Recently, we reported the first electrochemical NO release approaches from a reservoir of inorganic nitrite by generating copper(I) species, from either a copper wire electrode or a water soluble copper complex.[23,24] In the copper wire electrode-based system, the electrode material is cost-effective but it suffered from low NO flux and large fluctuations in the NO release profile. The soluble copper complex system releases a more steady and tunable NO flux, but platinum or gold wires were used as electrode materials, which are too expensive for widespread commercial use. Herein, we describe an electrochemical pulse sequence applied to a Cu^o wire working electrode within a single lumen catheter model that achieves a more stable, higher flux and longer-term NO generation. The NO can be easily released on demand by turning "on" electrochemical pulse sequence, and the flux of NO can be modulated by applying different voltage pulses to the copper working electrode, which cannot be achieved by traditional chemical release. By employing this method to fabricate catheters, the NO flux from the catheter surface is increased by 100% compared with the earlier electrochemical system, and this enables successful *in vivo* demonstration of the thromboresistance of catheters prepared with the Cu^0 wire electrode-based catheter system. Further, we clearly show that by using different electrochemically modulated NO release profiles (compared to that reported in[23]), the model catheters are able to prevent biofilm

formation by CABSIs-inducing bacterial species. It is also demonstrated, for the first time, that only 3 h of electrochemically generated NO from the catheter surfaces can significantly disperse 2 d and 4 d old pre-formed biofilms by an *E. coli* bacterial strain that is well known to be associated with CAUTIs.

2.2 Experimental Details

2.2.1 Materials

Sodium nitrite, sodium chloride, ethylenediaminetetraacetic acid (EDTA) disodium salt, sodium phosphate dibasic heptahydrate, and sodium phosphate monobasic monohydrate were purchased from Sigma-Aldrich (St. Louis, MO) and used as received. Luria Bertani (LB) broth and LB agar were obtained from Fisher Scientific Inc. (Pittsburgh, PA). All aqueous solutions were prepared with deionized water from a Milli-Q system (18 MΩ cm^{-1}; Millipore Corp., Billerica, MA).

Polytetrafluoroethylene (PTFE)-coated silver wire (bare wire 0.125 mm o.d.; PTFE coated wire 0.176 mm o.d.) was purchased from Sigmund Cohn Corp. (Mount Vernon, NY). PTFE-coated Cu^{o} wire (bare wire 0.127 mm o.d.; PTFE coated wire 0.152 mm o.d.) was a product of Phoenix Wire Inc. (South Hero, VT). Single-lumen standard silicone tubing (0.51 mm i.d.; 0.94 mm o.d.) was purchased from Helix Medical (Carpentaria, CA). Silicone rubber sealant was obtained from Dow Corning (Midland, MI).

E. coli K-12 MG16653 and *S. aureus* ATCC 45330 were from the American Type Culture Collection.

2.2.2 Catheters Fabrication

The model catheter configuration consisted of a single-lumen, silicone rubber tubing (length: 3 cm), that was sealed at one end with silicone rubber sealant. A PTFE coated silver/silver chloride wire was utilized as the reference electrode (with 0.235 cm^2 surface area exposed) and a PTFE-coated Cu^o wire (with ~0.012 cm^2 surface area exposed) served as the working electrode within the lumen. The reservoir solution within the tubing was 1.0 M $NaNO_2$, 0.30 M NaCl, 0.02 M EDTA, 1.0 M phosphate buffer (pH 7.05). The PTFE was removed from the ends of both Ag^o and Cu^o wires to expose a length of 60 mm and 3 mm, respectively. Both wires were coiled and inserted in the lumen in a manner that prevents direct metallic contact with each other. Finally, the other end of the silicone rubber tubing was sealed with silicone rubber sealant, and left to cure in water for approximately 12 h.

2.2.3 Electrochemical Generation of Nitric Oxide

The NO releasing profile from each catheter was measured via a chemiluminescence NO analyzer (NOA) (Sievers 280, Boulder CO). The catheter was placed inside a glass cell, containing DI water; the solution was constantly purged with a stream of N_2 gas, and the electrochemically generated NO emitted from the outer surface of the catheter tubing was carried to the NOA. The Cu^o and Ag^o wires coming out of the catheters were connected to a portable potentiostat (CH Instruments 1206B, Austin TX). To generate NO, a voltage pulse sequence was applied to the Cu^o wire working electrode. One cycle of the pulse sequence included a period of a cathodic pulse (-1.1, -1.2, -1.3 or -

1.4 V vs. Ag/AgCl wire), and another period involved an anodic pulse (+0.2 V vs. Ag/AgCl wire).

2.2.4 In Vivo Anti-Thrombotic Experiment in Rabbits

Briefly, one group of NO releasing catheters (low flux group, n=3) was tested using pulse sequence of 15 s at -1.25 V and 15 s at +0.20 V and the other group (high flux group, n=3) was tested using a pulse sequence of 15 s at -1.3 V and 15 s at +0.20 V. Two or three catheters were implanted into the jugular and/or femoral veins of each rabbit (~ 3 kg). One of the catheters was turned "on" by applying a pulse sequence described above and the other was turned "off" with open circuit. After 7 h, the catheters were explanted, a digital picture was taken, and the red pixels were counted using Image J software to represent the clot area. Animal handling and surgical procedures were approved by the University Committee on the Use and Care of Animals in accordance with university and federal regulations and a detailed protocol was reported elsewhere.[24]

2.2.5 Biofilm Growth Conditions and Plate Counting

***S. aureus* biofilms.** *Staphylococcus aureus* ATCC 25923 was used for the test. Catheters were mounted aseptically in the middle of a drip flow bioreactor (DFR 1110-4, BioSurface Technologies, Bozeman, MO) chambers. Each reactor chamber including the catheter was initially innoculated with 10 mL of a 100 fold-diluted bacterial culture that had been grown overnight with shaking at 37℃. After one hour incubation, fresh 10% strength of LB broth was dripped into the flow chamber at a flow rate of 100 mL/h. Biofilms were grown for 48 h at 37℃, by utilizing the drip flow biofilm reactor. The

channels of the reactor were constantly flushed with 10% LB broth for the entire time of the biofilm growth. Nitric oxide release was turned "on" during the 48 h experiment by applying cycles of 15 s at -1.3 V and 15 s at +0.2 V. At the end of the 48 h, each catheter was removed from the drip flow biofilm reactor and placed separately into a centrifuge tube containing 2 mL of 10 mM phosphate buffer saline, pH 7.4 (PBS). Each catheter was then homogenized in order to disintegrate the biofilm clumps and form a homogeneous cell suspension. Finally, each sample was 10-fold serially diluted and plated using the spread plating technique to assess cell viability.

***E. coli* biofilms**. *Escherichia coli* K-12 was used for this test. The bacterial strain was grown for either 48 or 96 h at 22℃ with catheters in the channel of the reactor but not turned "on" with the applied voltage pulse sequence. This specific temperature was chosen as it allowed *E. coli* biofilms to develop that had greater thickness and biomass. At the end of the 48 or 96 h, NO release was turned "on" for 3 h by applying cycles of 15 s at -1.3 V and 15 s at +0.2 V. The other growth conditions were the same as those used for *S. aureus* biofilms. Procedures to assess cell viability were also performed exactly as described above.

2.2.6 Biofilm Imaging

After either 2 or 4 d of biofilm growth, the NO releasing and control catheters (same assembly as NO release but electrodes in the catheters were not connected to potentiostat) to be used for fluorescence imaging were removed from the drip flow biofilm reactor and gently rinsed with 10 mM PBS. Unlike catheters utilized for plate-counting, these catheters were not homogenized; instead, they were stained with fluorescent dyes by using

Live/Dead BacLight Bacterial Viability kit (Invitrogen, Carlsbad, CA) for 20 min in the dark, exactly per the kit's instructions. Finally, each catheter was singly placed onto a cover-slip and its outer surface was visualized using an inverted fluorescent microscope (Olympus 1X71, Center Valley, PA), equipped with the appropriate filter sets.

2.3 Results and Discussion

2.3.1 Electrochemical Generation of Nitric Oxide

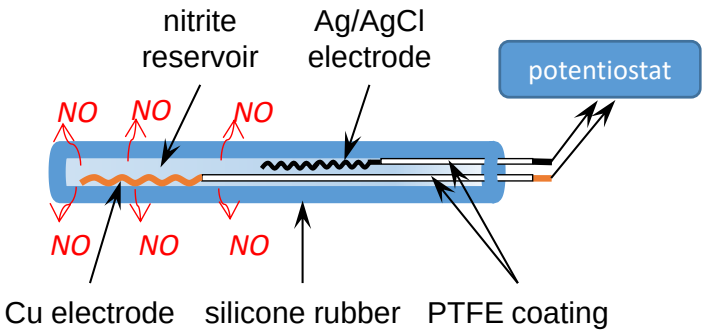

Figure 2.1. Schematic of a single-lumen electrochemically modulated NO releasing catheter.

The model catheter configuration consists of a single-lumen silicone rubber tubing that contains a nitrite reservoir and Cu^0 and Ag/AgCl wire electrodes (Figure 2.1). A pulse sequence of applied voltages to the Cu^o wire electrode is used to generate NO continuously from the nitrite ion reservoir within the catheter. The anodic pulse provides a transient level of Cu(I) ions that are capable of reducing nitrite to NO in accordance with the following reaction:

$$Cu(I) + NO_2^- + 2\ H^+ \rightarrow Cu(II) + NO + H_2O$$

However, oxidation of the copper electrode surface forms oxides of copper that passivate the surface, requiring applied cathodic voltages to regenerate a clean Cu^o surface that can create more Cu(I) ions upon re-oxidation.[23] Therefore, the pulse sequence of applied voltages must include repeated cycles of a cathodic voltage pulse followed by an anodic pulse (Figure 2.2a). In earlier work,[23] a pulse sequence containing cycles of 3 min at -0.92 V and 3 min at 0 V(vs. Ag/AgCl) was used to generate an average NO flux of 0.5 $\times 10^{-10}$ mol min^{-1} cm^{-2}, which fluctuates periodically from (0.25–0.75) $\times 10^{-10}$ mol min^{-1} cm^{-2} (see Figure 2.2b). This NO flux is not sufficient to prevent clotting *in vivo* and the fluctuation complicates the interpreting the relationship between NO flux and *in vivo* results. In order to obtain higher and more stable NO fluxes, in this work the effect of different pulse sequences on the NO release profile were compared. By using the pulse sequence of +0.2 V and -1.3 V, the average measured NO flux is now consistently >1.0 $\times 10^{-10}$ mol min^{-1} cm^{-2} (in absence of significant levels of oxygen, see below). As shown in Figure 2.2c, it is evident that fluctuations of the NO release profile are much larger if the pulse cycle time is every 6 min as compared with every 30 s. Note that for pulse cycles of every 6 min for 2 h, 20 spikes can be identified from the NO release profile detected by the NOA. This is because NO is only generated on the electrode during the anodic pulse—which is half of the cycle.

In another experiment, it was found that by further increasing the cathodic voltages from -1.0 V to -1.4 V (vs. Ag/AgCl wire), increased NO fluxes from the surface of the catheter tubing could be obtained (Figure 2.3). This is likely due to the fact that the more negative voltage can better regenerate a clean Cu^o surface. It was found that when cathodic pulses above -1.35 V are used, the baseline NO level (when the sequence is turned “off”)

also increases, probably due to the fact that the surface regenerated above this voltage is too active. When cathodic pulses < -1.35 V are used, the NO baseline level is consistently low (<0.2 $\times 10^{-10}$ mol min^{-1} cm^{-2}) when turned "off". Therefore, for remainder of the study, a pulse sequence with 15 s at +0.2 V and 15 s at -1.3 V was employed and with this sequence the catheters can release NO continuously for > 60 h (Figure 2.4).

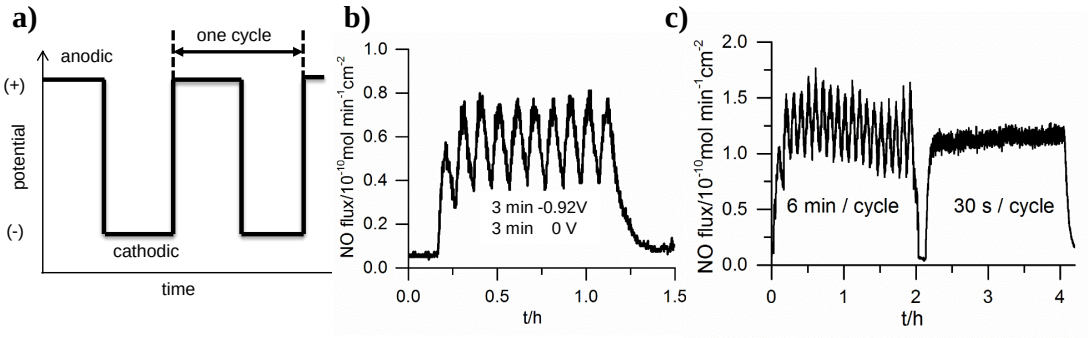

Figure 2.2. Effect of pulse cycle on NO release profile from surface of the silicone catheter from a copper wire electrode: (a) Schematic of applied voltage pulse sequence; (b) NO release profile from 6 min cycles using old pulse sequence (as in ref 23); with an anodic pulse of 3 min at 0 V and a cathodic pulse of 3 min at -0.92 V (vs. Ag/AgCl wire); (c) NO release profile of 6 min cycles and 30 s cycles, with an anodic pulse of +0.2 V and a cathodic pulse of -1.3 V (vs. Ag/AgCl wire).

The effect of O_2 level in the test solution in which the catheters were placed was also studied. In the presence of 10% and 21% O_2, the detected NO flux is reduced by 39% and 53%, respectively (Figure 2.5). This decrease in measured NO can be the result of two processes. First, the generated NO coming from the catheter can react with O_2 directly, within the catheter and within the gas phase that is purging the NO into the chemiluminescence instrument. Second, it is known that some Cu(I) species can reduce O_2 to superoxide radical, which can scavenge NO to form peroxynitrite.[25] It should be noted that the O_2 content in a vein is typically is much less than 10%, and within an artery

it is fairly close to this level (e.g., corresponding to 80-120 mm Hg). Hence, for the proposed catheters described here, it is likely that *in vivo*, the NO fluxes at the surface of the catheters should typically be > 0.8 $\times 10^{-10}$ mol min^{-1} cm^{-2}, whether the catheters are implanted in veins or arteries.

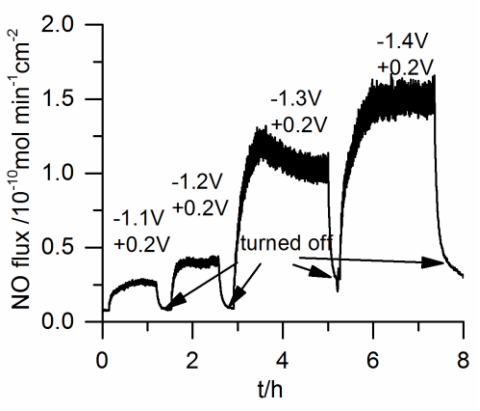

Figure 2.3. Effect of cathodic pulse voltage on NO release from a single-lumen catheter at 25 ℃. Each pulse cycle includes a 15 s cathodic voltage pulse and a 15 s anodic voltage pulse. The potentials are vs. Ag/AgCl wire.

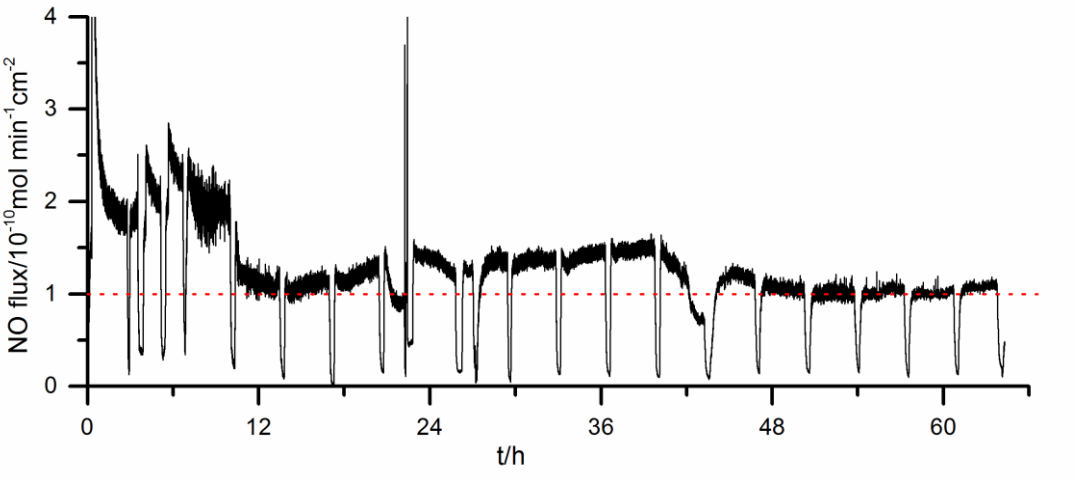

Figure 2.4. NO release from a single-lumen silicone catheter using repeated pulse cycles of 15 s at -1.3 V and 15 s at +0.2 V at 37 ℃. The dotted line indicates a surface NO flux of 1.0 $\times 10^{-10}$ mol min^{-1} cm^{-2}. Note that the catheter is intentionally turned "off" periodically to demonstrate the NO release can be modulated. The potentials are vs. a Ag/AgCl wire.

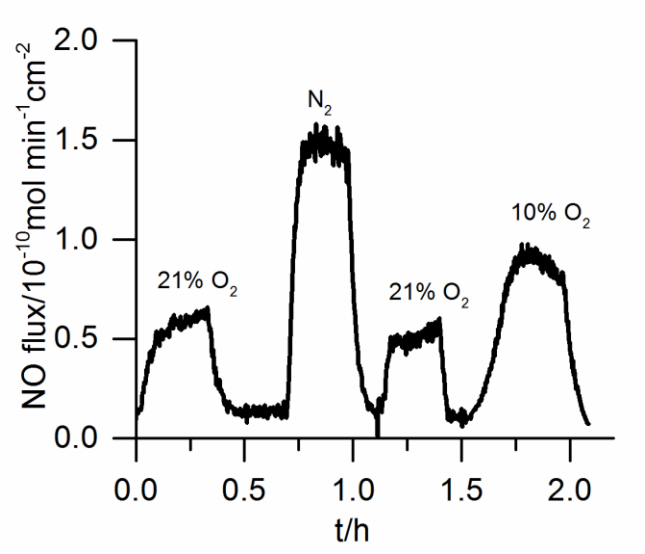

Figure 2.5. Effect of solution phase O_2 concentration on NO release from a single-lumen silicone catheter (37 ℃). Repeated pulse cycles of 15 s at -1.3 V and 15 s at +0.2 V are applied. Note that NO release is turned "off" when changing the purging gas.

2.3.2 Anti-Thrombotic Properties of NO Releasing Catheters In Vivo

To assess the antithrombotic activity of the electrochemical NO releasing catheters, the devices (both active and control catheters) were implanted into rabbit veins for 7 h. Catheters in the low flux group were set to exhibit an NO flux of ~0.7 $\times 10^{-10}$ mol min^{-1} cm^{-2} and those in the high flux group exhibit fluxes of ~1.1 $\times 10^{-10}$ mol min^{-1} cm^{-2} (via the applied voltage values for the cathodic pulse; see experimental section). As shown in Figure 2.6a, less thrombus formation was observed on the surface of the NO releasing catheters as compared with control catheters. However, the NO flux plays a critical role in this experiment, with a higher flux (~1.1 $\times 10^{-10}$ mol min^{-1} cm^{-2}) reducing the overall thrombus coverage by 62% ($n = 3$, $p < 0.001$), while a lower flux (~0.7 $\times 10^{-10}$ mol min^{-1} cm^{-2} reduces thrombus area by only 17% (Figure 2.6b; $n = 3$, $p < 0.05$) (reductions are

relative to average of control catheters without NO release). This agrees well with the fact that the endothelium layer of cells on the inner walls of blood vessels produces NO at a flux in the range of (0.5–4) $\times 10^{-10}$ mol min^{-1} cm^{-2} to prevent clotting, and dysfunction of NO producing the enzyme, eNOS, increases susceptibility to thrombophilia.[26] Note that NO released from the surface of the catheters has a short lifetime in blood (<1 s) due to reaction with oxyhemoglobin and, thus, will only induce a very localized antithrombotic effect, as compared with heparin, which usually induces a systemic effect.[27]

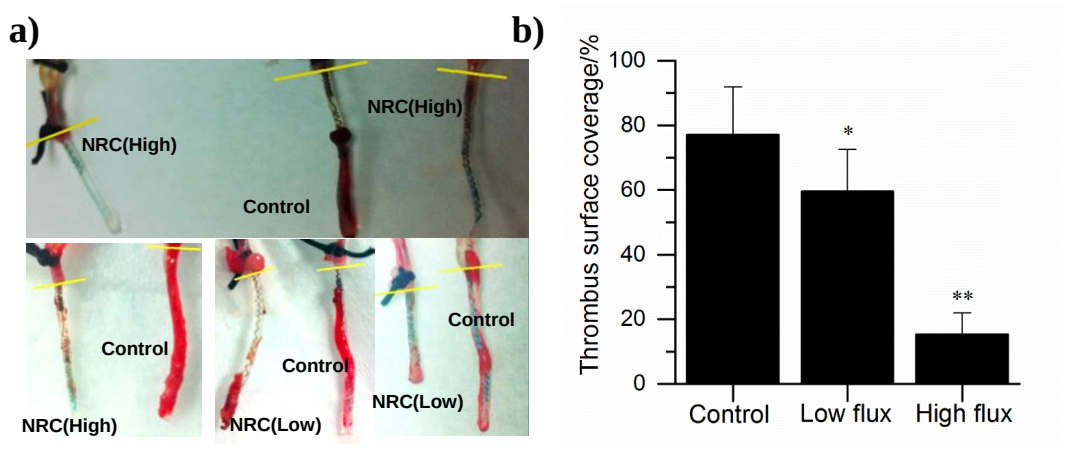

Figure 2.6. Antithrombotic effect of NO releasing catheters (NRC) in 7 h rabbit experiment: a) representative photos of high flux (NRC (High) ~1.1 $\times 10^{-10}$ mol min^{-1} cm^{-2}), low flux (NRC (Low) ~0.7 $\times 10^{-10}$ mol min^{-1} cm^{-2}) and control (Control, < 0.1 $\times 10^{-10}$ mol min^{-1} cm^{-2}) catheters after explantation; b) thrombus surface coverage quantified by counting the red pixels on the catheters from the photos (Low flux catheters: n = 3 rabbits, * $p < 0.05$; High flux catheters: n = 3 rabbits, **$p < 0.01$).

2.3.3 Biofilm Prevention Study

Since bacterial infections pose major clinical problem,[28] in prior work with the Cu-wire based NO release catheters, the effect of continuous e-chem NO release on the adhesion of *E. coli* and *A. baumannii* bacteria to the catheter surface within a CDC

bioreactor was examined. In this study, a drip flow bioreactor is used to allow growth of high biomass-biofilms close to the air liquid interface, which provides a standardized model that better represents *in vivo* conditions.[29] We first investigated the effect of NO on bacterial biofilm formation from a microbial species that is more prevalent with CABSI, *S. aureus*. We also examined whether effective dispersal of preformed, mature biofilms can be achieved with only 3 h of NO release turned "on" after the catheters were placed in the drip flow bioreactor to allow *E. coli* biofilm formation of over 2 and 4 d periods.

Since intravascular catheters necessitate continuous NO release to prevent clotting formation on their surfaces, biofilm dispersal was first studied by employing catheters that release NO continuously during the time exposed to *S. aureus* and media within the drip flow bioreactor. The *S. aureus* biofilms were grown for 48 h at 37℃, and NO was constantly generated electrochemically for the active catheters using pulse sequence of 15 s at -1.3 V and 15 s at +0.2 V. Corresponding controls containing the same nitrite reservoir as well as the Cu^{o} and Ag/AgCl wires but not connected to the potentiostat were also examined. Plate counts of viable bacteria present on the surface of the catheters demonstrate a 6 log-unit difference between control and NO releasing catheters (Figure 2.7; $n = 3$, $p < 0.01$).

It should be noted that *S. aureus* is an opportunistic pathogen capable of forming biofilms and causing chronic infections with high morbidity and mortality.[30,31] Furthermore, because *S. aureus* biofilms are purported to promote horizontal transfer of antibiotic determinants, they present an even greater challenge to successfully eradicate.[32] Thus, since the NO releasing catheter devices significantly lower the viable cell count of

S. aureus biofilms, this approach may represent an efficacious and relatively simple strategy to reduce this current serious complication in hospitalized patients.

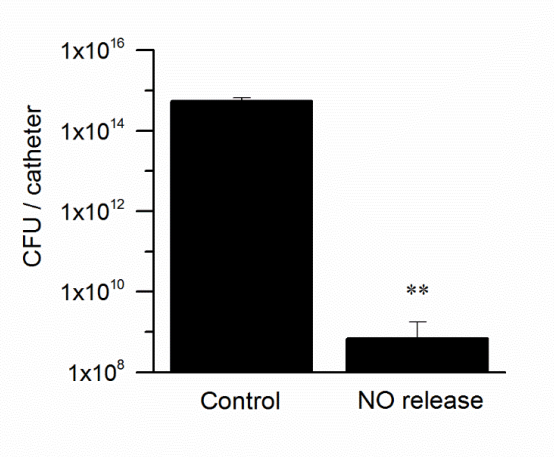

Figure 2.7. *S. aureus* biofilms developed on single-lumen catheters in a drip flow biofilm reactor for 48 h with the electrochemical NO release turned "on" continuously (only for NO release catheters) throughout the entire period of the biofilm growth. Plate counts of viable bacteria attached to the catheter surface after this period (n = 3, **p < 0.01).

It is also interesting to note that some bacterial infections can cause concomitant thrombosis. Indeed, invasive staphylococcal and streptococcal bacterial infections can promote hemostatic system malfunctions, which also lead to thrombosis.[33,34] Colonization by *S. aureus*, in addition to causing the majority of intravascular catheters-related infections,[35] can also induce platelet aggregation in vitro and induce the development of deep vein thrombosis *in vivo*.[36,37]

Because the plate count data for *S. aureus* biofilms showed a dramatic difference between continuous NO releasing and the control catheters, this result prompted an investigation into whether releasing NO only at the end of the biofilm growth period may still be sufficient to reduce bacterial viability on the surface of the catheter. Moreover, this strategy would conserve the nitrite reservoir, thereby significantly increasing the

operational NO release lifetime of any medical catheters developed based on this chemistry. This approach could be more viable for urinary catheters rather than intravascular devices, since thrombosis would not be an issue with such catheters and hence continuous NO release would not likely be required.

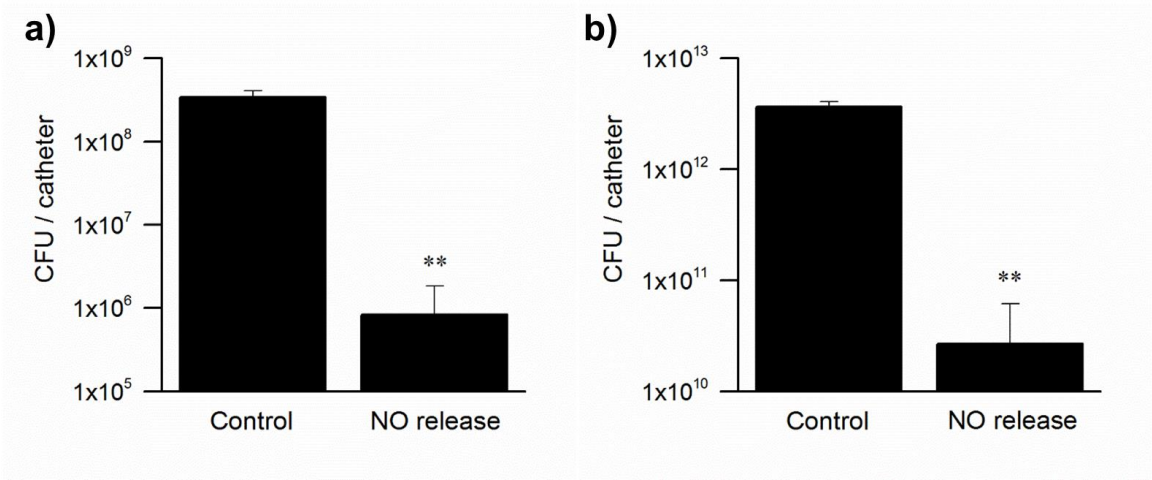

Figure 2.8. *E. coli* biofilm developed on single-lumen catheters in a drip flow biofilm reactor for a) 48 h and b) 96 h and NO release was then turned "on" only at the end of these periods for 3 h. Plate counts of viable bacteria attached to the catheter surface (n = 4 for both experiments, **p < 0.01).

Since *E. coli* is the cause of 80% of urinary tract infections (UTIs) in humans[38] and can easily adhere onto abiotic surfaces and mediate strong biofilm growth,[39,40] this bacterium was chosen to assess whether the catheters that are only turned "on" to generate NO at the end of the biofilm maturation process, can still abate cell viability significantly. Remarkably, as shown in Figure 2.8a, the electrochemical NO-release catheters can efficiently disperse 48 h *E. coli* biofilms by generating NO for only 3 h at relevant biological fluxes (1.0×10^{-10} mol min^{-1} cm^{-2}). Indeed, the bacterial count on the surface of the NO producing catheters is 3 log units lower than that found on the control catheters

(n = 4, $p < 0.01$). This finding is further validated by the fluorescent imaging data which illustrates that the bacterial surface coverage of the NO releasing catheters is noticeably less than the control catheters (Figure 2.9).

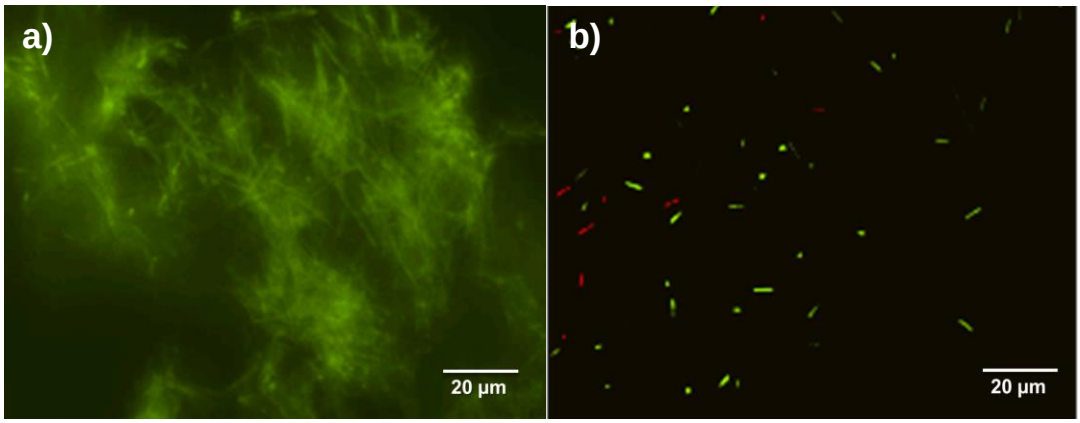

Figure 2.9. Representative fluorescent micrographs of surfaces of a) control and b) NO releasing catheters with live/dead staining. *E. coli* biofilms was grown for 48 h and NO is turned "on" for the NO releasing catheter for 3 h at the end of the growth before the imaging.

The matrix of extracellular polymeric substances, by increasing over colonization time, contributes to the adhesion properties of bacteria and enhances biofilm stability.[41-43] Because of this, both dispersal and eradication of biofilm structures are typically more problematic at later stages of biofilm development. Nonetheless, as demonstrated here, the electrochemical method of NO production from the surface of a catheter is efficient at inducing dispersal of 96 h old *E. coli* biofilms (Figure 2.8b). In fact, it is shown that the bacterial counts on the surfaces of catheters releasing NO for 3 h after a 4 d growth of biofilms are almost 3 log units lower than those on the control catheters (n = 4, $p < 0.01$). Consequently, these results demonstrate how the electromodulated NO releasing approach may also provide a novel strategy to reduce biofilm-induced UTIs over an extended time period of catheter placement, via a periodic generation of NO.

Because the proposed electrochemical NO generating system has considerable anti-biofilm properties, in future studies, it would be interesting to investigate whether local NO delivery at these low, non-toxic fluxes can also be efficient against antibiotic resistant, biofilm-forming microbial isolates. It has already been shown that NO can have an antimicrobial effect against multidrug-resistant uropathogenic *E. coli*.[44] In addition, a manganese nitrosyl, entrapped in the mesoporous material MCM-41, has been discovered to strongly inhibit the growth of drug-resistant *A. baumannii*.[45] Nevertheless, most of these studies to date have focused on the bactericidal properties of NO on planktonic cells. Because cells within biofilms are much more resistant than planktonic cells to antimicrobial agents,[6,46] it will be necessary to investigate whether NO released from the catheter configuration described in this work can also eradicate antibiotic-resistant isolates that have been grown to a mature biofilm stage on the surface of such devices.

2.4 Conclusions

In summary, it has been demonstrated that electrochemical release of NO from model catheters, which employ a copper wire electrode to generate Cu(I) ions to reduce nitrite to NO, can produce a relatively steady flux of NO from their surfaces for an extended time period by using the proper applied voltage pulse sequence. Such catheters were further shown to exhibit significant thromboresistance *in vivo* as well as anti-biofilm properties against bacteria that are known to be associated with high rates of hospital infections for both intravascular and urinary catheters. It should be noted that the single-lumen configuration used in this work is not practical for preparing operational catheters that could be employed clinically to infuse fluids or withdraw blood. However, we have

already demonstrated that electrochemical NO generation from multi-lumen catheters is possible, using the alternate Cu(II)-ligand mediated electrochemical reduction of nitrite within one lumen of the multi-lumen device.[24] Hence, efforts will now focus on using either of the two methods (Cu^o wire-based or Cu(II)-complex based) within full sized multi-lumen catheter configurations to demonstrate the anti-clotting and antimicrobial capability of this new approach with both intravascular and urinary catheters that could ultimately be employed in human studies.

2.5 References

(1) Umscheid, C. A.; Mitchell, M. D.; Doshi, J. A.; Agarwal, R.; Williams, K.; Brennan, P. J. *Infect. Control Hosp. Epidemiol.* **2011**, *32*, 101.

(2) Miller, D. L.; O'Grady, N. P. *J. Vasc. Interv. Radiol.* **2012**, *23*, 997.

(3) Oman, K. S.; Makic, M. B. F.; Fink, R.; Schraeder, N.; Hulett, T.; Keech, T.; Wald, H. *Am. J. Infect. Control*, *40*, 548.

(4) Zimlichman, E.; Henderson, D.; Tamir, O.; *et al*. *JAMA Internal Medicine* **2013**, *173*, 2039.

(5) Davies, D. *Nat. Rev. Drug Discovery* **2003**, *2*, 114.

(6) Mah, T.-F. C.; O'Toole, G. A. *Trends Microbiol.* **2001**, *9*, 34.

(7) Chung, K. K.; Schumacher, J. F.; Sampson, E. M.; Burne, R. A.; Antonelli, P. J.; Brennan, A. B. *Biointerphases* **2007**, *2*, 89.

(8) Ciobanu, C. S.; Groza, A.; Iconaru, S. L.; Popa, C. L.; Chapon, P.; Chifiriuc, M. C.; Hristu, R.; Stanciu, G. A.; Negrila, C. C.; Ghita, R. V.; Ganciu, M.; Predoi, D. *BioMed Research International* **2015**, *2015*, 926513.

(9) Stobie, N.; Duffy, B.; McCormack, D. E.; Colreavy, J.; Hidalgo, M.; McHale, P.; Hinder, S. J. *Biomaterials* **2008**, *29*, 963.

(10) Ding, X.; Yin, B.; Qian, L.; Zeng, Z.; Yang, Z.; Li, H.; Lu, Y.; Zhou, S. *J. Med. Microbiol.* **2011**, *60*, 1827.

(11) Jones, S. M.; Dang, T. T.; Martinuzzi, R. *Int. J. Antimicrob. Agents* **2009**, *34*, 360.

(12) Kuter, D. J. *The Oncologist* **2004**, *9*, 207.

(13) van Rooden, C. J.; Schippers, E. F.; Barge, R. M.; Rosendaal, F. R.; Guiot, H. F.; van der Meer, F. J.; Meinders, A. E.; Huisman, M. V. *J. Clin. Oncol.* **2005**, *23*, 2655.

(14) Loscalzo, J. *Circ. Res.* **2001**, *88*, 756.

(15) MacMicking, J.; Xie, Q.; Nathan, C. *Annu. Rev. Immunol.* **1997**, *15*, 323.

(16) Barraud, N.; Schleheck, D.; Klebensberger, J.; Webb, J. S.; Hassett, D. J.; Rice, S. A.; Kjelleberg, S. *J. Bacteriol.* **2009**, *191*, 7333.

(17) Cai, W.; Wu, J.; Xi, C.; Meyerhoff, M. E. *Biomaterials* **2012**, *33*, 7933.

(18) Nichols, S. P.; Schoenfisch, M. H. *Biomater. Sci.* **2013**, *1*, 1151.

(19) Riccio, D. A.; Schoenfisch, M. H. *Chem. Soc. Rev.* **2012**, *41*, 3731.

(20) Williams, D. L. H. *Acc. Chem. Res.* **1999**, *32*, 869.

(21) Keefer, L. K. *ACS Chem. Biol.* **2011**, *6*, 1147.

(22) Mowery, K. A.; Schoenfisch, M. H.; Saavedra, J. E.; Keefer, L. K.; Meyerhoff, M. E. *Biomaterials* **2000**, *21*, 9.

(23) Hofler, L.; Koley, D.; Wu, J.; Xi, C.; Meyerhoff, M. E. *RSC Adv* **2012**, *2*, 6765.

(24) Ren, H.; Wu, J.; Xi, C.; Lehnert, N.; Major, T.; Bartlett, R. H.; Meyerhoff, M. E. *ACS Appl. Mater. Interfaces* **2014**, *6*, 3779.

(25) Jourd'heuil, D.; Jourd'heuil, F. L.; Kutchukian, P. S.; Musah, R. A.; Wink, D. A.; Grisham, M. B. *J. Biol. Chem.* **2001**, *276*, 28799.

(26) Chen, A. F.; Ren, J.; Miao, C.-Y. *Jpn. J. Pharmacol.* **2002**, *89*, 327.

(27) Liu, X.; Miller, M. J. S.; Joshi, M. S.; Krowicka, H. S.; Clark, D. A.; Lancaster, J. R., Jr. *J. Biol. Chem.* **1998**, *273*, 18709.

(28) Costerton, J. W.; Stewart, P. S.; Greenberg, E. *Science* **1999**, *284*, 1318.

(29) Goeres, D. M.; Hamilton, M. A.; Beck, N. A.; Buckingham-Meyer, K.; Hilyard, J. D.; Loetterle, L. R.; Lorenz, L. A.; Walker, D. K.; Stewart, P. S. *Nat. Protoc.* **2009**, *4*, 783.

(30) Gotz, F. *Mol. Microbiol.* **2002**, *43*, 1367.

(31) Parsek, M. R.; Singh, P. K. *Annu. Rev. Microbiol.* **2003**, *57*, 677.

(32) Savage, V. J.; Chopra, I.; O'Neill, A. J. *Antimicrob. Agents Chemother.* **2013**, *57*, 1968.

(33) Boersma, R. S.; Jie, K. S. G.; Verbon, A.; van, P. E. C. M.; Schouten, H. C. *Ann. Oncol.* **2008**, *19*, 433.

(34) Donabedian, H.; Boyle, M. D. P. *Infect. Immun.* **1998**, *66*, 2362.

(35) Kiedrowski, M. R.; Horswill, A. R. *Ann. N. Y. Acad. Sci.* **2011**, *1241*, 104.

(36) Kerrigan, S. W.; Clarke, N.; Loughman, A.; Meade, G.; Foster, T. J.; Cox, D. *Arterioscler., Thromb., Vasc. Biol.* **2008**, *28*, 335.

(37) Martin, E.; Cevik, C.; Nugent, K. *Thromb. Res.* **2012**, *130*, 302.

(38) Campanha, M. T.; Hoshino-Shimizu, S.; Baquerizo, M. M. *Rev. Panam. Salud Publica* **1999**, *6*, 89.

(39) Gander, R. M.; Thomas, V. L. *Infect. Immun.* **1987**, *55*, 293.

(40) Ulett, G. C.; Mabbett, A. N.; Fung, K. C.; Webb, R. I.; Schembri, M. A. *Microbiology* **2007**, *153*, 2321.

(41) Danese, P. N.; Pratt, L. A.; Kolter, R. *J. Bacteriol.* **2000**, *182*, 3593.

(42) Ludecke, C.; Jandt, K. D.; Siegismund, D.; Kujau, M. J.; Zang, E.; Rettenmayr, M.; Bossert, J.; Roth, M. *PLoS One* **2014**, *9*, e84837.

(43) Reisner, A.; Haagensen, J. A. J.; Schembri, M. A.; Zechner, E. L.; Molin, S. *Mol. Microbiol.* **2003**, *48*, 933.

(44) Bang, C. S.; Kinnunen, A.; Karlsson, M.; Önnberg, A.; Söderquist, B.; Persson, K. *BMC Microbiol.* **2014**, *14*, 65.

(45) Heilman, B. J.; St. John, J.; Oliver, S. R. J.; Mascharak, P. K. *J. Am. Chem. Soc.* **2012**, *134*, 11573.

(46) Nickel, J. C.; Ruseska, I.; Wright, J. B.; Costerton, J. W. *Antimicrob. Agents Chemother.* **1985**, *27*, 619.

CHAPTER 3.

ELECTROCHEMICALLY MODULATED NO RELEASING BIOMEDICAL DEVICES VIA COPPER(II)-TRI(2-PYRIDYLMETHYL)AMINE MEDIATED REDUCTION OF NITRITE

3.1 Introduction

Biomedical devices are central to everyday medical care and intravascular catheters, in particular, play an indispensable role in monitoring patients by providing access to the blood and enabling infusion of drugs and nutrients. However, there are two major complications associated with the use of such devices; microbial infections and thrombosis/clotting. An estimated 80,000 catheter-related bloodstream infections (CR-BSIs) occur in patients within intensive care units (ICUs) in the United States each year, causing as many as 28,000 deaths and $2.3 billion in additional medical costs.[1] Thrombosis (i.e. clotting) is another major issue associated with catheter use, and this problem is only partly circumvented by intermittent or continuous heparin infusion. Additionally, use of heparin poses risk of systemic anticoagulation as well as heparin sensitivity in certain patients (including heparin induced thrombocytopenia (HIT)). Further, use of heparin does not prevent platelet activation and adhesion, the primary events in a foreign body induced coagulation process.[2]

Nitric oxide is an endogenously produced molecule (endothelial cells produce NO at a flux of (0.5–4.0) $\times 10^{-10}$ mol min^{-1} cm^{-2}) [3] that exhibits exceptional therapeutic potential, including killing bacteria[4] and preventing thrombosis.[5] Its short lifetime in blood (seconds) is both beneficial and challenging as the short-lived radical NO will only have a localized effect.[6] Thus, appropriate storage and delivery methods must be carefully considered as NO should be released precisely to a given area where it is needed. Strategies of doping NO donors such as diazeniumdiolates and *S*-nitrosothiols within polymer matrices have created new materials that exhibit improved biocompatibility in various *in vivo* blood contacting device/applications.[7,8] However, such NO donors are fragile and can lose NO during storage as a result of increased temperature or exposure to moisture or light. This increases the cost required for shipping and storage, limiting their utility in commercial biomedical products.

Nitric oxide generation via electrochemical reduction of nitrite could provide a cheap and controllable alternative method. However, direct nitrite reduction on metal electrodes is complicated and the products can vary from NO, N_2O, N_2, NH_2OH to NH_3, depending on pH, nitrite concentration, potential applied and nature of the metal electrode itself.[9,10] To achieve high selectivity towards NO generation, catalysts are necessary. Iron *meso*-tetrakis(4-*N*-methylpyridiniumyl) porphyrin has been shown to produce NO in a two-step electrolysis method in a flow system.[11] Recently, it was demonstrated that Cu^o electrodes can be used to generate NO from nitrite, via a pulsed applied potential sequence.[12] The sequence involved an anodic pulse to generate Cu(I) species and a subsequent cathodic pulse to clean the electrode.

Herein a simpler and much more attractive method to generate NO from a reservoir of nitrite ions is demonstrated using constant potential electrochemistry and the technique is applied to fabricate antithrombotic/antimicrobial catheters. In nature, Cu-containing nitrite reductases (E.C. 1.7.99.3) found in bacteria convert nitrite to NO via a 1 electron reduction.[13] Many Cu(II) complexes have been studied to mimic the active site of this enzyme,[14,15] as well as detect NO via fluorescence,[16] and several Cu(I) model systems have been shown to mediate nitrite reduction to NO.[17–19] In addition, Cu(II)-tri(2-pyridylmethyl)amine (Cu(II)TPMA) has been reported to catalyze the electrochemical reduction of nitrite to produce primarily N_2O.[20] In the present work we demonstrate that conditions can be tuned for this Cu(II)TPMA species to electrochemically generate predominately NO.

3.2 Experimental Details

3.2.1 Chemicals and Materials

Sodium nitrite, sodium chloride, sodium phosphate dibasic (99.95%), sodium phosphate monohydrate (99.5%), 3-(N-morpholino)propanesulfonic acid (99.5%), 3-(N-morpholino)propanesulfonic acid sodium salt (99.5%), copper(II) acetate monohydrate (99.99%), and tri(2-pyridylmethyl)amine (98%) were purchased from Sigma-Aldrich (St. Louis, MO) and used as received.

PTFE coated platinum (0.125 mm) and silver (0.127 mm) wires were purchase from Sigmund Cohn Corp. (Mount Vernon, NY). Single lumen standard silicone tubing (o.d. 1.47 mm, i.d. 1.96 mm) was purchased from Helix Medical (Carpentaria, CA) while dual

lumen silicone catheters (o.d. 2.34 mm) were provided by Cook Medical (Bloomington, IN).

Bacteria: *E. coli* EBW25113 was grown at 37 ℃ in Luria Bertani (LB) broth or LB agar plates. LB broth of 10% strength was used for biofilm development.

3.2.2 Bulk Solution Electrochemical Experiments

All electrochemical experiments were performed using a CH Instrument 1206B potentiostat. CVs were acquired in 5 mL of stationary solution in a three-electrode arrangement with a disk working electrode, Pt coil counter electrode and Ag/AgCl (3 M Cl^-) reference electrode.

Bulk electrolysis with different applied potentials were performed in a cell containing 5 mL solution of 2 mM Cu(II)TPMA, 100 mM nitrite and 0.1 M MOPS buffer. The gas product was then swept into a nitric oxide analyzer (NOA Sievers 280i, GE). The schematic of experiment setup is shown below in Figure 3.1.

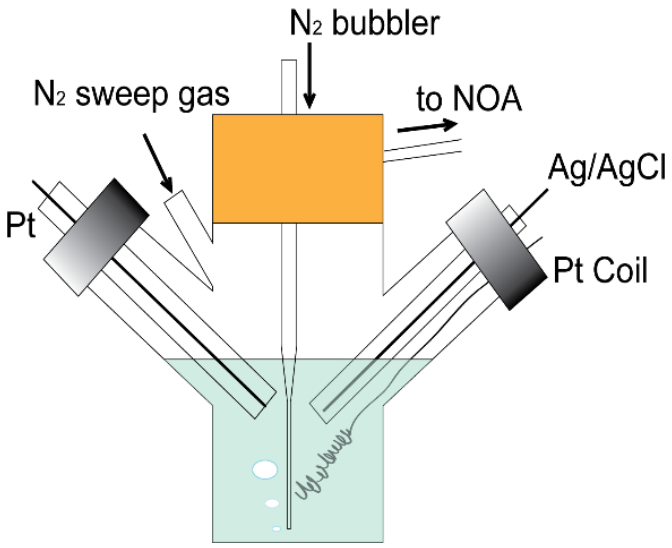

Figure 3.1. Experiment setup for bulk electrolysis of Cu(II)TPMA and nitrite solution.

3.2.3 Catheter Fabrication

A single lumen silicone rubber tubing (7.5 cm length, inner diameter 1.47 mm, and outer diameter 1.96 mm) was sealed at one end with silicone rubber sealant. A polytetrafluoroethylene (PTFE)-coated silver/silver chloride wire (with 0.080 cm^2 surface area exposed) was used as the reference electrode, and a PTFE-coated platinum wire (with 0.039 cm^2 surface area exposed) was used as the working electrode. The exposed ends of the respective wires were coiled separately. The coiled ends were inserted into the single lumen silicone rubber tubing so that the silver/silver chloride wire and the copper wire were not in direct metallic connection. A solution was loaded into the single lumen silicone rubber tubing. The solution included 2 or 4 mM Cu(II)TPMA, 0.4 M $NaNO_2$, and 0.2 M NaCl in 0.5 M MOPS buffer (pH 7.2). The silicone rubber tubing was then sealed to form a catheter. The PTFE-coated silver/silver chloride wire and PTFE-coated Pt wire extended out of the silicone rubber tubing as respective leads to the reference and working electrodes. A duel lumen catheter may be formed in a similar manner by introducing the solution and electrode into one of the two available lumens.

3.2.4 Gas Phase IR Experiment

A cell containing 10 mL of different concentrations of nitrite (50, 100 200 and 400 mM) in 2 mM CuTPMA, 0.2 M NaCl and 0.5 M MOPS buffer (pH 7.2) was used for bulk electrolysis. The solution was purged with Ar for 30 min before each experiment. A Pt wire electrode (0.32 cm^2) was used as working electrode and Ag/AgCl wire as reference and counter electrode. A constant potential (-0.4 V vs. 0.2 M Ag/AgCl) was applied for 3 h with stirring, after which the headspace gas was transferred into a vacuumed gas phase

IR cell using a cannula and analyzed using a Perkin-Elmer FT-IR. A prior calibration curve was obtained by adding different known amounts of saturated N_2O solution into 10 mL 0.5 M MOPS buffer (pH 7.2) to make 0.25, 1, 2 and 2.5 mM N_2O. Headspace N_2O was analyzed similarly and quantification was achieved by integration the N_2O feature peaks at 2235 and 2212 cm^{-1} in the IR spectra.[21]

3.2.5 Rabbit Experiments

Animal handling and surgical procedures were approved by the University Committee on the Use and Care of Animals in accordance with university and federal regulations and the detailed protocols are reported elsewhere.[22] Briefly, two catheters were implanted into the left and right jugular veins of ca. 3 kg anesthetized rabbits. The animals received no other anticoagulant or anti-platelet agent during the experiment. One of the catheters was "turned on" by applying a - 0.4 V vs. 0.2 M Cl^- Ag/AgCl reference and the other "turned off" with no potential applied. After 7 h, the catheters were explanted and a digital picture was taken and the red pixels were counted using Image J software to represent the clot area.

3.2.6 Numeric Simulation

Simulation was performed using COMSOL 4.3 b. To determine the NO distribution around the dual lumen catheter, a 2D space simulation was performed using the cross sectional geometry of the catheter. Since the catheter has a large length to diameter ratio, the edge effect of the two ends of the catheter can be neglected.

For NO distribution along the single lumen catheter, 2D-axial symmetry space was used. An NO flux of 7.4×10^{-9} mol min^{-1} cm^{-2} was set from the electrode surface in both cases, which is calculated based on NO release experimental data from the NOA. A diffusion profile with no convection is set with the stiff spring boundary condition across the solution-polymer phase boundary, which is used to ensure a continuous flux with partitioning of NO between the two phases (solution and polymer). Key boundary conditions and parameters are listed in Table 3.1. The diffusion and partition coefficients are based on literature data.[23-25]

Table 3.1. Boundary conditions used for simulating the NO diffusion from electrode surface through silicone rubber.

Boundary/ Domain	Boundary Conditions
Electrode surface	$N_1 = 7.4 \times 10^{-9}$ mol min^{-1} cm^{-2}
Inner solution	D_{NO_water}
Inner solution-silicone	$N_2 = 1000 \times (K*c_1-c_2)$
Silicone	$D_{NO\_silicone}$
Silicone-outer solution	$N_3 = 1000 \times (c_2-K*c_3)$
Outer solution	D_{NO_water}

N_1 is the flux of NO from electrode surface. N_2 is the flux of NO from the inner solution (Cu(II)TPMA and nitrite solution) into the silicone rubber. N_3 is the flux of NO from silicone rubber into the outer solution phase. D_{NO_water} and $D_{NO\_silicone}$ are the diffusion coefficient of NO in water and silicone rubber, respectively. K is the diffusion coefficient of NO in silicone phase over water phase.

3.2.7 ICP-OES Experiment

Nitric oxide releasing single lumen catheters were turned on (-0.4 V) and soaked in 3 mL PBS (pH 7.4) for 7 days (n = 3). The Cu content in both soaking PBS solution and the native PBS solution was detected by ICP-OES (inductively coupled plasma optical emission spectroscopy) and quantified via a calibration curve method.

3.3 Results and Discussion

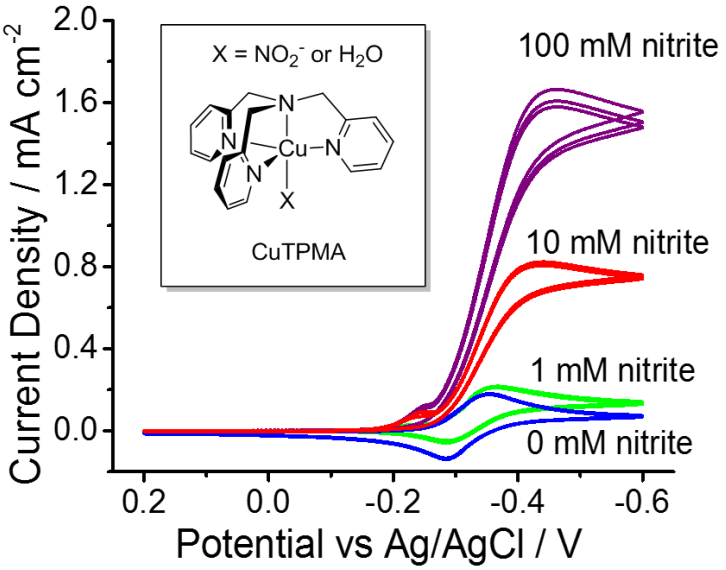

Figure 3.2. Cyclic voltammograms of 1 mM Cu(II)TPMA in 0.1 M MOPS buffer (pH 7.2) on a 0.0314 cm^2 gold disc electrode with different levels of nitrite in solution saturated with N_2. Scan rate is 50 mV/s. Inset: structure of Cu(II)TPMA.

Figure 3.2 shows the structure of Cu(II)TPMA (inset) and the resulting cyclic voltammetry (CV) of Cu(II)TPMA on a gold (Au) electrode in the presence of different levels of nitrite in solution. The reversible peaks in the absence of nitrite correspond to a one electron reduction from Cu(II) to Cu(I) within the complex, and the characteristic

catalytic peak in the presence of nitrite indicates that the nitrite is reduced by the Cu(I) species. The CVs observed are similar on platinum (Pt) and glassy carbon electrodes (Figure 3.3).

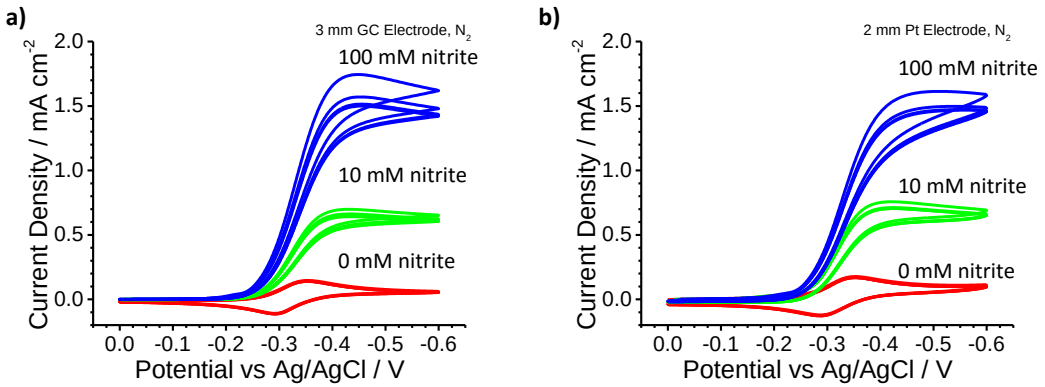

Figure 3.3. Cyclic voltammograms of 1 mM CuTPMA in 0.1 M MOPS buffer (pH 7.2) in a bulk solution experiment using a) 0.0707 cm^2 glassy carbon (GC) disk electrode; and b) 0.0314 cm^2 platinum disc electrode with different levels of nitrite in N_2 environment. Scan rate: 50 mV/s.

To detect the NO product, a bulk electrolysis experiment was performed by applying cathodic potentials in a cell that is connected to a chemiluminescence nitric oxide analyzer (NOA). A pH 7.2 3-(N-morpholino)propanesulfonic acid (MOPS) buffer was used for these experiments, since at a pH lower than 6, nitrite disproportionation occurs, producing background NO and NO_2. At pH higher than 8, it was observed that the activity of the catalyst decreases significantly and nitric oxide is not detected. Figure 3.4 demonstrates that a low, medium and high flux of NO release can be modulated by applying -0.2 V, -0.3 V and -0.4 V, respectively, to the working electrode (vs. 3 M Ag/AgCl reference electrode).

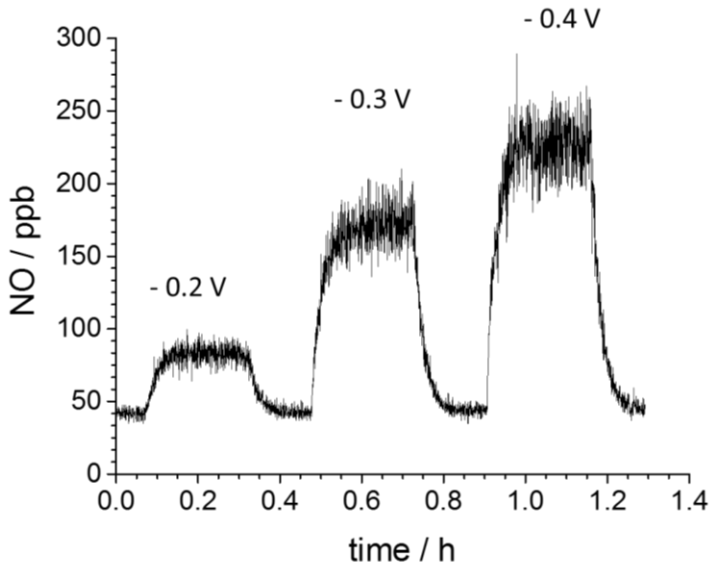

Figure 3.4. Modulation of NO generation in bulk solution by applying -0.2 V, -0.3 V and -0.4 V (vs. 3 M Cl^- Ag/AgCl) on a 0.071 cm^2 GC electrode. The solution contains 2 mM Cu(II)TPMA, 100 mM nitrite and 0.1 M MOPS buffer (pH 7.2).

To clarify the difference in product composition with an earlier paper[20] where N_2O was found to be the dominant product, bulk electrolysis experiments were performed. In these experiments, different levels of nitrite were present while applying a constant potential for 3 h, followed by careful analysis of the N_2O content by gas phase IR. It was found that N_2O is produced (from the reaction of Cu(I)TPMA with NO) but can be suppressed to a relatively low level (< 6%) when higher concentrations of nitrite are employed (see Figure 3.5 and Table 3.2). Note this low amount of N_2O is quite safe since up to 70% N_2O by volume is used routinely as an inhalation anesthetic in dentistry.[26] Previous studies have shown that Cu(I) complexes can disproportionate NO to generate N_2O and NO_2.[27,28] It is believed that the excess nitrite used in these experiments competitively binds to the Cu(I/II) center of the TMPA complex (after reduction of nitrite

to NO), and prevents NO binding to the Cu(I/II) center thereby suppressing N_2O generation. Note that NO only weakly binds to Cu(I) complexes.[28]

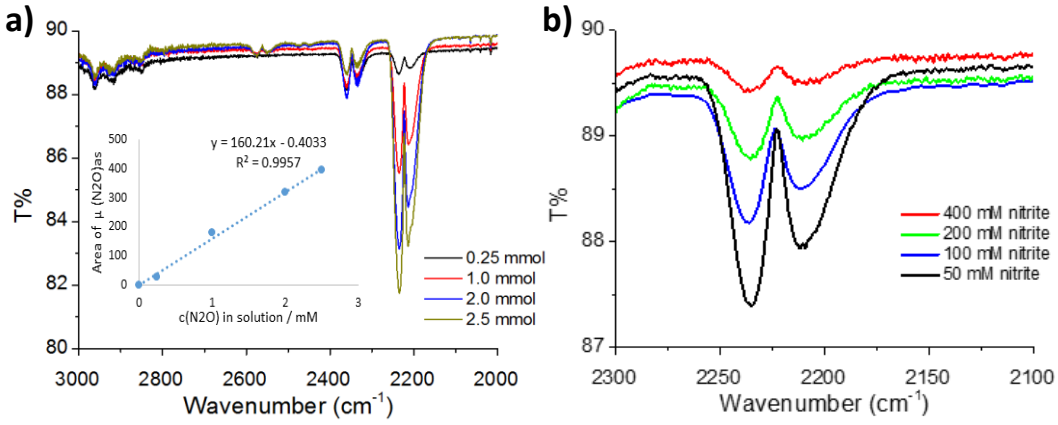

Figure 3.5. a) Gas phase IR spectra of headspace N_2O solution standards. Inset: calibration curve from integration of N_2O feature peaks at 2235 and 2212 cm^{-1}; b) gas-phase N_2O produced from bulk electrolysis of CuTPMA with different levels of nitrite present in the solution phase.

Table 3.2. Effect of nitrite concentration on the current efficiency and gaseous product ratio between NO and N_2O using CuTPMA mediated nitrite electrochemical reduction.

c (NO_2^-)/mM	**Area of $\mu(N_2O)_{asym}$**	**n(N_2O) /µmol**	**N_2O current efficiency**	**NO : N_2O**
50	91	2.9	68%	1 : 3.1
100	54	1.7	41%	1 : 0.5
200	28	0.9	21%	1 : 0.3
400	12	0.4	9%	1 : 0.06

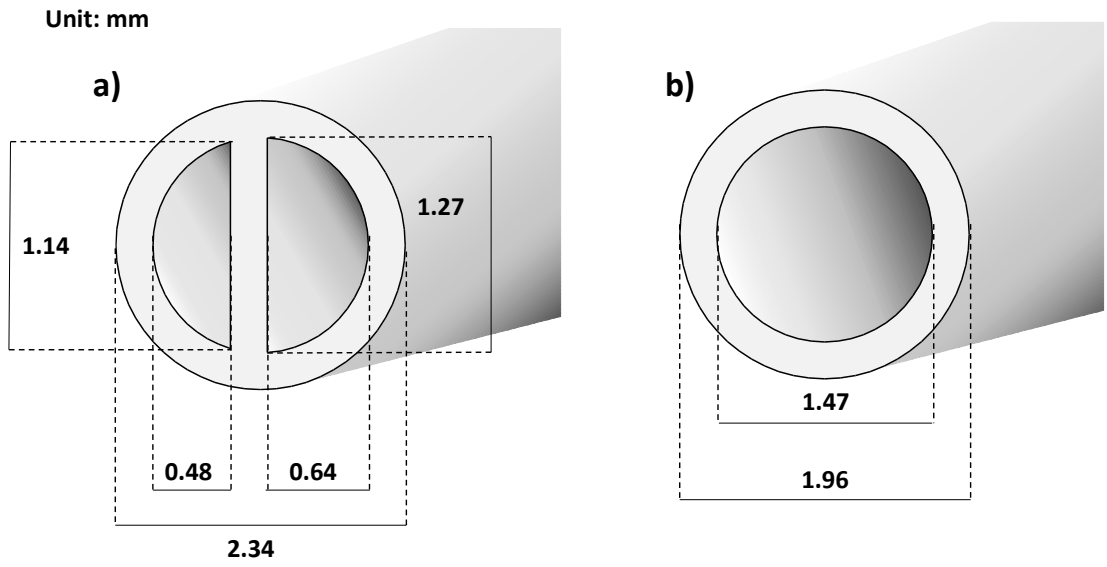

Figure 3.6. Cross sectional geometries of a) dual lumen and b) single lumen silicone catheters employed in these studies.

As proof-of-concept, such electrochemical NO release chemistry was applied to catheters as model biomedical devices to assess the antithrombotic and antimicrobial efficacy of this new NO release strategy. Nitric oxide releasing catheters (cross sectional geometries shown in Figure 3.6a) were fabricated by filling the lumen of silicone tubing with a solution containing 2 mM Cu(II)TPMA, 0.4 M nitrite, 0.2 M NaCl and 0.5 M MOPS buffer (pH 7.2). Teflon coated Pt and Ag/AgCl wires with 0.039 cm^2 (1 cm long) and 0.079 cm^2 (2 cm long) surface areas exposed, respectively, were used as the electrodes to conduct electrochemistry within the lumen (see Figure 3.7).

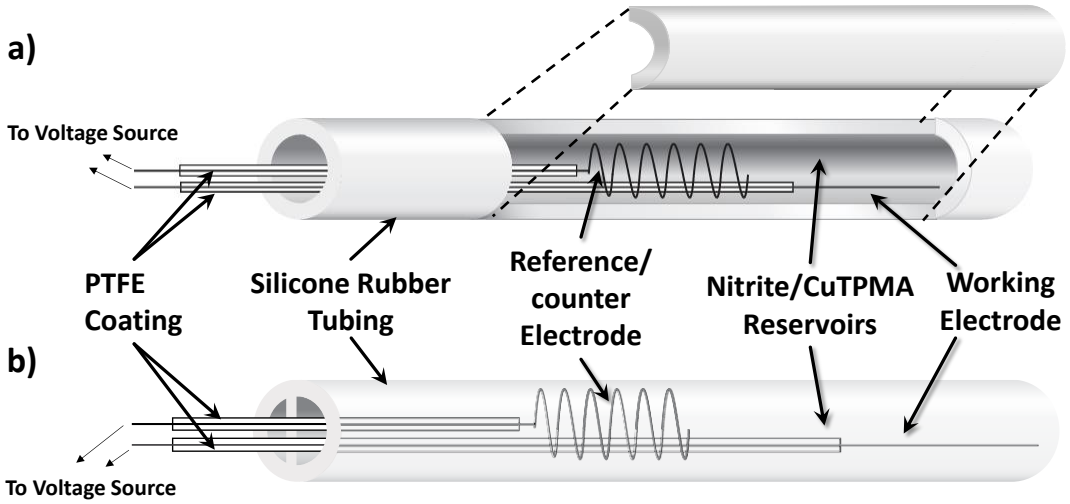

Figure 3.7. Schematics of a) single and b) dual lumen electrochemically modulated NO releasing catheter configurations examined in this work.

Finite element analysis modeling shows that NO flux out of the catheter mostly concentrates around the silicone surface near the working electrode. Hence, the flux is calculated based on the area of the device within a 3 cm long region encompassing the 1 cm exposed electrode, where >99.8% of the NO resides (see Figure 3.8).

Similarly, in the catheter configuration, the NO flux can be modulated by applying different voltage, and the observed flux, can vary from (0.4–3.0) $\times 10^{-10}$ mol min^{-1} cm^{-2} (Figure 3.9). Current efficiencies observed are up to 81% towards NO production and decrease as the applied potential is made more negative (see Table 3.3). To test the long-term stability of NO release, such devices were turned "on" and NO release monitored by chemiluminescence for an extended time period. We found that physiologically relevant NO fluxes (> 1.0 $\times 10^{-10}$ mol min^{-1} cm^{-2}) can be emitted from the catheter for more than 7 d (Figure 3.10).

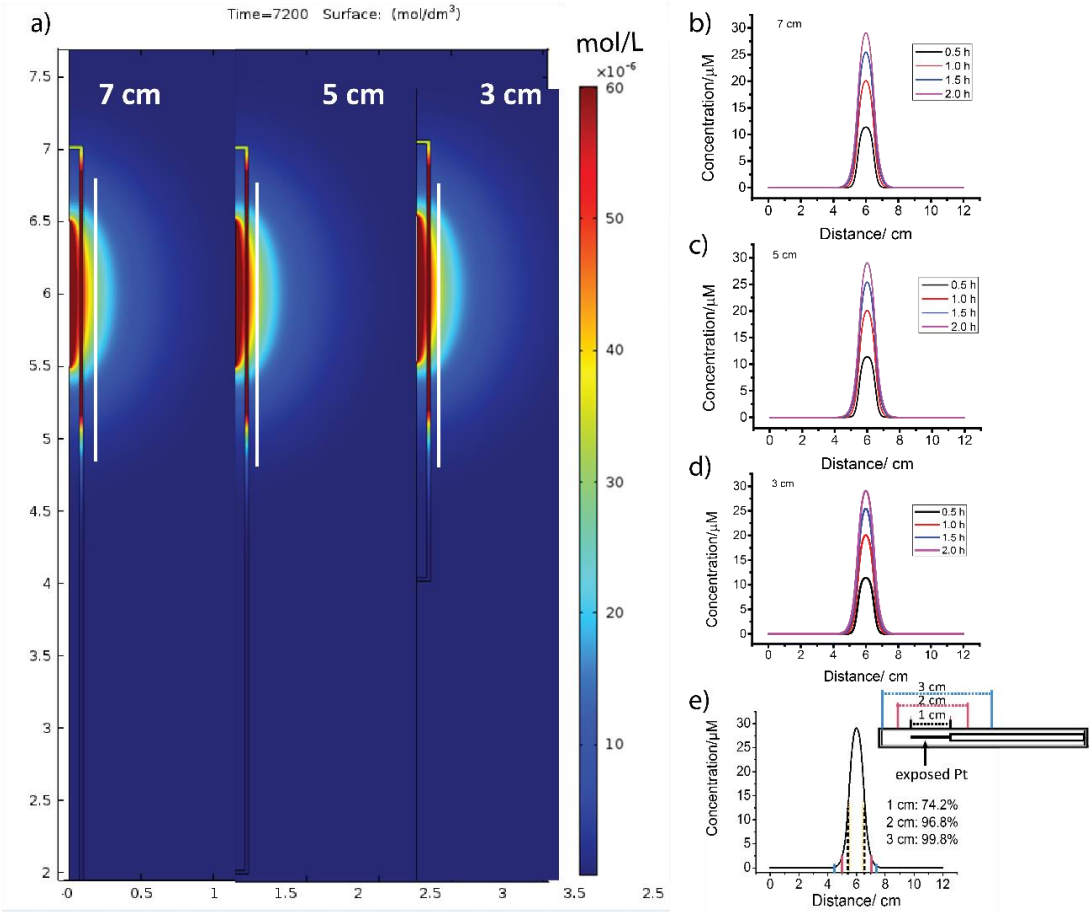

Figure 3.8. The concentration profile of 7, 5 and 3 cm catheters with 1 cm long active Pt surface; concentration profile 100 μm away from catheter surfaces of b) 7 cm c) 5 cm d) 3 cm in length along the direction of the white line at different time points; e) integration of concentration of a 7 cm catheter, with 1, 2 and 3 cm along a line 100 μm away from catheter surface near the exposed Pt electrode.

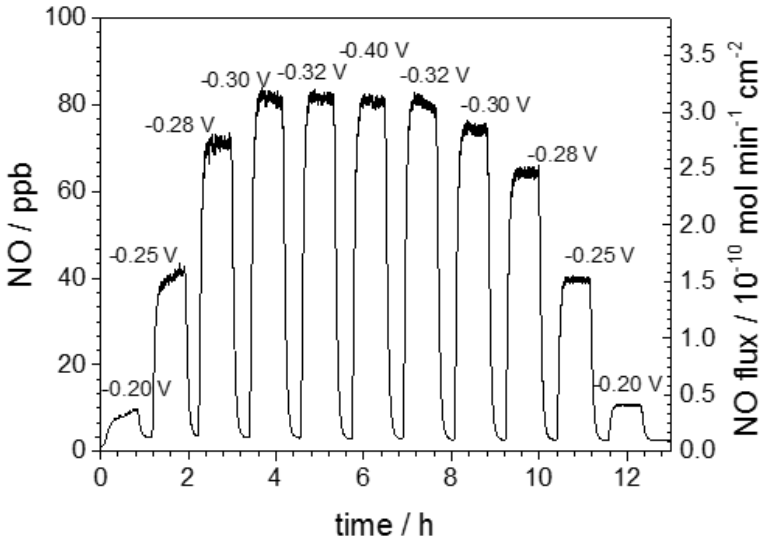

Figure 3.9. Modulation of NO flux from a single lumen catheter with 0.0798 cm^2 Pt wire. The solution contains 4 mM Cu(II)TPMA, 0.4 M $NaNO_2$, 0.2 M NaCl and 0.5 M MOPS (pH 7.2). Flux calculated based on the 3 cm silicone surface area near the Pt wire. Potentials are vs. 0.2 M Cl^- Ag/AgCl.

Table 3.3. Potential applied, NO flux, and NO current efficiency in the single lumen catheter.

Potential*/V	**NO flux/ 10^{-10} mol min^{-1} cm^{-2}**	**Faradaic efficiency**
-0.20	0.4	81%
-0.25	1.5	80%
-0.28	2.5	59%
-0.30	2.9	43%
-0.32	3.0	31%
-0.40	3.0	10%

* Potentials are vs. 0.2 M Cl^- Ag/AgCl

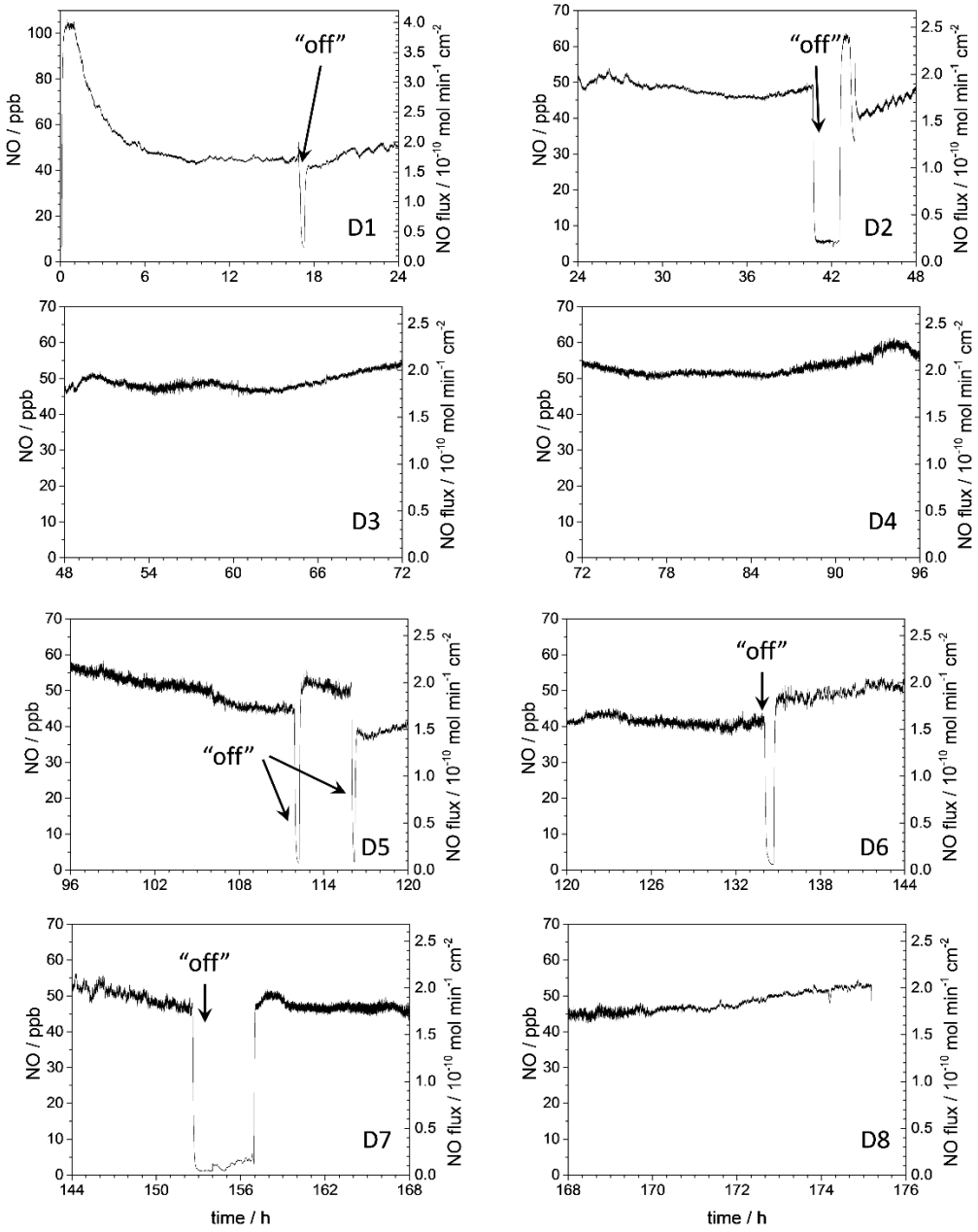

Figure 3.10. Nitric oxide release from a 7.5 cm long single lumen catheter with 0.080 cm^2 Pt wire. Inner solution contains 2 mM Cu(II)TPMA, 0.4 M $NaNO_2$, 0.2 M NaCl and 0.5 M MOPS (pH 7.2). NO turned "on" (- 0.4 V vs. 0.2 M Cl^- Ag/AgCl reference) for 8 d; periods of applied potential being turned "off" are also indicated.

To test the efficacy of this new NO release concept, 7 h *in vivo* testing was conducted by placing the two single lumen catheters described above in jugular veins of anesthetized rabbits with one of the catheters "turned on" (flux ~ 2.0×10^{-10} mol min^{-1} cm^{-2}) and the other "turned-off" (not linked to potentiostat; control). The degree of surface thrombus formation was assessed after removal and by using ImageJ 1.47 software[29] to determine the amount of clot covering the surface. The NO releasing catheters consistently exhibited reduced thrombosis ($p < 0.05$, $n = 3$), with an average of 88 ± 14% reduction in thrombus area when compared with the control catheters (Figure 3.11a and SL 1–3 in Figure 3.11c). This reduction in thrombus is not due to any significant temperature change for the active NO releasing catheters wired to the potentiostats owing to current flow. Indeed, based on simple calculations from Joule's law, the temperature change within the small volume of inner nitrite reservoir solution due to μA levels of current flow would be << 1 ℃ over a 24 h period.

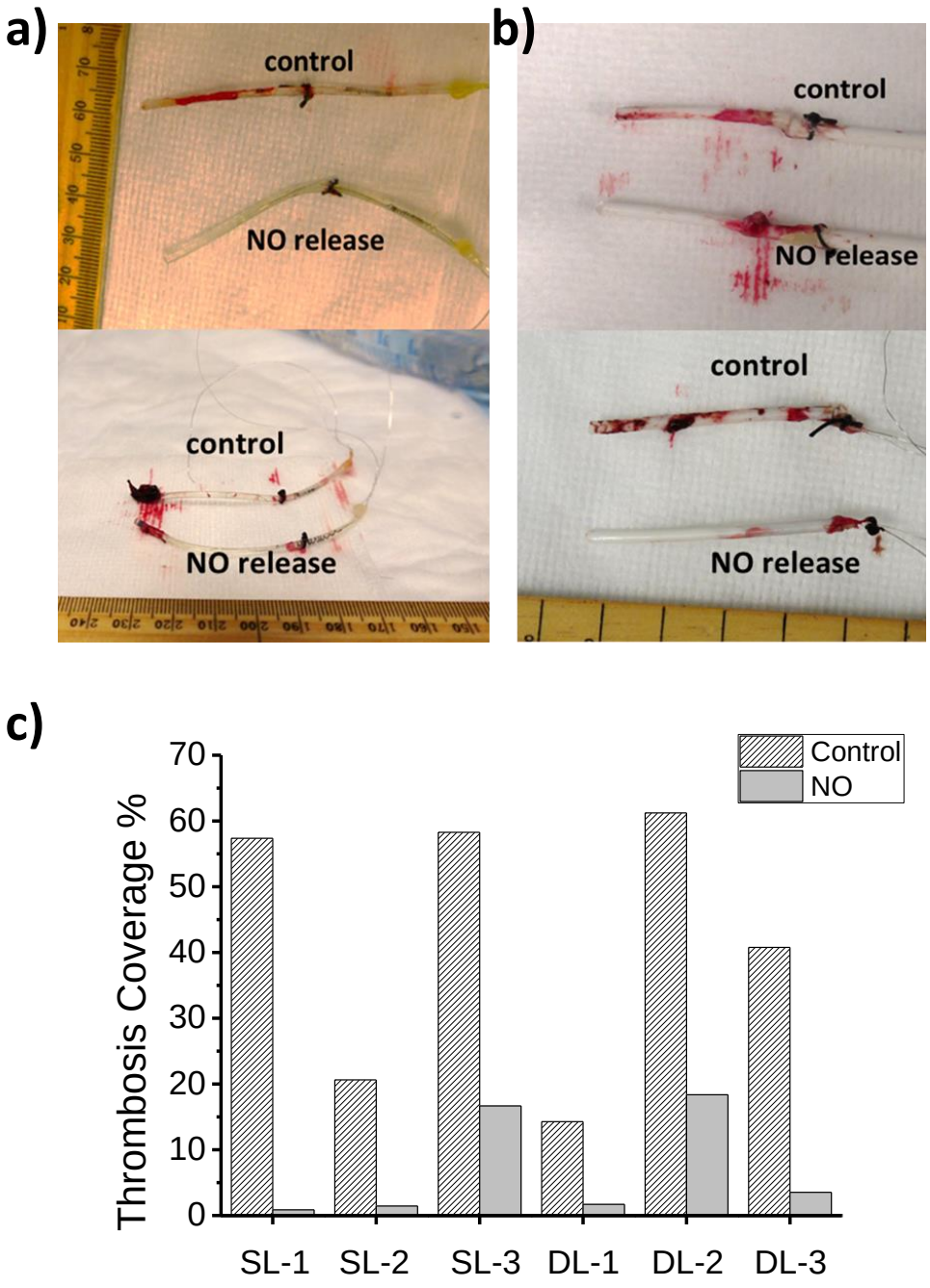

Figure 3.11. Antithrombotic effect of e-chem NO releasing catheters in veins of six rabbits for 7 h. Representative pictures of a) single and b) dual lumen catheters after removal from the vein; c) thrombosis coverage percentage on the catheters (single lumen: SL 1–3, dual lumen: DL 1–3).

In potential clinical practice, any e-chem NO releasing catheter would require at least one open lumen to sample blood or infuse agents and a second, closed-off lumen dedicated to NO release. Therefore, it is important to demonstrate that the new e-chem NO release methods could be adapted to such a configuration. This was accomplished using a dual lumen catheter (cross sectional geometry shown in Figure 3.6b). Although such a catheter's asymmetry could cause an uneven distribution of NO at the outer and inner surfaces of the lumens, the silicone rubber catheter material has a very high solubility and mobility for lipophilic NO,[24,25] that provides a reservoir for the e-chem generated NO and improves the distribution of the gas. Indeed, such effect is confirmed by finite element analysis simulations, as similar NO concentrations are found near the surfaces of the two respective lumens after 30 min of NO generation (see Figure 3.12). *In vivo* thrombosis experiments with the dual lumen configuration also showed significant reduction of thrombosis on NO releasing catheters ($p < 0.05$, $n = 3$) with an $83 \pm 12\%$ reduction of the thrombosis area compared with corresponding controls in the same animals (Figure 3.11b and DL 1–3 in Figure 3.11c).

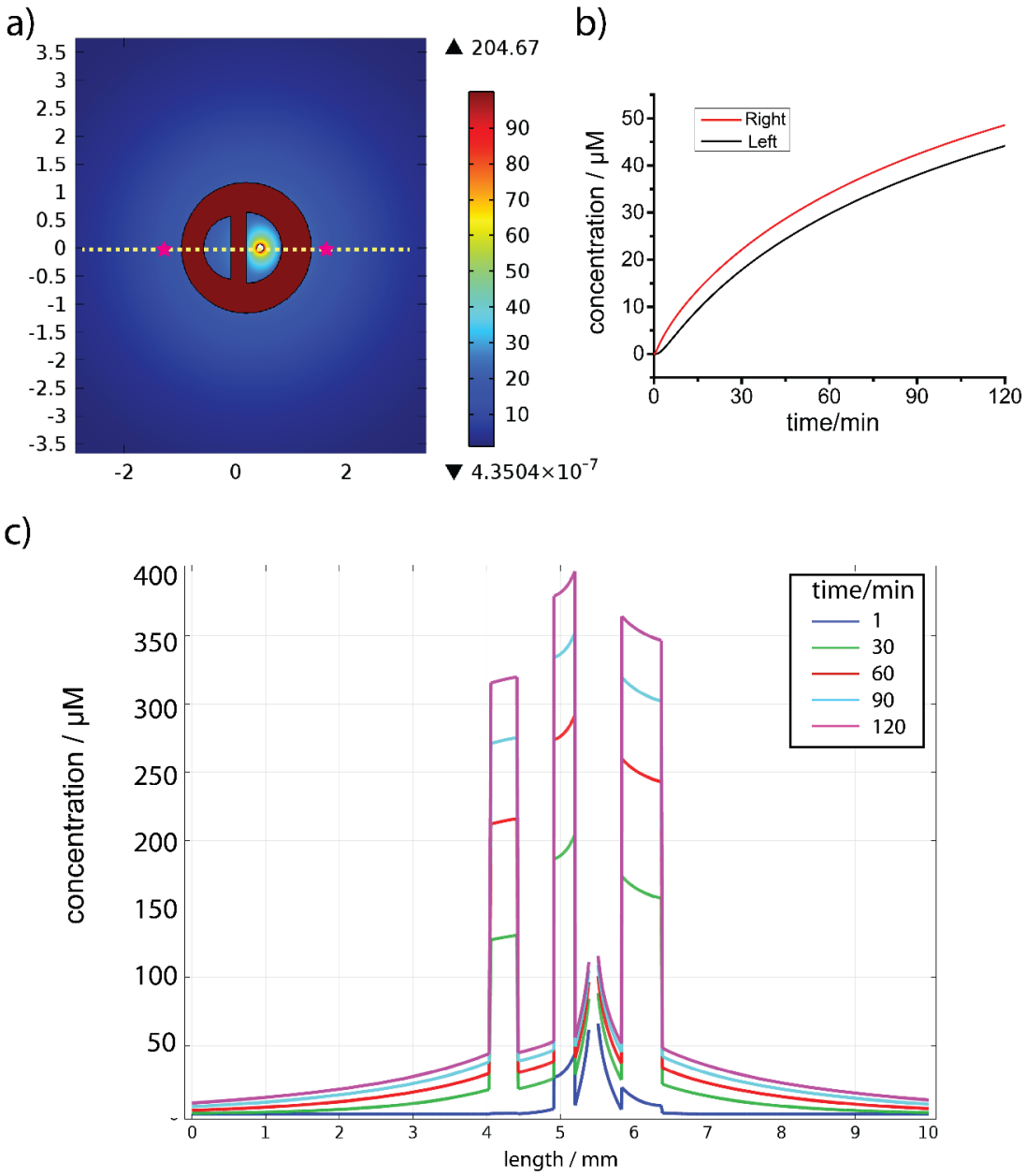

Figure 3.12. Distribution of NO concentration around the cross-section of a dual lumen silicone catheter (via COMOSOL Multiphysics): a) color map of NO concentration after 30 min of NO generation from the electrode surface; b) concentration vs. time at 100 µm from left- and right-side of the catheter surface (indicated by pink star in the color map; c) concentration profile on the cut line crossing the electrode (yellow dashed line in the color map).

To assess the antimicrobial/antibiofilm activity of the new e-chem NO releasing catheters, the total adhered viable bacteria on their surfaces after exposure to a flowing stream of medium containing the bacteria for 3 d was determined. The dual lumen catheters were tested in a drip flow bioreactor system, which mimics the catheter environment *in vivo*. The catheter and its peripheral environment (channel surface) were first inoculated with high number of bacteria (~10^8 CFU/channel) and then flushed continuously with fresh high nutrient medium (1/10 Laurie Broth) to remove any unattached cells and allow biofilm development on surfaces. Then, *E. coli* biofilms were grown on the catheter with continuous medium flowing (100 mL/h) for 3 d and the NO release was "turned on" for only 3 h each day (at flux of 0.6×10^{-10} mol min^{-1} cm^{-2}). Even with this low flux of NO release and with this release turned on only periodically, bacterial plate counts showed a > 1000-fold decrease of viable bacteria on the channel surfaces in which the NO releasing catheters (n = 5) were placed and a > 100-fold decrease in viable bacteria on the catheter surfaces (Figure 3.13 a and b) when compared to controls. The reduction of biofilm formation on the channel walls was so significant that it could easily be observed visually (Figure 3.13 c). It should be noted is that the biofilm data presented here are viable bacterial counts on the entire surface of the channel.

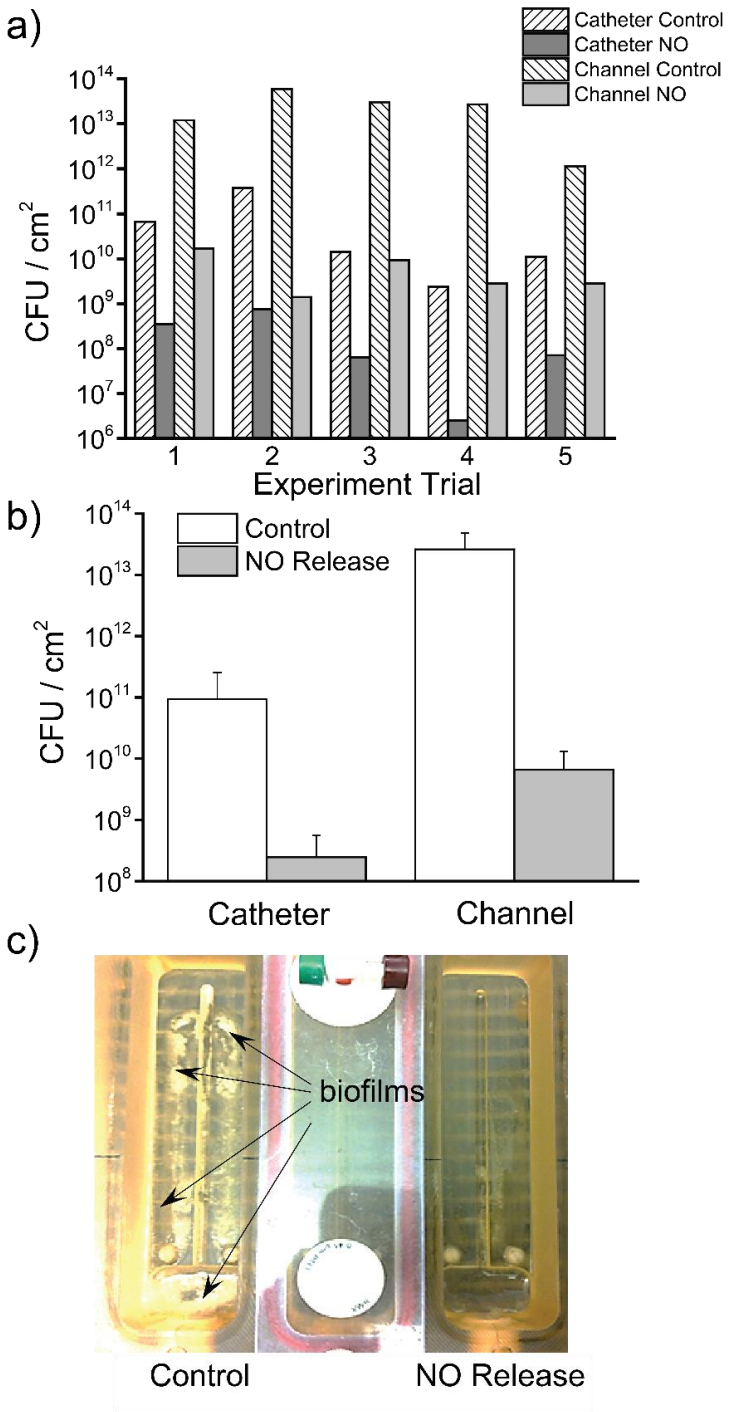

Figure 3.13. *E. coli* biofilm developed on dual lumen catheters in a drip flow reactor for 3 d with NO turned on for 3 h each day. a) and b): Plate count of the number of viable bacteria attached to the catheter surface and channel surface; c) picture shows the dramatic reduction of biofilm (indicated by arrow) formed on the channel with NO releasing catheter.

One potential concern is the competing reaction of oxygen with reduced Cu(I)TPMA. However, the CV of 1 mM Cu(II)TPMA with nitrite looks similar in air and in N_2 (Figure S-7), suggesting oxygen reduction has little effect under such conditions. The rabbit and biofilm experiments described above all were conducted in the presence of oxygen, and the data obtained in these experiments suggest that physiological levels of oxygen do not significantly suppress NO production by competing for the Cu(I)TPMA sites.

In the long term, the potential leaching of Cu is also important to consider. Literature suggests that Cu(II) ions cannot transport through silicone rubber to any significant degree[30] and this was confirmed by conducting a 7 d Cu leaching test. The soaking solution contains no copper species above the trace background levels found initially within the PBS (see Table 3.4).

Table 3.4. Result of 7 day Cu leaching experiment determined by ICP-OES.

Sample	Intensity	Concentration /ppb
Native PBS	3675 ± 263	10 ± 4
7 d Soaking of catheters is PBS	3591 ± 293	10 ± 4

3.4 Conclusions

In summary, electrochemically controlled NO releasing catheters have been developed using Cu(II)TPMA mediated nitrite reduction and these devices exhibit significant thromboresistance and antiseptic activity. Longer term (i.e., 3–7 d) *in vivo* experiments to test thromboresistance in freely moving animals are now being planned

with such catheters using miniaturized battery powered potentiostats to control the NO release fluxes of the devices. The NO flux control in real-time via such chemistry should also enable development of excellent $NO_{(g)}$ sources with different temporal release pattern for other biomedical applications, including a new generation of infection-resistant urinary catheters and wound healing patches, as well as NO inhalation therapy equipment for critically ill patients.

3.5 References

(1) O'Grady, N. P.; Alexander, M.; Burns, L. A.; Dellinger, E. P.; Garland, J.; Heard, S. O.; Lipsett, P. A.; Masur, H.; Mermel, L. A.; Pearson, M. L.; Raad, I. I.; Randolph, A. G.; Rupp, M. E.; Saint, S. *Clin. Infect. Dis.* **2011,** *52*, e162.

(2) Geary, R. L.; Koyama, N.; Wang, T. W.; Vergel, S.; Clowes, A. W. *Circulation* **1995,** *91*, 2972.

(3) Vaughn, M. W.; Kuo, L.; Liao, J. C. *Am. J. Physiol.: Heart Circ. Physiol.* **1998,** *274*, H2163.

(4) Nichols, S. P.; Schoenfisch, M. H. *Biomater. Sci.* **2013,** *1*, 1151.

(5) Loscalzo, J. *Circ. Res.* **2001,** *88*, 756.

(6) Pacher, P.; Beckman, J.; Liaudet, L. *Physiol. Rev.* **2007,** *87*, 315.

(7) Frost, M. C.; Rudich, S. M.; Zhang, H.; Maraschio, M. A.; Meyerhoff, M. E. *Anal. Chem.* **2002,** *74*, 5942.

(8) Major, T. C.; Brant, D. O.; Reynolds, M. M.; Bartlett, R. H.; Meyerhoff, M. E.; Handa, H.; Annich, G. M. *Biomaterials* **2010,** *31*, 2736.

(9) Duca, M.; Kavvadia, V.; Rodriguez, P.; Lai, S. C. S.; Hoogenboom, T.; Koper, M. T. M. *J. Electroanal. Chem.* **2010,** *649*, 59.

(10) Duca, M.; van der Klugt, B.; Koper, M. T. M. *Electrochim. Acta* **2012,** *68*, 32.

(11) Chi, Y.; Chen, J.; Aoki, K. *Inorg. Chem.* **2004,** *43*, 8437.

(12) Höfler, L.; Koley, D.; Wu, J.; Xi, C.; Meyerhoff, M. E. *RSC Adv.* **2012,** *2*, 6765.

(13) Adman, E. T.; Murphy, M. E. P. Copper Nitrite Reductase. In *Handbook of Metalloproteins;* Messerschmidt, A., Huber, R., Poulos T., Wieghardt, K., Eds.;Wiley: New York, 2001; pp 1381.

(14) Merkle, A. C.; Lehnert, N. *Dalton Trans.* **2012,** *41*, 3355.

(15) Casella, L.; Carugo, O.; Gullotti, M.; Doldi, S.; Frassoni, M. *Inorg. Chem.* **1996,** *35*, 1101.

(16) Tan L; Wan A, Li H. *Analyst* **2013**, *138*, 879.

(17) Halfen, J. A.; Mahapatra, S.; Wilkinson, E. C.; Gengenbach, A. J.; Young, V. G.; Que, L.; Tolman, W. B. *J. Am. Chem. Soc.* **1996,** *118*, 763.

(18) Kujime, M.; Izumi, C.; Tomura, M.; Hada, M.; Fujii, H. *J. Am. Chem. Soc.* **2008,** *130*, 6088.

(19) Kumar, M.; Dixon, N. A.; Merkle, A. C.; Zeller, M.; Lehnert, N.; Papish, E. T. *Inorg. Chem.* **2012,** *51*, 7004.

(20) Komeda, N.; Nagao, H.; Kushi, Y.; Adachi, G.; Suzuki, M.; Uehara, A.; Tanaka, K. *Bull. Chem. Soc. Jpn.* **1995,** *68*, 581.

(21) Zheng, S.; Berto, T. C.; Dahl, E. W.; Hoffman, M. B.; Speelman, A. L.; Lehnert, N. *J. Am. Chem. Soc.* **2013,** *135*, 4902.

(22) Yan, Q. Y.; Major, T. C.; Bartlett, R. H.; Meyerhoff, M. E. *Biosens. Bioelectron.* **2011,** *26*, 4276.

(23) Zacharia, I.; Deen, W. *Ann. Biomed. Eng.* **2005,** *33*, 214.

(24) Abraham, M. H.; Gola, J. M. R.; Cometto-Muniz, J. E.; Cain, W. S. *J. Chem. Soc., Perkin Trans. 2* **2000,** 2067.

(25) Mowery, K. A.; Meyerhoff, M. E. *Polymer* **1999,** *40*, 6203.

(26) Kanagasundaram, S. A.; Lane, L. J.; Cavalletto, B. P.; Keneally, J. P.; Cooper, M. G. *Arch. Dis. Child.* **2001,** *84*, 492.

(27) Ruggiero, C. E.; Carrier, S. M.; Tolman, W. B. *Angew. Chem., Int. Ed.* **1994,** *33*, 895.

(28) Fujisawa, K.; Tateda, A.; Miyashita, Y.; Okamoto, K.-i.; Paulat, F.; Praneeth, V. K. K.; Merkle, A.; Lehnert, N. *J. Am. Chem. Soc.* **2008,** *130*, 1205.

(29) Rasband, W. S. U. S. National Institutes of Health, Bethesda, Maryland, USA, *http://imagej.nih.gov/ij/* **1997-2012**.

(30) Donaldson, N.; Baviskar, P.; Cunningham, J.; Wilson, D. *J. Biomed. Mater. Res., Part A* **2012,** *100A*, 588.

CHAPTER 4.

IMPROVED IN VIVO PERFORMANCE OF AMPEROMETRIC OXYGEN (PO_2) SENSING CATHETERS VIA ELECTROCHEMICAL NO GENERATION/RELEASE

4.1 Introduction

Levels of chemical species in blood, including blood gases (pH, partial pressure of O_2 (PO_2), partial pressure of CO_2 (PCO_2)), electrolytes (Na^+, K^+, Ca^{2+}), glucose, and lactate, provide invaluable information for the diagnosis and treatment of hospitalized patients.[1,2] Currently, these analytes are intermittently measured *in vitro* with point-of-care devices using blood samples, which provides only periodic information, leaving large gaps in time between blood draws. Continuous monitoring of these species directly within blood vessels would greatly improve the quality of health care for critically ill patients.[3,4] Indeed, the development of intravascular devices that can monitor key physiological species in real-time is the "holy grail" in the field of chemical sensors. Despite extensive efforts over several decades, there are currently no sensing devices available that can achieve this goal, mostly due to poor biocompatibility of the devices once placed intravascularly (IV) within flowing blood.[5-7] One of major complications is the formation of clots/thrombus, which occurs within hours after blood contact.[8] The thrombus can isolate the sensors from the

bulk of the blood and cause unreliable analytical results.[9] Intravascular thrombus formation also has the intrinsic risk to embolize and affect vital organs in the patient.[10]

In blood vessels, healthy endothelial cells generate nitric oxide (NO) at the flux from (0.5–4.0) $\times 10^{-10}$ mol min^{-1} cm^{-2}, and one of the functions of NO is to inhibit platelet activation/aggregation and prevent clotting at the surface of the endothelial cell layer.[11-13] Inspired by this knowledge, NO release/generation strategies have been adopted for the development of more biocompatible IV devices, including electrochemical sensors.[14-19] The traditional NO releasing sensors rely on coatings on the surface of the devices that contain NO donors (either by entrapping or covalent attachment) that decompose and generate NO spontaneously both *in vivo* and under storage in buffer solution.[20,21] Such passive NO release strategies are expensive and have shelf-life issues due to the instability of many NO donors utilized to date. There are also concerns about leaching of NO donors and/or byproducts into the blood stream. These issues have, impeded their adaptation into clinical settings. Strategies based on NO generation from endogenous *S*-nitrosothiol (RSNO) species using immobilized catalysts on the surface of the sensors have also been pursued.[15] However, the levels of endogenous RSNOs are likely too variable from patient to patient to guarantee that enough surface NO can be generated to prevent platelet adhesion and clotting for each and every patient.

Recently, a completely new electrochemical method has been reported to produce very controllable NO generation by electrochemical reduction of inorganic nitrite ions catalyzed by a copper(II)-ligand complex.[22] Not only can the NO generation/release be actively controlled “on” and “off”, but also the flux of the NO release from the device surface can be readily modulated within the physiologically relevant range, by applying

different voltages to an inner working wire electrode. This "on-demand" NO release method is highly desirable for implantable sensors for several reasons, including: 1) during the storage, the NO release can be turned "off" and thus the reservoir of NO precursor is preserved; 2) sodium nitrite as the NO donor is very stable and inexpensive compared to NO donors like diazeniumdiolates and *S*-nitrosothiols; and 3) the levels of NO release can be modulated *in vivo*, with low levels for most of the time to prevent clotting, and higher levels turned on only periodically to better prevent/manage risk of infection.

In this study, for the first time, the concept of combining electrochemical NO generation/release with intravascular chemical sensors to improve their *in vivo* analytical performance is investigated. Specifically, a dual lumen catheter-type amperometric PO_2 sensor (i.e., one lumen dedicated to electrochemical NO generation and the second lumen used for PO_2 sensing) is developed to demonstrate this concept. Such devices can be fabricated conveniently using commercial dual lumen silicone rubber catheter tubing without any NO releasing/generating coating. The performance of these sensors is further evaluated in rabbit and pig models for up to 21 h, both in veins and in arteries. The sensors were exposed to a wide range of PO_2 in *vivo* from ~20 mmHg to ~480 mmHg, by changing ventilator levels of fraction of inspired oxygen (FiO_2).

4.2 Experimental Details

4.2.1 Reagents and Instrumentation

Sodium nitrite, copper acetate, tris(2-pyridylmethyl)amine (TPMA), sodium chloride, sodium bicarbonate, sodium carbonate, potassium chloride, and HEPES buffer

were obtained from Sigma-Aldrich (St. Louis, MO). Teflon® PFA-coated silver (0.127 mm OD) and platinum wires (0.125 mm OD) are products of A-M Systems (Sequim, WA). All solutions were prepared with Milli-Q water (Millipore Corp., Billerica, MA). Dual-lumen silicone catheters (7 Fr) were gifted from Cook Medical Inc. (Bloomington, IN). Silicone rubber adhesive (RTV-3140) was obtained from Dow Corning (Midland, MI). Tanks of gas with varying levels of O_2 balanced in N_2 were products from Cryogenic Gas Inc. (Detroit, MI).

All electrochemical experiments were performed using CH Instruments multi-channel potentiostats (1000C, Austin, TX) and a BioStat potentiostat (ESA Biosciences Inc., Chelmsford, MA). Nitric oxide release from the catheters was measured using a Sievers Nitric Oxide Analyzer (GE Instruments, Boulder, CO). Blood gas values from blood samples drawn from the test animals were measured using a 700 series blood gas analyzer (Radiometer America Inc., Brea, CA).

4.2.2 Fabrication of Catheter-Type Electrochemical NO Releasing PO_2 Sensors

The procedures used were modified from those reported previously.[22,23] A long dual lumen catheter (see dimensions in Figure 4.1) was cut to 7 cm in length, and both lumens were sealed at one end with silicone rubber adhesive. The larger lumen was filled with a solution containing 4 mM CuTPMA (see Chapter 3 for preparation), 0.4 M $NaNO_2$, 0.2 M NaCl and 0.5 M HEPES (pH 7.2). A Teflon® PFA-coated Pt wire (3 cm exposed) and a Ag/AgCl wires (5 cm exposed) were inserted into the lumen as working and reference electrodes, respectively. The smaller lumen was filled with 0.15 M KCl in 0.1 M bicarbonate/carbonate buffer (pH 10) and a PFA-coated Pt wire (only tip exposed) as well

as a Ag/AgCl wire (3 cm exposed) were inserted for oxygen sensing. The openings of the lumens at the proximal end were then sealed (around the wires) with silicone rubber adhesives and left cured in water overnight.

4.2.3 Calibration of PO_2 Sensor

Catheter sensors were immersed in PBS bubbled with different levels of O_2 (0%, 10%, 21%, 100%) at the flow rate of ~500 mL/min. The PO_2 sensing lumen of the catheter was polarized at -700 mV in PBS with 0% O_2 for 1 h before calibration. At each level of PO_2, NO release was switched either from "on" to "off" or from "off" to "on", by applying -400 mV between the working and reference electrodes within the NO generating lumen. Note that the two lumens are separate electrochemical cells and the lead wires from each lumen are connected to different channels of a multi-channel potentiostat. To determine response times, the sensors were switched between solutions pre-saturated with 0% O_2 and 21% inspired O_2. The response time corresponds to the time needed to reach 90% of the steady-state current response after changing the oxygen level.

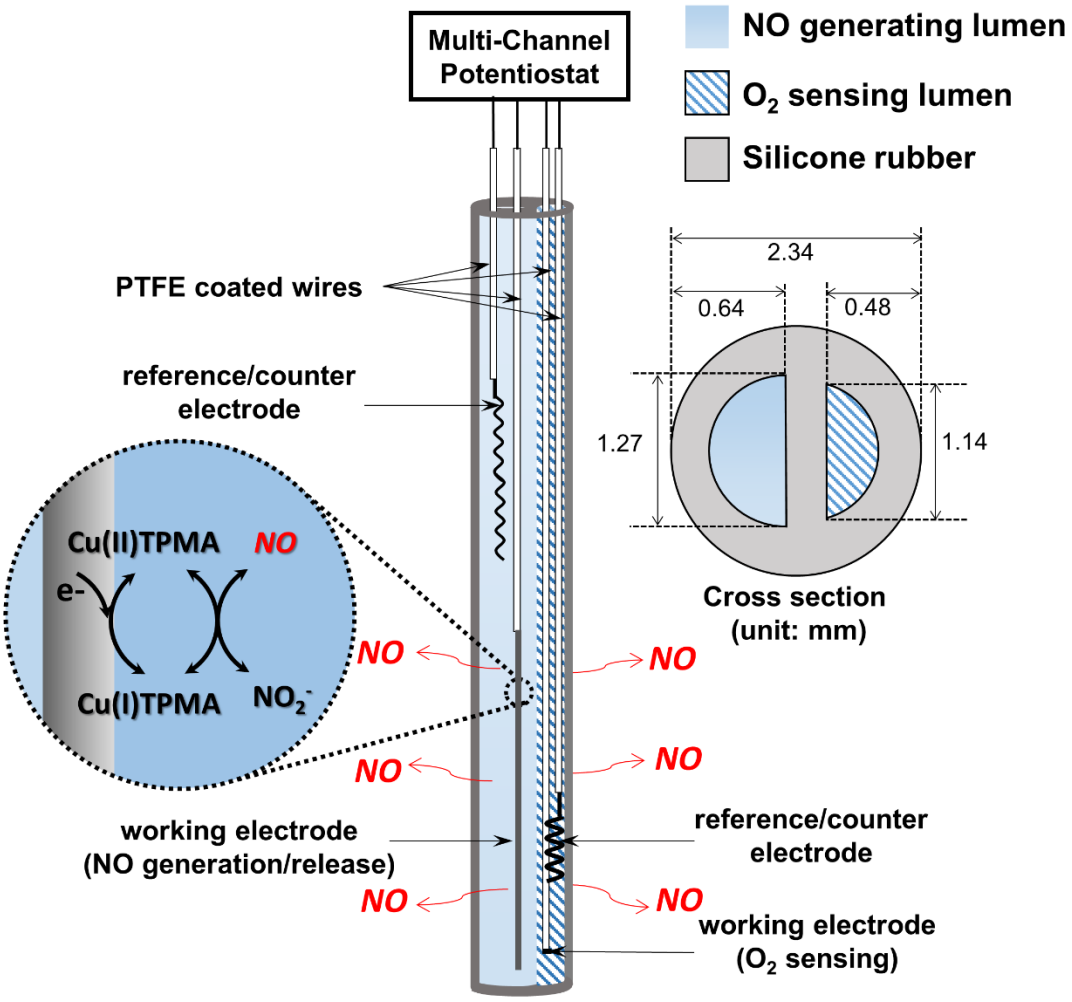

Figure 4.1. Schematic of dual-lumen catheter-type electrochemical NO generating/releasing PO_2 sensor with cross section geometry of catheter.

4.2.4 In Vivo Experiments

The procedures used were in compliance with the University Committee on the Use and Care of Animals as well as federal regulations and were reported elsewhere.[15] Briefly, New Zealand white rabbits (~3 kg, n = 5) were placed under anesthesia for the 7 h experiments. Two catheter-type PO_2 sensors were placed in the jugular veins and connected to potentiostats with NO release lumen switched "on" for one of the sensors.

No other anticoagulant or antiplatelet agents were administrated to the rabbits during the experiments. The initial FiO_2 was 100%. During the latter part of the experiment, the FiO_2 level was changed to 21% for ~1 h and then switched back to 100%. Venous blood was drawn every 30 min to test for PO_2 values using the blood gas analyzer as the reference method. To calibrate the sensors *in vivo*, the *ex vivo* data point at the 30 min time point after implantation was used as a one-point calibration, with intercept determined by a prior benchtop calibration of the oxygen sensing portion of the catheter. The continuous signal from the sensors was compared with the intermittent *in vitro* blood PO_2 values. The sensors with the blood vessels intact were then explanted after systemic heparinization to prevent necrotic thrombosis during vessel harvesting. Digital pictures were then taken and the red pixels were counted using Image J software to quantify clot area.[23,24]

Similar experiments were performed using a porcine model (~50 kg, n = 4) for 21 h. The sensors were placed in the femoral and carotid arteries via an open cut-down allowing for continuous blood flow past the sensors. The FiO_2 level was maintained at 21% and changed periodically to 100% for a 1 h period (ca. every 6 h). Arterial blood was drawn every hour to assess the accuracy of the PO_2 values provided by the implanted sensors. Similar to the experiments with rabbits, sensors and vessels were explanted at the end of the experiments to allow for quantification of clot burden.

4.2.5 Signal Processing and Statistics

The *in vivo* data from the sensors were recorded every second and averaged every 30 s to reduce the electronic noise as well as the size of the data set. A Student's t-test

(two-tail, paired) was used to evaluate the significance of the data sets. Linear regression and R^2 were used to evaluate the accuracy and correlation, respectively.

4.3 Results and Discussion

4.3.1 Rationale for Sensor Design

A commercial dual-lumen silicone catheter (cross section geometry shown in Figure 4.1) was used to fabricate the electrochemical NO releasing PO_2 sensors. Silicone rubber is preferred because it is highly permeable towards both the analyte, O_2, and the anticlotting agent, NO, while impermeable towards the components of the inner reservoir ions/species.[22,25] One lumen of the catheter is dedicated to O_2 sensing, using the cross-section distal tip of a PFA-coated Pt wire working electrode. It is held at a cathodic potential (-0.7 V vs. Ag/AgCl) where reduction of O_2 occurs to yield a steady-state current proportional to PO_2 levels. The other lumen is dedicated to NO generation/release and contains a reservoir of sodium nitrite (0.4 M) and CuTPMA (4 mM) catalyst. Note that although the cross-section geometry of the dual lumen catheter is not symmetric, it can be shown by finite element analysis (via Comsol Multiphysics® software) that the NO distribution is symmetrically enhanced around the entire dual lumen catheter assembly because of the high diffusivity and solubility of this neutral lipophilic gas molecule in the silicone rubber (see Figure 4.2).

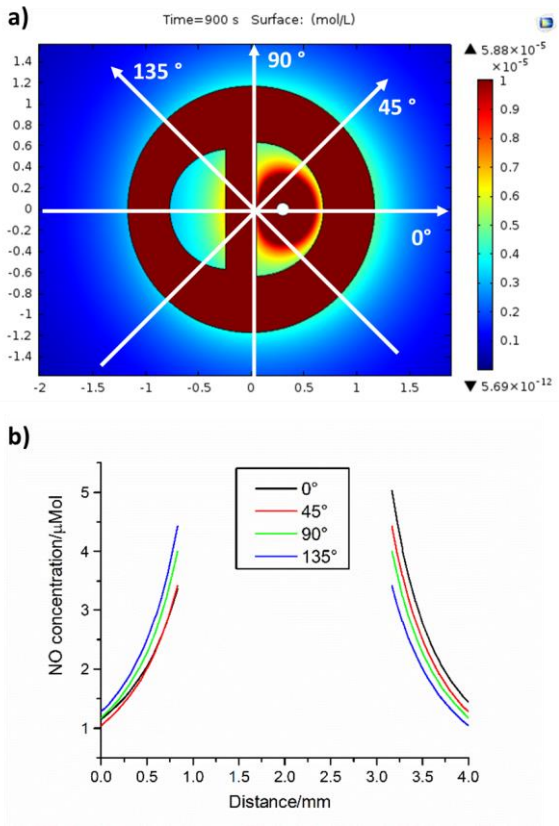

Figure 4.2. Distribution of NO levels around a dual lumen catheter after 900 s in the presence of air from simulation via Comsol Multiphysics®: a) Concentration color map near catheter surface; b) concentration of NO outside the catheter along the lines dissecting the catheter at 0 °, 45 °, 90 ° and 135 °, as indicated in a).

4.3.2 Sensor Performance on the Benchtop

The first study involved assessing the compatibility of the O_2 sensing with the electrochemical NO generation process. The design of the sensor facilitates such investigation, since the two electrochemical systems reside within the two separate lumens of the same catheter device and the NO generation lumen can be easily turned "on" and "off" by applying -0.4 V to the Pt working electrode within that lumen. Thus, the exact same sensor can be studied with and without NO release, merely by disconnecting the

electrode leads from the NO generating lumen to the potentiostat. The O_2 sensor was found to be fully compatible with NO release, as no noticeable amperometric signal changes were observed for the O_2 sensor when NO generation was switched "on" or "off" at each O_2 level during the calibration (see Figure 4.3). This is expected as the reaction between NO and O_2 is second order with respect to NO, implying that the reaction is slow when the concentration of NO is low.[26] This is true for the catheters under investigation, as they generate a relatively low flux of NO, ~1.5 $\times 10^{-10}$ mol min^{-1} cm^{-2} (see below). The high solubility of O_2 in silicone rubber also sufficiently supplies O_2 to the electrode surface even if a portion of the O_2 does react with NO.

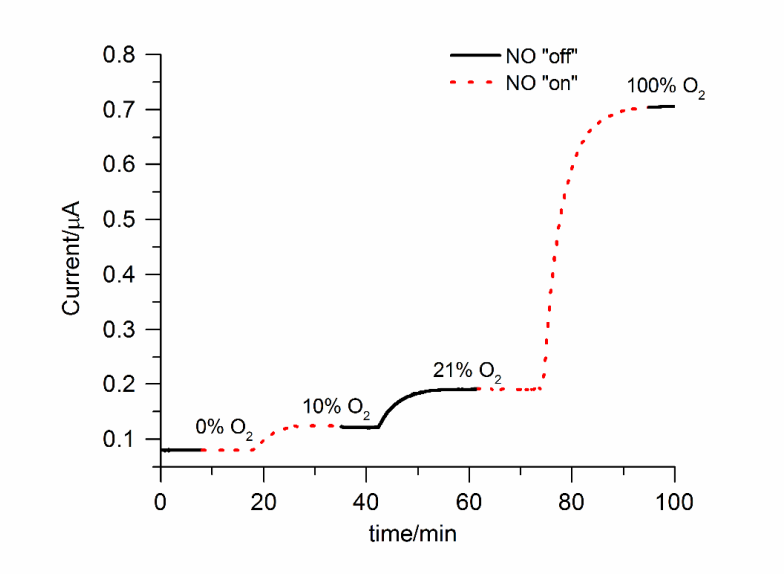

Figure 4.3. Calibration curve of *P*O_2 sensing catheters on the benchtop with NO generation/release switched "on" and "off" as indicated.

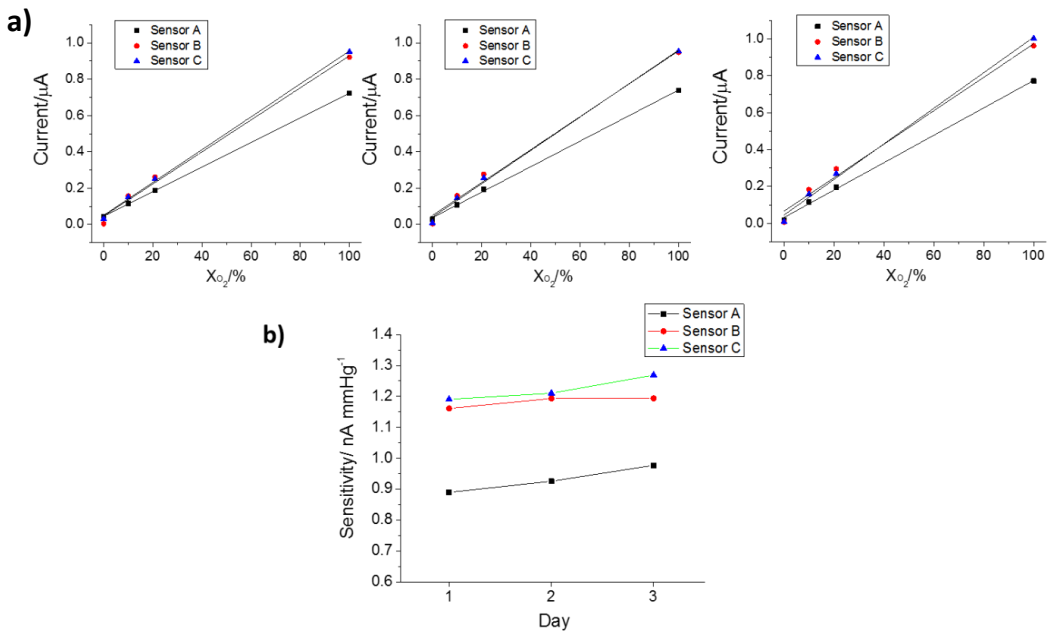

Figure 4.4. Stability of the PO_2 sensing catheters over 3 d: a) calibration curve of three sensors on different days with continuous NO generation/release; b) summary of the change in sensitivity over 3 d period for each of the three sensors.

In benchtop studies, the sensors exhibited stable amperometric calibrations during storage at 37 ℃ over 3 d with continuous NO generation/release (Figure 4.4). The response time of the PO_2 sensors were ca. 7 min (Figure 4.5), primarily determined by the dimensions (e.g., wall thickness) of the dual lumen catheters employed in these studies. Although not ideal, this response time is sufficient to be clinically useful, especially compared to the current situation where PO_2 can only be measured *ex-vivo* using samples of fresh blood. The response time for standard Clark-type O_2 sensor also depends on the dimension of the sensor (membrane thickness, distance between the electrode to the membrane etc.), but since the membranes can be very thin for *ex-vivo* sensors, the response times of these devices are generally 1 min or so. This is not possible when the wall of the

catheter is being used as the gas permeable membrane, since wall thickness needs to be large enough to provide the catheter mechanical strength to be placed within a blood vessel.

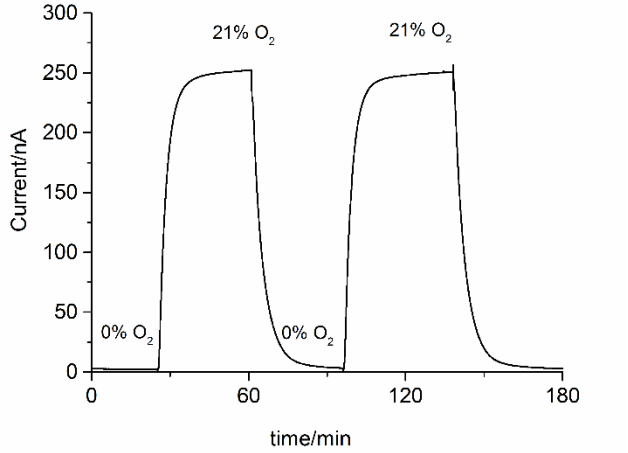

Figure 4.5. Typical reversible response of the electrochemical NO generation PO_2 sensing catheter under investigation.

The NO release of such devices was also examined. The sensing catheters released NO, as measured by chemiluminescence measurements,[27] at an average surface flux of $>1.0 \times 10^{-10}$ mol min^{-1} cm^{-2} (based on the area inserted in blood vessels) for 72 h, which is more than sufficient for the short-term proof-of-concept studies reported here (see Figure 4.6). The duration of the NO release in these particular devices is limited primarily by the small volume of the NO generation reservoir solution containing nitrite ions (~30 μL). The duration of NO generation/release can be readily extended, if necessary, by increasing the volume or concentration of sodium nitrite within the reservoir. It has been shown that devices that have a larger reservoir (using longer catheters) can exhibit NO release at relevant fluxes for >7 d.[22] This provides a simple solution for extending the NO release

duration since only a relatively small portion of the device needs to reside within the blood vessels. The surface region of NO release can be controlled by situating the active NO generating electrode near the distal end where the catheter is implanted within the blood vessel.[22] Increasing the concentration of nitrite in the reservoir without changing the volume, though effective for longer-term NO release, is limited by the further increase in osmotic pressure, which could potentially compromise the stability of the device over longer-term use.

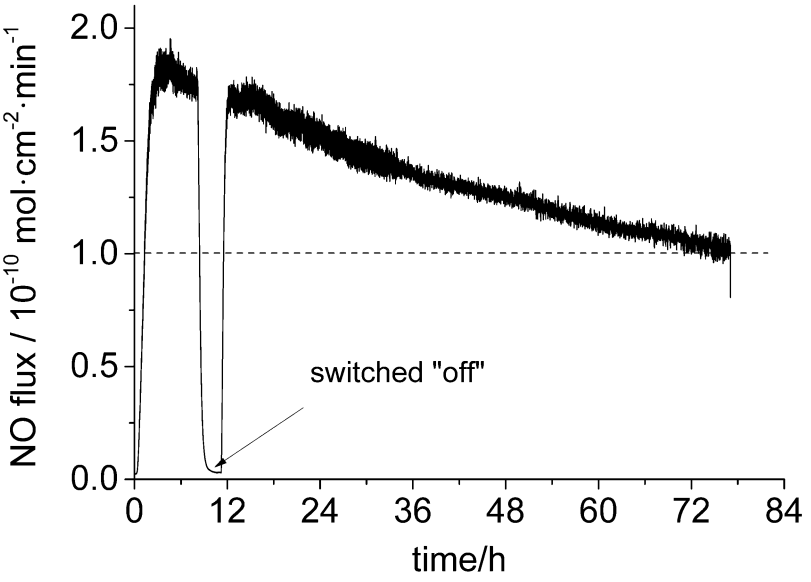

Figure 4.6. NO release profile from an electrochemical NO generation/release PO_2 sensing catheter. NO release was switched "off" at ~ the 8th h to demonstrate the control of the release.

4.3.3 Sensor Performance In Vivo

The catheter-type PO_2 sensors were first studied in rabbit veins over a 7 h period. The sensors were purposely challenged with lower venous PO_2 levels during the latter period of the experiment, by switching the FiO_2 from 100% to 21%. The NO releasing

sensors measured the PO_2 levels accurately and are able to follow both the decrease of PO_2 at the ~4 h time point and the recovery of PO_2 at the ~5.5 h time point (see Figure 4.7a as representative example). In contrast, the signal from the control sensors started to deviate negatively during the latter time period of the experiment, and although the sensors responded to a decrease of PO_2 at ca. the ~4 h mark, the levels measured were not accurate (negative deviation from *in vitro* blood-gas instrument values) and the responses were not able to fully recover back when the PO_2 was changed to the higher level via increasing the FiO_2 level. This was due to the formation of the large blood clots on the control sensor (see Figure 4.7b, as example). Thrombus formation around the catheter surface can create a local environment that has lower O_2 level because of the consumption of oxygen by platelets and other cells within the clot.[9] Overall, the NO releasing sensors induce less clot formation than the control sensors as measured by imaging the surface of the catheters after explantation from the rabbit after 7 h (see Figure 4.7c for data for n = 5 rabbits, $p < 0.05$).

Since the PO_2 level is different within each individual animal at different time points, the accuracy of the sensors was evaluated by quantitating the deviations (**Dev**) of the PO_2 values provided by the sensors vs. those provided from the *in vitro* blood sample PO_2 measurements at the same time point, assuming the *in vitro* measured values are 100% accurate. The deviation can be calculated as:

$$\textbf{\%Dev} = ((PO_{2\ \text{sensor}} - PO_{2\ \text{reference}})/PO_{2\ \text{reference}}) \times 100$$

where $PO_{2\ \text{sensor}}$ is the measured PO_2 from catheter-type sensors and $PO_{2\ \text{reference}}$ is the measured PO_2 from the blood gas analyzer using the discrete blood samples. In general, the NO releasing sensors showed deviations within ±15% and the differences are not significant at each time point ($p > 0.2$, n = 5 rabbits, Figure 4.7d), while the control sensors

exhibited significant negative deviations at time points >4 h after they were implanted within veins ($p < 0.05$, n = 5 rabbits, Figure 4.7d). It should be noted that venous PO_2 values are typically much lower and encompass a relatively narrow range (25–50 mmHg) compared to arterial blood (see below for porcine experiments). Small changes in the venous PO_2 values provide information about tissue perfusion.[28] The effective functionality of NO releasing PO_2 catheter sensors within veins has not been evaluated previously.

For testing the proposed sensors *in vivo* over longer time periods and over a wider range of PO_2 levels, the catheter sensors were further implanted within pig arteries for 21 h. Again, the FiO_2 was varied between 100% and 21% to challenge the sensors with different arterial PO_2 levels *in vivo*. As in the rabbit experiments, the sensors with electrochemical NO release followed the changes in PO_2 more accurately and reversibly while the control sensors without NO generation turned "on" start to exhibit negative deviations from *in vitro* measured PO_2 levels after 6 h (Figure 4.8a). Overall, the NO releasing sensors provided more reliable PO_2 values for the entire 21 h *in vivo* experiments (n = 4 pigs, $p > 0.1$ at each time point) while the controls sensors, after 6 h of implantation, showed a significant negative deviation of >20% at almost every time point (n = 4 pigs, $p < 0.05$ at each time point except for the 16th h, see Figure 4.8b). Note that the ability to follow active modulation of PO_2 in both veins and arteries were demonstrated for the first time for these new NO releasing PO_2 sensors.

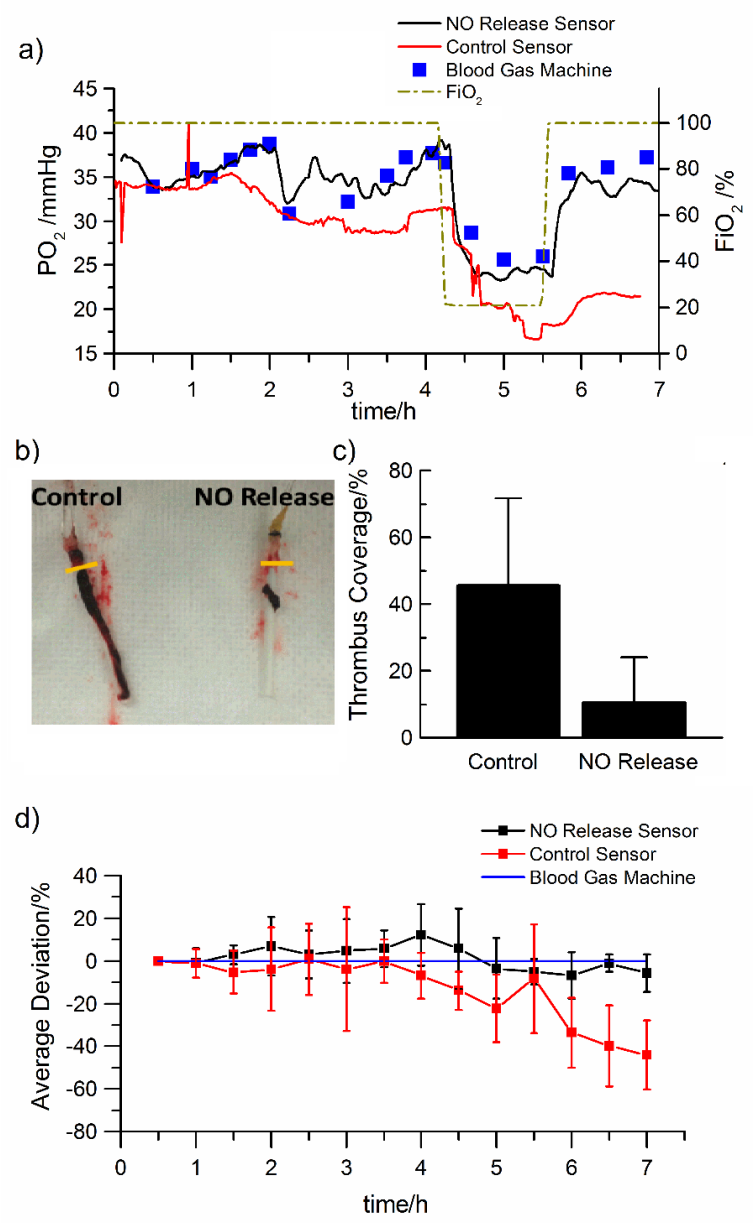

Figure 4.7. Performance of electrochemical NO generating/releasing PO_2 sensors implanted in rabbit veins for 7 h: a) representative response for a NO releasing sensor (black) and a control sensor (red) compared with blood draw *in vitro* test values (blue square); the FiO_2 levels were changed purposely between 100% to 21% (dash dot) to vary venous PO_2; b) representative photo illustrating the degree of clot formation on the surface of the control and the NO releasing sensors after being explanted; c) average thrombus coverage on NO releasing sensors vs. control sensors (n = 5 rabbits, $p < 0.05$); d) average deviation of the NO releasing sensors (black) and control sensors (red) from the reference method (blue). Error bars indicate standard deviations.

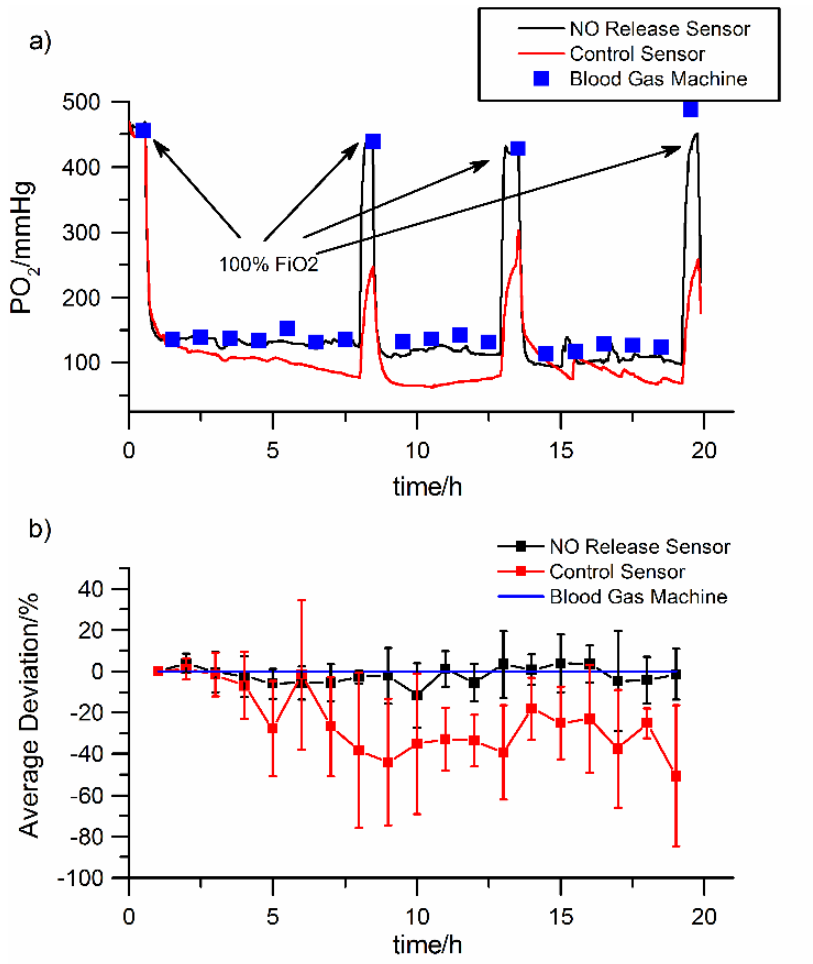

Figure 4.8. Performance of electrochemical NO generating/releasing PO_2 sensors implanted in pig arteries for 21 h: a) representative current response for a NO releasing sensor (black) and a control sensor (red) compared with blood draw *in vitro* test values (reference method, blue square). Arrows indicate where FiO_2 changes from 21% to 100%; b) average deviation of the NO release sensors (black) and control sensors (red) from the reference method (blue). Error bars indicate standard deviations.

The measurements from both rabbit veins and pig arteries can also be combined and compared with the reference method to assess their overall analytical performance *in vivo* (see Figure 4.9). Data points after the 4 h time point in the rabbits and after the 6 h time point in pigs were included in the comparison, since it generally takes time to observe

the lowered analytical results for the control sensors (accumulation of clots/thrombus takes time). The NO releasing sensors exhibited good correlation ($R^2 = 0.97$) and accuracy for PO_2 measurements with an average deviation of $-2 \pm 11\%$, whereas the control sensors yielded much poorer correlation ($R^2 = 0.43$) and a deviation of $-31 \pm 28\%$. Based on the periodic blood sample tests as reference method (n = 84), 96% of the measurements from NO generating/releasing sensors were within ±20% error, while only 32% of the measurements from control sensors were within ±20% error (Figure 4.9). Linear regression was performed on these measurements to obtain slopes for the results from the electrochemical PO_2 sensors vs. those from the reference *in vitro* measurement method. The electrochemical NO releasing sensors yielded a slope of 0.90 (not shown in Figure 4.9 for clarity), indicating good overall accuracy. The control sensors, in contrast, exhibited a slope of 0.51, indicating an overall 49% suppression of the signals. Again, this is most likely due to thrombus formation and concomitant entrapped metabolically active cells on the surfaces of the control catheters.

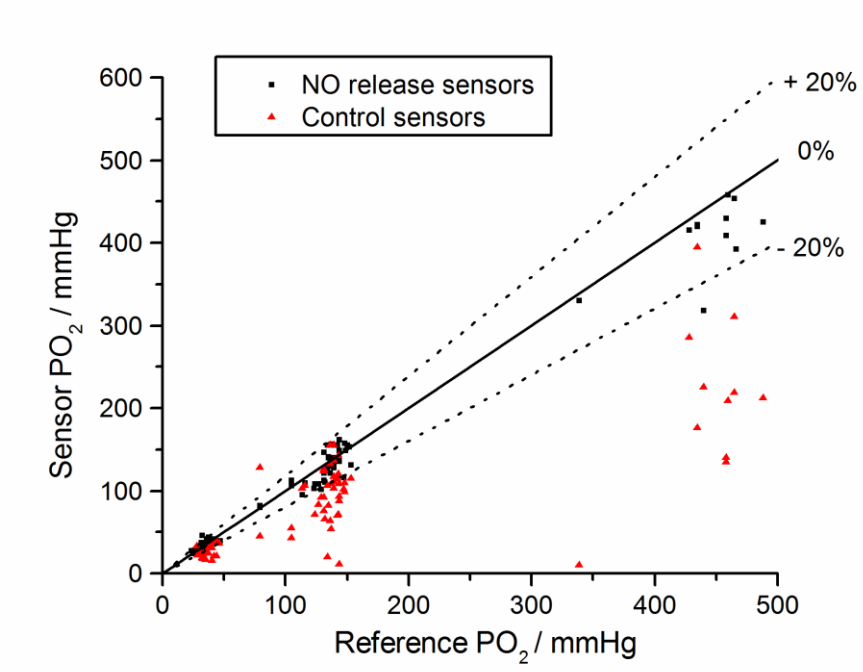

Figure 4.9. Comparison of measured PO_2 from catheter-type sensors *in vivo* vs. reference method from blood samples. Data contain all the measurements > 4 h time point in rabbit experiments and > 6 h time point in pig experiments. Black squares represent results from the NO generating/releasing sensors. The red triangles represent the measurements from the control sensors. Dash lines and solid line indicate ±20% error and 0% error, respectively.

4.4 Conclusions

Catheter-type amperometric PO_2 sensors incorporating a novel electrochemical NO generating/release system have been developed. These NO releasing sensors were implanted in both veins and arteries of animal models for up to 21 h and yield less clot formation and more accurate analytical results. This method could provide a general strategy for improving the hemocompatibility of a wide variety of blood contacting sensors/devices. Further, owing to the potent antimicrobial properties of NO,[29] such electrochemical NO generating devices could also greatly lower the risk of infection, which

is another major issue with intravascular sensors and other devices, especially when the dwelling time is longer than 24 h. It is envisioned that low level of NO can be used to prevent clotting but can be increased for short periods (3 h per day etc.) to better kill bacteria.[21] This can be readily achieved by the new electrochemical NO release system investigated in this study. Longer-term (7 d) *in vivo* investigation of the new IV-PO_2 sensor design in freely-moving animals are currently being planned.

4.5 References

(1) Bloom, B. M.; Grundlingh, J.; Bestwick, J. P.; Harris, T. *Eur. J. Emerg. Med.* **2014**, *21*, 81.

(2) Shapiro, N. I.; Howell, M. D.; Talmor, D.; Nathanson, L. A.; Lisbon, A.; Wolfe, R. E.; Weiss, J. W. *Ann. Emerg. Med.* **2005**, *45*, 524.

(3) The Juvenile Diabetes Research Foundation Continuous Glucose Monitoring Study Group; *N. Engl. J. Med.* **2008**, *359*, 1464.

(4) Martin, D. S.; Grocott, M. P. W. *Crit. Care Med.* **2013**, *41*, 423.

(5) Frost, M. C.; Wolf, A. K.; Meyerhoff, M. E. In *Detection Challenges in Clinical Diagnostics*; The Royal Society of Chemistry, 2013, pp 129.

(6) Ganter, M.; Zollinger, A. *Br. J. Anaesth.* **2003**, *91*, 397.

(7) Wilson, G. S.; Gifford, R. *Biosens. Bioelectron.* **2005**, *20*, 2388.

(8) Hu, W.-J.; Eaton, J. W.; Ugarova, T. P.; Tang, L. *Blood* **2001**, *98*, 1231.

(9) Wu, Y.; Meyerhoff, M. E. *Talanta* **2008**, *75*, 642.

(10) Burns, K. E. A.; McLaren, A. *Can. Respir. J.* **2009**, *16*, 163.

(11) Vaughn, M. W.; Kuo, L.; Liao, J. C. *Am. J. Physiol. Heart Circ. Physiol.* **1998**, *274*, H2163.

(12) Wang, G.-R.; Zhu, Y.; Halushka, P. V.; Lincoln, T. M.; Mendelsohn, M. E. *Proc. Natl. Acad. Sci. U. S. A.* **1998**, *95*, 4888.

(13) Förstermann, U.; Sessa, W. C. *Eur. Heart J.* **2012**, *33*, 829.

(14) Frost, M. C.; Rudich, S. M.; Zhang, H.; Maraschio, M. A.; Meyerhoff, M. E. *Anal. Chem.* **2002**, *74*, 5942.

(15) Wu, Y.; Rojas, A. P.; Griffith, G. W.; Skrzypchak, A. M.; Lafayette, N.; Bartlett, R. H.; Meyerhoff, M. E. *Sens. Actuators, B Chem.* **2007**, *121*, 36.

(16) Yan, Q. Y.; Major, T. C.; Bartlett, R. H.; Meyerhoff, M. E. *Biosens. Bioelectron.* **2011**, *26*, 4276.

(17) Shin, J. H.; Schoenfisch, M. H. *Analyst* **2006**, *131*, 609.

(18) Schoenfisch, M. H.; Mowery, K. A.; Rader, M. V.; Baliga, N.; Wahr, J. A.; Meyerhoff, M. E. *Anal. Chem.* **2000**, *72*, 1119.

(19) Marxer, S. M.; Robbins, M. E.; Schoenfisch, M. H. *Analyst* **2005**, *130*, 206.

(20) Keefer, L. K. *Annu. Rev. Pharmacool. Toxicol.* **2003**, *43*, 585.

(21) Williams, D. L. H. *Acc. Chem. Res.* **1999**, *32*, 869.

(22) Ren, H.; Wu, J.; Xi, C.; Lehnert, N.; Major, T.; Bartlett, R. H.; Meyerhoff, M. E. *ACS Appl. Mater. Interfaces* **2014**, *6*, 3779.

(23) Ren, H.; Colletta, A.; Koley, D.; Wu, J.; Xi, C.; Major, T. C.; Bartlett, R. H.; Meyerhoff, M. E. *Bioelectrochemistry* **2015**, *104*, 10.

(24) Schneider, C. A.; Rasband, W. S.; Eliceiri, K. W. *Nat. Methods* **2012**, *9*, 671.

(25) Zacharia, I.; Deen, W. *Ann. Biomed. Eng.* **2005**, *33*, 214.

(26) Lewis, R. S.; Deen, W. M. *Chem. Res. Toxicol.* **1994**, *7*, 568.

(27) Coneski, P. N.; Schoenfisch, M. H. *Chem. Soc. Rev.* **2012**, *41*.

(28) Soller, B. R.; Idwasi, P. O.; Balaguer, J.; Levin, S.; Simsir, S. A.; Salm, T. J. V.; Collette, H.; Heard, S. O. *Crit. Care Med.* **2003**, *31*, 2324.

(29) Schairer, D. O.; Chouake, J. S.; Nosanchuk, J. D.; Friedman, A. J. *Virulence* **2012**, *3*, 271.

CHAPTER 5.

DOSAGE EFFECT OF NITRIC OXIDE (NO) AND ITS SYNERGY WITH ANTIBIOTIC AGAINST PSEUDOMONAS AERUGINOSA BIOFILM USING CONTROLLED RELEASE OF NO FROM AN ELECTROCHEMICAL SYSTEM

5.1 Introduction

A multitude of chronic infections that arise from different medical situations, such as catheter related/induced infections,[1] patients with cystic fibrosis,[2] or endocarditis,[3] etc. are caused by *Pseudomonas aeruginosa* and its biofilms. Such infections are usually hard to cure, not only because this opportunistic pathogen itself often develops resistance towards a broad spectrum of antibiotics, but also because of its ability to form biofilms in different environments.[4,5] To date, treatment of bacterial biofilm-related infections in hospitals mostly relies on prolonged exposure to high-dosage antibiotics.[6] However, such antibiotic treatments alone are usually not successful because these conventional antibiotics more effectively target the planktonic cells instead of biofilm. Furthermore, overdose of antibiotics increases the risks of inducing multi-drug resistant strains or "superbugs" and other side effects.[7] For infections related to indwelling devices (e.g., catheters), the biofilms/devices eventually have to be physically removed. This infection challenge calls for new methods with capabilities to quickly eradicate bacterial biofilms while still ensuring safety to the host.

One proposed effective strategy is to use a small molecule—nitric oxide (NO), which is produced endogenously by the human immune system to fight bacterial infection during host defense.[8] Over the past decade, NO donors themselves as well as NO releasing materials have been investigated to either prevent biofilm formation or to remove existing biofilms.[9-17] However, these NO release strategies often have uncontrolled NO burst release, and sometimes result in complications from leaching of the NO donors themselves as well as their degradation products, which obscure the true effects of NO.[18,19] In addition, the effectiveness of short-term steady NO release at physiologically-safe fluxes against mature biofilms is not clear, though these fluxes, ranging from (0.5–4.0) $\times 10^{-10}$ mol min^{-1} cm^{-2} (0.5–4.0 flux), are frequently targeted for the development of many NO releasing implants, including catheters and stents.[20,21] Furthermore, the overall effect of NO at different fluxes, including the role of flux on the killing of bacteria and/or dispersal of biofilms, needs to be clarified. If the decrease in biofilm by NO release is mainly due to the detachment of live cells from the biofilm, the behavior of theses detached bacteria and the risk they pose to the host also needs further investigation. In addition to the anti-biofilm effect of NO, it has recently been found that endogenous NO produced by bacteria can protect them against antibiotics.[22] These intriguing yet different ways that bacteria interact with NO requires more careful study of the dosage effect so that effective control of bacteria via NO release can be developed.

In this study, to evaluate effects of NO at different dosages against bacterial biofilms, especially in the physiological flux range that is nontoxic to the host cells, we utilize a recently developed, highly controllable electrochemical NO release catheter system.[16] Using this catheter model we investigate the effect of different fluxes of NO

release on mature *P. aeruginosa* biofilms. The NO flux from the device surface can be controlled readily by applying different voltages across two wire electrodes within a lumen of the catheter containing nitrite ions and a copper(II)-complex. Herein, we demonstrate that short-term (3 h) NO release at low physiological flux is able to significantly reduce surface-attached mature biofilms. These levels of NO are also shown to display a synergic effect with gentamicin against the bacteria in biofilms.

5.2 Experimental Details

5.2.1 Catheter Fabrication and NO Release Profile Measurement

The procedures used were similar to those reported previously.[16,23] A single lumen silicone tube was cut to 6 cm in length and sealed at one end with silicone rubber adhesive. The lumen was filled with a solution containing 4 mM copper(II)-tri(2-pyridylmethyl)amine, 0.4 M $NaNO_2$, 0.2 M NaCl and 0.5 M HEPES buffer (pH 7.2). A Teflon® PFA-coated Pt wire (3 cm exposed) and a Ag/AgCl wire (5 cm exposed) were inserted into the lumen as working and reference electrodes, respectively. The openings of the lumens at the proximal end were then sealed (around the wires) with silicone rubber adhesive and left to cure in water overnight (see Figure 5.1). The NO release profile of the catheters was controlled by applying different voltages, and outer surface NO flux was measured with a Nitric Oxide Analyzer (Sievers 280i, GE Analytics, Boulder, CO), as reported previously.[24]

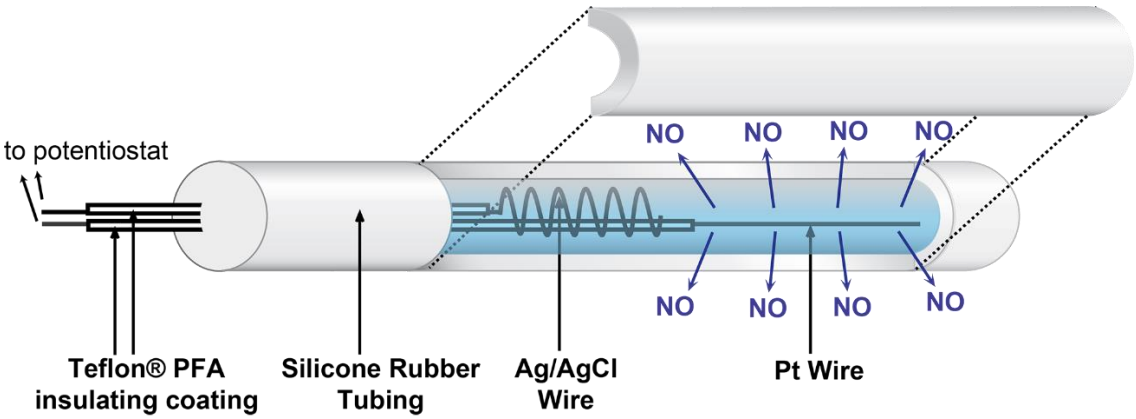

Figure 5.1. Schematic of the electrochemical NO releasing catheter employed in this study, with cutaway view showing the inside configuration of the catheter.

5.2.2 Bacterial Strain and Biofilm Growth

Pseudomonas aeruginosa PAO1 wild-type strain was obtained from University of Washington (UW Genome Sciences, Seattle WA).[25] The bacterial strain was maintained on Luria Bertani (LB) agar plate and grown in LB broth. Biofilm was developed in a CDC bioreactor (Biosurface Technologies, Bozeman, MT). Briefly, the electrochemical NO releasing catheters were fixed on the holders of CDC bioreactor. Four mL of overnight grown *P. aeruginosa* wild-type PAO1 culture were inoculated into the CDC bioreactor at final concentration about 10^6 CFU/mL and the CDC bioreactor was left still for 1 h before introducing fresh 10% LB media at 100 mL/h using a peristaltic pump and starting the magnetic stirrer to generate shear force. The biofilms were allowed to develop in the bioreactor for 7 d at 37 ℃, and the catheter pieces were then taken out aseptically from the reactor and gently rinsed in sterile PBS to remove any loosely attached bacteria. The catheters were then subject to NO induced bacteria dispersal studies.

5.2.3 Microscopic Observation

The catheters with 7 d grown biofilm were placed in a convertible flow cell (CFCAS0003, Stovall Life Science, Greensboro, NC) and the two ends of catheters were secured on surface by water-proof glue in order to observe the surface biofilm with a microscope. LB broth (10%) was continuously provided to the flow cell by a peristaltic pump at a flow rate of 10 mL/h. Biofilm dispersal was monitored using a fluorescence microscope (Olympus IX71, Center Valley, PA) equipped with Fluorescence Illumination System (X-Cite 120, EXFO) and appropriate filter sets. Image and video were obtained using an oil immersion 60× objective lens.

5.2.4 Dose-Response Studies of NO on 7 Day Biofilms

The catheters with 7 d biofilms were transferred into 5 mL of PBS in a 15-mL corning centrifuge tube. The wires of the catheters were connected to a multi-channel potentiostat (1000C, CH Instrument, Austin, TX), with the platinum wire connected to the working electrode lead, and the silver wire to the reference and counter leads. The NO release was then turned "on" for 3 h, by applying the voltages required to achieve the flux desired (e.g., -0.22 V for 0.3 flux, -0.23 V for 0.5 flux, -0.26 V for 1.2 flux, -0.275 V for 1.5 flux, and -0.325 V for 3.0 flux).[16] The solution remained static during the experiment. After 3 h of NO release, the viable bacterial cells on the catheter surfaces were quantified by plate counts. Briefly, the catheters were taken out of the PBS and the inner filling solutions of the catheters were carefully removed using a syringe from the rear side of the catheters. Three cm of the catheter was cut off into a 2 mL of fresh PBS and homogenized with the highest speed (TH, OMNI International, Kennesaw, GA) and the homogenized

buffer was serially diluted by 10-fold each time with PBS. Fifty μL of each dilution was plated onto LB agar plates and the plates were incubated overnight at 37 ℃ for colony counting.

The bacteria released to the buffer media during the 3 h NO release experiment were also quantified as described above. The buffer media was homogenized before serial dilutions and plate counts. The catheter samples at each flux level were run in triplicate and Student's t-test was used for statistical analysis.

5.2.5 Susceptibility Tests of Planktonic Cells towards NO and/or Gentamicin

A set of NO release catheters were placed in PBS with ~10^7/mL overnight grown bacteria and NO release was turned "on" for 3 h and 24 h without stirring. The control catheters were set up the same way except that the NO release was turned "off". The bacteria in the PBS were quantified by plate count following the same protocol as described above.

5.2.6 Combination of NO Release with Antibiotic Treatment

The experimental procedures of this study were similar to that of the dosage response study described above. The biofilm attached catheters were placed in PBS with varying concentration of gentamicin (ranging from 0 to 500 μg/mL) and the NO was turned "on" at 1.5 flux immediately after being submerged in buffer. After 3 h treatment, the bacteria remaining on the catheter pieces as well as those within the media were quantified by plate counting as described above.

To further demonstrate the resistance of biofilm-detached cells to gentamicin, the catheters with preformed biofilms were also placed in PBS without gentamicin/NO release first for 3 h. Then, the buffers soaking the catheter was further homogenized as described above and treated with gentamicin of varied concentrations (0-500 μg/mL) for another 3 h. Plate counts of the soaking solutions were again performed as described above.

5.3 Results

5.3.1 Nitric Oxide Release Profile of the Catheters

The real time NO release profile of the electrochemical NO release catheters was tested via chemiluminescence as described in the Material and Methods section. As shown in Figure 5.2, these catheters exhibit a very steady NO release profile under a given constant applied voltage. Furthermore, the flux of NO from the catheter surface could be readily modulated in the range from 0–3.2 flux, simply by applying different voltages to the electrode wires. The ability of such modulation allows biofilms to be grown without release of NO from the catheter, while a given amount/flux of NO release can be turned "on" at appropriate times thereafter as defined by the study.

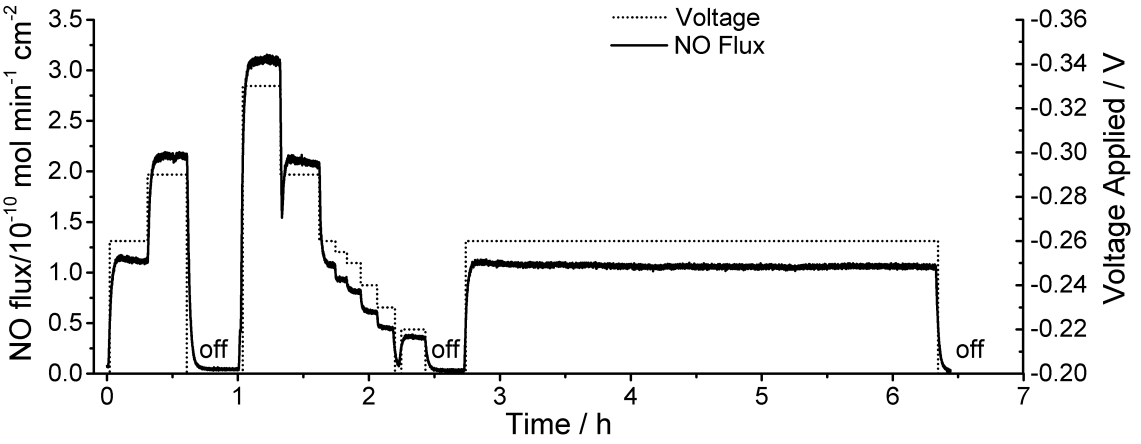

Figure 5.2. Modulation of surface NO fluxes from an electrochemical NO releasing catheter by different applied voltages applied to the metal wire electrodes.

5.3.2 Dosage Effect Studies of NO on 7 Day Biofilms

The effect of NO on mature 7 d *P. aeruginosa* biofilms formed on the catheter surface was monitored under microscope in real-time. The procedures are summarized Figure 5.3A. During the 3 h when the NO was turned "on" at 1.5 flux, the coverage of bacterial biofilms became significantly less dense (Figure 5.3B), suggesting that the NO release prompted the dispersal of biofilms from the catheter surface. The biofilms on the control device, a catheter containing the same solutions and wires but not connected to the potentiostat, remained mostly intact (Figure 5.3C).

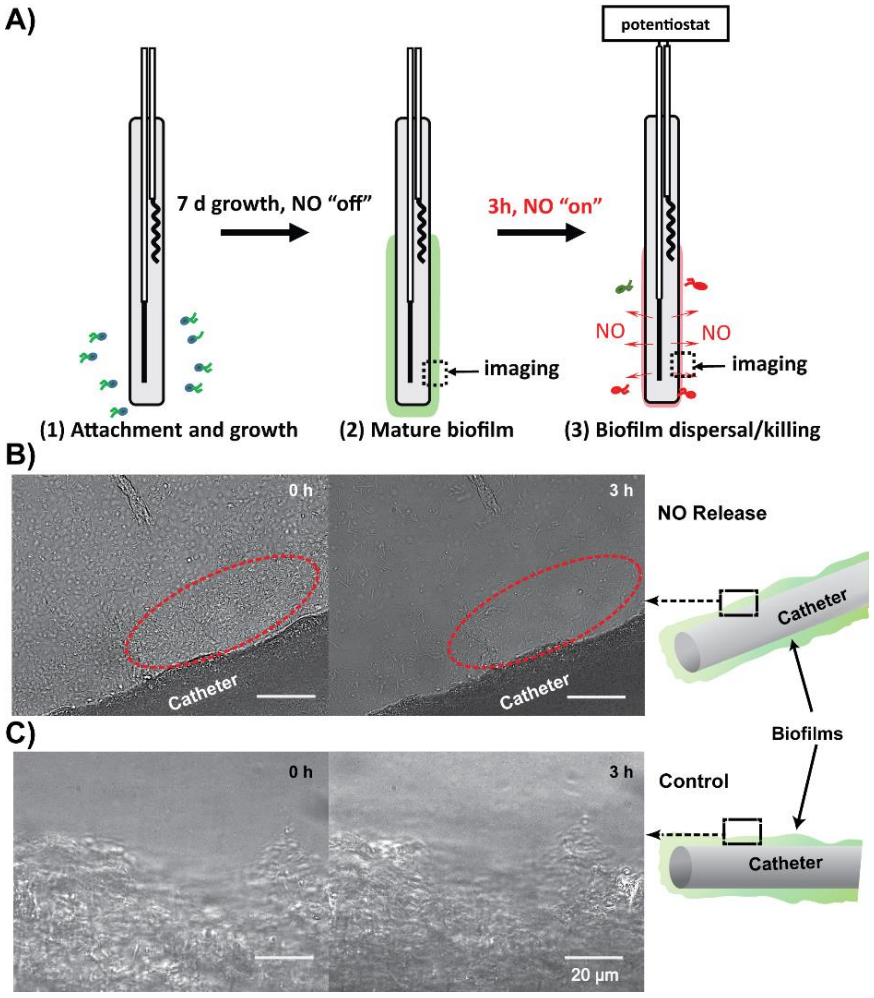

Figure 5.3. Imaging 7 d *P. aeruginosa* biofilms with 3 h of NO release at surface flux of 1.5×10^{-10} mol min^{-1} cm^{-2}: A) Illustration of the experiment procedure and areas on the catheter that are under imaging; B) representative images of NO release catheter and its biofilm at 0 and 3 h; C) representative images of control catheter and its biofilm at 0 and 3 h.

As shown in Figure 5.3, 3 h NO release at 1.5 flux resulted in dispersing mature biofilms from the catheter surface. To evaluate the effects of different surface NO flux levels on mature biofilms, catheters with 7 d preformed *P. aeruginosa* biofilms grown onto the catheter surfaces were transferred into fresh PBS before different NO fluxes were turned "on" electrochemically. After NO was released for 3 h at given fluxes, both the

bacteria on the catheter surfaces (in biofilms) and those detached/dispersed into the PBS media were quantified by viable plate counts. On the catheter surfaces, NO release at 0.3 flux for 3 h reduced the attached bacteria by 86%, and the effects became stronger as the NO flux was increased, reaching a 3 log reduction with NO flux > 1.5 flux (see Figure 5.4 and Table 5.1). During 3 h experiments without NO release, a small portion of the bacteria in the biofilms detached spontaneously into the media (about 3.5%, see Table 5.1). With NO release at 0.3 flux, the number of viable bacteria in the media increased by 88% on average as compared to the control, revealing a significant biofilm dispersal effect of the electrochemically released NO. Overall, the number of total viable cells decreases both on catheter surfaces and in media as the NO flux increases (Table 5.1), indicating a simultaneous dispersing and killing effect with increased NO flux.

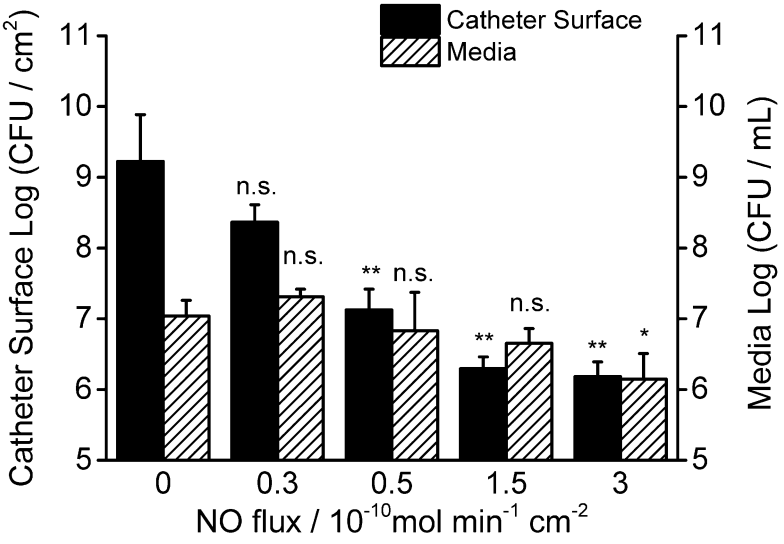

Figure 5.4. Dosage response of 3 h NO release on 7 d *P. aeruginosa* biofilms. Viable bacteria counts A) on the surface of catheters and B) within the media after NO release for 3 h in the PBS. Asterisk denotes statistical significance at each flux compared with 0 flux (n.s.: $p > 0.05$, * $p < 0.05$, ** $p < 0.01$).

Table 5.1. Effect of NO flux on dispersing and killing of mature 7 d *P. aeruginosa* biofilms.

NO flux /10^{-10} mol min^{-1} cm^{-2}	**0**	**0.3**	**0.5**	**1.5**	**3.0**
Attached viable cells	96.5%	13.4%	0.8%	0.1%	0.1%
Detached viable cells	3.5%	6.6%	2.2%	1.4%	0.5%
Total viable cells	100.0%	20.0%	2.9%	1.6%	0.5%

5.3.3 Killing Kinetic Studies on Biofilm and Planktonic Cells

Since NO is effective in reducing bacteria in mature biofilms on the catheter surface after such a short period of exposure (3 h), we studied the kinetics of killing with 1.5 flux of NO. As can be seen in Figure 5.5 (left two columns), approximately a 2 log unit decrease in the number of surface viable bacteria was observed after 3 h and an additional 1 log decrease was obtained after 24 h of NO release treatment.

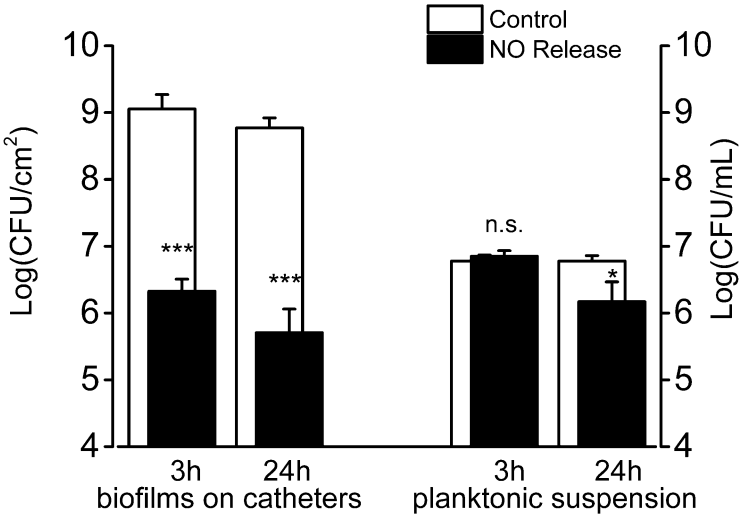

Figure 5.5. Effect of 3 h and 24 h NO release (1.5 flux unit) treatment towards *P. aeruginosa* biofilms (7 d) on the catheters and its planktonic counterparts in the PBS. Asterisk denotes statistical significance (n.s.: $p > 0.05$, * $p < 0.05$, ** $p < 0.01$, *** $p < 0.001$).

Such NO killing kinetics studies were also performed on the planktonic cells in PBS. After 3 h of NO release, no obvious killing was observed, wherease 24 h of NO release killed 54% of bacteria (Figure 5.5, right two columns). The much less killing effect of NO towards planktonic cells is likely because the level of NO is the highest at the surface of the catheter, and diminishes rapidly within the bulk solution due to reaction of NO with oxygen and components of bacteria (proteins, etc.).[26-28]

5.3.4 Synergistic Effect of NO Release with Antibiotic

Since NO is less effective in killing bacterial cells in the media (as shown above), we next explored if more effective killing could be achieved by combining the NO release with conventional antibiotic treatment. We used gentamicin in this study, as this aminoglycoside has been previously employed in the treatment of gram-negative bacteria infections, including *P. aeruginosa*.[29] The catheters with mature *P. aeruginosa* biofilms were placed in PBS containing different concentrations of gentamicin (ranging from 0-500 μg/mL), and NO release was controlled electrochemically. Without NO release (control), bacteria in the biofilms were highly resistant towards gentamicin at concentrations up to 500 μg/mL, with less than a 1 log reduction (see Figure 5.6A). As a control, the *P. aeruginosa* planktonic cells were completely eradicated (> 7 log reduction) in 3 h at 500 μg/mL (Figure 5.6B), confirming previous studies in the literature[30] that cells in biofilms are much less susceptible to antibiotic treatment. However, a significant synergistic effect was observed when NO release was combined with gentamicin. Release of NO at 1.5 flux, together with 25 μg/mL gentamicin in the buffer resulted in a combined ca. 3 log reduction

of the surface viable cells. The effect was enhanced further to > 3 log reduction with 100 μg/mL gentamicin and close to a 5 log reduction with 500 μg/mL gentmicin (Figure 5.6A).

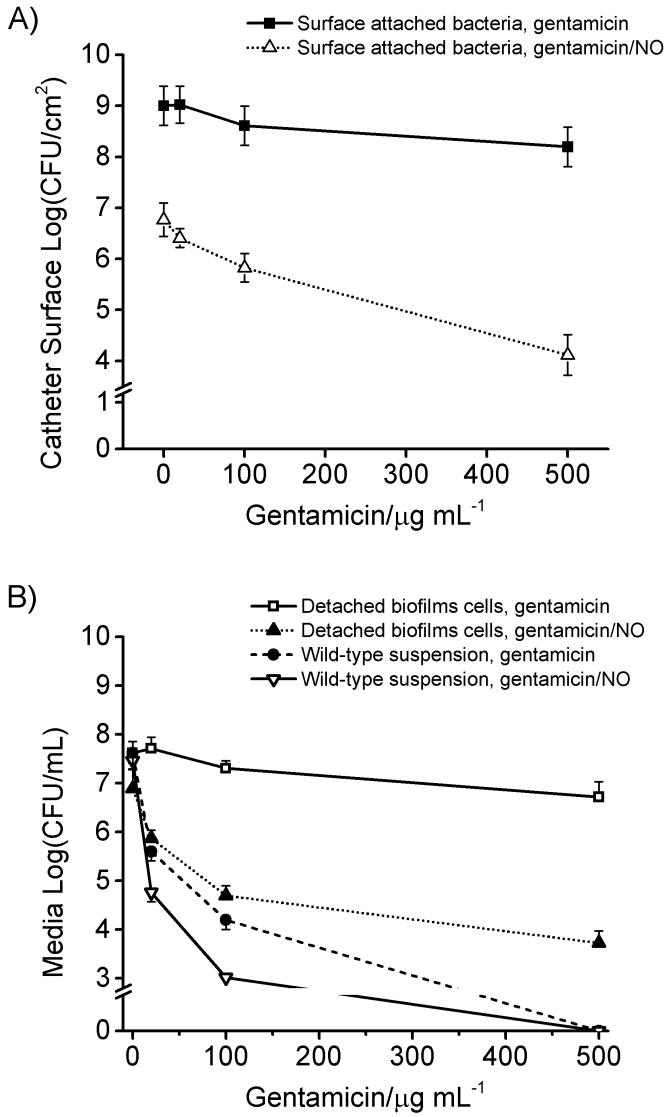

Figure 5.6. Combination of NO release with different concentrations of gentamicin against 7 d *P. aeruginosa* biofilms. A) Surface attached bacterial biofilm after 3 h treatment of gentamicin (gentamicin), and gentamicin with simultaneous NO release at 1.5 flux (gentamicin/NO); B) biofilm-detached/released bacteria vs. planktonic suspension control in the media with different treatments: 3 h exposure to different concentration of gentamicin (gentamicin); 3 h NO release at 1.5 flux in the presence of varied concentration of gentamicin (gentamicin/NO).

The synergistic effect between NO and genamicin was also investigated towards the cells detached/released into the media from the biofilms. Without NO release, the detached/released cells in the media were highly resistant to gentamicin over the entire concentration range investigated (< 0.5 log reduction with up to 500 μg/mL gentamicin treatment) (Figure 5.6B, solid line with square). Similar resistance was also observed even when the detached/released cells were homogenized first before the antibiotic treatment (data not shown), which is in contrast to the high suspectibility of the wild-type planktonic cells in the media (Figure 5.6B, dash line with solid circle). However, this resistance was significantly reduced when gentamicin was combined with simultaneous NO release, with almost a 2 log reduction of the viable cells when 25 μg/mL of gentamicin was combined with a 1.5 flux of NO. (Figure 5.6B) The reduction was further enhanced to > 3 log unit when 100 and 500 μg/mL of gentamicin was combined with NO at the same flux, indicating a significant synergistic effect of gentamicin and NO (Figure 5.6B, dotted line with triangle).

Release of NO also enhances the killing efficacy of gentamicin against planktonic suspension of *P. aeruginosa,* leading to an additional 1 log reduction of the cells at 25 and 100 μg/mL of gentamicin when NO was simultaneously released at 1.5 flux (Figure 5.6B, solid line with triangle).

5.4 Discussion

5.4.1 Killing Effect of NO on Biofilms on the Surface vs. Planktonic Cells in the Media

For the biofilms attached to the catheter surface, it was found that the higher the flux of NO release, the less viable bacteria remained on the surface (Figure 5.4). The wild-

type *P. aeruginosa* expresses NO reductase (*nor*) in the biofilms, which is believed to prevent the accumulation of "toxic" NO during denitrification.[31] In this study, we found that the exogenous NO release in the physiological range is still effective in killing such bacteria within the biofilms. On the other hand, the planktonic cells in the media (both the planktonic suspension as well as the cells detached/released by the biofilms) exhibits less susceptibility to the NO release (Figure 5.4 and Figure 5.5). Overall, the NO release at 0.3 to 3.0 flux units can effectively decrease the total viable bacteria on surfaces and bacteria detached in the surrounding solution and its killing effect is positively correlated with NO dosage (Table 5.1).

5.4.2 Modeling of the Transport of NO

The reduced killing efficacy displayed by the similar fluxes of NO against planktonic cells in the media vs. cells in the biofilms is quite interesting. There are several potential explanations for this. First, because NO is released constantly from the surface of the catheter, the concentration of NO should be highest immediately adjacent to the surface. This is where the bacterial cells are attached and the level of NO decreases as distance from the catheter increases. Secondly, the lower diffusivity of gases in the biofilm matrix might lead to the further accumulation of NO locally near the catheter's surface.[5] Further, deep inside the biofilms, the environment is usually near anoxic; this means that loss of NO by reaction with O_2 will be reduced, resulting in a higher effective NO concentration than within an ambient air environment. To investigate all these effects, a 1-D axial symmetry model was set up and the diffusion equations were solved by numeric simulation under each condition (Figure 5.7A). Indeed, all these hypotheses were verified

by the simulation. Under all conditions investigated, NO concentration is highest at the catheter surface and decreases as the distance to the catheter surface increases (Figure 5.7B). When the diffusivity was set to 60% of the that in water in ambient air environment to represent the diffusion in biofilms [5], the accumulation effect is observed, with increases of 22% and 9% in the NO concentration at the catheter surface and 100 μm away from the catheter surface, respectively (Figure 5.7B). When the O_2 environment was switched from ambient to anoxic, a 1.7× increase in NO concentration is predicted on the catheter surface (Figure 5.7B).

On the other hand, under ambient air, NO concentration at 1 mm away from the catheter is only ~5% of that on the catheter surface after 5 min of NO release. This means bacteria in the bulk of the media are exposed to far less effective NO and, therefore, are not susceptible towards the NO killing effect. It should be noted that this model only considers the diffusion and reaction of NO with O_2 and neglects the complications from uptake of NO by the bacteria as well as other reactions. However, these complications should not change the qualitative effects predicted by the model.

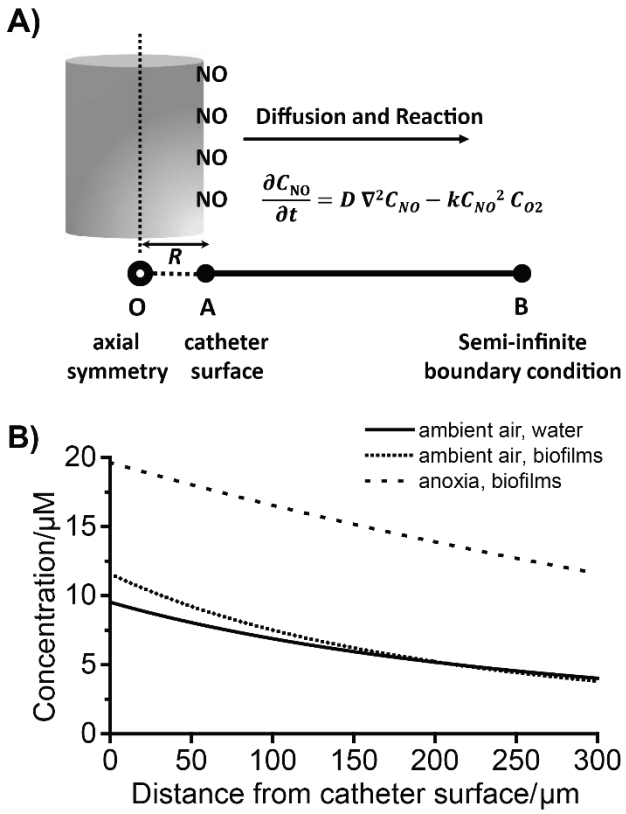

Figure 5.7. Effect of O_2 environment and diffusivity of NO on the NO concentration profile near the catheter surface via simulation. A) Illustration of the 1-D axial symmetry model. Point O represents axial symmetric line for the catheter; Point A is catheter surface where constant NO at 1.5 flux is released; Point B represents semi-infinite boundary condition where concentration of NO is 0. *R* is the radius of the catheter. B) NO concentration profile after NO release is "on" for 5 min: normal diffusivity (diffusivity in water) with ambient air (solid line); 60% diffusivity (slower diffusion in biofilms) with ambient air (short-dotted line) and 60% diffusivity in anoxic environment (deep inside biofilms, dashed line).

5.4.3 Synergistic Treatment Effect of NO Release and Gentamicin

The synergistic effect between NO and biocides has previously been shown in the treatment of gram-positive and gram-negative planktonic bacteria[32] as well as multi-species biofilms from water distribution systems.[10] Controversially, endogenous NO

produced by bacteria also has been reported to increase the resistance of bacteria toward broad-spectrum of antibiotics.[22] In our study, the synergy between the NO and gentamicin treatment were observed in killing bacterial cells in biofilms, biofilm detached/released cells, as well as planktonic cells (Figure 5.6). Several mechanisms have been proposed regarding the aminoglycoside resistance in *P. aeruginosa*, including enzymatic modification (phosphorylation, acetylation, adenylation, etc.) of the aminoglycoside species,[33] changes in the membrane permeability,[34] and altered ribosome binding sites.[35] Evidence shows that NO can upregulate genes involved in energy metabolism.[36] Therefore, we postulate that NO increases the permeability of the membrane by increasing the metabolism, thereby accelerating the energy-dependent process of gentamicin uptake.[37] Detailed studies are warranted on how NO might modify the genes related to antibiotic-resistance and their expression, to better understand such a mechanism.

As indicated above, *P. aeruginosa* biofilms are highly resistant toward antibiotic treatment. What is surprising is that the cells detached/released from the biofilm have enhanced capacity for resisting gentamicin, regardless of whether they are aggregated together or suspended as single cells. This is in contrast to their planktonic counterparts. Since bacteria in biofilm are highly heterogeneous in genetics,[38] it is very likely that the detached/released cells have genetically mutated and become antibiotic resistant. Further investigation is needed to better understand and verify such a mechanism.

The results from this study also suggest that for the biofilm associated infections in hospitals, the challenge might not be just the biofilms themselves, which are notoriously hard to remove. The highly resistant cells released from the biofilms should also receive

attention, as these motile cells may circulate and grow inside the body to cause secondary or systemic infections while escaping from the traditional antibiotic treatments.

The fact that a very low amount of NO release is effective in removing the biofilms over a very short time period demonstrates a potent way to resolve the significant problem of biofilms that partially cause the large number of catheter associated infections that kills more than 20,000 patients in hospitals each year in the U.S. alone.[39] Indeed, the use of multi-lumen catheter devices in which one lumen is dedicated to the electrochemical NO release system utilized in these studies should be quite useful, even if the devices are turned "on" for NO release for only a few hours each day. For cystic fibrosis patients, where *P. aeruginosa* biofilms pose huge challenge, NO released from acidified nitrite has already been shown to be effective in reducing *P. aeruginosa* biofilms within the airways and lungs of patients afflicted with this disease.[40] However, acidified nitrite also produces nitrogen dioxide (NO_2), which is toxic towards both the host and the pathogens. In this case, inhalation of low dose NO from an electrochemical gas phase NO generation system should be an attractive alternative to treat this disease as the NO can be produced on demand and at a rate of release that can be carefully controlled electrochemically, potentially enabling in-home low-dose NO inhalation therapy for such patients.

5.5 Conclusions

Electrochemical NO release from a catheter tubing surface has been utilized to study NO's effect on mature *P. aeruginosa* biofilms. Dosage response studies revealed that a significant killing effect of NO at physiological fluxes ($>0.5 \times 10^{-10}$ mol min^{-1} cm^{-2}) occurs, reducing mature *P. aeruginosa* biofilms by more than 2 log units. In the absence

of NO, both the bacteria in the biofilms and those detached/released from the biofilms were highly resistant towards antibiotic treatment, but became more susceptible when exposed to NO. Synergy between NO and gentamicin was found against biofilm and detached cells. Up to a 6 log unit reduction of biofilms bacteria on the catheter surface was observed upon the combined exposure of the biofilms to a 1.5 flux of NO for 3 h and 500 μg/mL gentamicin. Such a combination of NO release with existing antibiotics might provide a potent treatment for infections caused by resistant bacteria. This study provides additional insight into the potential treatment of biofilm-related infections using various NO therapies alone or in combination with gentamicin.

5.6 References

(1) Cole, S. J.; Records, A. R.; Orr, M. W.; Linden, S. B.; Lee, V. T. *Infect. Immun.* **2014**, *82*, 2048.

(2) Folkesson, A.; Jelsbak, L.; Yang, L.; Johansen, H. K.; Ciofu, O.; Hoiby, N.; Molin, S. *Nat Rev Micro* **2012**, *10*, 841.

(3) Yilmaz, M.; Sunar, H.; Mert, A. *Infection* **2013**, *41*, 243.

(4) Werner, E.; Roe, F.; Bugnicourt, A.; Franklin, M. J.; Heydorn, A.; Molin, S.; Pitts, B.; Stewart, P. S. *Appl. Environ. Microbiol.* **2004**, *70*, 6188.

(5) Stewart, P. S. *J. Bacteriol.* **2003**, *185*, 1485.

(6) Aslam, S. *Am. J. Infect. Control* **2008**, *36*, S175.e9.

(7) Spellberg, B.; Guidos, R.; Gilbert, D.; Bradley, J.; Boucher, H. W.; Scheld, W. M.; Bartlett, J. G.; Edwards, J.; America, t. I. D. S. o. *Clin. Infect. Dis.* **2008**, *46*, 155.

(8) Bogdan, C. *Nat. Immunol.* **2001**, *2*, 907.

(9) Barraud, N.; Hassett, D. J.; Hwang, S.-H.; Rice, S. a.; Kjelleberg, S.; Webb, J. S. *J. Bacteriol.* **2006**, *188*, 7344.

(10) Barraud, N.; Storey, M. V.; Moore, Z. P.; Webb, J. S.; Rice, S. A.; Kjelleberg, S. *Microb Biotechnol* **2009**, *2*, 370.

(11) Hetrick, E. M.; Shin, J. H.; Paul, H. S.; Schoenfisch, M. H. *Biomaterials* **2009**, *30*, 2782.

(12) Schairer, D. O.; Chouake, J. S.; Nosanchuk, J. D.; Friedman, A. J. *Virulence* **2012**, *3*, 271.

(13) Sulemankhil, I.; Ganopolsky, J. G.; Dieni, C. A.; Dan, A. F.; Jones, M. L.; Prakash, S. *Antimicrob. Agents Chemother.* **2012**, *56*, 6095.

(14) Riccio, D. A.; Coneski, P. N.; Nichols, S. P.; Broadnax, A. D.; Schoenfisch, M. H. *ACS Appl. Mater. Interfaces* **2012**, *4*, 796.

(15) Cai, W.; Wu, J.; Xi, C.; Meyerhoff, M. E. *Biomaterials* **2012**, *33*, 7933.

(16) Ren, H.; Wu, J.; Xi, C.; Lehnert, N.; Major, T.; Bartlett, R. H.; Meyerhoff, M. E. *ACS Appl. Mater. Interfaces* **2014**, *6*, 3779.

(17) Colletta, A.; Wu, J.; Wo, Y.; Kappler, M.; Chen, H.; Xi, C.; Meyerhoff, M. E. *ACS Biomaterials Science & Engineering* **2015**, *1*, 416.

(18) Mowery, K. A.; Schoenfisch, M. H.; Saavedra, J. E.; Keefer, L. K.; Meyerhoff, M. E. *Biomaterials* **2000**, *21*, 9.

(19) Arora, D. P.; Hossain, S.; Xu, Y.; Boon, E. M. *Biochemistry* **2015**, *54*, 3717.

(20) Frost, M. C.; Reynolds, M. M.; Meyerhoff, M. E. *Biomaterials* **2005**, *26*, 1685.

(21) Ren, H.; Coughlin, M. A.; Major, T. C.; Aiello, S.; Rojas Pena, A.; Bartlett, R. H.; Meyerhoff, M. E. *Anal. Chem.* **2015**, *87*, 8067.

(22) Gusarov, I.; Shatalin, K.; Starodubtseva, M.; Nudler, E. *Science* **2009**, *325*, 1380.

(23) Ren, H.; Colletta, A.; Koley, D.; Wu, J.; Xi, C.; Major, T. C.; Bartlett, R. H.; Meyerhoff, M. E. *Bioelectrochemistry* **2015**, *104*, 10.

(24) Zheng, Z.; Ren, H.; VonWald, I.; Meyerhoff, M. E. *Anal. Chim. Acta* **2015**, *887*, 186.

(25) Winsor, G. L.; Lam, D. K. W.; Fleming, L.; Lo, R.; Whiteside, M. D.; Yu, N. Y.; Hancock, R. E. W.; Brinkman, F. S. L. *Nucleic Acids Res.* **2011**, *39*, D596.

(26) Poole, R. K.; Hughes, M. N. *Mol. Microbiol.* **2000**, *36*, 775.

(27) Tsukahara, H.; Ishida, T.; Mayumi, M. *Nitric Oxide* **1999**, *3*, 191.

(28) Kumita, H.; Matsuura, K.; Hino, T.; Takahashi, S.; Hori, H.; Fukumori, Y.; Morishima, I.; Shiro, Y. *J. Biol. Chem.* **2004**, *279*, 55247.

(29) Tam, V. H.; Kabbara, S.; Vo, G.; Schilling, A. N.; Coyle, E. A. *Antimicrob. Agents Chemother.* **2006**, *50*, 2626.

(30) Stewart, P. S.; Costerton, J. W. *Lancet* **2001**, *358*, 135.

(31) Kakishima, K.; Shiratsuchi, A.; Taoka, A.; Nakanishi, Y.; Fukumori, Y. *Biochem. Biophys. Res. Commun.* **2007**, *355*, 587.

(32) Privett, B. J.; Deupree, S. M.; Backlund, C. J.; Rao, K. S.; Johnson, C. B.; Coneski, P. N.; Schoenfisch, M. H. *Mol. Pharm.* **2010**, *7*, 2289.

(33) Wright, G. D. *Curr. Opin. Microbiol.* **1999**, *2*, 499.

(34) Mingeot-Leclercq, M.-P.; Glupczynski, Y.; Tulkens, P. M. *Antimicrob. Agents Chemother.* **1999**, *43*, 727.

(35) Shakil, S.; Khan, R.; Zarrilli, R.; Khan, A. *J. Biomed. Sci.* **2008**, *15*, 5.

(36) Barraud, N.; Schleheck, D.; Klebensberger, J.; Webb, J. S.; Hassett, D. J.; Rice, S. A.; Kjelleberg, S. *J. Bacteriol.* **2009**, *191*, 7333.

(37) Taber, H. W.; Mueller, J. P.; Miller, P. F.; Arrow, A. S. *Microbiol. Rev.* **1987**, *51*, 439.

(38) Stewart, P. S.; Franklin, M. J. *Nat Rev Micro* **2008**, *6*, 199.

(39) Klevens, R. M.; Edwards, J. R.; Richards, C. L.; Horan, T. C.; Gaynes, R. P.; Pollock, D. A.; Cardo, D. M. *Public Health Rep.* **2007**, *122*, 160.

(40) Major, T. A.; Panmanee, W.; Mortensen, J. E.; Gray, L. D.; Hoglen, N.; Hassett, D. J. *Antimicrob. Agents Chemother.* **2010**, *54*, 4671.

CHAPTER 6.

EXPERIMENTAL AND SIMULATION STUDIES OF TRANSPORT OF NO THROUGH BIOMEDICAL GRADE POLYMERS AND ITS EFFECT ON LOCAL NO FLUX DISTRIBUTION ON MEDICAL DEVICES

6.1 Introduction

Biocompatibility is central to the design and performance of medical devices. The issues of biocompatibility include clot formation on blood contacting devices,[1] foreign body response on subcutaneous implants,[2] biofilm formation and microbial infections on all types of invasive devices.[3] One promising means to combat all of these issues with a single agent is to employ nitric oxide (NO), an endogenous molecule with potent antithrombotic, antimicrobial and immune suppressing properties.[4-7] However, because NO is a gas molecule and is relatively reactive, the use of NO donors together with proper release methods are necessary to deliver NO locally to be effective.[8] Nitric oxide donors can either be covalently attached to or non-covalently incorporated within polymers,[9,10] and such polymers are then used either as coatings for devices, including intravascular sensors, or as the bulk material of the devices (e.g., catheters, intravascular sensors and stents).[11-13]

Two types of biomedical polymers, silicone rubber[14-17] and polyurethanes,[18-20] are extensively used in creating NO releasing materials because of their innate compatibility

with NO release chemistry, appropriate mechanical properties and stability *in vivo*.[21] However, the transport properties of such polymers with respect to NO diffusion rates, partition coefficients, etc. have been less studied. Such transport properties can significantly affect the observed NO release profile, including surface flux of NO, longevity of release, duration to reach steady state release, as well as the NO release distribution of NO around the surface of actual devices. Such transport properties, once known, can help predict the NO release profile and NO distribution around the devices, and therefore help guide the optimal design/configuration of devices for biomedical medical applications.

Mowery *et al.* did examine the transport of NO in polymers and obtained apparent diffusion coefficients for PVC, silicone rubber and two aliphatic polyether polyurethanes.[22] Although useful in predicting the average flux at steady-state, transient processes, transport processes involving chemical reactions, and local flux distribution cannot be accurately described by using apparent diffusion coefficients alone. This is because this coefficient includes the mixed processes of both diffusion and partitioning. Polymers with same apparent diffusion coefficient can display very different NO release profiles and distributions under non-steady-state conditions. Moreover, the transport properties of NO in newly developed polyurethanes that have been shown to exhibit improved stability and biocompatibility *in vivo* have not been reported.[23]

To better understand the time-dependent NO transport and release processes in polyurethanes and to improve the design of NO releasing scaffolds and devices, in this study, the transport properties of different polyurethanes, including classic aliphatic, aromatic polyether polyurethanes, as well as newly developed silicone and polycarbonate

containing polyurethanes are examined. The *true* diffusion coefficients of NO in these polymers are studied separately from the partition process. Finally, finite element analysis is used to simulate the effects of diffusion and partitioning on the NO release profile as well as distribution of NO at the outside surface of multi-lumen catheter, and the simulation results are compared with experimental data.

6.2 Theory

6.2.1 Gas Transport in Polymers: Diffusion and Solution

Transport of gas through polymers can be described by two different processes—diffusion and solution. Solution is the process of gas partitioning between the polymer phase and the gas or liquid phase, and therefore the term partition and solution are used interchangeably in this chapter. Figure 6.1 summarizes a general 1-D model for NO permeation from one stream (upstream) into another stream (downstream) through a polymer layer, which describe the transport process in the diffusion experiments conducted in this study, as well as NO release process from a NO reservoir inside a polymeric membrane, e.g., electrochemical (e-chem) NO release system.

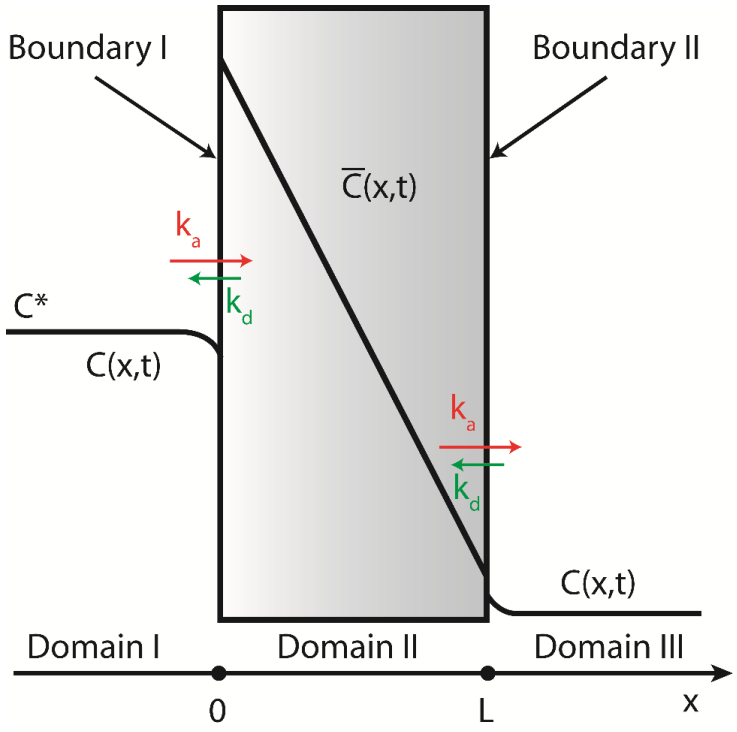

Figure 6.1. Schematic for NO permeation through polymer film/wall with thickness of *L*.

Suppose gas molecules dissolved in a solution (Domain I) with bulk concentration C^* need to permeate through a polymeric membrane (Domain II) and enter the downstream solution on the other side of the membrane (Domain III). First, the dissolved gas in Domain I needs to be transported to close proximity to the polymer/solution interface (Boundary I) by diffusion (diffusion coefficient *D*) and convection. Second, the gas close to the interface (Boundary I) must partition between the polymer and solution phases. This partitioning process can be viewed as two elementary steps: adsorption (transfer from solution into polymer, with a first order heterogeneous rate constant k_a); and desorption (transfer from polymer into solution, with a first order heterogeneous rate constant k_d). The ratio of k_a/k_d determines the partition coefficient *K* between the two phases. In the third step, the gas molecules that partition into the polymer domain (Domain II) are transported to the other

interface of the membrane (x = L) by diffusion (diffusion coefficient $\bar{D}$; the bar denotes the membrane phase). The fourth step, again, involves partitioning of gas molecules between polymer/solution interface (Boundary II) with the same k_a and k_d as in the second step. Finally, the gas molecules that has entered the receiving solution (Domain III) will be transported away. The driving force for all these processes is the chemical potential gradient, or equivalently, the concentration gradient in this study.

Several assumptions are made to simplify the mathematical model for the diffusion process shown in Figure 6.1. First, we assume that all the diffusion processes are Fickian. That is, the magnitude of flux is proportional to the concentration gradient, and the diffusion coefficient is concentration independent. This assumption is a valid as the gas molecule are small and the concentration of gas in the experiment is low, ensuring no significant change of the polymer, structurally or dynamically, by the presence of the diffusing gas molecules (i.e., no swelling or plasticization). Secondly, the membrane is isotropic and homogeneous. This should be macroscopically true for the polymers under study. Based on these assumptions, diffusion equations in the three domains coupled by partitioning in 1-D as well as the corresponding initial values and boundary conditions are shown below:

Domain I

$$\frac{\partial C(x,t)}{\partial t} = D\frac{\partial^2 C(x,t)}{\partial^2 x} \tag{1}$$

$$C(-\infty, t) = C(x, 0) = C^* \tag{2}$$

$$J(0,t) = k_d\bar{C}(0,t) - k_a C(0,t) = k_d[\bar{C}(0,t) - KC(0,t)] \tag{3}$$

Domain II:

$$\frac{\partial \bar{C}(x,t)}{\partial t} = \bar{D}\frac{\partial^2 \bar{C}(x,t)}{\partial^2 x} \tag{4}$$

$$\bar{J}(0,t) = -J(0,t) = k_d[KC(0,t) - \bar{C}(0,t)] \tag{5}$$

$$\bar{J}(L,t) = [k_a C(L,t) - k_d \bar{C}(L,t)] = k_d[KC(L,t) - \bar{C}(L,t)] \tag{6}$$

$$C(x,0) = 0 \tag{7}$$

Domain III:

$$\frac{\partial C(x,t)}{\partial t} = D\frac{\partial^2 C(x,t)}{\partial^2 x} \tag{8}$$

$$J(L,t) = -\bar{J}(L,t) = k_d[\bar{C}(L,t) - KC(L,t)] \tag{9}$$

$$C(+\infty,t) = C(x,0) = 0 \tag{10}$$

Equations (1) (4) (7) are diffusion equations in the different domains, and the other equations are initial values and boundary conditions. Equations (3) (5) and Eqs (6) (9) couple diffusion in Domains I, II and in Domains II, III, respectively, by enforcing a continuous flux across the boundaries.

For the diffusion experiment, assuming stirring provides sufficient mixing in Domain I, the concentration of NO in solution can be treated as homogeneous during the experiment. A large amount of solution volume in Domain I as compare to the membrane volume (Domain II) ensures that concentration of NO in Domain I remains essentially unchanged in the time scale of a typical diffusion experiment. The homogeneity and time invariance of NO concentration simplifies Eqs (1) and (2) to:

$$C(x,t) = C^*, \text{ for } x < 0\ , \tag{11}$$

Assuming fast partition equilibrium at the interface, the Eqs (3) and (5) can be reduced to:

$$\bar{C}(0,t) = KC(0,t) = KC^* \tag{12}$$

Similarly, because NO in the downstream (Domain III) is rapidly pumped into the detector for measuring the rate of NO transport, the concentration of NO in Domain III is essentially zero at all times. Eqs (8) and (10) are therefore reduced to:

$$C(x,t) = 0 \text{ , for } x > L \tag{13}$$

And by analogy for fast equilibria, Eqs (6) and (9) become:

$$\bar{C}(L,t) = KC(L,t) = 0 \tag{14}$$

Under these conditions, the complicated coupled diffusion in three domains is simplified into the diffusion process in Domain II alone, with governing equation Eq (4) and boundary conditions provided by Eqs (12) and (14) and initial value, Eq (7).

Such diffusion equations can be solved exactly, and integrating the flux at x=L over time yields:

$$Q(L,t) = \frac{\overline{D}KC^*}{L}\left(t - \frac{L^2}{6\overline{D}} + \frac{2L^2}{\pi^2\overline{D}}\sum_{n=1}^{\infty}\frac{(-1)^{n+1}}{n^2}\exp\left(-\frac{\overline{D}n^2\pi^2\mathrm{t}}{L^2}\right)\right) \tag{15}$$

where $Q(L,t)$ denotes the amount of gas that penetrates the membrane per unit area at time *t*. When *t* -> ∞, the exponential term is dropped:

$$Q(L,t) = \frac{\overline{D}KC^*}{L}\left(t - \frac{L^2}{6\overline{D}}\right) \tag{16}$$

Therefore, plot of the amount of permeated gas versus time will approach a linear asymptote as t-> ∞, with an intercept at the x axis:

$$\tau = \frac{L^2}{6\overline{D}} \tag{17}$$

τ is defined as the time lag. Once the membrane thickness *L* and time lag τ are obtained, the diffusion coefficient can be calculated from Eq (17).

First derivative of Eq (15) gives:

$$J(L,t) = \frac{\overline{D}KC^*}{L} + \frac{2\overline{D}KC^*}{L}\sum_{n=1}^{\infty}(-1)^n \exp\left(-\frac{\bar{D}n^2\pi^2 \mathrm{t}}{L^2}\right) \qquad (18)$$

The first term of Eq (18) corresponds to the steady-state portion of the flux, whereas the second term corresponds to the transient portion of the flux. As t -> ∞, the flux reaches steady-state:

$$J(L,t) = \frac{\overline{D}KC^*}{L} \qquad (19)$$

From the steady-state flux, $\overline{D}K$ can be obtained. Together with the $\overline{D}$ obtained from the transient time lag, the partition coefficient *K* can also be determined. This forms the basis for measurement of both the diffusion coefficients and partition coefficients of NO in this study for a variety of biomedical polymers.

Under other conditions, for example, electrochemical NO generation from catheters (as reported in Chapters 2 and 3, see Figures 2.1 and 3.7 for the schematics), the assumption of effective stirring in Domain I is no longer valid and a diffusion layer will exist within the inner source solution phase. Therefore, diffusion equations in Domain I and II need to be coupled together. Distribution of NO around an actual catheter surface is also of interest during the application of these type of devices. Under this circumstance, however, the 1-D model is not sufficient to describe the distribution process. This complicated case can be solved in higher dimension numerically using finite element analysis, which is described within the next section.

6.3 Experimental and Simulation Methods

6.3.1 Materials and Instrument

Sodium nitrite (99.99%), potassium iodide, and sulfuric acid were purchased from Sigma-Aldrich (St. Louis, MO) and used as received. All the solutions were prepared with deionized water from a Milli-Q system (18 MΩ cm^{-1}; Millipore Corp., Billerica, MA).

Carbosil 20 80A and Bionate 80A were from DSM (Heerlen Netherlands), while Elast-Eon 5-325 80A (E5-325) was from AorTech International plc (Weybridge, UK). Tecoflex SG-80A and Pellethane 80AE were gifts from Lubrizol (Cleveland, Ohio). Silicone rubber sealant (RTV-3140) was a product of Dow Corning (Midland, MI).

6.3.2 Membrane Preparation

All the polyurethane films were prepared by casting a 10 wt% solution of the polymer in THF in a 6 cm diameter glass O-ring on a glass slide. The slide was left to dry in a fume hood for 24 h and then placed under vacuum for further drying for another 4 h period. Silicone rubber films were prepared by casting a suspension of RTV sealant in THF within a 6 cm Teflon O-ring on a Teflon slide with 48 h drying under ambient conditions. Selective chemical properties of all the polymers used in this study are listed in Table 6.1.

Table 6.1. Chemical properties of silicone and polyurethanes used in this study.

Polymer Name	Description	PDMS /%	Soft Segment	Hard Segment	Hard Segment/%	Density /(g mL^{-1})
Silicone	Silicone rubber	100	PDMS	-	-	1.05
Elast-Eon 5-325	Silicone Polyether Polyurethane	66	PDMS:PHMG (98:2) [24]	MDI:BDO	32.5 [24]	1.08
Tecoflex SG-80A	Polyether Polyurethane	0	PTMG	HMDI:BDO	40 [25]	1.04
Carbosil 20-80A	Silicone Polycarbonate Polyurethane	20	PHEC: PDMS (66:34)	MDI:BDO	40-45 [26]	1.16
Pellethane 80AE	Polyether Polyurethane	0	PTMG	MDI:BDO	45 [27]	1.11
Bionate 80A	Polycarbonate Polyurethane	0	PHEC[26]	MDI:BDO	35 [26]	1.19

PDMS = poly(dimethylsiloxane); PHMG = poly(hexamethylene oxide); PTMG = poly(tetramethylene oxide); PHEC = poly(1,6-hexyl 1,2-ethyl carbonate); MDI = 4,4′-methylene-bis(phenyl isocyanate); HMDI = 4,4′-methylene-bis(cyclohexyl isocyanate); BDO = 1,4-butanediol.

6.3.3 NO Transport Measurements

In a diffusion cell, a membrane was clamped in between the two parts of the cell (see Figure 6.2 for the experimental setup). Solutions of 0.1 M H_2SO_4 and 5% KI were pre-purged with N_2 for 20 min to remove O_2. A 3.5 mL aliquot of each solution was then added to the left side of the diffusion cell. Afterwards, each side of the cell was purged thoroughly with N_2 again for another 20 min to eliminate O_2. The solution on the left side was then vigorously stirred throughout the entire time of the experiment. Then, the time

was recorded when a 50 µL aliquot of a $NaNO_2$ standard solution (5 mM) was injected into the 7 mL solution on the left side of the cell. The NO flux was measured in real time with chemiluminescence using a nitric oxide analyzer (NOA) (Sievers 280i, GE Analytics, Boulder CO) until the steady-state flux was reached on the right side of the cell.

Alternatively, 0.1 M H_2SO_4 and 5% freshly made ascorbic acid can also be used to generate NO from nitrite solutions, when I_2 adsorption was found to be significant on the polymer surface.

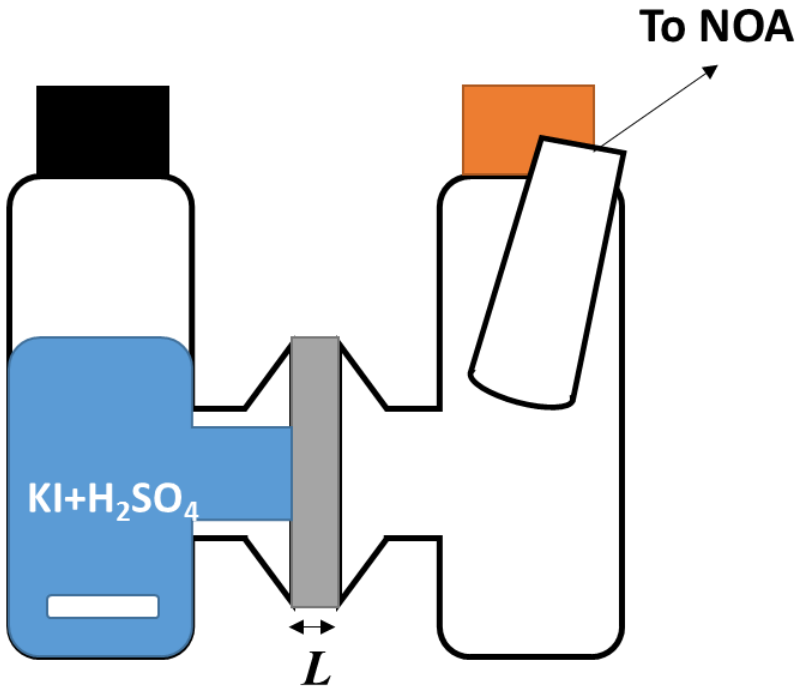

Figure 6.2. Schematic for the diffusion experiment performed in this study. The polymeric membrane is clamped between two parts of the diffusion cells. The left cell is filled with KI and H_2SO_4 to generate NO when nitrite is added. The right cell is connected directly to nitric oxide analyzer (NOA).

6.3.4 Fabrication of Electrochemical NO Releasing Silicone and PU Catheters

Standard silicone tubing was purchase from VWR. PU tubing was prepared by dip coating of a 15 wt% of SG80A in THF on a 2.0 mm diameter straight stainless steel mandrel (McMaster-Carr, IL). The tubing obtained had a ~0.3 mm wall thickness and were cut off for the fabrication of the electrochemical NO releasing catheters. The procedures were similar manner as previously reported (see Experimental Details in Chapter 3).[28,29]

6.3.5 Measurement of Asymmetric Release by Agar Immobilization

An electrochemical NO releasing catheter was mounted on a glass slide with tape. A hot 1% agar was poured onto the glass slide so that the agar incorporated the catheter when cold. The agar was further cut so that the cross sectional geometry was rectangular with catheter in the center. The NO release was then turned on, and nitrite content at each side of the catheter was measured by measuring the nitrite content using chemiluminescence. Briefly, the agar sample was dissolved in DI water, and aliquots of the solution was injected into a cell containing degassed 5% KI and 0.1 M H_2SO_4 solution to convert nitrite to NO. The cell was connected to a nitric oxide analyzer for NO measurement via chemiluminescence.

6.3.6 Simulation Methods

Finite element analysis via Comsol Multiphysics (5.0b) was used to simulate the effect of partition coefficient and diffusion coefficient on the NO release profiles when using single lumen catheters and the NO distribution when employing multi-lumen catheters.

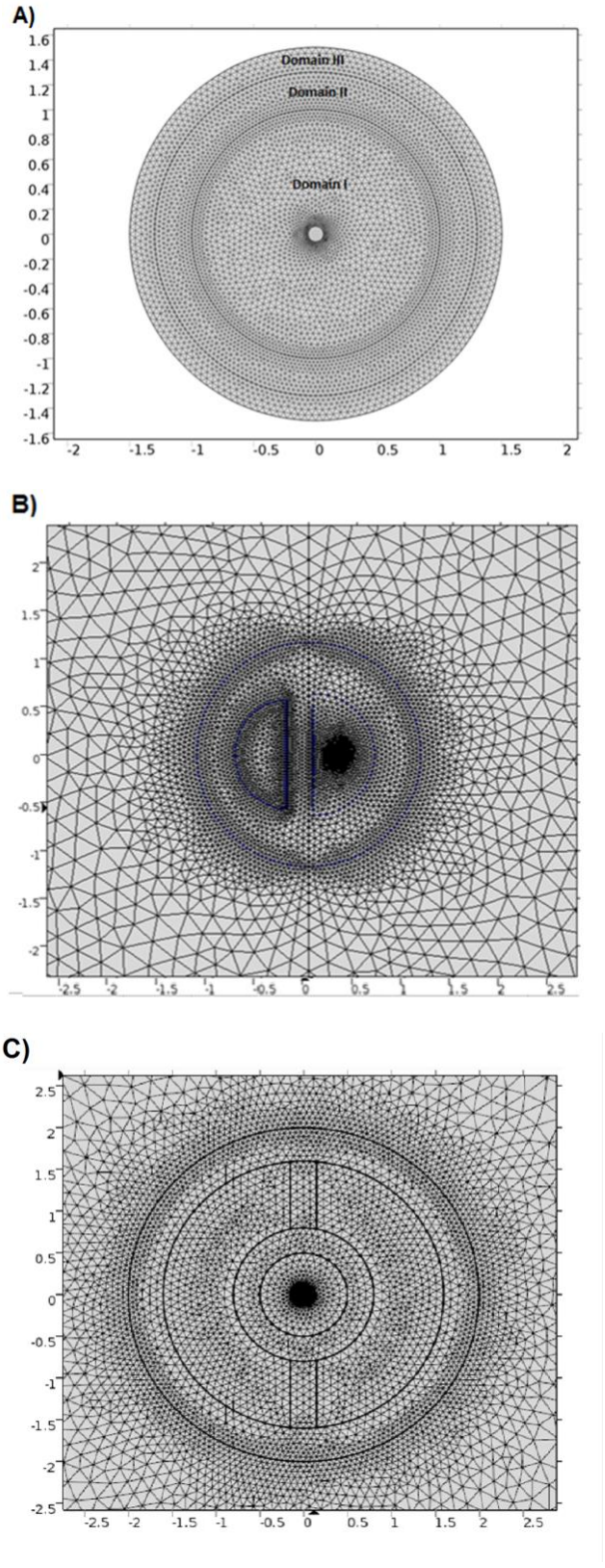

Figure 6.3. Geometry and meshing for (A) single lumen, (B) commercial dual lumen, and (C) proposed symmetric triple lumen catheter used in the finite element analysis.

Table 6.2. Parameters used in finite element analysis.

Symbol	Description	Value
D	Diffusion coefficient for NO in water	2.21×10^{-5} cm ^{2}s^{-1}
N	Flux of NO at electrode surface	6.4×10^{-9} mol cm^{-2}min^{-1}
K	Partition coefficient	0.5, 1, 2, 5, 10
$\overline{D}$	Diffusion coefficent for NO in polymers	5.0×10^{-7}, 2.0×10^{-6}, 1.0×10^{-5}, 5.0×10^{-5} cm^2 s^{-1}
OD_cat	Outer diameter of the single lumen catheter	2.6 mm
ID_cat	Inner diameter of the single lumen catheter	2.0 mm
OD_ele	Outer diameter of the electrode	0.125 mm

For response time estimation, a 2-D model of the cross-section of a single lumen catheter was implemented. Similar 2-D equations for diffusion coupled by partition as described in Eqs (1) (4) (7) and (3) (5) (6) (9) are the governing equations for this transport study, except the Neumann boundary condition of constant flux at the electrode surface was used instead of constant concentration. In Domain III, an NO sink at 0.2 mm away from the catheter surface was purposely set to mimic the fact that NO is removed from the surface of the catheter very fast, either into the NOA by purging, or reacting with oxyhemoglobin when placed within the bloodstream *in vivo*. For simulation of the distribution of NO around the outer surface of multi-lumen catheters, a similar model was used except the cross-section geometry was different. The geometry and meshing of the model are shown in Figure 6.3, and the related parameters are shown in Table 6.1.

6.4 Results and Discussion

6.4.1 Diffusion Studies of NO Through Polyurethanes

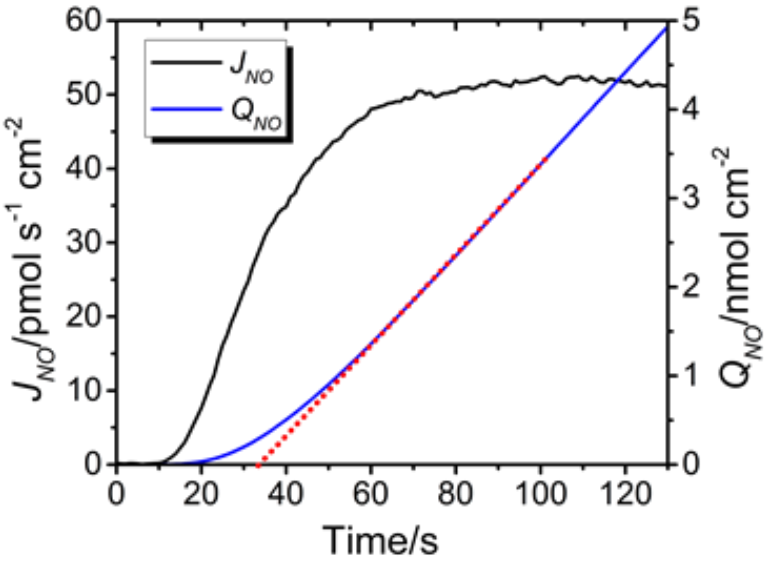

Figure 6.4. Typical NO flux profile (J_{NO}, black) and amount of permeated NO (Q_{NO}, red) vs. time for 368 μm E5-325 polyurethane at 25 ℃ in a diffusion experiment. Red dotted line denotes the asymptote used for deriving the time lag.

A typical NO flux and accumulative amount of permeated NO vs. time for NO diffusion through an E5-325 PU membrane is shown in Figure 6.4. From the steady-state flux, together with membrane thickness, $\overline{DK}$ can be obtained according to Eq. 19. After integration of the flux vs. time, an accumulated amount of permeated NO is obtained, which can be used to estimate time lag (τ) and calculate the diffusion coefficient. Similar experiments were performed for the different polyurethane and silicone rubber films (structure description and selected physical properties of all the polymers under

investigation are listed in Table 6.1) at both 25 ℃ and 37 ℃. The measured coefficient and partition coefficients of NO in these polymers are summarized in Table 6.3.

Table 6.3. Summary of diffusion coefficients and partition coefficients of NO in various polymers obtained in this study.

Polymer	$\overline{D}_{298K}$ /10^{-6} cm^2 s^{-1}	$\overline{D}_{310K}$ /10^{-6} cm^2 s^{-1}	K_{298K}	K_{310K}
Silicone	16 ±2	20 ±4	5 ±1	4 ±1
E5-325	6 ±1	8.5 ±0.8	3.8 ±0.5	3.3 ±0.3
PU SG80A	1.2 ±0.5	1.9 ±0.5	2.5 ±0.8	2.2 ±0.3
Carbosil 20 80A	0.66 ±0.09	1.4 ±0.5	1.2 ±0.4	0.3 ±0.1
Pellethane 80A	0.5 ±0.1	0.8 ±0.3	1.5 ±0.4	1.1 ±0.2
Bionate 80A	0.3 ±0.1	0.7 ±0.1	0.7 ±0.2	0.6 ±0.1

The diffusion coefficient of NO ($\overline{D}$) determined in the different polymers is negatively correlated to the density (ρ) of the polymer (see Figure 6.5). This can be understood by the free volume theory,[30] which suggests that diffusion in a polymer occurs by hopping between the holes of free volume, with the relationship:

$$\log \overline{D} = A - \frac{B}{f_v} \tag{20}$$

where *A* and *B* are constants related to the size of the penetrants and hole size of the polymer matrix, respectively, and f_v is the fraction of free volume. Assuming similar densities of different polymer chains (occupied volumes) in this study, the specific density of a polymer

is negatively proportional to f_v. In fact, a direct relationship between f_v and $\overline{D}$ has been established experimentally by diffusion and positron annihilation lifetime experiments.[31]

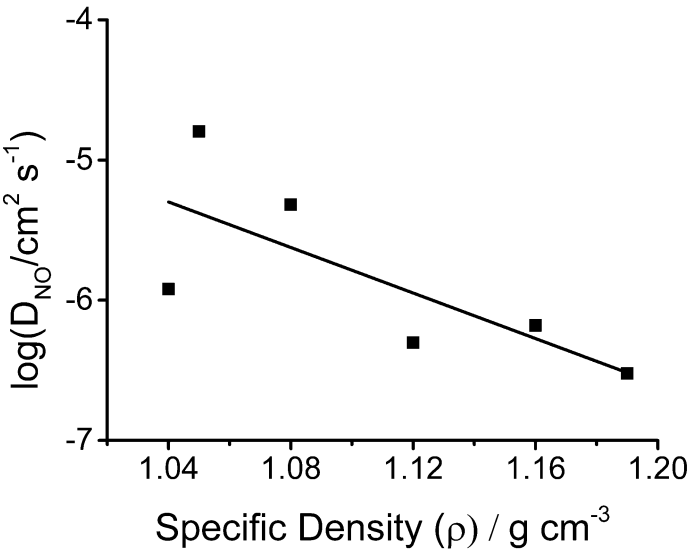

Figure 6.5. Specific density (ρ) of polymers vs. log of diffusion coefficient for NO (D_{NO}). Correlation coefficient r = -0.75 for ρ vs. the log D_{NO}.

The PDMS polymer chain is flexible with a low barrier for rotation, which allows a large free volume and therefore fast diffusion for penetrants like NO. Such a large free volume of PDMS is also indicated by the low glass transition temperature (T_g) of neat PDMS (-112 ℃).[32] This explains the fact that silicone rubber has the highest $\overline{D}$ for NO, and all the PUs containing PDMS segments examined in this study exhibit significantly higher diffusion coefficients for NO than similar PUs without the PDMS segments (e.g. E5-325 vs. Pellethane, Carbosil vs. Bionate).

The polycarbonate chain (PHEC), while having a low T_g of -70 ℃ in the neat form, can form strong hydrogen bonds with urethane components in PUs.[32] Such hydrogen bonding significantly decreases the free volume by closer packing and a reduction in chain

mobility, which is also indicated by the much higher *T*g (-7 ℃) of the PHEC segments in polycarbonate copolymers of PUs.[32] This reduced free volume of PHEC chain in PUs explains the relatively slow diffusion of NO in Bionate and Carbosil.

PU SG80A and Pellethane are both pure PUs with polyether as soft segments but exhibit quite different NO diffusion properties. SG80A contains urethane segments from 4,4′-methylene-bis(cyclohexyl isocyanate) (HMDI) and 1,4-butanediol (BDO), whereas Pellethane contains urethane segments from 4,4′-methylene-bis(phenyl isocyanate) (MDI) and BDO.[25,27,33] As the aromatic MDI is more rigid than the aliphatic HMDI, PUs with segments from MDI have a larger barrier for chain rotation and therefore lower free volume. Therefore, PU SG80A exhibits a greater diffusion coefficient for NO than Pellethane.

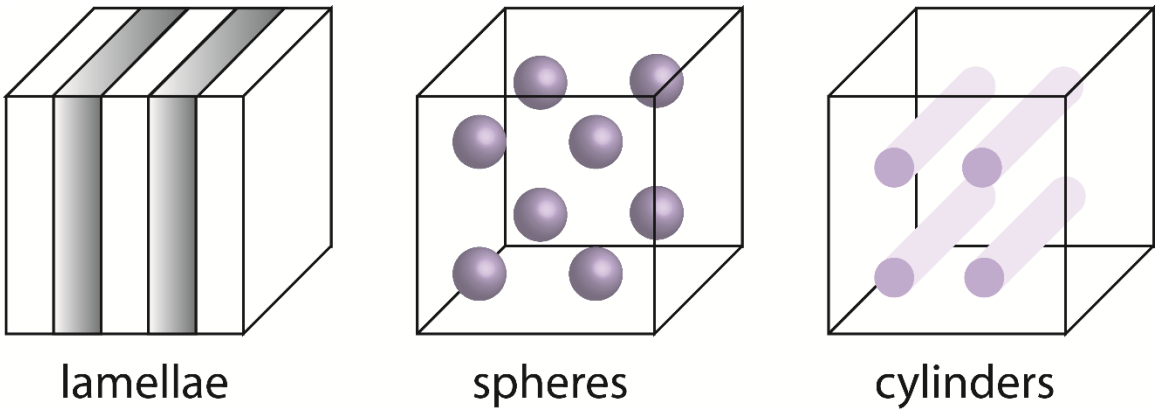

Figure 6.6. Cells of typical morphology (lamellae, spheres and cylinders) for block copolymers with phase separation.

In addition to the chain flexibility and free volume, polymer morphology in block copolymers also significantly affect the diffusion of gas molecules.[34] This is especially true for polyurethanes as they tend to micro-phase separate into different morphologies, including continuous phase with spheres, cylinders and lamellae.[35] The exact morphology

depends on the miscibility of the blocks, stoichiometry of the blocks, and preparation conditions (including thermal history).[36] In PUs with some PDMS within the copolymer chain, such as E5-325 and Carbosil, the PDMS segments undergo phase separation of nearly 100%.[32,37] This allows the fraction of the PDMS phase to be simply represented by the stoichiometry. Effective media theory has been proposed to model diffusion within polymer blends with different morphology, including spheres, cylinders and lamellae.[38] Such methods were first developed for solving issues of conductivity of composite materials, and the derived equations can be directly applied for diffusion by changing the conductivity into permeability. The diffusion of gas in PUs can be modeled by considering compositions of cells with morphologies as shown in random orientation as shown in Figure 6.6. The relationship between volume fraction of PDMS phase and the predicted diffusion coefficient from different morphologies are plotted in Figure 6.7.

E5-325 possesses segments of PDMS and MDI:BDO, and the PDMS content is as high as 66%. This micro-morphology can be described as two phases comprising a continuous PDMS phase (66%) and discontinuous hard segment phase. From Figure 6.7A, the point for E5-325 lies close to the predicted line for a cylinder of a hard phase in PDMS. However, a volume fraction of 66% is likely to be near the percolation threshold.[39] Predictions near the percolation threshold using this method often involves large error.[40]

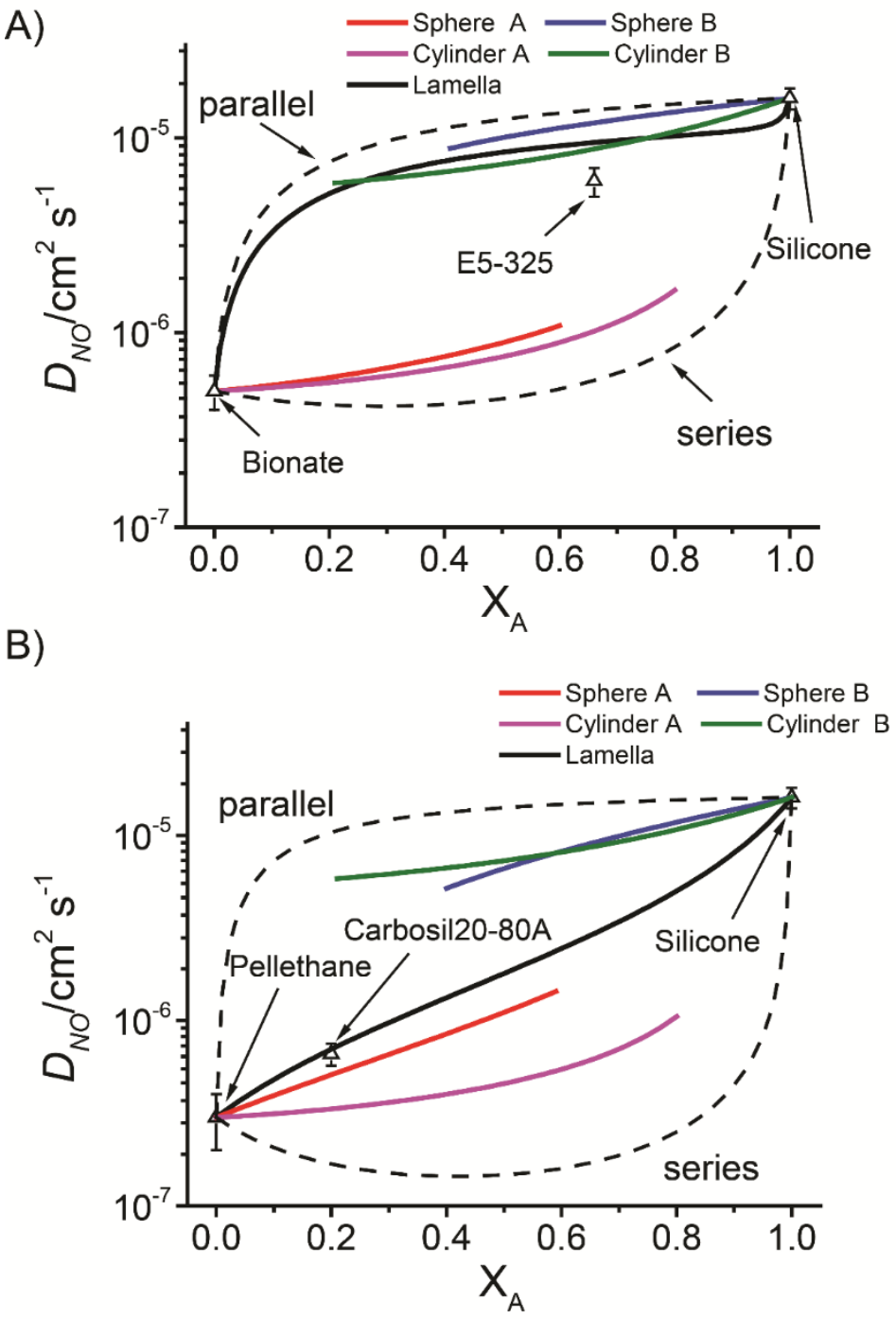

Figure 6.7. Diffusion coefficient of NO (D_{NO}) vs. volume fraction of PDMS (X_A) in polymer based on different morphology for (A) Silicone-PU, and (B) Polycarbonate-Silicone-PU.

For Carbosil-20, the PDMS chains phase separate completely due to low compatibility with other chains. From percolation theory, PDMS, with a volume fraction of 20%, is less likely to form a continuous phase. Significant mixing of PHEC and the hard segment occurs, and only 10–15% of hard segment phase is separated (~4% of total volume). To simplify the description using a two-phase model, the small amount of separated hard segment phase can be neglected. Therefore, the morphology is described as continuous PHEC mixed phase with islands of PDMS. From Figure 6.7B, it is likely that Carbosil-20 contains a lamellae structure of the PDMS component and the PHEC component.

Diffusion coefficients and partition coefficients were obtained only at 25 ℃ and 37 ℃ as these temperatures are most relevant for biomedical applications. As expected when the temperature increases, the diffusion coefficients of NO increase for all the polymers tested. We did not attempt to derive an Arrhenius activation energy from the two temperature data points. The activation energies would contain contributions from both the diffusant (NO) and the polymers and is less useful considering the complex composition and phase transitions of the different polymers at different temperatures.

Errors in the diffusion experiments stem from many factors with major ones being the exact thickness of the membrane, the uncertainty arising from the response time of the NOA (2 s), and effectiveness of convection from stirring to NO source solution.

In the experiment, asymmetry exists for the membrane as one side is contacting water (Domain I) while the other side is contacting gas (Domain III). Such asymmetry, could potentially have an effect on the adsorption and desorption processes at the interfaces. In this experiment, the adsorption and desorption processes are assumed to occur very fast

for both the water/polymer interface and the gas/polymer interface. If such an assumption is valid, the effect of asymmetry at the interface would be negligible. The purpose for having gas on the other side instead of solution is to minimize the error by greatly decreasing the response time for the NO detection and to ensure that the downstream concentration is effectively zero at all times by quickly forcing the arriving NO into the detector.

6.4.2 Effect of $\overline{D}$ and K on Response Time of NO Release

Partition and diffusion affect NO transport in polymers and therefore can affect the NO release profile of some systems. Particularly, the time it takes for NO release to reach steady-state, defined as the response time, is of importance as it can affect the performance/functionality of NO releasing device. Catheters made from silicone and SG 80A with electrochemical NO release system have been used to demonstrate such an effect. With the same geometry, catheters with different materials show very different diffusion profiles (see Figure 6.8). For a pure PDMS catheter, the surface flux of NO reaches steady-state within 5 min, whereas for a catheter made with PU SG80A, it takes more than 60 min to reach steady-state. This is explained by the fact that the diffusion coefficient of NO in silicone is 13 times greater than that in PU SG 80A (see Table 6.3).

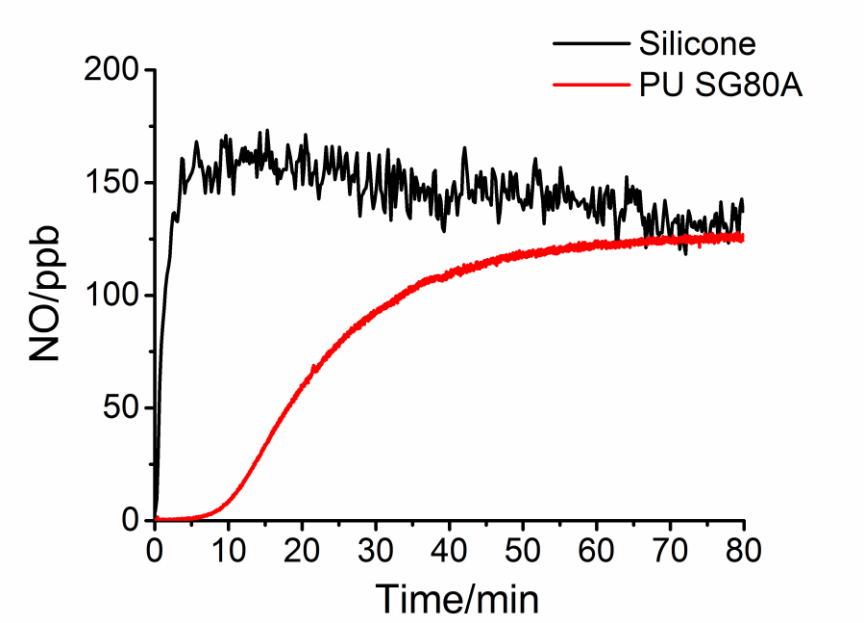

Figure 6.8. NO release profile for electrochemical NO releasing catheters made from silicone and PU SG80A determined by a nitric oxide analyzer. The catheters are 2.6 mm in o.d. and ~0.3 mm in wall thickness.

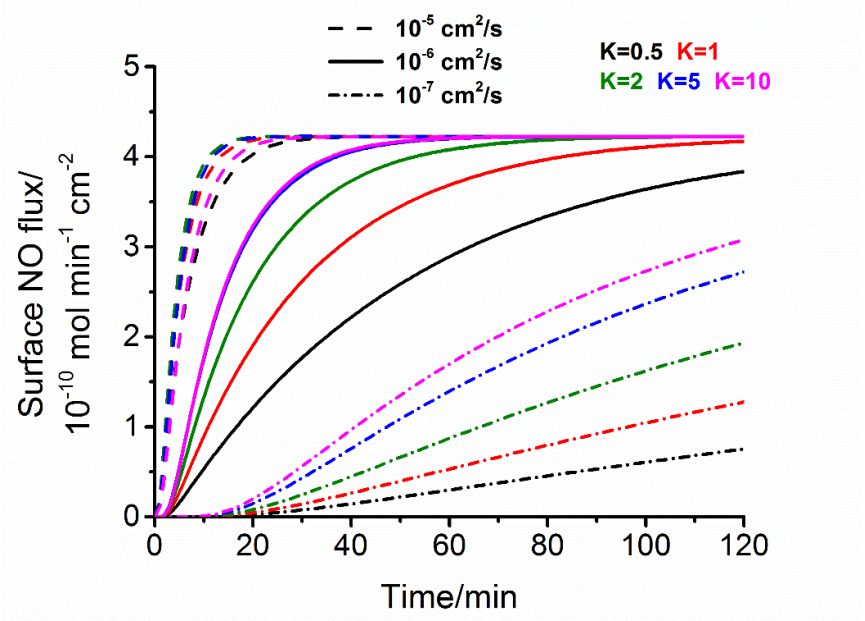

Figure 6.9. Effect of diffusion and partition on NO release profile from electrochemical NO releasing catheters as determined by simulation.

The effect of $\overline{D}$ and K of NO in polymers on the NO release profile from a single lumen catheter was further investigated via finite element analysis using Comsol Multiphysics. From the simulation result, the response time of NO release becomes faster as $\overline{D}$ and K increase (see Figure 6.9). This result together with results of $\overline{D}$ and K in the diffusion study (Table 6.3) illustrates that to achieve a faster response time in electrochemical NO releasing catheters, silicone is the preferred material. For a normal single lumen catheter with 0.3 mm wall thickness, the response time for silicone and E5 will be $\leq$ 20 min. The other polymers that have low $\overline{D}$ and K values for NO, although not ideal for electrochemical catheter application, could be used as release barriers to slow down the release of NO, or to prevent burst release. For example, in drug delivery using nanoparticles, where prolonged release is often hard to achieve, calls for use of materials with low permeability as the outer barrier.[41]

6.4.3 The Effect of $\overline{D}$ and K on NO Distribution on Multi-Lumen Catheters

Another aspect of NO release is the distribution of NO on the surface of the devices. For example, application of electrochemical NO release in catheters requires multi-lumen catheters because one of the lumens needs to be sacrificed for the electrochemical NO generation system. However, as most commercial multi-lumen catheters are not centrosymmetric, NO distribution around the outer surfaces of such catheters are likely to be asymmetric. On the other hand, using a polymer with a high partition coefficient could serve as a reservoir for NO release, and that coupled with a high diffusion coefficient could promote a more symmetrical distribution of NO. Both $\overline{D}$ and K, therefore, could impact the distribution of NO, besides the geometry of the device.

To study such asymmetry effects, a commercial dual lumen silicone catheter was simulated using $\overline{D}$ and K values obtained in this study. Such a catheter has already been used in practice for conducting antithrombotic, antimicrobial studies as well as for preparing new NO release PO_2 sensing catheters (see Chapter 3, 4, 5).[29,42] The local surface flux distribution for this catheter configuration is plotted in Figure 6.10a. To quantify the worst case scenario of asymmetry, the ratio of the highest and the lowest local fluxes on the surface is used and is called maximum surface flux ratio (see Figure 6.10d). The surface flux of NO increases as the time increases, and the maximum surface flux ratio decreases to <2 after 20 min in the absence of O_2 (Figure 6.10). With ambient O_2 reacting with NO, the surface flux reaches a steady-state after 30 min, and the maximum surface flux ratio reaches 2.5 (Figure 6.10). Such asymmetry was also probed experimentally by measuring the cumulative nitrite content (released NO reacts with O_2 to form nitrite) at different sides of catheter in an agar gel into which e-chem NO releasing catheter was placed (experimental setup shown in Figure 6.11A). As shown in Figure 6.11B, the results from the experiment agree well with the simulation.

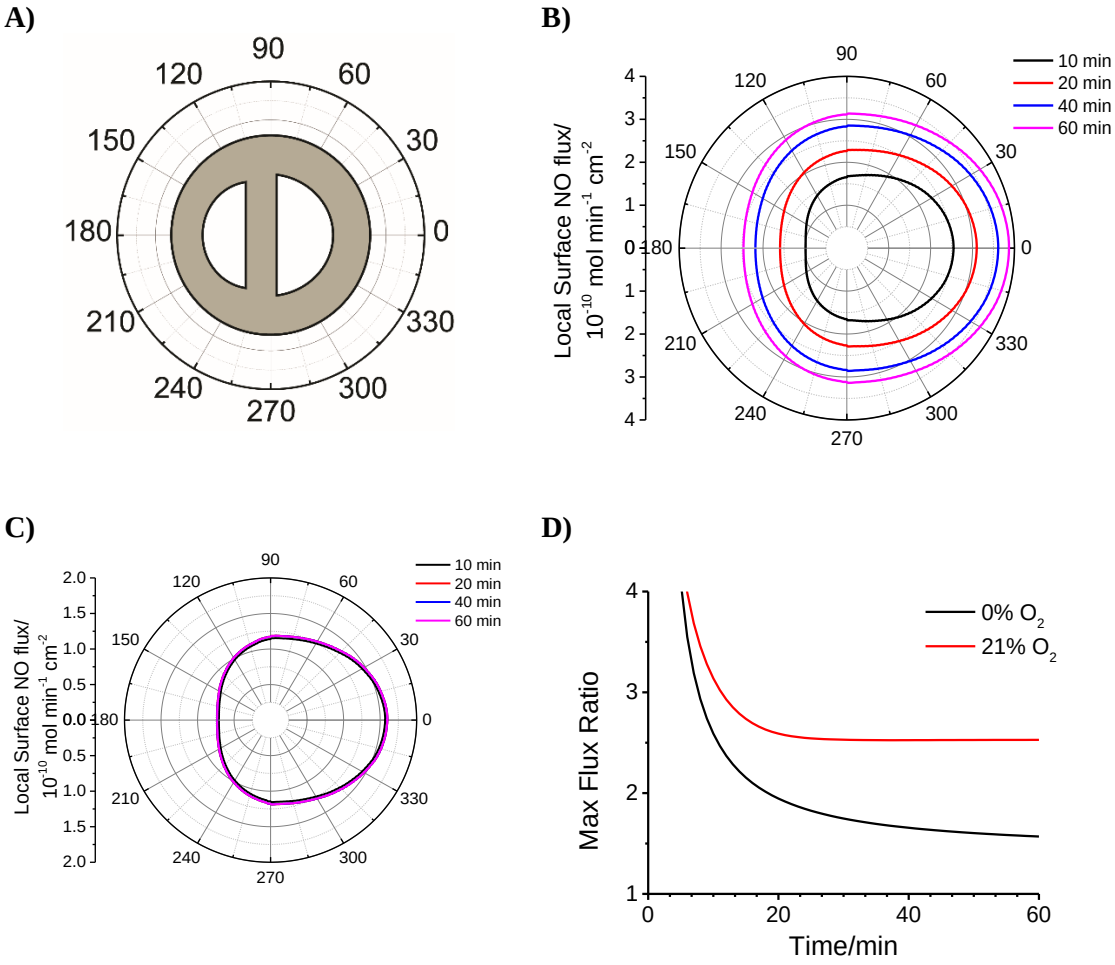

Figure 6.10. Local surface flux of NO on a Cook 7 Fr dual lumen PDMS catheter at room temperature in N_2 and in air. A) illustration of the polar angel for the dual lumen catheter; B) polar graph showing the local surface flux at different time in 0% and C) in 21% O_2; D) Maximum surface flux ratio vs. time under 0 and 21% O_2.

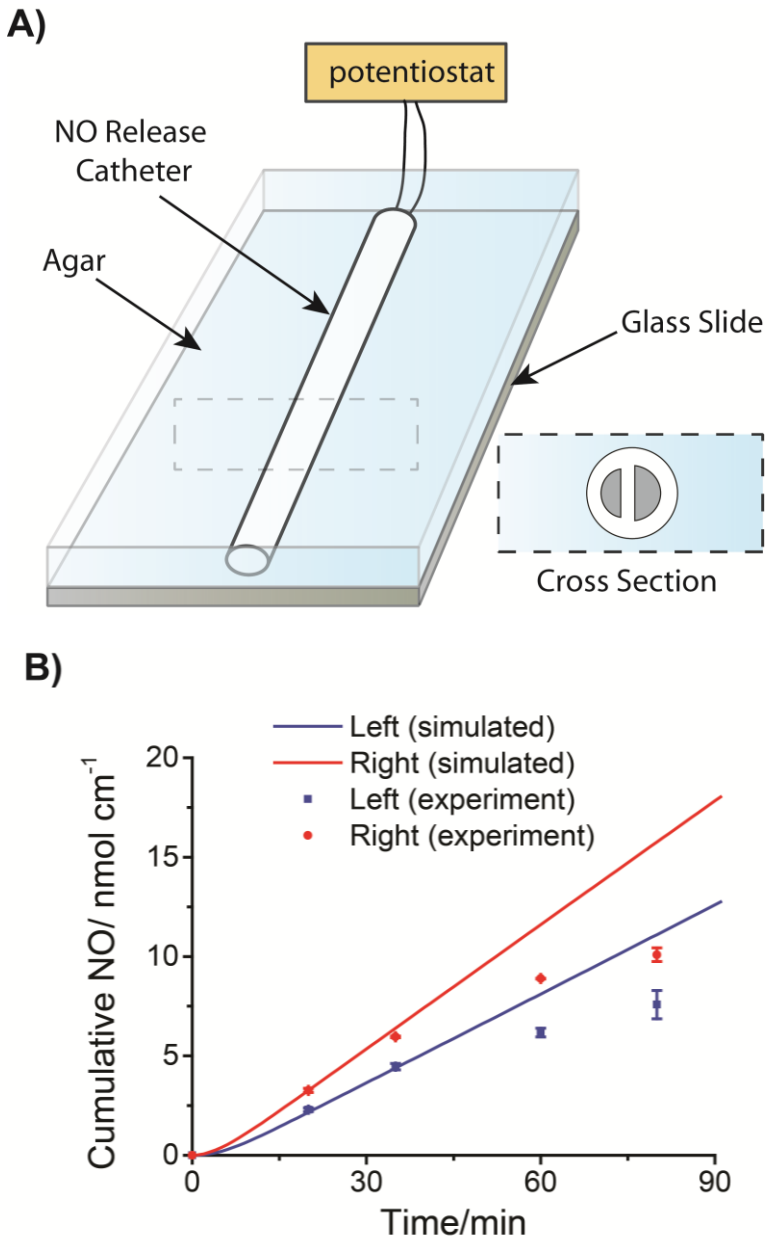

Figure 6.11. Experiment probing the distribution of NO by around a dual lumen catheter. A) experimental setup of catheter immobilization using agar; B) cumulative NO in the left and right domain of the catheter as measured by the agar immobilization experiment (dot) and simulation (line).

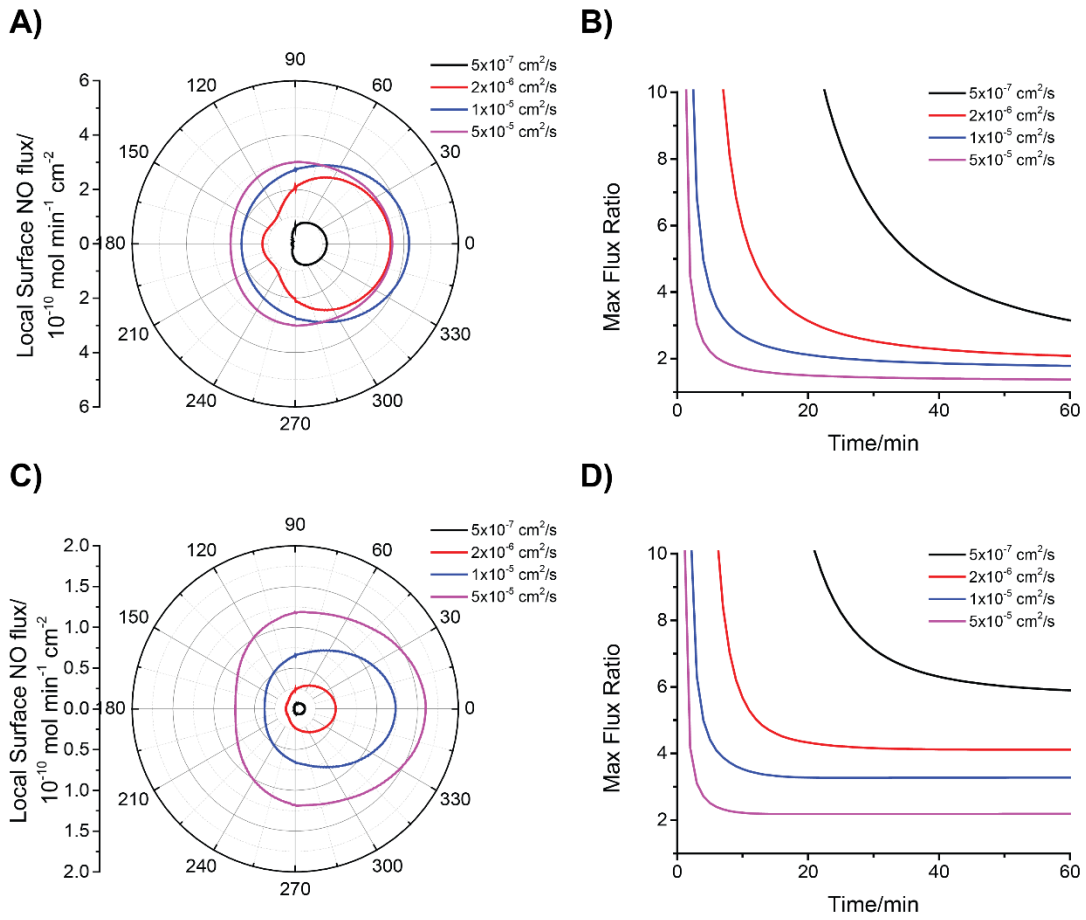

Figure 6.12. Effect of diffusion coefficient ($\overline{D}$) on distribution of NO on a catheter (same configuration of the Cook 7 Fr dual lumen catheter as shown in Figure 6.10) at 20 min. Partition coefficient K = 2.5. A) Polar graph of distribution of NO flux at catheter surface at 0% O_2; B) maximum flux ratio vs. time at 0% O_2; C) Polar graph of distribution of NO flux at catheter surface at 21% O_2; D) maximum flux ratio vs. time at 21% O_2.

Using this geometry of the commercial dual-lumen catheter as an example, the effect of different values of $\overline{D}$ and K on the NO distribution was further studied by simulation. The lowest diffusion coefficient (5×10^{-7} cm^2 s^{-1}) shows the most asymmetric distribution of surface NO flux, with a maximum surface flux ratio of >10 (see Figure 6.12 A). Such a large asymmetry is partially a transient effect as the low diffusion coefficient

allows NO to permeate through one side of the catheter before a significant amount of NO appears at the other side. With longer times (> 60 min), the asymmetry decreases (see Figure 6.12 B). However, during all of the 60 min period used for our simulations, the symmetry is always significantly better with larger diffusion coefficients. The same trend is true when reaction of NO with O_2 is also considered, although the exact asymmetry is worse compared to under same conditions but without taking into account the reaction of NO with O_2 (See Figure 6.12 C and D)

The effect of partition coefficient on the distribution is more complex and is time-dependent. Without O_2, the largest partition coefficient (K = 10; NO has favorable solubility in polymer phase) yields the lowest average flux of NO release at the 20 min (see Figure 6.13 A and B). This is likely because with high partition coefficient, more NO needs to be dissolved in the polymer phase before being released. A partition coefficient of 2 shows the best distribution at all time points. With 21% O_2, the average surface flux increases as K increases, but the trend for distribution changes with time. K = 2 offers the best distribution within the first 18 min, and K = 5 shows a better distribution between 18 and 36 min (see Figure 6.13 c and d). After 36 min, a K = 10 exhibits the best distribution, reaching a steady rate of 3.6 after 70 min (Figure 6.13d).

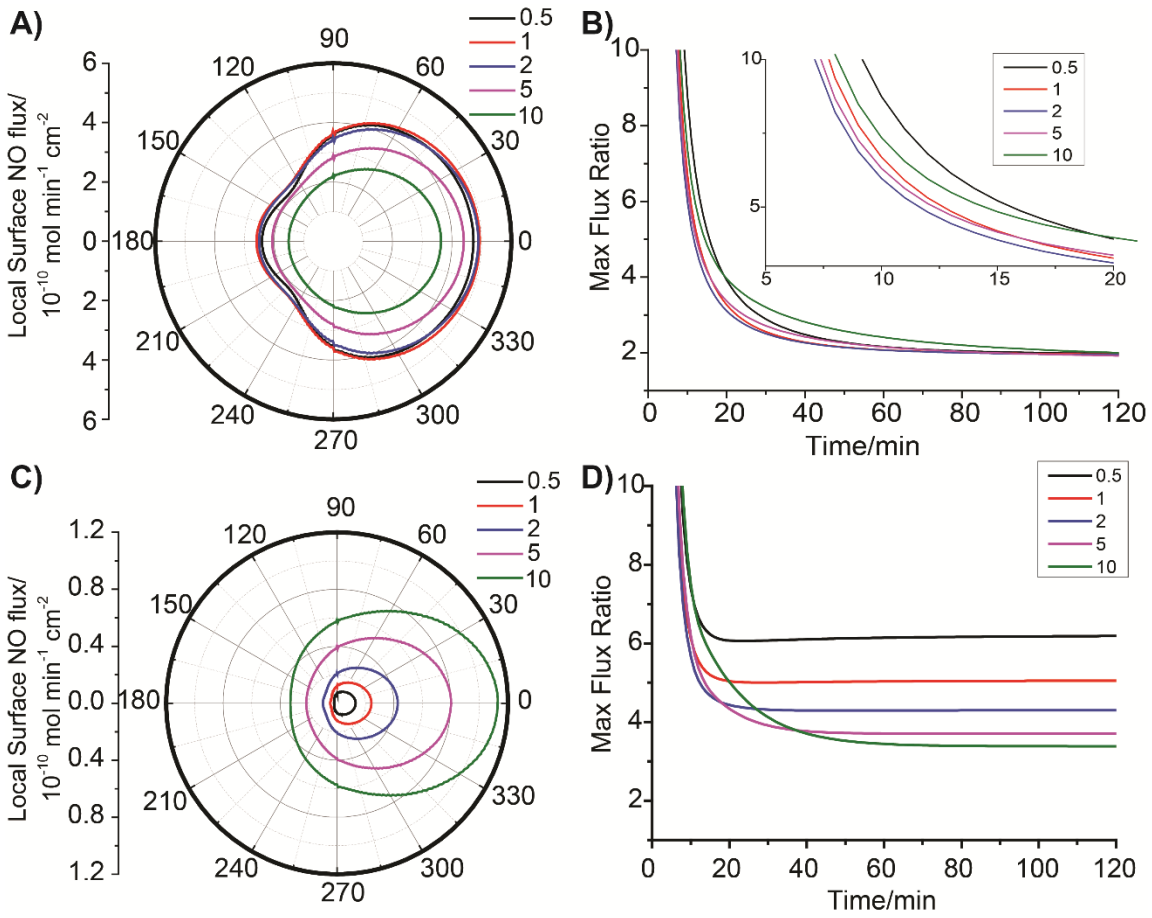

Figure 6.13. Effect of partition coefficient (*K*) on distribution of NO for Cook 7 Fr dual lumen catheter at 20 min in 0% O_2 and 21% O_2. Diffusion coefficient $\overline{D} = 2\times10^{-6}$ cm^2 s^{-1}. A) Polar graph of distribution of NO flux at catheter surface without O_2; B) maximum flux ratio vs time without O_2; C) Polar graph of distribution of NO flux at catheter surface with 21 %; D) maximum flux ratio vs time with 21% O_2.

A more symmetric design has also been proposed (cross-section geometry shown in Figure 6.3C) and the distribution of NO for this design was also investigated by simulation methods. The distribution of NO is indeed more symmetric for this more symmetric design; the maximum ratio of local surface fluxes falls below 2 after 20 min for $\overline{D}$ from 5.0 $\times10^{-7}$ cm^2 s^{-1} to 5.0 $\times10^{-5}$ cm^2 s^{-1} at a constant partition coefficient (see Figure

6.14A). Similarly, the maximum ratio of local surface flux also falls below 2 after 20 min for *K* ranging from 0.5 to 10 at a constant diffusion coefficient (see Figure 6.14B).

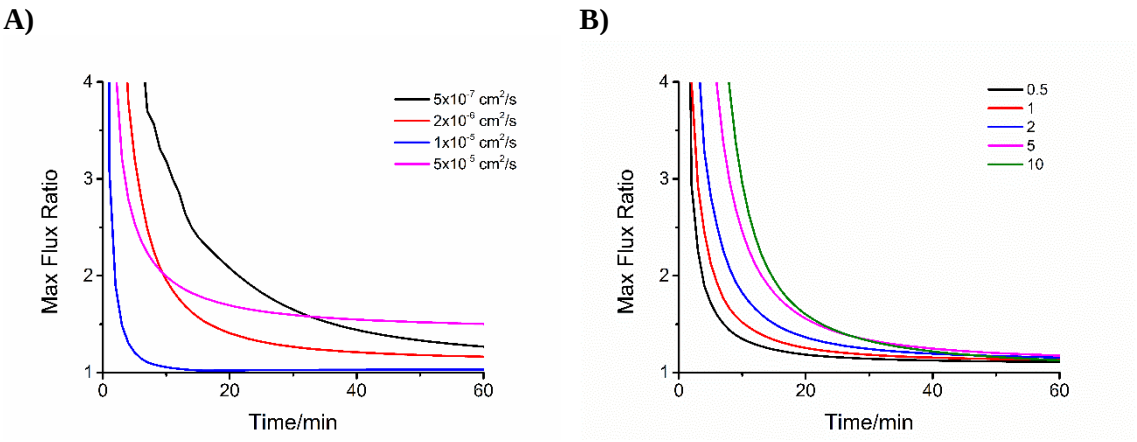

Figure 6.14. Effect of diffusion coefficient ($\overline{D}$) and partition coefficient (*K*) of NO in the polymer on the maximum ratio of local flux on an electrochemical NO releasing catheters with a more symmetric design as shown in Figure 6.3C. A) varied $\overline{D}$ with *K* = 2; B) varied *K* with $\overline{D}$ = 2×10^{-6} cm^2 s^{-1}.

6.5 Conclusions

Diffusion and partition coefficients for NO in silicone and different polyurethanes have been studied using a time lag method. The diffusion coefficients for block co- and tripolymer PUs containing PDMS segments are explained by effective medium theory with different morphologies. The effect of $\overline{D}$ and *K* on NO release response time as well as asymmetric NO distribution at the outermost surfaces of single and dual-lumen catheters have been examined both experimentally and by simulation. Polymers with large $\overline{D}$ and *K* for NO exhibit faster response times. Catheters made from polymers with larger $\overline{D}$ yield enhanced distribution of NO on the outer surface of the catheter. A more symmetric design

for multi-lumen catheter has been proposed, and the NO distribution is indeed more symmetric for all the partition coefficients and diffusion coefficients modeled. Overall, diffusion and partition coefficients of NO in polymers together with finite element analysis provide a powerful means in studying and designing novel NO releasing devices, especially new type of electrochemically generated NO catheters recently reported by our group.[29,42]

6.6 References

(1) Park, K.; Mosher, D. F.; Cooper, S. L. *J. Biomed. Mater. Res.* **1986**, *20*, 589.

(2) Anderson, J. M.; Rodriguez, A.; Chang, D. T. *Semin. Immunol.* **2008**, *20*, 86.

(3) Stewart, P. S.; Costerton, J. W. *Lancet* **2001**, *358*, 135.

(4) Saavedra, J. E.; Southan, G. J.; Davies, K. M.; Lundell, A.; Markou, C.; Hanson, S. R.; Adrie, C.; Hurford, W. E.; Zapol, W. M.; Keefer, L. K. *J. Med. Chem.* **1996**, *39*, 4361.

(5) Fang, F. C. *Nitric Oxide* **2012**, *27, Supplement*, S10.

(6) Bogdan, C. *Nat. Immunol.* **2001**, *2*, 907.

(7) Carpenter, A. W.; Schoenfisch, M. H. *Chem. Soc. Rev.* **2012**, *41*.

(8) Wallis, J. P. *Transfus. Med.* **2005**, *15*, 1.

(9) Frost, M. C.; Reynolds, M. M.; Meyerhoff, M. E. *Biomaterials* **2005**, *26*, 1685.

(10) Riccio, D. A.; Schoenfisch, M. H. *Chem. Soc. Rev.* **2012**, *41*.

(11) Amoako, K. A.; Archangeli, C.; Handa, H.; Major, T.; Meyerhoff, M. E.; Annich, G. M.; Bartlett, R. H. *ASAIO J.* **2012**, *58*, 238.

(12) Schoenfisch, M. H.; Mowery, K. A.; Rader, M. V.; Baliga, N.; Wahr, J. A.; Meyerhoff, M. E. *Anal. Chem.* **2000**, *72*, 1119.

(13) Wu, B. Y.; Wang, Y.; Roy-Chaudhury, P.; Meyerhoff, M. E. *Abstr Pap Am Chem S* **2009**, *237*.

(14) Zhang, H. P.; Schoenfisch, M. H.; Meyerhoff, M. E. *Abstr Pap Am Chem S* **1999**, *218*, U452.

(15) Frost, M. C.; Rudich, S. M.; Zhang, H.; Maraschio, M. A.; Meyerhoff, M. E. *Anal. Chem.* **2002**, *74*, 5942.

(16) Zhang, H.; Annich, G. M.; Miskulin, J.; Osterholzer, K.; Merz, S. I.; Bartlett, R. H.; Meyerhoff, M. E. *Biomaterials* **2002**, *23*, 1485.

(17) Colletta, A.; Wu, J.; Wo, Y.; Kappler, M.; Chen, H.; Xi, C.; Meyerhoff, M. E. *ACS Biomater. Sci. Eng.* **2015**, *1*, 416.

(18) Reynolds, M. M.; Hrabie, J. A.; Oh, B. K.; Politis, J. K.; Citro, M. L.; Keefer, L. K.; Meyerhoff, M. E. *Biomacromolecules* **2006**, *7*, 987.

(19) Coneski, P. N.; Schoenfisch, M. H. *Polymer Chemistry* **2011**, *2*.

(20) Reynolds, M. M.; Saavedra, J. E.; Showalter, B. M.; Valdez, C. A.; Shanklin, A. P.; Oh, B. K.; Keefer, L. K.; Meyerhoff, M. E. *J. Mater. Chem.* **2010**, *20*, 3107.

(21) Lamba, N. M.; Woodhouse, K. A.; Cooper, S. L. *Polyurethanes in biomedical applications*; CRC press, 1997.

(22) Mowery, K. A.; Meyerhoff, M. E. *Polymer* **1999**, *40*, 6203.

(23) Tanzi, M. C.; Mantovani, D.; Petrini, P.; Guidoin, R.; Laroche, G. *J. Biomed. Mater. Res.* **1997**, *36*, 550.

(24) Osman, A. F.; Edwards, G. A.; Schiller, T. L.; Andriani, Y.; Jack, K. S.; Morrow, I. C.; Halley, P. J.; Martin, D. J. *Macromolecules* **2012**, *45*, 198.

(25) Solís-Correa, R. E.; Vargas-Coronado, R.; Aguilar-Vega, M.; Cauich-Rodríguez, J. V.; Román, J. S.; Marcos, A. *J. Biomater. Sci. Polym. Ed.* **2007**, *18*, 561.

(26) Wiggins, M. J.; MacEwan, M.; Anderson, J. M.; Hiltner, A. *J. Biomed. Mater. Res. A* **2004**, *68*, 668.

(27) Coury, A. J.; Slaikeu, P. C.; Cahalan, P. T.; Stokes, K. B.; Hobot, C. M. *J. Biomater. Appl.* **1988**, *3*, 130.

(28) Hofler, L.; Koley, D.; Wu, J.; Xi, C.; Meyerhoff, M. E. *RSC Adv* **2012**, *2*, 6765.

(29) Ren, H.; Colletta, A.; Koley, D.; Wu, J.; Xi, C.; Major, T. C.; Bartlett, R. H.; Meyerhoff, M. E. *Bioelectrochemistry* **2014**, *104C*, 10.

(30) Fujita, H. *Polym. J.* **1991**, *23*, 1499.

(31) Wang, Z. F.; Wang, B.; Yang, Y. R.; Hu, C. P. *Eur. Polym. J.* **2003**, *39*, 2345.

(32) Hernandez, R.; Weksler, J.; Padsalgikar, A.; Choi, T.; Angelo, E.; Lin, J. S.; Xu, L.-C.; Siedlecki, C. A.; Runt, J. *Macromolecules* **2008**, *41*, 9767.

(33) Mizumoto, D.; Nojiri, C.; Inomata, Y.; Onishi, M.; Waki, M.; Kido, T.; Sugiyama, T.; Senshu, K.; Uchida, K.; Sakai, K.; Akutsu, T. *ASAIO J.* **1997**, *43*, M500.

(34) Shah, N.; Sax, J. E.; Ottino, J. M. *Polymer* **1985**, *26*, 1239.

(35) Mishra, A.; Aswal, V. K.; Maiti, P. *The Journal of Physical Chemistry B* **2010**, *114*, 5292.

(36) Yuliya, B.; Marie, U. In *Polymers for Personal Care and Cosmetics*; American Chemical Society: 2013; Vol. 1148, p 65.

(37) Pongkitwitoon, S.; Hernández, R.; Weksler, J.; Padsalgikar, A.; Choi, T.; Runt, J. *Polymer* **2009**, *50*, 6305.

(38) Sax, J.; Ottino, J. M. *Polymer Engineering & Science* **1983**, *23*, 165.

(39) Diederichsen, K. M.; Brow, R. R.; Stoykovich, M. P. *ACS Nano* **2015**, *9*, 2465.

(40) Kirkpatrick, S. *Phys. Rev. Lett.* **1971**, *27*, 1722.

(41) Hofmeister, I.; Landfester, K.; Taden, A. *Angew. Chem. Int. Ed.* **2015**, *54*, 327.

(42) Ren, H.; Coughlin, M. A.; Major, T. C.; Aiello, S.; Rojas Pena, A.; Bartlett, R. H.; Meyerhoff, M. E. *Anal. Chem.* **2015**, *87*, 8067.

CHAPTER 7.

ELECTROCHEMICAL GENERATION OF NO FOR POTENTIAL APPLICATION IN INHALED NO THERAPY

7.1 Introduction

As discussed in Chapter 1, nitric oxide (NO) is endogenously produced and plays key roles in several physiological processes, including inducing vasodilation, preventing platelet adhesion/activation and promoting wound healing and angiogenesis.[1-6] Nitric oxide is also a potent antimicrobial agent released by macrophages and nasal epithelial cells to fight infection.[7,8] Inspired by these functions, NO releasing materials have been developed and applied in different medical devices to improve their biocompatibility.[9,10] In addition, direct inhalation of nitric oxide (INO) has become a mainstay of intensive care for lung failure, since its first medical application 20 years ago.[11] INO induces preferential pulmonary vasodilation and lowered pulmonary vascular resistance.[12] As a result, INO has been approved for use in persistent pulmonary hypertension of newborn babies (PPHN) and has been demonstrated to improve oxygenation and reduce the need for the higher-risk extracorporeal membrane oxygenation (ECMO) therapy.[13,14] INO is essential in neonatology, lung transplantation, and pulmonary hypertension. Although currently only approved for treatment of PPHN, INO has shown beneficial effect on other illnesses including pneumonia,[15] ARDS (acute respiratory distress syndrome),[16] stroke,[17] and

cardiopulmonary bypass.[18] Recent studies have also reported the use of INO as an inhaled antiseptic agent in the treatment of cystic fibrosis[19] and tuberculosis.[20] Further, the anti-inflammatory properties of INO have also been reported to modulate the immune response and promote survival in patients with malaria,[21] a disease that affects 225–600 million worldwide each year.[22] Long-term use of INO has been studied in some ambulatory patients with pulmonary hypertension,[23] pulmonary fibrosis,[24] and COPD (chronic obstruction pulmonary disorder).[25] INO has also been demonstrated to provide neuroprotection and reduce brain damage.[26]

At present, INO requires a gas cylinder of NO and a complex delivery device to regulate and monitor NO and is considered one of the most expensive drugs in neonatal medicine.[27] The cost of implementing INO is $3000 per day per patient and the cost at the University of Michigan Hospital alone is $4.8M per year.[28] Despite the expense of this system, the INO therapy is still considered cost effective in terms of decreasing the need for ECMO and essential to prevent death of some neonates.[29] The cost mostly stems from the very expensive NO tank at ppm levels, which is a consumable and needs to be relatively fresh. This is because NO undergoes disproportionation to form N_2O and highly toxic NO_2, especially at elevated pressure, limiting the use-life of a cylinder of NO >800 ppm in medical applications.[30] On the other hand, the entire INO distribution system, especially the NO cylinder, is heavy and cumbersome. Because of the high cost and the complexity of the system, INO is unavailable in many hospitals, and is not practical for outpatient usage. An inexpensive yet portable device for INO is the key in making the INO available to more patients around the world, facilitating clinical trials of INO therapy on more diseases as described above, and ultimately making INO available for home use.

GeNO Inc. is developing a NO generation technique based on catalytic conversion of liquid NO_2/N_2O_4 into NO.[31] However, using highly toxic NO_2 as the starting material induces significant safety concerns. Generation of NO from N_2 and O_2 via pulsed electrical discharges has also been demonstrated for INO application.[32] However, NO generation is concomitant with formation of toxic NO_2 and O_3, which needs further scrubbing before use.

In earlier work reported in this dissertation (see Chapters 3), generation of NO via electrochemical reduction of inexpensive nitrite ions was demonstrated and NO in 0-400 ppb range at 0.2 L/min can be achieved by applying different potentials to the working electrode.[33,34] Such an *in situ* electrochemical NO generation system is very attractive for INO as the NO can be produced on demand, and the NO levels produced can be easily regulated. However, INO requires a much wider NO concentration range (up to 200 ppmv) at higher flow rates (from 1–5 L/min), which is 100–100,000 times higher than the original design that was described in our earlier work. In this chapter, the generation of gas phase NO at concentrations relevant for INO therapy is explored using the new electrochemical NO generation system.

7.2 Experimental Details

7.2.1 Chemical and Materials

Sodium nitrite (99.99%), HEPES acid (99.5%), HEPES sodium salt (99.5%), copper(II) sulfate pentahydrate (99.999%), and 1,4,7-trimethyl-1,4,7-triazacyclononane (Me_3TACN) (97%) were purchased from Sigma-Aldrich (St. Louis, MO) and used as

received. All aqueous solutions were prepared with deionized water (18 M Ω cm^{-1}) from a Milli-Q system (Millipore Corp., Billerica, MA). Platinum (Pt) mesh (99.9%, 52 mesh, 50 × 50 mm) was obtained from Sigma-Aldrich (St. Louis, MO), and a gold (Au) mesh electrode (99.99%, 52 mesh, 50 × 50 mm) was a product of Alfa Aesar (Ward Hill, MA). Teflon® PFA-coated platinum wires (0.125 mm OD) from A-M Systems (Sequim, WA) were used as lead wires for the mesh electrodes. NO (45 ppm) and NO_2 (20 ppm) standards were products from Cryogenic Gas Inc. (Detroit, MI).

All the electrochemical experiments were performed on either a Gamry 600 potentiostat or a CH Instrument 760 potentiostat. The generation of NO was measured in real time via chemiluminescence by an NO analyzer from GE Analytics (Boulder, CO).

7.2.2 Experimental Setup

A homemade glass cell with port for a bubbler and gas outlet was filled with 80 mL solution of 7 mM $CuMe_3TACN$, 1.0 M $NaNO_2$ and 0.5 M HEPES buffer (pH 7.3). Further electrochemical characterization of the $Cu(II)Me_3TACN$ complex is described in Appendix A. The platinum mesh electrode and the Au mesh electrode were submerged in the solution and physically separated by a fritted glass bubbler to prevent short circuit. In the case where the potential on the working electrode needs to be determined, a reference electrode was added to the system. The fritted glass bubbler was used to produce smaller bubbles so that the mass transfer of generated NO between aqueous phase and gas phase is greatly enhanced. For long term experiments (electrolysis > 8 h), especially at higher flow rate (>1.0 L/min), the carrier gas (e.g., N_2) was first passed through a 1.0 M NaCl solution to

take up some water (i.e., humidified) before entering the electrochemical cell, preventing the drying of the solution in the cell.

7.2.3 Detection of N_2O, NO_2 and Aerosol

N_2O detection was carried out similar to a previously reported method based on gas phase IR spectroscopy.[35] Briefly, the INO solution underwent bulk electrolysis at a constant current of 5 mA for 30 min. The headspace of the cell was then sampled into the IR gas cell and quantification was based on integration of N_2O feature peaks at 2235 and 2212 cm^{-1} in the IR spectra using a calibration curve.

NO_2 was detected based on photolysis of NO_2 to generate NO (see Figure 7.1 for the schematic). The gas phase sample was passed through a photochemical reactor equipped with 350 nm UV lamp (Rayonet RPR-600, Branford, CT) in a U-shape glass tube before feeding into the nitric oxide analyzer (NOA). The increased signal in the presence of the UV lamp being turned on was used for NO_2 quantification. NO_2 at levels of 1–20 ppmv (achieved by mixing different ratios of standard NO_2 with N_2 using a mass flow controller) was employed to calibrate the photolysis-chemiluminescence system to obtain NO_2 conversion efficiency.

Aerosol was detected by passing the gas into a septum sealed deoxygenated DI water for 5, 10 and 20 min, followed by removal of the dissolved NO by purging with high purity N_2 for 10 min. The nitrite in the solution was quantified using chemiluminescence. Briefly, an aliquot of the solution was injected to a cell containing 0.1 M H_2SO_4 and 5% KI solution that is connected to the nitric oxide analyzer.

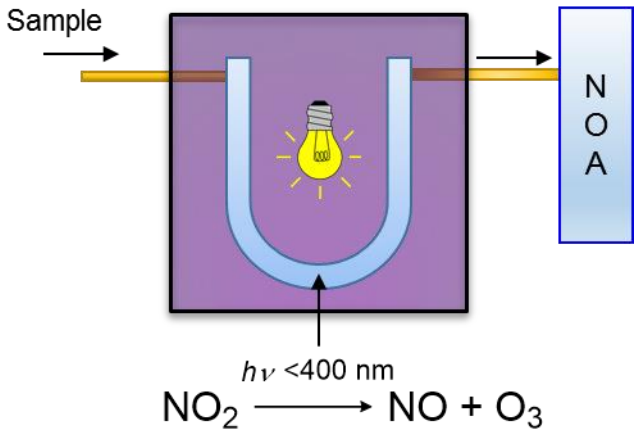

Figure 7.1. Experimental setup for chemiluminescence detection of NO_2. The sample is passed through a UV photochemical reactor and NO_2 is converted to NO, which is subsequently detected by nitric oxide analyzer (NOA).

7.3 Results and Discussion

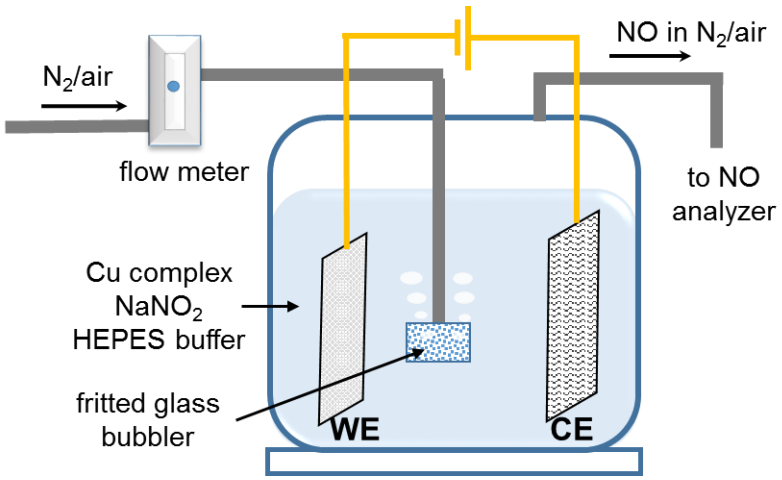

Figure 7.2. Schematic of bulk electrolysis cell for INO generation. WE: working electrode (Pt mesh); CE: counter electrode (Au mesh). The solution contains 7 mM $CuMe_3TACN$, 1.0 M $NaNO_2$ and 0.5 M HEPES buffer (pH 7.3).

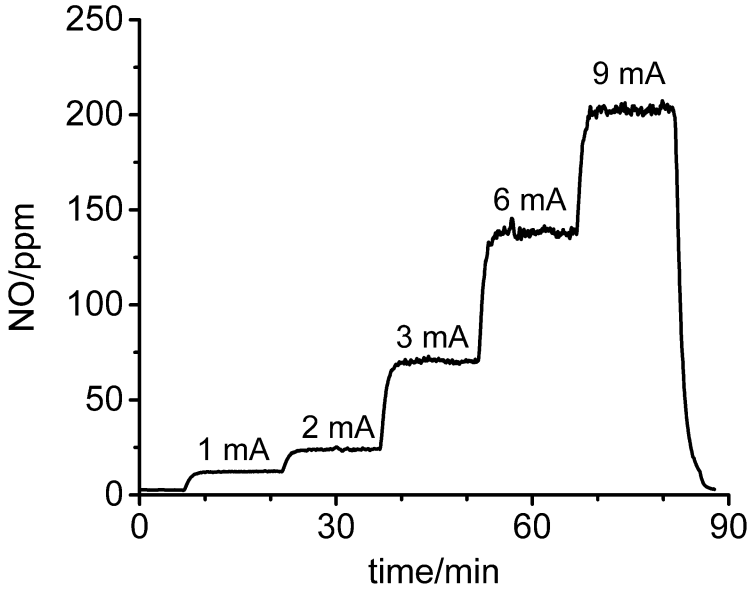

Figure 7.3. Modulation of NO concentration in gas phase by applying different constant currents. The bubbling gas is N_2 at 1 L/min. The solution contains 7 mM $CuMe_3TACN$, 1.0 M $NaNO_2$ and 0.5 M HEPES buffer (pH 7.3).

The electrochemical NO delivery system was accomplished in a glass cell for generation of gas phase NO for potential application in INO. The schematic is shown in Figure 7.2. In this two electrode system, a Pt mesh electrode was the working electrode and a Au mesh was the counter electrode. By applying different constant currents between the electrodes, different concentrations of NO (from 0-200 ppm) can be generated in the gas phase, and the NO concentration is very stable (Figure 7.3). The time for NO concentration to change from one level to another is less than 5 min, demonstrating a good temporal control of the system (Figure 7.3). In this NO generation system, the constant current method was used to generate NO in contrast to the constant potential method introduced in the earlier catheter studies (see Chapter 3).[34] There are several reasons behind this preference. First, gas phase NO concentration is proportional to the NO flux

from the electrode surface at steady-state, which, in turn, is directly determined by the current on the working electrode. Therefore, the constant current method provides a more stable NO concentration/generation rate and is less sensitive to fluctuations in temperature or solution composition. Another advantage is that the constant current method consists of only two electrodes – a reference electrode is not necessary, making the electronics much simpler.

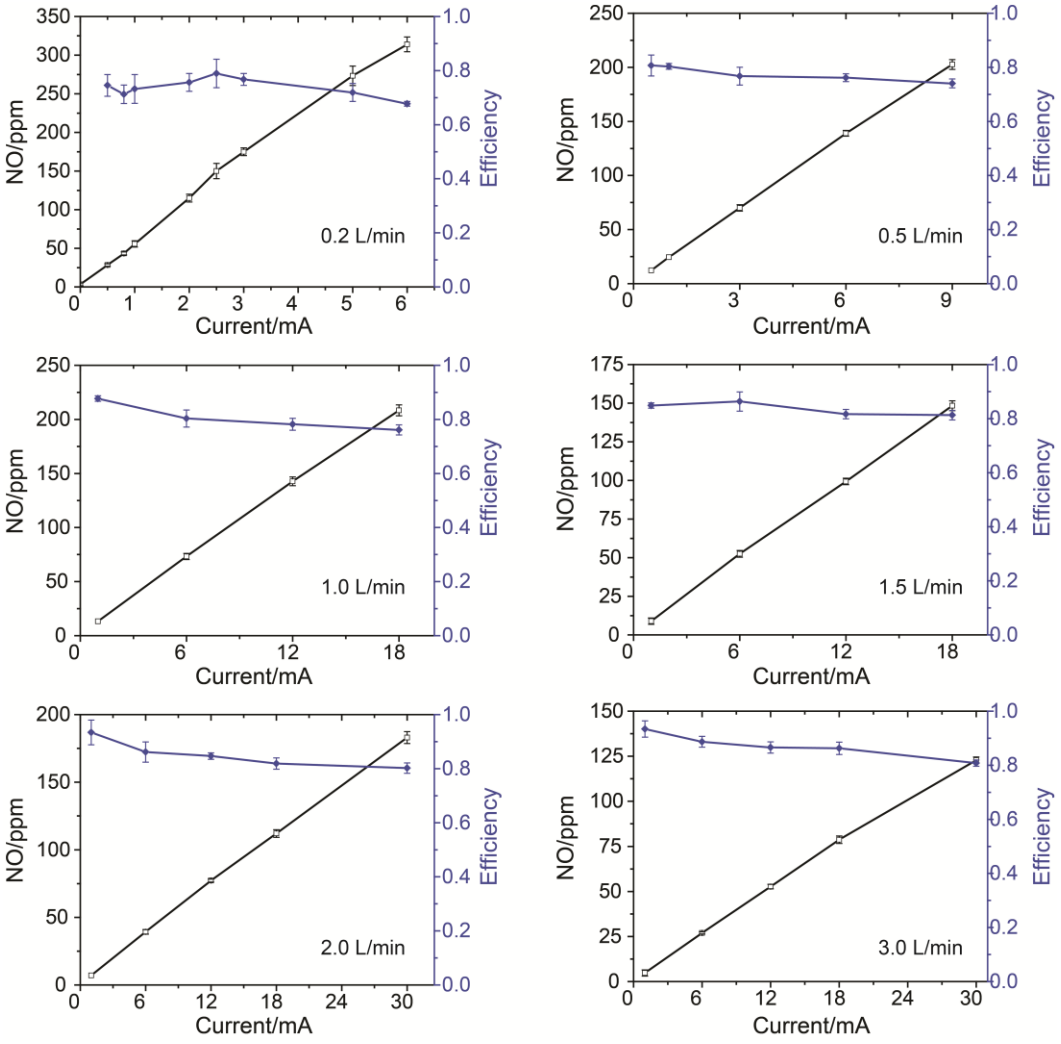

Figure 7.4. Current vs. NO concentration in the gas phase at different flow rates and the corresponding faradaic efficiency. The solution contains 7 mM $CuMe_3TACN$, 1.0 M $NaNO_2$ and 0.5 M HEPES buffer (pH 7.3).

At different flow rates of the purge gas from 0.2 L/min to 3.0 L/min, NO concentrations of 10–150 ppm in N_2 can be generated by applying different currents matching the flow rate (Figure 7.4). Higher flow rates require higher current to yield the same NO concentration because of the dilution effect of the carrier gas. Under a given flow rate, the NO concentration in the gas phase is proportional to the current applied (as shown in Figure 7.4), and the associated faradaic efficiency is relatively stable (fluctuation < 10%) for different currents. This is because the system operates within 50% of the limiting current where no significant side reactions occur. Also, the measured efficiencies are relatively high considering that both of the working and counter electrodes are in the same cell solution where reaction/consumption of product on the counter electrode is inevitable, and contributes to some decrease in efficiency.

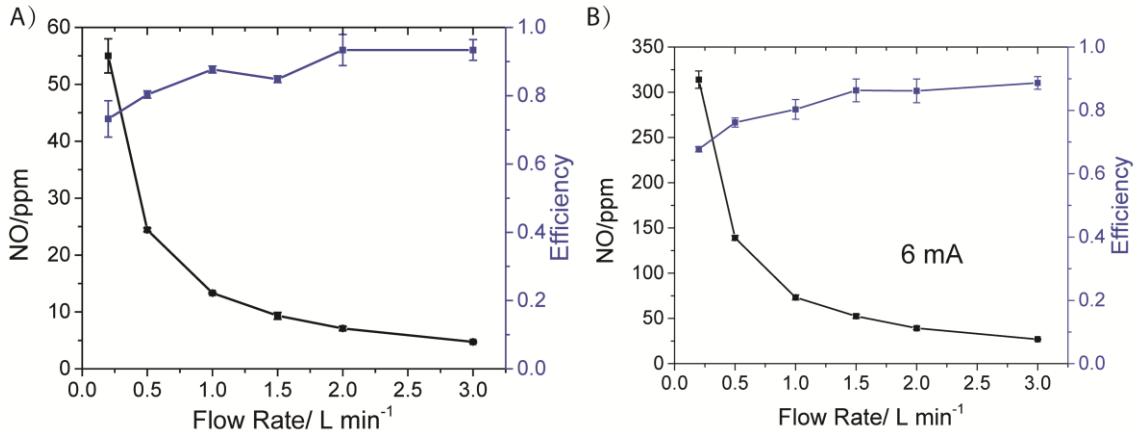

Figure 7.5. Effect of flow rate on NO concentration in the gas phase and current efficiencies at A) 1 mA and B) 6 mA.

The current efficiency increases as the bubbling/purge flow rate increases (Figure 7.5). This enhanced effect of bubbling/flow rate on current efficiency results from two processes. Higher flow rate induces more efficient mass transfer, for both the catalyst to

get to the surface of the working electrode, as well as the substrate (nitrite) mixing with reduced catalyst very near the surface after the Cu(I)-ligand complex is formed. Also, higher flow rate captures/purges more NO over a given time period, decreasing the concentration of NO in solution more effectively, preventing the cross reaction of product NO at the counter electrode, where oxidation to NO_2 could occur.

Nitric oxide generated from the electrochemical device is fresh at ambient pressure because the NO is produced *in situ*, avoiding production of N_2O and toxic NO_2 from disproportionation of NO, which remains a problem for NO in high pressure cylinders. The produced NO in N_2 is pure with no NO_2 or N_2O detected in the gas phase, which is also indicated by the relatively high overall current efficiency. No significant nitrite containing aerosol (<5 ppb) was detected.

Based on the amount of nitrite (1.0 M) in the solution, the amount of NO (in moles) that can be produced from this electrochemical device is equivalent to more than 10 full cylinders of INO commercially available (D-size, 800 ppm, 2000 psig), yet the size of the device is less 20% of one cylinder. Indeed, the bulk electrolysis of the one volume of nitrite solution (80 mL) yielded a stable NO concentration in the gas phase that would be equivalent to more than 2 cylinders of NO (See Figure 7.6).

In addition, the NO generating solution is very stable under ambient conditions. During such storage in air for 60 days, the solution produced similar amount of NO at given current on different days (Figure 7.7). Moreover, the same electrodes and electronics are also very stable and can be reused many times; the consumables are only the solution, which is very inexpensive compared to the current INO cylinder.

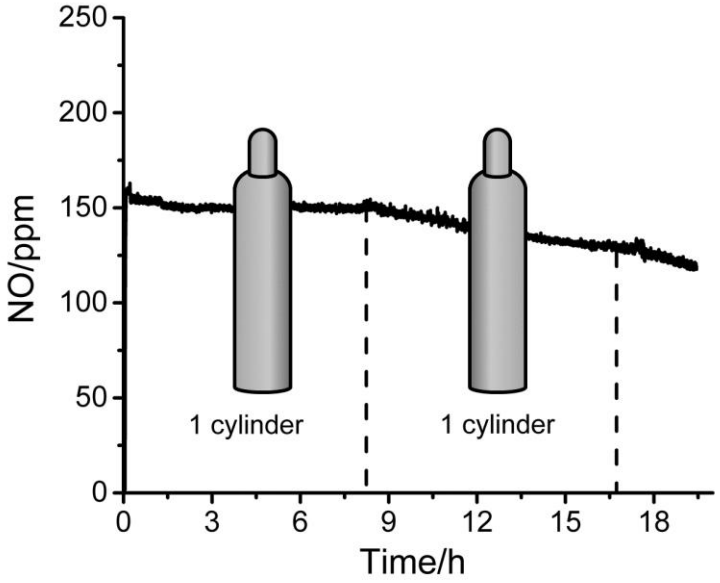

Figure 7.6. Electrochemical NO generation for INO at 3L/min from the same 80 mL solution at 36 mA.

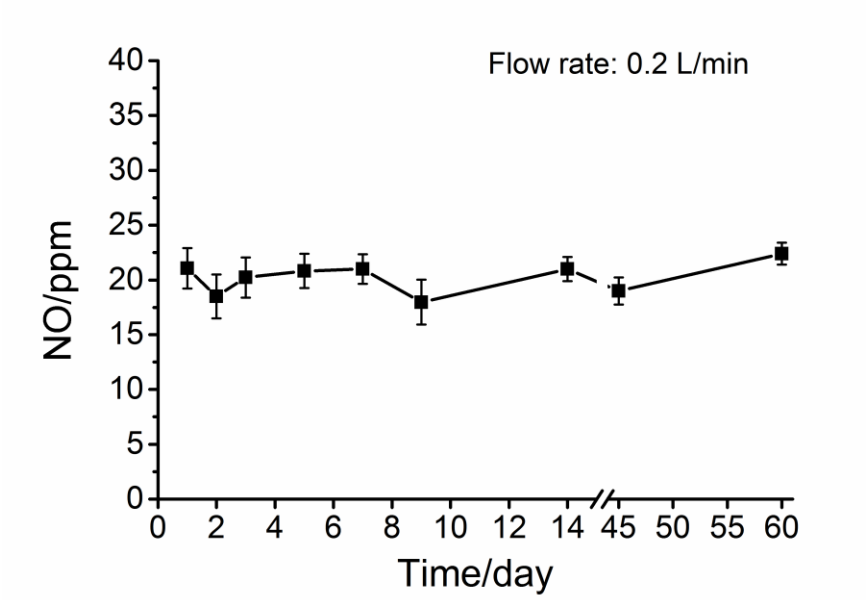

Figure 7.7. NO generation from the same solution at 0.5 mA for 4 h each day. The solution is stored at ambient conditions for up to 60 days.

It is desirable to demonstrate that instead of N_2, air can also serve as a carrier gas. Using this system, ppm levels of NO in air can still be produced with essentially no NO_2 detected (<1 ppm) (Figure 7.8), although the concentration of NO is much lower (~80% reduction at 5 mA) than that if the carrier gas is N_2 under the same conditions. This is likely due to the reaction of NO and O_2 with water to form nitrite, as well as the scavenging of Cu(I) by O_2. Since NO is generated at the surface of the electrode, its concentration is highest at the electrode surface. Reaction between NO and O_2 is second order with respect to NO both in the gas phase and in the solution phase, producing an increased reaction rate at higher NO concentrations. The NO_2 concentration from reaction of NO with air is shown in Figure 7.9 based on rate constant in the literature.[36] In the gas phase, it takes 12 s to produce 1 ppm of NO_2 from the reaction of 200 ppm NO and air. In the solution phase, the product of NO oxidation is nitrite. This explains why no significant NO_2 (<1 ppm) is produced even when air was used as a carrier gas in the experiment. This is likely because most of the reaction between NO and O_2 occurs in the solution phase. Overall, air can be used as carrier/bubbling gas for the electrochemical NO generation system, granting the system the potential to be transferred into a more portable device for use of INO at more sites, even at home. In order to produce higher levels of INO for hospital use, using N_2 as the purge gas and then combining this stream with a given flow of oxygen immediately before entering the patient would be the preferred arrangement.

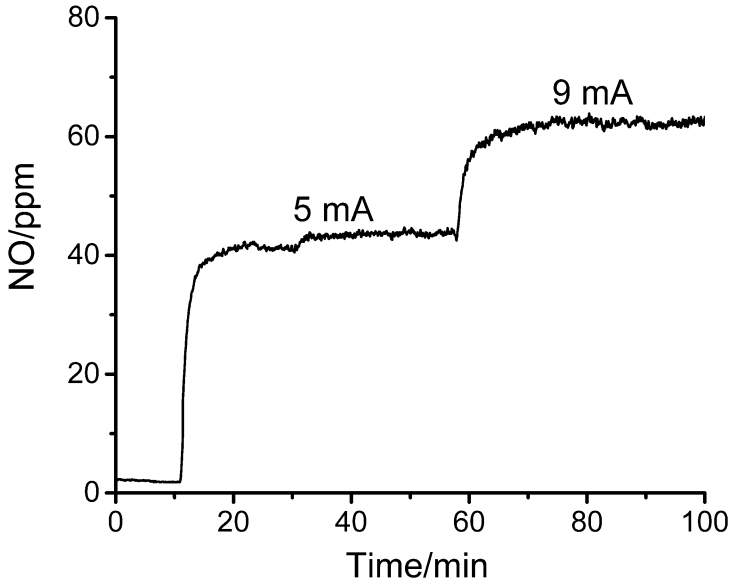

Figure 7.8. NO generation in gas phase using air as bubbling gas. Flow rate of air is 0.2 L/min.

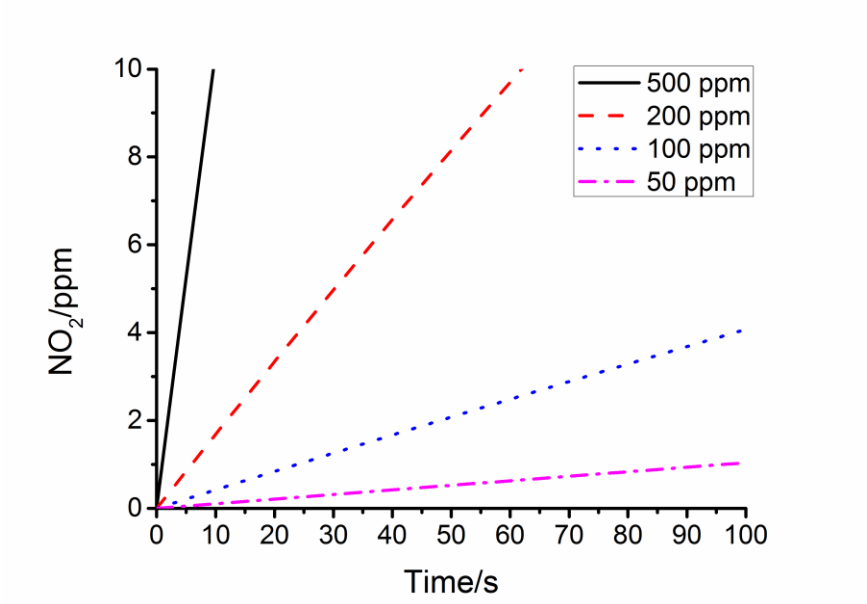

Figure 7.9. NO_2 produced from reaction of NO at different concentration with air in the gas phase vs. duration of the reaction based on rate equation $d[NO_2]/dt=2\ k\ [NO]^2[O_2]$, where $k = 6.0 \times 10^3$ $M^{-2}\ s^{-1}$.

For a more compact design, silicone rubber bundles can also be employed as a gas exchange device directly inside the electrolyte solution (see Figure 7.10). Again, as shown in Figure 7.11, NO levels over a clinically useful range can be generated in the gas phase, although the overall efficiency is slightly lower than the direct bubbling in the electrochemical cell. Further, there is a longer lag period to change the gas phase levels to a new steady-state value when changing current applied. This is likely because the rate is governed by the gas exchange at the solution/polymer and polymer/gas interfaces.

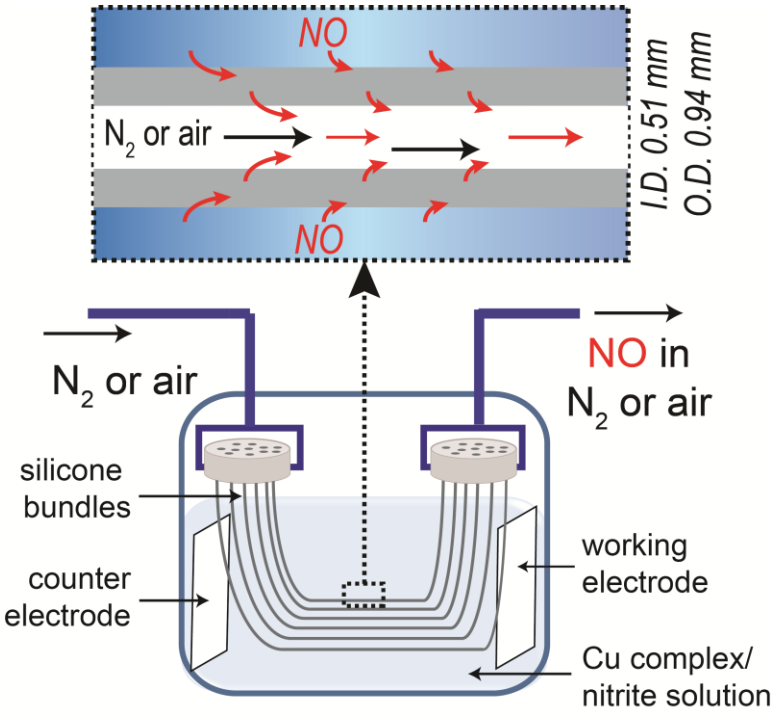

Figure 7.10. Silicone rubber bundle design for gas exchange in electrolysis solution for INO generation.

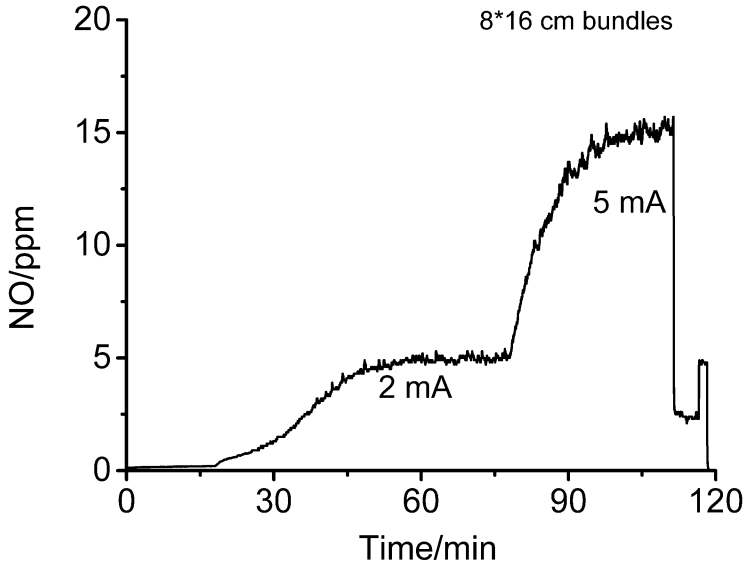

Figure 7.11. NO generation from using silicone rubber bundle in the electrolysis solution for gas exchange. The bundles contain 8 silicone tubing (i.d. 0.51 mm, o.d. 0.94 mm, length 16 cm). Flow rate of N_2 passing the bundles is 2 L/min.

7.4 Conclusions

In conclusion, using constant current method, relatively pure NO can be generated from electrochemical reduction of nitrite at the surface of a Pt mesh electrode. The concentration of NO in the gas phase can range from 1–150 ppm at different flow rates, which is relevant for INO therapy and can potentially be a substitute for the NO tank currently used in the hospital. The electrochemical INO system is robust and stable, and NO concentration in the gas phase can be easily tuned by applying different constant currents. The system can also operate using air as carrier gas for NO, suggesting the possibility of developing a more portable INO device. Such system can be readily adapted for oxygenator application, where a sweep gas of NO can potentially alleviate significant issues of clot formation in the use of oxygenators during open heart surgery and ECMO.

Finally, this robust NO generator can serve as a tool for fundamental biological/physiological studies requiring a given NO concentration in the gas phase, e.g. effect of NO on airway related diseases, both *in vitro* and *in vivo*.

7.5 References

(1) Fang, F. C. *J. Clin. Invest.* **1997**, *99*, 2818.

(2) Luo, J.-d.; Chen, A. F. *Acta Pharmacol. Sin.* **2005**, *26*, 259.

(3) Wallis, J. P. *Transfus. Med.* **2005**, *15*, 1.

(4) Williams, D. L. H. *Org. Biomol. Chem.* **2003**, *1*, 441.

(5) Mellion, B. T.; Ignarro, L. J.; Ohlstein, E. H.; Pontecorvo, E. G.; Hyman, A. L.; Kadowitz, P. J. *Blood* **1981**, *57*, 946.

(6) Chaux, A.; Ruan, X. M.; Fishbein, M. C.; Ouyang, Y.; Kaul, S.; Pass, J. A.; Matloff, J. M. *The Journal of Thoracic and Cardiovascular Surgery* **1998**, *115*, 604.

(7) Rouby, J. *Am. J. Respir. Crit. Care Med.* **2003**, *168*, 265.

(8) Halpenny, G. M.; Mascharak, P. K. *Anti-Infective Agents in Medicinal Chemistry (Formerly `Current Medicinal Chemistry - Anti-Infective Agents)* **2010**, *9*, 187.

(9) Frost, M. C.; Reynolds, M. M.; Meyerhoff, M. E. *Biomaterials* **2005**, *26*, 1685.

(10) Carpenter, A. W.; Schoenfisch, M. H. *Chem. Soc. Rev.* **2012**, *41*.

(11) Pepke-Zaba, J.; Higenbottam, T.; Dinh-Xuan, A. T.; Stone, D.; Wallwork, J. *The Lancet* **1991**, *338*, 1173.

(12) Creagh-Brown, B. C.; Griffiths, M. J.; Evans, T. W. *Critical Care* **2009**, *13*, 221.

(13) Roberts Jr, J. D.; Fineman, J. R.; Morin, F. C.; Shaul, P. W.; Rimar, S.; Schreiber, M. D.; Polin, R. A.; Zwass, M. S.; Zayek, M. M.; Gross, I. *N. Engl. J. Med.* **1997**, *336*, 605.

(14) *N. Engl. J. Med.* **1997**, *336*, 597.

(15) Blomqvist, H.; Wickerts, C.; Andreen, M.; Ullberg, U.; ÖOUrtqvist, Å.; Frostell, C. *Acta Anaesthesiol. Scand.* **1993**, *37*, 110.

(16) Dellinger, R. P.; Trzeciak, S. W.; Criner, G. J.; Zimmerman, J. L.; Taylor, R. W.; Usansky, H.; Young, J.; Goldstein, B. *Critical Care* **2012**, *16*, R36.

(17) Charriaut-Marlangue, C.; Bonnin, P.; Gharib, A.; Leger, P.-L.; Villapol, S.; Pocard, M.; Gressens, P.; Renolleau, S.; Baud, O. *Stroke* **2012**, *43*, 3078.

(18) Ardehali, A.; Hughes, K.; Sadeghi, A.; Esmailian, F.; Marelli, D.; Moriguchi, J.; Hamilton, M. A.; Kobashigawa, J.; Laks, H. *Transplantation* **2001**, *72*, 638.

(19) Ratjen, F.; Gärtig, S.; Wiesemann, H.; Grasemann, H. *Respir. Med.* **1999**, *93*, 579.

(20) Long, R.; Jones, R.; Talbot, J.; Mayers, I.; Barrie, J.; Hoskinson, M.; Light, B. *Antimicrob. Agents Chemother.* **2005**, *49*, 1209.

(21) Bergmark, B.; Bergmark, R.; De Beaudrap, P.; Boum, Y.; Mwanga-Amumpaire, J.; Carroll, R.; Zapol, W. *The Pediatric infectious disease journal* **2012**, *31*, e250.

(22) *World Health Organization. WHO Guildelines for the Treatment of Malaria*; World Health Organization: Geneva, Switzerland, 2010.

(23) Channick, R. N.; Johnson, F. W.; Williams, P. J.; Auger, W. R.; Fedullo, P. F.; Moser, K. M.; Newhart, J. W. *CHEST Journal* **1996**, *109*, 1545.

(24) Yung, G. L.; Kriett, J. M.; Jamieson, S. W.; Johnson, F. W.; Newhart, J.; Kinninger, K.; Channick, R. N. *The Journal of Heart and Lung Transplantation* **2001**, *20*, 1224.

(25) Vonbank, K.; Ziesche, R.; Higenbottam, T.; Stiebellehner, L.; Petkov, V.; Schenk, P.; Germann, P.; Block, L. *Thorax* **2003**, *58*, 289.

(26) Garry, P. S.; Ezra, M.; Rowland, M. J.; Westbrook, J.; Pattinson, K. T. *Exp. Neurol.* **2015**, *263*, 235.

(27) Subhedar, N.; Dewhurst, C. *Archives of Disease in Childhood. Fetal and Neonatal Edition* **2007**, *92*, F337.

(28) Cole, F. S.; Alleyne, C.; Barks, J. D.; Boyle, R. J.; Carroll, J. L.; Dokken, D.; Edwards, W. H.; Georgieff, M.; Gregory, K.; Johnston, M. V.; Kramer, M.; Mitchell, C.; Neu, J.; Pursley, D. M.; Robinson, W. M.; Rowitch, D. H. *Pediatrics* **2011**, *127*, 363.

(29) Angus, D. C.; Clermont, G.; Watson, R. S.; Linde-Zwirble, W. T.; Clark, R. H.; Roberts, M. S. *Pediatrics* **2003**, *112*, 1351.

(30) Tsukahara, H.; Ishida, T.; Todoroki, Y.; Hiraoka, M.; Mayumi, M. *Free Radical Res.* **2003**, *37*, 171.

(31) Lovich, M. A.; Fine, D. H.; Denton, R. J.; Wakim, M. G.; Wei, A. E.; Maslov, M. Y.; Gamero, L. G.; Vasquez, G. B.; Johnson, B. J.; Roscigno, R. F.; Gilbert, R. J. *Nitric Oxide* **2014**, *37*, 66.

(32) Yu, B. L.; Muenster, S.; Blaesi, A. H.; Bloch, D. B.; Zapol, W. M. *Sci. Transl. Med.* **2015**, *7*.

(33) Ren, H.; Colletta, A.; Koley, D.; Wu, J.; Xi, C.; Major, T. C.; Bartlett, R. H.; Meyerhoff, M. E. *Bioelectrochemistry* **2015**, *104*, 10.

(34) Ren, H.; Wu, J.; Xi, C.; Lehnert, N.; Major, T.; Bartlett, R. H.; Meyerhoff, M. E. *ACS Appl. Mater. Interfaces* **2014**, *6*, 3779.

(35) Peng, B.; Meyerhoff, M. E. *Electroanalysis* **2013**, *25*, 914.

(36) Tsukahara, H.; Ishida, T.; Mayumi, M. *Nitric Oxide* **1999**, *3*, 191.

CHAPTER 8.

CONCLUSIONS AND FUTURE DIRECTIONS

8.1 Conclusions

As demonstrated within this dissertation, nitric oxide (NO), an endogenously produced small molecule, has many favorable physiological functions and can be used for improving the performance/biocompatibility of various medical devices from catheters to intervascular devices, as well as for certain treatments (e.g., chronic wounds, respiratory diseases etc.). Controllable and inexpensive methods for release/delivery of NO would significantly facilitate the application of NO in various medical settings. This thesis has focused on the development of electrochemical methods for modulated NO release from inexpensive inorganic nitrite salts.

In Chapter 2, the NO generation was optimized from a Cu^0 wire-based system in a catheter configuration. Nitric oxide was generated by a pulse sequence containing anodic and cathodic pulses in sequence, and NO surface fluxes $>1 \times 10^{-10}$ mol min^{-1} cm^{-2} were shown to be readily generated from a single lumen catheter for more than 60 h. Such electrochemical NO releasing catheters showed reduced clotting *in vivo* and prevented the formation of biofilms on their surfaces from *S. aureus* and *E. coli* in drip flow bioreactor experiments.

In Chapter 3, an alternate electrochemical NO generation method was developed using a copper(II)-ligand complex, CuTPMA, as a catalyst for electrochemical reduction of nitrite. A constant reductive potential was applied on the working electrode to generate NO, and NO fluxes from (0–3.2) $\times 10^{-10}$ mol $min^{-1}cm^{-2}$ can be readily modulated by applying different potentials in a single lumen catheter setup. Such a catheter was shown to release NO continuously for more than 8 days. Such NO release was also applied in a dual-lumen catheter configuration and exhibited significant anti-clotting properties *in vivo*. It was further demonstrated that NO release for a short period of time (3 h) each day was sufficient to prevent the microbial biofilm formation on the catheter surface for over a 3-day period.

This electrochemical NO release system using CuTPMA as the electron transfer mediator/catalyst was further utilized for the development of a catheter-type electrochemical NO releasing PO_2 sensor, as described in Chapter 4. This PO_2 sensor was based on the commercial dual lumen catheter. One of the lumens was dedicated to electrochemical NO release as described in Chapter 3, and the other lumen was dedicated for PO_2 sensing, similar to a Clark-type O_2 sensor.[1] This newly-developed NO releasing PO_2 sensing catheter provided much more accurate PO_2 values when implanted in rabbit veins for 7 h and pig arteries for 21 h when compared with the control PO_2 sensors without electrochemical NO release, which deviated negatively from the true value based on intermittent blood draws and *in vitro* measurements.

In Chapter 5, the facile control of the NO release from the catheter surface was further utilized for fundamental dosage studies of NO on dispersal/killing of mature microbial biofilm. NO release for 3 h in the physiologically relevant range showed

significant killing of mature *P. aeruginosa* biofilms. Synergy between NO release and addition of the antibiotic gentamicin to the test media was also found. This study not only demonstrated that electrochemical NO release provides a robust tool for fundamental microbiological studies, but also suggests a viable means for controlling biofilm related infection in medical settings.

In Chapter 6, transport of NO within and through polymers was studied to better understand/optimize the design of medical devices utilizing NO release. The transport properties (diffusion coefficient and partition coefficient) of NO in different biomedical grade polymers were measured via diffusion experiments. Such properties were then applied to finite element analysis (FEA) for simulating the NO release profile as well as its distribution in commercial dual lumen catheters. The FEA method proves to be a useful tool in designing the optimal geometry of medical devices that exhibit NO release, especially utilizing the new electrochemical NO generating scheme described in Chapter 3.

In Chapter 7, the Cu(II)-ligand complex mediated electrochemical NO release was further adapted for potential application in inhaled NO (INO) therapy. NO concentrations from 0–150 ppmv were produced in the gas phase using a constant current method with large area mesh electrodes, with no significant levels of NO_2 or N_2O detected. This study further extends NO generation via the electrochemical method to a much higher concentration range, and demonstrates the possibility of using such a method for replacing the expensive tanks of NO employed for INO therapy in hospitals around the world.

Preliminary screening and characterization of various Cu(II)-ligand complexes as catalysts for NO generation from nitrite are provided in Appendix A.

Overall, the electrochemical NO generation systems described in this thesis provide a versatile and robust means to create different NO-based medical devices. One of the biggest advantages is the easy control of NO release levels. The release of NO not only can be gated "on" and "off", but the flux of NO release can also be modulated temporally by applying either different currents or different voltages to the working electrodes within the various devices.

8.2 Future Directions

8.2.1 Screening of More Cu(II)-Ligand Complexes for Better Catalysts

Future directions involve both fundamental and applied studies. For fundamental studies, more efficient and robust catalysts need to be developed for NO generation from nitrite. Some modification of the existing catalysts can be potentially helpful in this regard. The structures of some potentially useful Cu(II)-ligand complexes are shown in Figure 8.1.

Preliminary data have already already been collected with 3-[bis(2-pyridylmethyl)amino]propionate (BMPA-Pr, Figure 8.1C n = 2). This complex exhibits quasi-reversible electron transfer on Pt electrode (peak separation of ~90 mV) with $E_{1/2}$ = -0.325 V vs. Ag/AgCl (3 M Cl^-) and catalyzed reduction of nitrite with faradaic efficiency of NO > 30%.

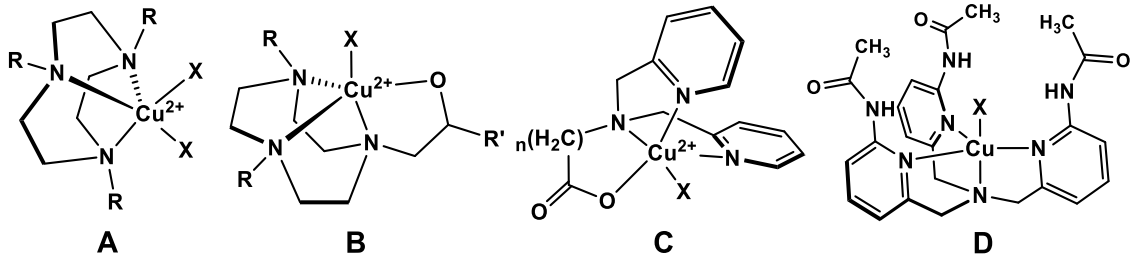

Figure 8.1. Structures of new TACN derivatives and Cu(II) complexes that can be investigated in future work. A) Cu(II)R_3TACN$(X)_2$, R = -Et, -*i*Pr, -CH_2CH_2OH, or -*i*PrOH; B) asymmetric TACN derivatives: R' = H (alcohol group) or carbonyl (carboxylate group); C) BMPA-carboxylate derivatives; n = 1–3; D) Cu(II)TAPMA(X)]. X = NO_2^-, H_2O/HO^-, CH_3COO^-, or Cl^-, depending on experimental conditions.

8.2.2 Exploration of Other Electrode Materials/Modification of the Electrodes

Other inert and inexpensive electrode materials can be explored for use with the Cu(II)-ligand complex-based electrochemical NO generation system. Preliminary studies suggest that carbon fibers can be used in a catheter setup for electrochemical NO generation. Stainless steel can also be used for NO generation, although the efficiency is lower, and some corrosion of the electrode occurs. Further enhancement of the stability of these electrodes by anodization or by plating with inert metal (e.g., Au or Pt) on the surface should be considered.

Another direction for future research would be to modify the surface of suitable electrodes with the Cu(II) catalysts, thereby converting a homogeneous catalysis system to a more robust/reusable heterogeneous one. This modification can be achieved either by click chemistry (Figure 8.2A),[2] or by electrooxidation of a catalyst containing aryl carboxylate groups on a graphitic surface (Figure 8.2B),[3] or electroreduction of a diazonium salt,[4] as well as formation of self-assembly monolayer of catalysts on a gold

electrode (Figure 8.2C).[5] A catalyst with a large π system can also be noncovalent adsorbed onto a carbon surface by π- π interaction.[6]

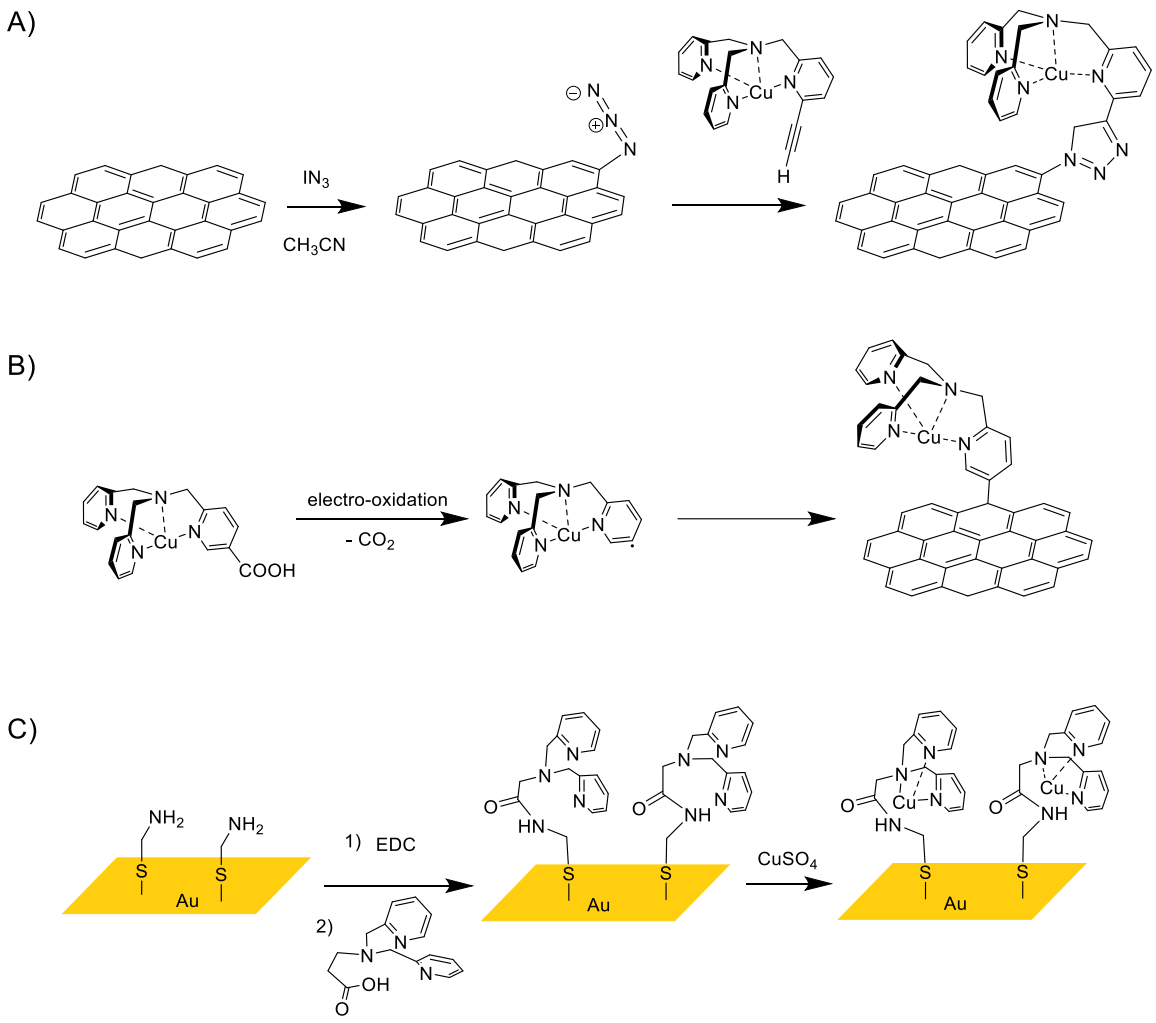

Figure 8.2. Various approaches to immobilize Cu(II)-ligand catalysts onto different electrode surfaces. A) Click chemistry to bind catalyst onto a graphitic surface; B) electro-grafting by coupling of an aryl radical to the graphitic surface via electrochemical oxidation of an aryl carboxylic acid; and C) attachment of catalyst to gold surface by a cystamine mediated self-assembly monolayer.

In addition, Cu(II) complexes with a tridentate ligand could be potentially be bound to a pyridine or imidazole containing polymer, like poly(vinylpyridine) (PVPy) or poly(vinylimidazole) (PVI). The structure of the resulting Cu(II)-containing polymers are shown in

Figure **8.3**. Electron hopping between Cu sites can render the film conductive and such polymeric film can be cast onto the electrode surface for further catalytic studies.

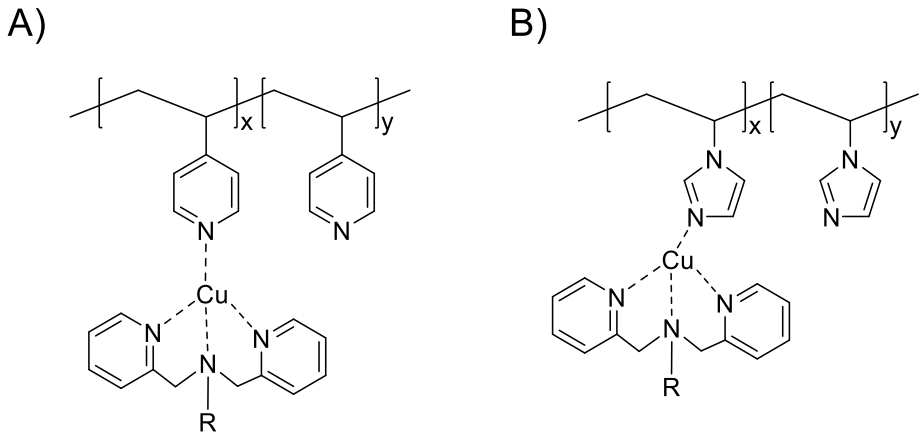

Figure 8.3. Attachment of Cu(II)-tridentate-ligand complexes to A) poly(vinylpyridine) and B) poly(vinylimidazole).

8.2.3 Development of a Galvanic NO Release System or Photocatalytic System

With a better understanding of the Cu(II) catalysts, the system could be adapted to a galvanic system where no external voltage source is required. This can be achieved by coupling the reaction on the working electrode to another reaction on the counter electrode, that has its own redox potential that would create a galvanic cell that would discharge spontaneously to drive the reduction of nitrite.

On the other hand, a photocatalytic system where NO release from reduction of nitrite is driven by light will also be an interesting direction to pursue. This can be achieved using a p-type semiconductor with band edge more negative than the formal potential for catalytic reduction of nitrite (e.g., GaAs[7]).

8.2.4 Optimization in Catheters for Longer Term NO Release

Longer term NO release in the catheter configuration can be optimized by using a more concentrated solution of nitrite and catalyst, ultimately for long-term animal studies. On the other hand, a method that involves changing the solution inside the catheter can also be explored. Figure 8.4 illustrates a configuration of a catheter in which the inner filling solution can be easily changed or circulated, providing the potential to greatly prolong the NO release lifetime.

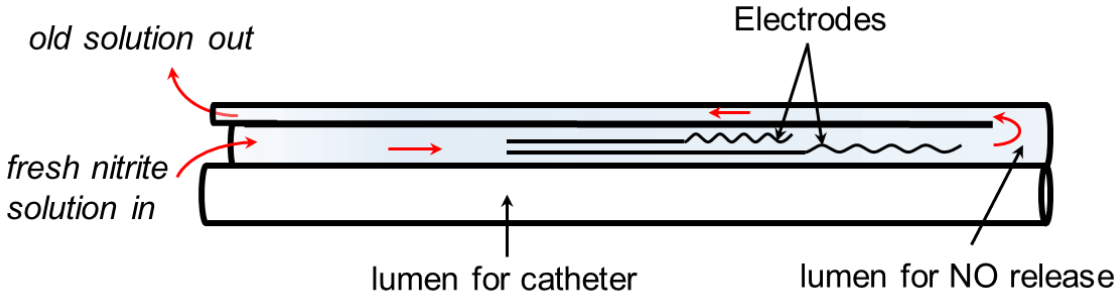

Figure 8.4. Concept of circulating/changing the inner filling nitrite solution for electrochemical NO release.

8.2.5 More Fundamental Antimicrobial Studies

Utilizing the facile temporal control of the NO release, the effect of NO on biofilms at different stages of its formation should be possible. For example, the dosage effect of

NO can be studied at the stage of initial attachment and the stage of colonization and growth of the bacteria (see Figure 1.1 in Chapter 1).

In this dissertation, the pulsed/periodic release of NO on biofilm was only studied at 3 h/day for 3 days. Other release frequencies should also be examined to determine the most efficient release frequency for preventing biofilm formation for a number of different microbes.

Synergy between NO and antibiotics should be further investigated on other pathogenic bacteria strains, as well as using other common antibiotics (e.g., cephalosporin, commonly used to treat *S. aureus* biofilm) to test the generality of such synergy. Ultimately, such synergy can be studied *in vivo* for both catheter-associated urinary tract infections (CAUTIs) and catheter-associated bloodstream infections (CABSIs), using the new electrochemical NO release catheter technology developed as part of this dissertation work.

8.2.6 Improvement of Systems for INO

For the INO project, a better design taking the whole system into account, including reactions on both the anode and cathode, to improve the overall efficiency should be further investigated. The working and counter electrodes can be separated by an ion conductive membrane (e.g., Nafion), or by adding some anode depolarizer (electroactive species that can be oxidized on the counter electrode) to decrease the potential for NO oxidation or O_2 generation at the surface of the counter electrode. Ideally, such an anode depolarizer can also serve as a proton source (e.g., $N_2H_4 \rightarrow N_2 + 4H^+ + 4e^-$) while being compatible with the cathode reaction.

The application of gas phase NO generated from the electrochemical system may be applicable for biological/physiological studies, e.g. airway related diseases, both *in vitro* and *in vivo*. Development of a more portable device based on pumped air as the carrier gas should also be beneficial in expanding the use of INO to more places, and potentially for treatment of more diseases, including convenient home use. The availability of suitable NO sensors that can detect the levels of the NO gas entering the patient is essential for such a system, and these sensors should provide signals that can servo-regulate the potential or current applied to the working electrode, thereby controlling the concentration of inhaled NO to a precise level.

The research reported in this thesis only touched the surface in terms of fundamental and applied studies possible for the electrochemical NO generating/release concept. Clearly, research in this area should be expanded on a number of fronts to realize the full potential of this relatively simple approach.

8.3 References

(1) Clark, L. C.; Wolf, R.; Granger, D.; Taylor, Z. *Continuous Recording of Blood Oxygen Tensions by Polarography*, 1953; Vol. 6.

(2) Devadoss, A.; Chidsey, C. E. D. *J. Am. Chem. Soc.* **2007**, *129*, 5370.

(3) Andrieux, C. P.; Gonzalez, F.; Savéant, J.-M. *J. Am. Chem. Soc.* **1997**, *119*, 4292.

(4) Bahr, J. L.; Yang, J.; Kosynkin, D. V.; Bronikowski, M. J.; Smalley, R. E.; Tour, J. M. *J. Am. Chem. Soc.* **2001**, *123*, 6536.

(5) Xiao, Y.; Ju, H.-X.; Chen, H.-Y. *Anal. Chim. Acta* **1999**, *391*, 73.

(6) Blakemore, J. D.; Gupta, A.; Warren, J. J.; Brunschwig, B. S.; Gray, H. B. *J. Am. Chem. Soc.* **2013**, *135*, 18288.

(7) Krishnan, R. In *Encyclopedia of Electrochemistry*; Wiley-VCH Verlag GmbH & Co. KGaA: 2007.

APPENDIX A.

SUMMARY OF BEHAVIOR OF VARIOUS CU(II)-LIGAND COMPLEXES AS CATALYSTS FOR NO GENERATION VIA ELECTROCHEMICAL REDUCTION OF NITRITE

A.1 Summary of the Electrochemical Properties Cu-Ligand Complexes

In Chapter 3, CuTPMA was studied as a catalyst for NO generation by electrochemical reduction of nitrite ions. In addition to this catalyst, other copper-ligand complexes have also been screened for similar NO generation from nitrite. The ligands for these Cu(II) complexes can be categorized into three classes: 1) alkyl tripodal ligands, including tris(2-aminoethyl)amine (TREN) and its derivative tris[2-(dimethylamino)ethyl]amine (Me_6TREN); 2) pyridyl containing tripodal ligands, including tris(2-pyridylmethyl)amine (TPMA), 3-[bis(2-pyridylmethyl)amino]propionate (BMPA-Pr), and 2-ethylthio-*N*,*N*-bis(pyridin-2-yl)methylethanamine (BMPA-SEt); and 3) tridentate cyclic compounds, including 1,4,7-triazacyclononane (TACN) and its *N*-methyl derivative, 1,4,7-trimethyl-1,4,7-triazacyclononane (Me_3TACN). The structures of these compounds are shown in Figure A.1.

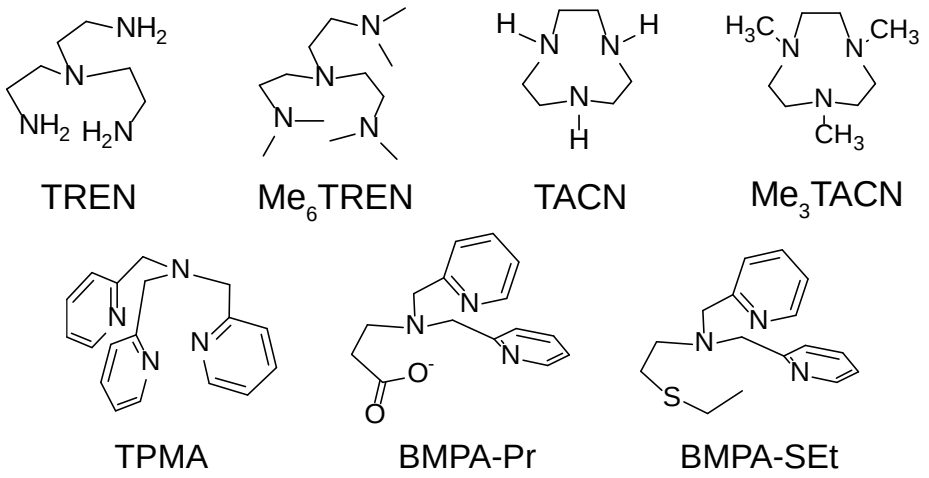

Figure A.1. Structures of ligands that form strong Cu(II) complexes that have been studied in this work for electrochemical reduction of nitrite.

Using cyclic voltammetry and bulk electrolysis in the presence of nitrite, these Cu(II)-ligand complexes were characterized for their formal potential, and their maximum NO production rate in the presence of 1 mM catalyst and 0.1 M nitrite. The results are summarized in Table A.1. These experiments were conducted using a 2 mm diameter Pt disk electrode with 1 mM Cu(II)-ligand complexes in 5 mL 0.1 M HEPES buffer solution (pH 7.3). $E_{1/2}$ is determined from the midpoint of cathodic and anodic peak potentials in CV at scan rate of 50 mV/s under N_2. Maximum NO generation rate was determined by a nitric oxide analyzer (NOA) during bulk electrolysis of the same solution in the presence of 0.1 M $NaNO_2$ solution at potential more negative than the catalytic wave for reduction of nitrite. Faradaic efficiency was calculated based on the ratio of amount of NO measured in the NOA measurement divided by Faraday's constant to the charge passed based on the integration of the current.

Table A.1. Summary of electrochemical properties of catalyst in aqueous solution.[†]

Ligand	$E_{1/2}$ /V (vs. Ag/AgCl)	Max NO Rate * /μmol $s^{-1}cm^{-2}$	Faradaic Efficiency *
TREN	-	-	< 0.1 %
Me_6TREN	-0.25	-	< 0.1 %
TACN	-0.24	-	< 0.1 %
Me_3TACN	-0.24	5.7	-0.30V: 93%
BMPA-Pr	-0.32	1.1	-0.30V: 32%
BMPA-SEt	+0.25	-	<0.1 %
TPMA	-0.33	9.9	-0.32V: 28%

[†] This data was collected in collaboration with Mr. Andrew Hunt from Dr. Lehnert Lab.
* 1 mM $Cu^{II}L$, 0.1 M nitrite, 0.1 M HEPES buffer (pH 7.3).

A.2 Study of Cu(II)Me_3TACN as Catalyst for NO Generation from Nitrite

Among these catalysts, $CuMe_3$TACN has the highest faradaic efficiency for NO generation. The cyclic voltammogram (CV) of $CuMe_3$TACN in the presence of different concentrations of nitrite is shown in Figure A.2. The cathodic wave increases as the nitrite concentration increases, indicating the catalytic reaction likely through an EC' mechanism, similar to that observed for CuTPMA.[1] In the bulk electrolysis, NO at different fluxes can be generated by applying different voltages before the limiting current is reached (Figure A.3).

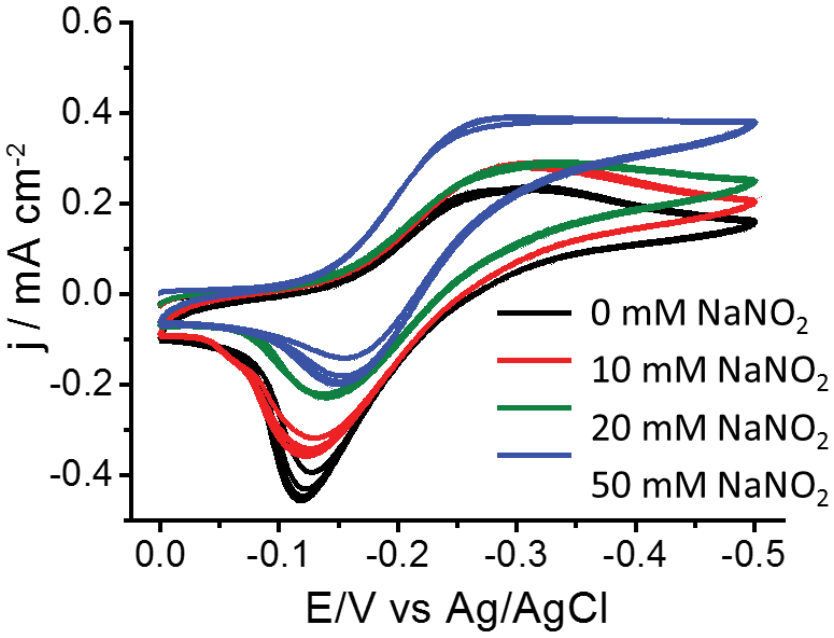

Figure A.2. Cyclic voltamogram of 1 mM Cu(II)Me_3TACN in 0.1 M HEPES buffer (pH 7.3) in the presence of different concentrations of $NaNO_2$.

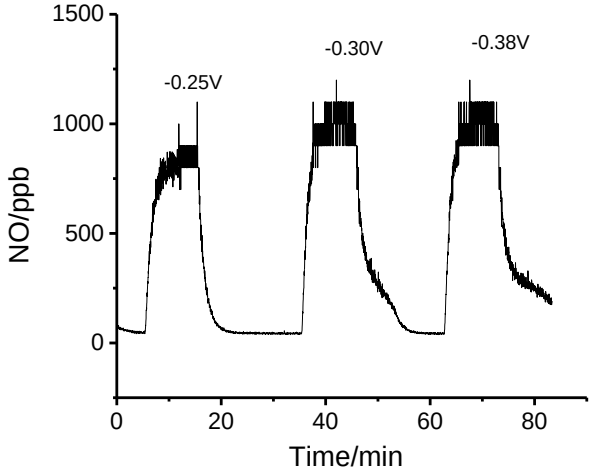

Figure A.3. NO release to gas phase from a 5 mL solution of 1 mM Cu(II)Me_3TACN, 50 mM $NaNO_2$, 0.1 M HEPES (pH 7.3), 0.1 M NaCl by different applied potential to a 2 mm diameter Pt working electrode. Solution was continuously purged with nitrogen at flow rate of 50 mL/min.

The $CuMe_3TACN$ and nitrite solution was also studied in a single lumen catheter. The configuration of the catheter is the same as in Figures 3.6 and 3.7A. The generated NO showed relatively stable flux for more than 16 h. The average faradaic efficiency is 70%. At the end of the experiment, Cu^o is deposited on the working electrode as evidenced by a stripping peak of Cu^o in a fresh buffer solution (data not shown, also evidenced from the anodic peak ~-0.05 V in the CVs $CuMe_3TACN$ at 0 or low levels of nitrite; see Figure A.3).

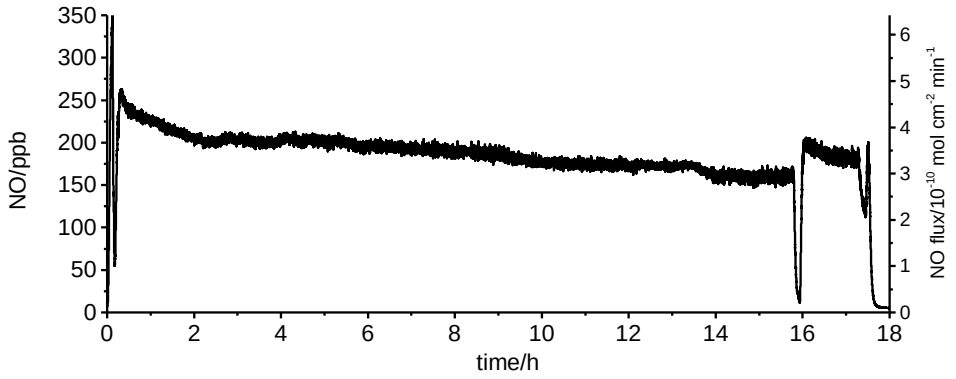

Figure A.4. NO release from a single lumen catheter (i.d. 1.47 mm; o.d. 1.96 mm, 6 cm) using 0.5 mM Cu(II)Me_3TACN, 0.5 M $NaNO_2$, 0.4 M HEPES and 0.16 M NaCl as inner solution. Pt wire (o.d. 0.127 mm) was exposed for 2 cm and Ag/AgCl wire was exposed for 4 cm and coiled. Applied potential was -0.3 V vs Ag/AgCl wire.

A.3 Side Reaction of $CuMe_3TACN$—Disproportionation of Cu(I)

The Cu^0 deposited on the electrode surface is surmised through disproportionation of the electrochemically generated Cu(I)-ligand complex. This was examined in more detail by conducting voltammetry on a 25 um microelectrode so that a higher scan rate can be achieved without significant complications from charging currents. As shown in Figure A.5, the anodic peak at ~ -0.05 V is highly dependent on the scan rate. The peak area

decreases as the scan rate increases. This is because at higher scan rates, the homogeneous reaction (disproportionation) kinetics is slow compared to the scan rate, and most of the Cu(I) is not able to disproportionate before being re-oxidized back to the inert Cu(II) in the reverse scan.

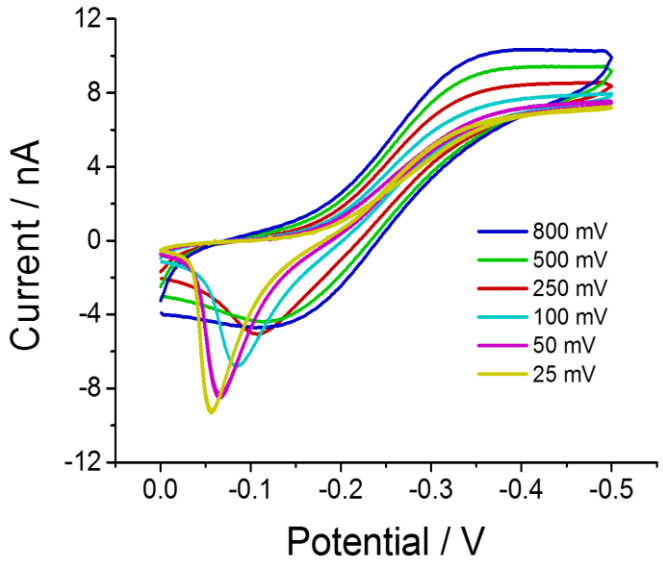

Figure A.5. Cyclic voltammogram of 2 mM $CuMe_3TACN$ in 0.1 M HEPES buffer on a 25 μm Pt microelectrode at different scan rates. The peak on the anodic scan near -0.05 V correspond to the stripping of Cu^0 on the electrode surface.

A 2-D axial symmetry model for the 25 μm microelectrode was built to simulate the kinetics of the disproportionation reaction during the scans of CVs. Bulter-Volmer kinetics was assumed as the boundary conditions on the electrode surface.[2] The diffusion equation for Cu(I) was coupled with homogeneous disproportionation reaction $d[Cu^0]/dt = k^{dis}[Cu(I)]^2$, where k^{dis} is the second order rate constant for the disproportionation reaction. The simulated CV (without showing the anodic peak from stripping) at different scan rates is shown in Figure A.6. The amount of Cu^0 generated from simulation was compared with

that from the CV in the experiments using Faraday's law ($Q = nF$) by integrating the anodic peak. Simulation using a homogeneous rate constant of $k^{dis} = 1.2 \times 10^2$ M^{-1} s^{-1} yields a good fit with the experiment results at all scan rates (See Figure A.7).

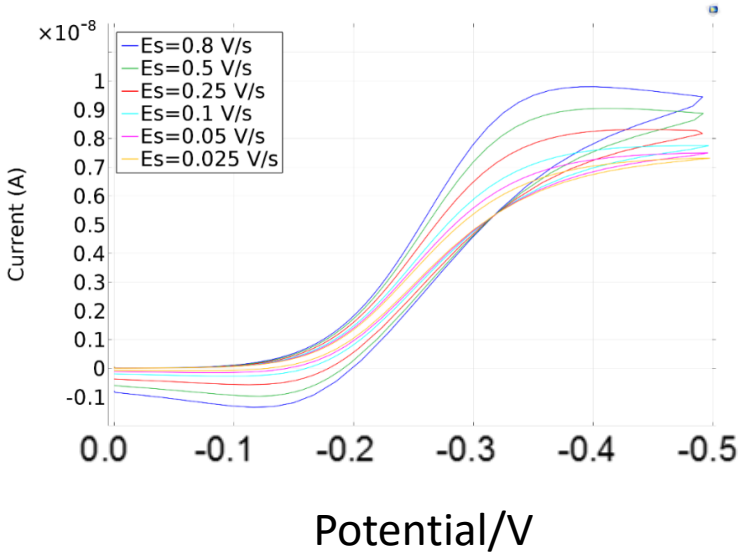

Figure A.6. Simulated CV of 2 mM $CuMe_3TACN$ on a 25 μm Pt microelectrode at different scan rate. The reaction of disproportionation of Cu(I) was included.

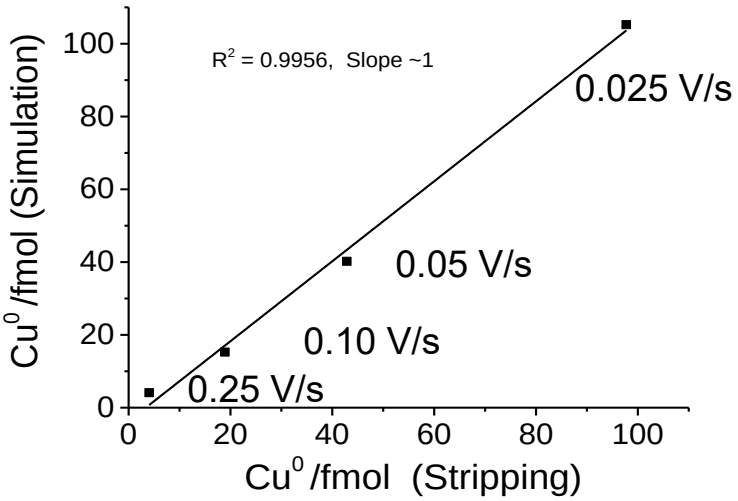

Figure A.7. Comparison of deposited Cu from experiment and simulation. The stripping peak at ~-0.05 V was used to calculate amount of deposited Cu^o.

Such disproportionation was also found in the CuTACN complex, which has a similar structure with $CuMe_3TACN$. The disproportionation reaction for CuTACN is much faster than that for $CuMe_3TACN$, with $k^{dis} = 2.50 \times 10^3\ M^{-1}\ s^{-1}$. This indicates that Cu(I)TACN is less stable than Cu(I)Me_3TACN, which explains why no nitrite reduction was observed for CuTACN. Structurally, the methyl groups in $CuMe_3TACN$ provide more steric and therefore slow down the disproportionation reaction, which needs two Cu(I) complex to approach each other in close proximity.

A.4 References

(1) Ren, H.; Wu, J.; Xi, C.; Lehnert, N.; Major, T.; Bartlett, R. H.; Meyerhoff, M. E. *ACS Appl. Mater. Interfaces* **2014**, *6*, 3779.

(2) Bard, A. J.; Faulkner, L. R. *Electrochemical Methods: Fundamentals and Applications, 2nd Edition*; John Wiley & Sons, 2001.